Solder flux chemistry and climatic reliability of electronics: optimization of flux chemistry for robust performance

Feng Li

PhD Thesis

Solder flux chemistry and climatic reliability of electronics

Optimization of flux chemistry for robust performance
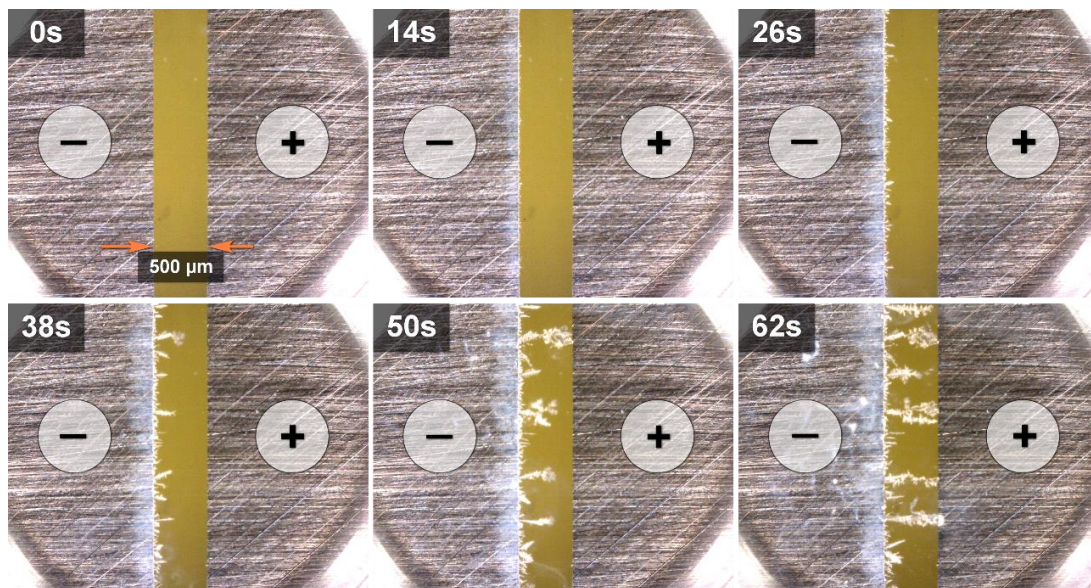
PhD Thesis

Feng Li

Solder flux chemistry and climatic reliability of electronics

Optimization of flux chemistry for robust performance

PhD Thesis

by

Feng Li

April 2021

Supervisors:

Professor Rajan Ambat

Senior Scientist Morten Stendahl Jellesen

Section of Materials and Surface Engineering

Department of Mechanical Engineering

Technical University of Denmark (DTU)

Produktionstorvet 425

DK-2800, Kgs. Lyngby, Denmark

To see the world

Things dangerous to come to

To see behind walls

Draw closer

To find each other

And to feel

That is the purpose of life

----*The Secret Life of Walter Mitty*

Quoted from the movie I saw on the flight to CPH.

PREFACE

This thesis is submitted in candidacy for a PhD degree from Technical University of Denmark. The project entitled "Solder flux chemistry and climatic reliability of electronics: optimization of flux chemistry for robust performance" has been carried out at the Department of Mechanical Engineering, Section of Materials and Surface Engineering, under supervision of Professor Rajan Ambat and Senior Scientist Morten Stendahl Jellesen. This PhD project was a part of research work in the CELCORRr/CreCon consortium (https://celcorr.dtu.dk/), collaborated with Inventec Performance Chemicals (https://www.inventec.dehon.com/en/). The duration of this PhD programme was from January 2018 to April 2021.

PREFACE

ACKNOWLEDGEMENT

ABSTRACT

Corrosion reliability of electronic devices has become a significant issue today due to the growing trend towards miniaturization, wide spread use, and issues such as cleanliness of the printed circuit board assembly (PCBA). Today, 70-80% of the electronic devices are manufactured using no-clean solder flux, which leave flux residue on printed circuit board assemblies (PCBAs). No-clean flux residues are hygroscopic; thereby assisting water film formation on the PCBA surface under humid conditions. Water film connecting between biased points on a PCBA surface can result in electrochemical failure modes such as leakage current failures due to parasitic circuit formation and electrochemical migration (ECM).

The motivation of this PhD project is to obtain a deeper understanding of the impact of flux chemistry in general and particularly the activator chemistry on the solderability and climatic reliability of electronics with an aim to develop better flux formulation satisfying both aspects. The no-clean flux chemistry used today introduce different types of flux residues as localized and potentially corrosive contamination on the PCBA after the soldering process. Some of these residues are highly harmful from the humidity point of view due to their difference in the hygroscopic and ionic nature. The main objective of this work is to characterize and optimize flux formulations by identifying new flux activator compounds or combinations, characterizing the feasibility of new activator compounds for soldering, and evaluating the climatic reliability of PCBAs produced by wave soldering process as well as reflow soldering process. Work has also focused on the corrosion mechanism of Sn-Ag-Cu (SAC) solder alloys and the impact of the flux residue on the protection performance of conformal coatings, which aims to provide a systematic understanding of the protective performance.

Chapter 1 provides a brief introduction of the climatic reliability issues of the electronics and scope of the PhD thesis. Chapter 2 reviews the humidity interaction on a PCBA surface, contamination (flux residue), and conformal coating, which provide a full picture of humidity impact on electronic devices. Further, the corrosion failure mode of powered electronic devices, literature on potential flux activator candidates, and the evaluation methods and techniques for this project was summarized. Chapter 3 provides a summary of the materials and testing methods used in the PhD project.

Research work carried out in this thesis has summarized in 6 journal papers listed from Chapter 4-9, which are published or intended for journal publication. Chapter 4 investigated the corrosion mechanism of five types of SAC solder alloys with Ni, Sb, Bi alloying additives. Chapter 5-7

investigated the solderability and humidity robustness when using alkanolamines, amino acids and dicarboxylic acids with amine additives as flux activator in wave solder flux. Chapter 8 investigated the impact of the different types of flux activators on the climatic reliability of surface-mount devices specially focusing on reflow-soldering process and residue. Chapter 9 focused on the impact of the flux residue on the protection performance of 3 types of conformal coatings. Finally, Chapter 10 provides an overall discussion based on the research outcome and Chapter 11 shows the conclusions from the present work and further perspectives in this field.

Overall, investigations showed better humidity performance and solderability when using amino acid and blend WOA-amine activators in the flux formulation. The combined results from the investigations show that the solderability of flux activator depend upon the strength of the carboxyl and amino groups under soldering temperature, while the humidity robustness of the flux residue depend upon the interaction or reaction between water, dicarboxylic acids, and amines. Glutamine as amino acid candidate provides good wetting properties and humidity robustness in comparison with dicarboxylic acids presently used in commercialized flux chemistry. Diethanolamine and triethanolamine are not feasible from the humidity point of view because of their hydrophilic character due to the hydroxyl group and strong protonation behavior of amino group, while 0.2 wt.% tripropylamine and naphthyamine additives were shown to significantly improve the humidity robustness of succinic acid based wave solder flux.

For the conformal coating investigation, performance depends upon the level of cleanliness of the PCB and chemistry of flux residue. The presence of highly hygroscopic flux residue increased moisture absorption to the conformal coating, delamination, and failure. The increased adhesion of the elastomeric acrylate coating was shown to be a key parameter explaining better performance even on highly flux contaminated PCB.

Corrosion reliability investigation of SAC solder alloys showed that the corrosion behavior primarily depends upon the distribution homogeneity of the Ag_3Sn intermetallic compounds. For InnoLot alloy, Bi additive acted as cathode and form micro-galvanic corrosion cell with Sn/Sb solid solution and Sb additive reduced the corrosion current density.

RESUMÉ

Klimatisk pålidelighed af elektronik er blevet et væsentligt problem i dag på grund af den voksende tendens mod miniaturisering, udbredt anvendelse og at sikre renhed af færdig producerede printkort. I dag er 70-80% af printkort fremstillet ved hjælp af såkaldt "no-clean" loddesystemer, som vil efterlade flusrester på printkort. Sådanne flusrester kan være hygroskopiske og derved øge risiko for dannelse af vandfilm på printkort under fugtige forhold. En sådan dannet vandfilm kan danne elektrolytisk forbindelse mellem forskellige metalliske elementer på printkortet, hvilket kan resultere i korrosion, lækstrømme og elektrokemisk migration.

Motivationen for dette ph.d.-projekt er at opbygge en dybere forståelse af indflydelsen af fluskemi generelt med fokus op effekten af aktivatiorer på loddeevne og klimatisk pålidelighed. På sigt kan der udvikles optimerede flus systemer der både sikrer loddevne og har minimal effekt såfremt der dannes vandfilm på printkort overfladen. Den "no-clean" flusteknologi, der anvendes i dag, efterlader forskellige typer flusrester efter loddeprocessen. Nogle af disse rester er meget skadelige på grund af deres hygroskopiske og ledningsevnebærende egenskaber. Hovedformålet med projektet er at optimere flusformuleringen ved at identificere nye flusaktivatorforbindelser eller kombinationer, og karakterisere disse lodningegenskaber samt at evaluere den klimatiske pålidelighed af printkort produceret ved bølgelodningsproces samt reflow-lodningsproces. Arbejdet fokuserer også på korrosionsmekanismen af Sn-Ag-Cu (SAC) lodde-legeringer og indflydelsen af flusrester på beskyttelsesevnen for laksystemer.

Kapitel 1 giver en kort introduktion af de klimatiske pålidelighedsspørgsmål reevante for elektronikken samt en afgrænsning af ph.d.-afhandlingens omfang. Kapitel 2 gennemgår interaktion mellem fugt og printkort, effekten af forurening (flusrester) og lak systemer. Desuden gennemgåes korrosionsfejlstilstande samt litteratur om potentielle flusaktivator-kandidater og evalueringsmetoder heraf. Kapitel 3 giver et resumé af de materialer og testmetoder, der anvendes i ph.d.-projektet.

Forskningsarbejde udført i denne afhandling er opsummeret i 6 tidsskriftartikler fra kapitel 4-9, som er publiceret eller beregnet til tidsskriftpublikation. Kapitel 4 undersøger korrosionsmekanismen for fem typer af SAC lodde legeringer med Ni, Sb og Bi legeringsadditiver. Kapitel 5-7 undersøger lodbarhed og effekter af fugt ved anvendelse af alkanolaminer, aminosyrer og dicarboxylsyrer med amintilsætningsstoffer som flusaktivator til brug for bølgelodning. Kapitel 8 undersøger virkningen af de forskellige typer af flusaktivatorer på den klimatiske pålidelighed af overflademonterede komponenter med specielt fokuserer på reflow-loddeproces og flusrester.

Kapitel 9 fokuserer på virkningen af flusrester på beskyttelsesevnen for 3 typer af lak systemer. Endelig giver kapitel 10 en samlet diskussion og kapitel 11 viser konklusionerne fra det nuværende arbejde og yderligere perspektiver på dette felt.

Samlet set viste undersøgelser bedre fugt modstandsdygtighed og loddeevne ved anvendelse af aminosyrer og blandede WOA-aminaktivatorer i flusformuleringen. De kombinerede resultater fra undersøgelserne viser, at lodbarheden afhænger af styrken af carboxyl- og aminogrupperne under loddetemperatur, mens ledningsevnen afhænger af interaktionen eller reaktionen mellem vand, dicarboxylsyrer og aminer. Glutamin som aminosyrekandidat giver god fugt modstandsdygtighed og fugtstabilitet i sammenligning med dicarboxylsyrer, der anvendes i kommercialiseret fluskemi. Diethanolamin og triethanolamin er ikke velegnede på grund af deres hydrofile karakter; hydroxylgruppen og den stærke protoneringsadfærd af aminogruppen, mens 0,2 vægtprocent tripropylamin og naphthyaminadditiv viste bedre egenskaber.

Til undersøgelse af laksystemer fandtes en sammenhæng mellem fugtmodstandsdygtighed og printkortets renhed samt kemiske opbygning af tilbageværende flusrester. Tilstedeværelsen af meget hygroskopiske flusrester øgede fugtabsorptionen til den lakken og resulterer i delaminering og manglende beskyttelse. God vedhæftning af den elastomere acrylatbelægning klarede sig bedst selv på ganske høje koncentrationer af flus forurenende printkort.

Korrosionsundersøgelse af SAC-lodde legering viser, at korrosionsadfærden primært afhænger af fordelingen af Ag_3Sn intermetalliske forbindelser. For InnoLot-legering fungerede Bi-additiv som katode og dannede mikro-galvanisk korrosionscelle med Sn/Sb, og det blev vist at Sb-additiv resulterede i en reduceret korrosionsstrømstæthed.

LIST OF ABBREVIATIONS

AC   Alternating Current

AFM   Atomic force Microscopy

AH   Absolute Humidity

AR   Acrylic Resin

ATR   Attenuated Total Reflectance

BET   Brunauer-Emmett-Teller

BSE   Backscattering Electron

CA   Chronoamperometry

CAF   Conductive Anodic Filament

CVD   Chemical Vapour Deposition

DC   Direct Current

DEA   Diethanolamine

DIPA   Diisopropanolamine

DRH   Deliquescence Relative Humidity

EA   Ethanolamine

ECM   Electrochemical Migration

E_{corr} Corrosion Potential

EDS   Energy Dispersive Spectroscopy

EIS   Electrochemical Impedance Spectroscopy

ER   Epoxy Resin

ERH   Efflorescence Relative Humidity

FR-4   Glass-reinforced Epoxy Laminate

FT-IR   Fourier Transform Infrared Spectroscopy

GAB   Guggenheim-Absernon-de Boer

HASL   Hot Air Solder Leveling

IC   Intergrated Circuit

i_{corr} Corrosion Current Density

IMC	Intermetallic Compound
LC	Leakage Current
LOM	Light Optical Microscopy
MTTF	Mean Time to Failure
OCP	Open Circuit Potential
PCB	Printed Circuit Board
PCBA	Printed Circuit Board Assembly
pKa	Acid Dissociation Constant
PR	Parylene Resin
RH	Relative Humidity
RoHS	Restriction of Hazardous Substances Directive
SAC	Sn-Ag-Cu
SE	Secondary Electron
SEM	Scanning Electron Microscopy
SIR	Surface Insulation Resistance
SKPFM	Scanning Kevin Probe Force Microscopy
SMD	Surface-Mount Device
SMT	Surface-Mount Technology
SR	Silicone Resin
TEA	Triethanolamine
TEL	Thin Electrolyte Layer
THB	Thermal Humidity Bias
TIPA	Triisopropanolamine
TTF	Time to Failure
UR	Urethane Resin
WD	Water Droplet testing
WEEE	Waste Electrical and Electronic Equipment Directive
WOA	Weak Organic Acid
XRD	X-ray diffraction

LIST OF PUBLICATIONS

PUBLICATIONS AS FIRST AUTHOR

1. **F. Li**, V. Verdingovas, K. Dirscherl, G. Harsányi, B. Medgyes, R. Ambat, Influence of Ni, Bi, and Sb additives on the microstructure and the corrosion behavior of Sn–Ag–Cu solder alloys, J. Mater. Sci. Mater. Electron. 31 (2020) 15308–15321. doi:10.1007/s10854-020-04095-y.

2. **F. Li**, K. Piotrowska, M.S. Jellesen, R. Ambat, Alkanolamines as activators in no-clean flux systems: Investigation of humidity robustness and solderability, Mater. Sci. Mater. Electron. (2021). doi:10.1007/s10854-020-05235-0.

3. **F. Li**, I. Mantis, M.S. Jellesen, R. Ambat, Amino acids as activators for wave solder flux systems: investigation of solderability and humidity effects, submitted to Journal of Electronic Materials.

4. **F. Li**, M.S. Jellesen, R. Ambat, Comparative study of tripropylamine and naphthylamine as additives in wave solder flux: investigation of solderability and humidity effects, to be submitted to Journal of material science: Materials in Electronics.

5. **F. Li**, A.R. Lakkaraju, M.S. Jellesen, R. Ambat, Effect of reflow process related flux residue on the climatic reliability of surface-mount electronic devices, to be submitted to Journal of Materials Processing.

6. **F. Li**, V. Verdingovas, I. Mantis, M.S. Jellesen, R. Ambat, Influence of no-clean solder flux residue on the corrosion protection of conformal coatings used in electronics, to be submitted to Progress in Organic Coatings.

JOINT PUBLICATIONS AS CO-AUTHOR

1. A. Khangholi, **F. Li**, K. Piotrowska, S. Loulidi, R. Ambat, G. Van Assche, A. Hubin, I. De Graeve Humidity Robustness of Plasma-Coated PCBs, J. Electron. Mater. 49 (2020) 848–860. doi:10.1007/s11664-019-07714-5.

2. K. Piotrowska, **F. Li**, R. Ambat, Thermal decomposition of binary mixtures of organic activators used in no-clean fluxes and impact on PCBA corrosion reliability, Solder. Surf. Mt. Technol. 32 (2019) 93–103. doi:10.1108/SSMT-05-2019-0020.

3. K. Piotrowska, **F. Li**, R. Ambat, Transformation of reflow solder flux residue under humid conditions, submitted to Microelectronics Reliability.

4. I. Mantis, **F. Li**, M.S. Jellesen, R. Ambat, Protective Properties of Fluoropolymer Coating for PCBs under Cyclic Climatic Conditions, submitted to Microelectronics Reliability.

5. H. Conseil-Gudla, **F. Li**, R. Ambat, Profiling trapped reflow residues on circuit board assemblies and interaction with humidity, to be submitted to Journal of material science: Materials in Electronics.

CONFERENCE PAPER AND PRESENTATION

1. **F. Li**, V. Verdingovas, B. Medgyes, R. Ambat, Corrosion reliability of lead-free solder systems used in electronics, Proceedings of the 40th International Spring Seminar on Electronics Technology (ISSE), 2017 . IEEE.
2. **F. Li**, V. Verdingovas, B. Medgyes, R. Ambat, Corrosion reliability of lead-free solder systems used in electronics, Proceedings 2018 IMAPS Nordic Conference on Microelectronics Packaging (NordPac 2018) . IEEE, p. 67-71.
3. **F. Li**, V. Verdingovas, B. Medgyes, R. Ambat, Investigation of microstructure and corrosion reliability of Sn-Ag-Cu based Lead-free Solder Alloys, Eurocorr 2018, Kraków, Poland.
4. **F. Li**, K. Piotrowska, M.S. Jellesen, R. Ambat, Electrochemical study on etching ability and humidity robustness of organic amines used in the solder flux systems, Eurocorr 2019, Seville, Spain.
5. **F. Li**, A.R. Lakkaraju, M.S. Jellesen, R. Ambat, Effect of wave and reflow solder flux residue on the corrosion reliability of electronics, Eurocorr 2020, Vitrual.

TABLE OF CONTENT

1. Introduction

1.1. Background

Today, electronic devices are used in a variety of fields, including communication, computer, business and retail electronics, industrial electronics, instrumentation, aerospace, military etc [1]. Electrification of vehicles is an example, which will increase the use of electronics in the automotive industry. For lower price, high processing speed, lower energy consumption and smaller sizes, miniaturization of electronics became the trend today with size reduction at component level, Printed Circuit Board Assembly (PCBA) level, and device level. Design of the component also changed over the years from leaded components to Ball Grid Assembly (BGA) type changing the corresponding soldering process for PCBA, which significantly reduced the pitch distance of the electrodes (layouts) on PCBA surface. Similar scenario can be seen for passive chip components mounted PCBA that have undergone severe size reduction.

For many applications, service environment for the electronics could be very harsh, hence require better corrosion reliability. PCBAs are inherently susceptible to corrosion when exposed to varying humidity and temperature conditions due to multiple factors, such as base materials and component material make up, PCBA design such as pitch distance between biased points, contamination on the PCBA. **Figure 1.1** shows a schematic of the multiple factors contributing to the corrosion reliability of electronics. When the water film forms on the PCBA surface connecting biased points resulting in electrochemical cell formation, ionic residues on the surface makes the water film good electrolyte. Residues also determine the humidity boundary for failure due to their hygroscopic nature.
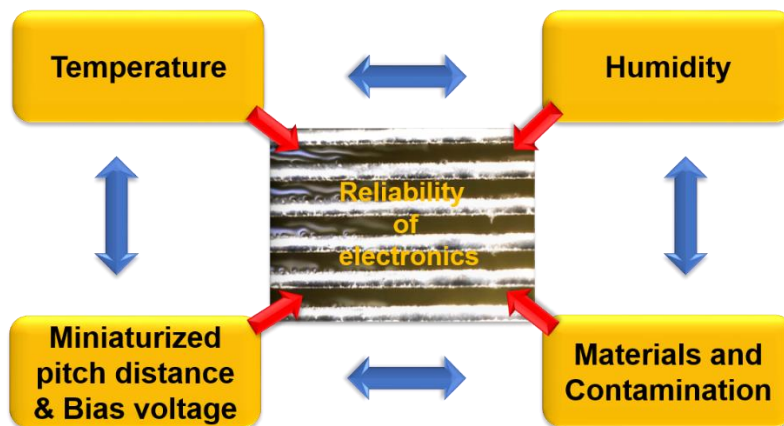
Figure 1.1 Factors affecting humidity related corrosion reliability of electronics

Climatic factors causing corrosion in electronics are related to the varying climate conditions during service such as day/night humidity and temperature fluctuations and seasonal changes, precipitation levels, and atmospheric contaminations. Although, electronics parts are protected by packaging, humidity can enter the device depending on the tightness of the packaging.

Electronic parts are usually never come in contact with large amount of water. However, under conducive conditions, thin water film can build up on PCBA surface depending on the surrounding humidity level, differential temperature, and ionic contamination on the surface. Although, the exact nature of functionality issues arising from the effect of exposure conditions vary depending on the specificity of the involved electronic part, major influence is due to the metallic parts undergoing corrosion that leads to total electrical failure and interference on functionality. Such failures can be intermittent or permanent depending on the existence of the conductive climatic conditions as well as failure modes.

Ionic contaminations on the PCBA acts as accelerators for the electronic corrosion [9]. The source of ionic contamination on the PCBA can be distinguished as external contamination and intrinsic contamination. The external contamination was induced by the service environment, including corrosive salts, dust and corrosive gases etc, while the intrinsic contamination source was mainly from the presence of the process-related no-clean flux residue [9]. The external contamination source can be avoided using conformal coating, potting, and robust enclosure design. In comparison, intrinsic no-clean flux residue contamination play a vital role on electronic corrosion. Hence, intrinsic contamination existing on the PCBA surface is more important and controlling this factor will increase overall inherent humidity robustness of the PCBA.

Residue on the PCBA surface can be either ionic or non-ionic in nature, although ionic residues are more problematic from the point of view of humidity interaction. Cleanliness of materials, components, and manufacturing processes are integrated together on a PCBA surface with contribution from each, although the assembling process (last step) namely the automated soldering process has significantly higher contribution. This has direct connection to the use of no-clean flux because the removal of flux residue during the soldering process solely depends on the kinetics of the thermal decomposition process, which is never complete due to variations in the temperature profile and short exposure time at higher temperatures.

No-clean flux with WOA activators has been occupied 70-80% of the market [12][16] due to the trend of halogen-free and the elimination of volatile organic cleaning agents [13]. WOAs like linear dicarboxylic acids, namely: glutaric acid, succinic acid, and adipic acid etc., were used as

activators in the formulation of commercial solder fluxes [13] today. The WOA flux activators in flux residue can cause corrosion of electronic system due to the interaction of humidity, temperature and applied voltage [22]. The WOA activator is hygroscopic in nature [23], which results in reduction of humidity level required for condensed water film formation. The WOA flux activators are water soluble [6]. Consequently, the ionization of carboxyl group of WOA increases the conductivity of the condensed water on the PCB surface, which accelerated the high leakage current and ECM failures under voltage bias loading [6]. With higher temperature exposure, the solubility of WOA in water increased, which will increase the risk of the corrosion and decline the robustness of electronic devices.

The art of the no-clean flux aims at decomposing or evaporating the solid content in the flux after soldering process to obtain PCB assemblies with minimal flux residue or residue-free surface [6]. However, in reality the manufacturing process conditions are not able to eliminate the presence of flux residues formed through wave soldering process, selective wave soldering process, rework & repair process, and reflow soldering process [17]. In general, PCBAs produced due to reflow soldering process provided better corrosion performance than the other soldering process due to the special morphology of the residue, however, corrosion failures can occur over extended period of exposure to humidity [21]. Sometime, PCBAs are protected from humidity using the conformal coating. However, protection performance of the conformal coatings also depends upon the cleanliness of the PCBA surface, type of residue present, and compatibility between coating material and residue. Presence of ionic residues between the PCBA board and conformal coating results in delamination of the coating, water film build up, and corrosion related failures, while the humidity boundary for failures depends on the chemistry of the residue.

1.2. Scope of the thesis

The main objective of this PhD project is to build deep understanding on the flux chemistry effect on humidity related reliability issues of electronics with an aim to develop knowledge that can be used for making robust flux systems satisfying both climatic reliability requirements and solderability. Part of the PhD work was focused on investigations about new flux activators based on Amines and Amino acid systems individually or together with presently used Weak Organic Activators (WOAs). Overall objective was to develop feasible methods for making optimized flux formulations better than the one existing today. For flux activator investigations, focus was on liquid flux systems used for wave soldering process. Effect of flux residue from reflow soldering process was also investigated as a function activator chemistry and PCBA design effects on humidity related reliability. Many solder alloy powders are used in flux formulations, which will

have varying effects on corrosion reliability. Corrosion effects of various solder alloys chemistry was investigated by correlating microstructure, electrochemical behavior, and effects on humidity related reliability aspects. Finally the effect of flux residue on the performance of conformal coating was investigated in detail for 3 different types of conformal coating namely acrylated polyurethane, silicone rubber, and elastomeric acrylate. The focus different investigations carried out in this thesis are the as following:

- **Influence of Ni, Bi, and Sb additives on the microstructure and the corrosion behavior of Sn–Ag–Cu solder alloys**

This work was aim to investigate the influence of the Ni, Sb, and Bi additives on the microstructure and corrosion properties of SAC alloy under DC loading. The ECM susceptibility of SAC alloys were correlated to the micro-galvanic corrosion mechanism by electrochemical methods and microstructural investigations.

- **Alkanolamines as activators in no-clean flux systems: investigation of humidity robustness and solderability**

This work focused on comprehensive understanding of the performance of alkanolamines as potential activators for the flux system with detailed analysis of their behavior under humid conditions using electrochemical methods, while the solderability effect was investigated using wetting force measurements and hot plate spreading tests. Properties of alkanolamines were compared with with typical WOA activators used today.

- **Amino acids as activators for wave solder flux systems: Investigation of solderability and humidity effects**

This work focused on understanding the humidity robustness of four amino acids as flux activators, while the humidity effects and solderability of these activators are compared with commercial WOA flux activators.

- **Comparative study of tripropylamine and naphthylamine as additives in wave solder flux: investigation of solderability and humidity effect**

Tripropylamine and naphthyamine were investigated as representative materials for alkyl-amine and aromatic amine. This study systematically investigated the function of these amine additives in WOA activator based flux formulation under wave soldering condition and the effect of flux residue on humidity robustness of PCBA.

- **Effect of reflow process related flux residue on the climatic reliability of surface-mount electronic devices**

This work investigated the effect of activators in reflow flux paste on humidity related reliability issues. Work focused on the evolution of flux residue under humidity exposure, and how the release of activator can cause reliability issues. The role of flux residue spreading and component stand-off height on the climatic reliability of PCBA were investigated using electrochemical impedance spectroscopy.

- **Influence of no-clean solder flux residue on the corrosion protection of conformal coating used in electronics**

This investigation focused on the effect of the flux residue on the moisture barrier properties and adhesion properties of conformal coating on PCBA surface. Electrochemical impedance spectroscopy and leakage current testing were used to monitor the water interaction on the coatings during climatic exposure in relation with the ECM susceptibility of coated PCBA.

1.3. Structure of the thesis
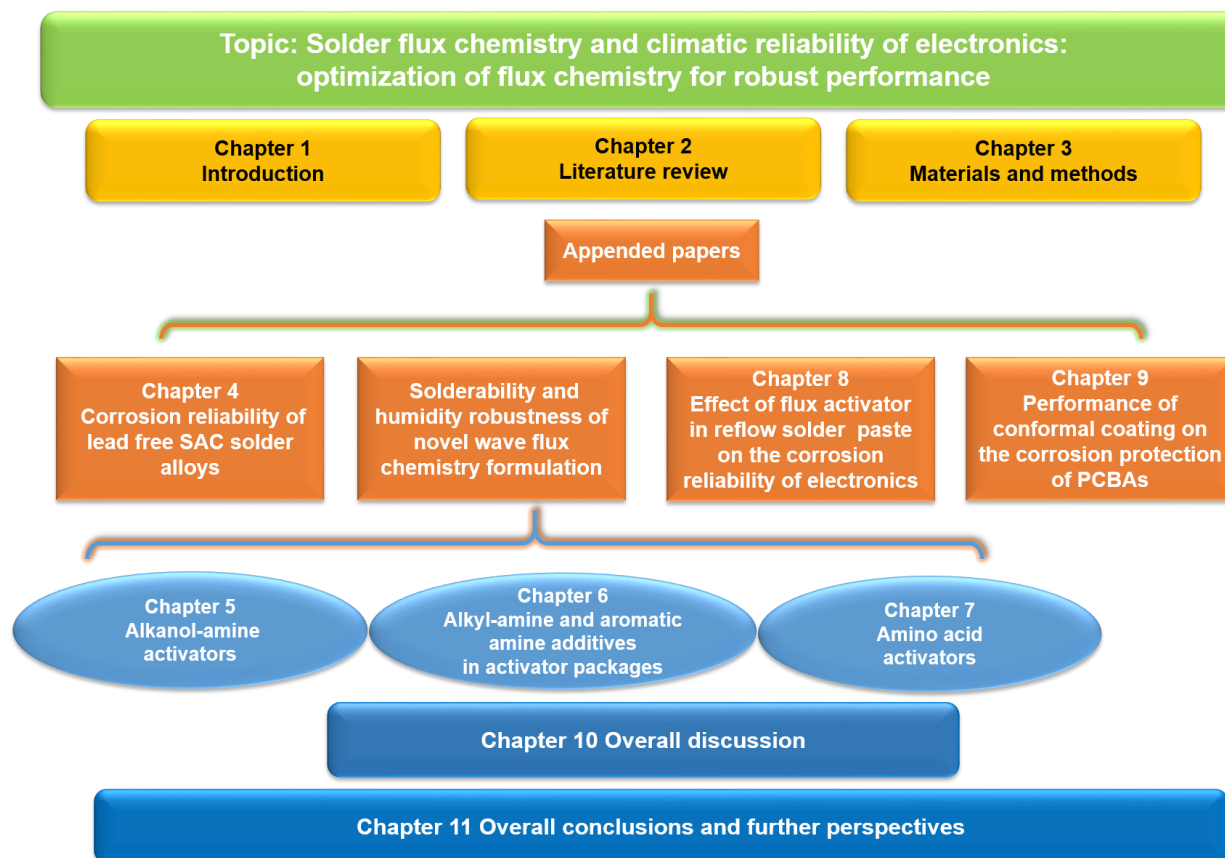
Figure 1.2 Bird view diagram showing structure of the PhD thesis.

Bird view diagram of the PhD thesis is shown in **Figure 1.2**, which consists of 11 chapters. Chapter 1 provides the overall introduction to the topic and scope of the thesis. Chapter 2 provide

detailed background, literature analysis connected to the PhD topic, and discussion of mechanisms related to electrochemical failure modes. Chapter 3 summarizes the materials and experimental used as part of various investigations. Outcome of the research activities are presented as manuscripts published or intended for publication in Journal. Chapter 4-9 cover this. Chapter 4 presents the investigation of the corrosion of solder alloys. Investigation of different flux activators effect on humidity robustness and solderability are presented in Chapter 5-7. Chapter 9 presents the investigation on reflow flux residue and humidity effect, while chapter 10 present the influence of the flux residue on the protection performance of conformal coatings. Finally, chapter 10 provides the overall discussion on the work and chapter 11 demonstrates the conclusions and further perspectives.

2. Literature review

The corrosion reliability of electronics is attributed to the interaction of humidity and other atmospheric contaminants with parts of the devices under application environment. Among various components of environmental conditions, humidity plays a big role as in most cases electronics systems are enclosed, therefore to a large extent filter the particulate contaminations. PCBA is the most important part of an electronic device, and there are several inherent factors of the PCBA will influence humidity related reliability issues. Ionic contamination one of the key dues to its influence on the water fill formation and effects on its electrolytic properties. The contamination such as flux residue with WOA on the PCBA usually is in hygroscopic and ionic nature, which is able to accelerate the water condensation and increasing the corrosivity by dissolution. As result, the corrosion related failure such as electrochemical migration, conductive anodic filament or galvanic corrosion were accelerated on the PCBA under humid conditions.

2.1. Humidity and dew point

Water molecule is a polar molecule and presents as liquid phase under ambient temperature and pressure. It contains two O-H bonds where the angle in between is 140.45°. The oxygen atom in the molecule is electronegative, therefore, the oxygen atom has negative charge and hydrogen atoms possess positive charge. The dipole between hydrogen and oxygen atoms induced attraction is known as hydrogen bond. The strong hydrogen bonds in water molecule provide the cohesion between water, other polar molecules, and surfaces.

Water vapour present in the atmosphere as an important trace component, and the volume fraction in the ambient air is in a range of 0.4 – 1.0%. The concentration of water vapour in the air is called humidity. Absolute humidity (AH) measures the grams of water vapour in dry air, which depends on the temperature as hot air can hold more water. The AH value is the mass of the water vapour (m_{H_2O}) over the total volume of the air and water vapour mixture $(V_{atomsphere})$ as shown in **Equation 2.1**. **Equation 2.2** shows that the relative humidity (RH) is the percentage ratio of partial pressure of the water vapour (p_{H_2O}) to the equilibrium saturated vapour pressure of the water $(p_{equilibrium})$ at a particular temperature. The Mollier diagram is a graphic demonstration of the relative humidity, temperature and the enthalpy as shown in **Figure 2.1**, which shows that the vapour pressure of water in the air depends on temperature with higher temperature can carry more water content. Therefore, saturation level of vapor pressure increases with temperature; hence, vapor pressure corresponds to a particular RH level at low temperature results, lower vapor pressure and RH at high temperature. Curve corresponding to

100% RH is corresponds to the dew point under various temperature, where the air cannot hold more water vapour and hence form liquid water on cooled surface. In the temperature range between - 45°C and 60°C, the dew point can be approximately calculated using Magnus formula (**Equation 2.3**) with an accuracy of ±0.35°C, where T_{dp} is dew point temperature in degree Celsius, T is ambient temperature in degree Celsius, and RH is relative humidity.
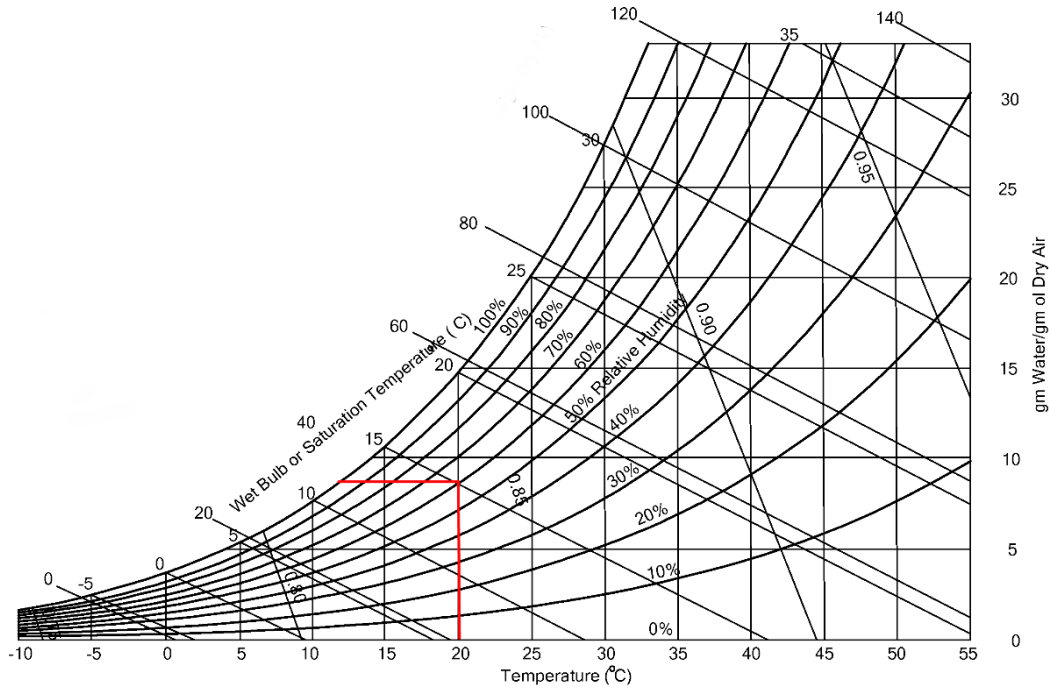
Figure 2.1 *Psychrometric chart (Mollier diagram) at 1 atm total pressure, adapted from [1].*

$$AH = \frac{m_{H_2O}}{V_{atomsphere}} \qquad \textbf{\textit{Equation 2.1}}$$

$$RH = \frac{p_{H_2O}}{p_{equilibrium}} \times 100 \qquad \textbf{\textit{Equation 2.2}}$$

$$T_{\mathrm{dp}} = \frac{243.12(\ln\left(\frac{\mathrm{RH}}{100}\right) + \frac{17.62\mathrm{T}}{243.12+T})}{17.62 - \ln\left(\frac{\mathrm{RH}}{100}\right) - \frac{17.62\mathrm{T}}{243.12+T}} \qquad \textbf{\textit{Equation 2.3}}$$

2.2. Humidity interaction with PCBAs

Figure 2.2 shows various ways of interaction between water vapour and amorphous solid objects includes surface interaction, condensed water, and internalized water, which in total sub-divided into five water-solid interactions modes namely adsorption, deliquescence, capillary condensation, absorption and crystal hydrate formation [2]. Electronic devices consist of PCBAs, coating materials, potting materials, and enclosure with a variety of polymers, metals/alloys, ceramics, and other chemicals [3][4]. Practically, the humidity related failures are related to relative humidity due to the dew point induced water layer formation between electrodes with bias voltage [5]. The

water-solid interaction modes are dependent on the materials, chemicals, design of PCBAs as well as the exposed climate, which may induce parasitic circuit on the surfaces and interfaces once substantial level of water film forms, hence possibly interfere the function of electronic devices [6][5]. Moreover, since many types of metals and alloys, for example: copper, tin, aluminum, silver, nickel, and gold etc., used in the electronics for packaging and functioning perspective, condensation of water triggered the formation corrosion cell on the PCBAs and lead to corrosion related failure of electronics [7][8][9]. Therefore, the understanding of the humidity interaction with different materials and surfaces used for electronics is important.
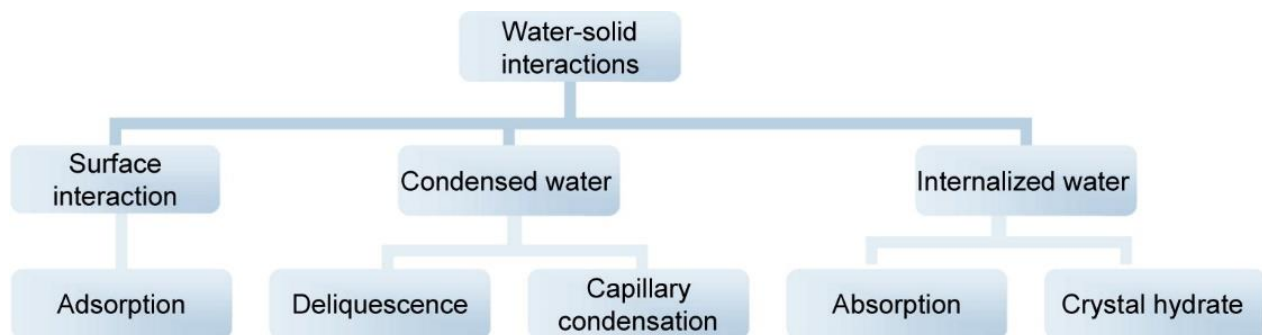
Figure 2.2 Summary chart of water-solid interaction, adapted from [2].

2.2.1. Humidity interaction with clean surface of PCBAs

Water adsorption

The water activity can be expressed as the equilibrium RH of the atmosphere surrounding the solid objects. In practice, the water-solid interactions between humidity and surface of PCBAs include adsorption and water condensation. The water adsorption behavior of PCBAs surface is related to surface energy and water activity, whereas the condensation is related to exposed climate, temperature changes, and hygroscopic nature of the surface.

For the water adsorption, many types of semi-empirical isotherm models were used to estimate the water activity on the solid surface, such as the Brunauer Emmett-Teller (BET) equation, the Guggenheim-Abserson-de Boer (GAB) model, the Halsey model, the Henderson model, the Iglesias-Chirife model, the Langmuir Equation, the Oswin model, , the Peleg model, and the Smith model [10]. Particularly, BET equation is preferred since the fundamental assumption of Langmuir equation do not hold to estimate the first water monolayer adsorption [11][12]. **Figure 2.3** shows the physical model of BET equation (Equation 2.4), where N represents the number of the water manolayers formed on the surface of PCBAs, the RH represents the relative humidity in the scale

of 0-1, E_0 represents the energy of water bounding to the surface, E is the energy of water evaporation [5].
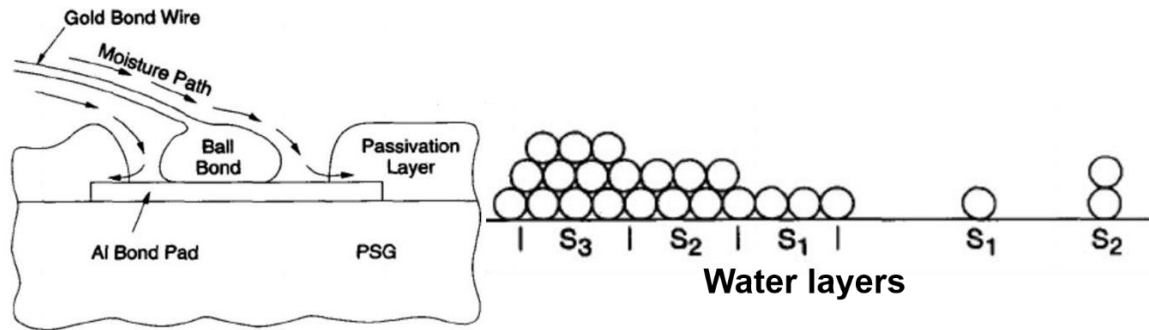
Figure 2.3 *The interference of moisture to the surface of PCBA and BET model of multilayer adsorption, adapted from* [12].

$$N = \frac{(RH)e^{\frac{E_0-E}{kT}}}{(1-RH)[1+(RH)(e^{\frac{E_0-E}{kT}}-1)]} \quad \textbf{\textit{Equation 2.4}}$$

For the laminate polymer materials with moderate surface energy, E is equal to E_0. Therefore, the equation can be expressed to **Equation 2.5**.

$$N = \frac{RH}{1-RH} \quad \textbf{\textit{Equation 2.5}}$$

For the ceramics and metals materials in PCBAs with high surface energy, the E_0 is much larger than E. Therefore, the equation can be simplified to **Equation 2.6**.

$$N = \frac{RH}{1-RH} + 1 \quad \textbf{\textit{Equation 2.6}}$$

Compared to the moderate laminate polymer materials (regular surface), the hydrophilic materials (high energy surface) always adsorb one more layer over the low humidity range before saturation, as shown in **Figure 2.4** [5].
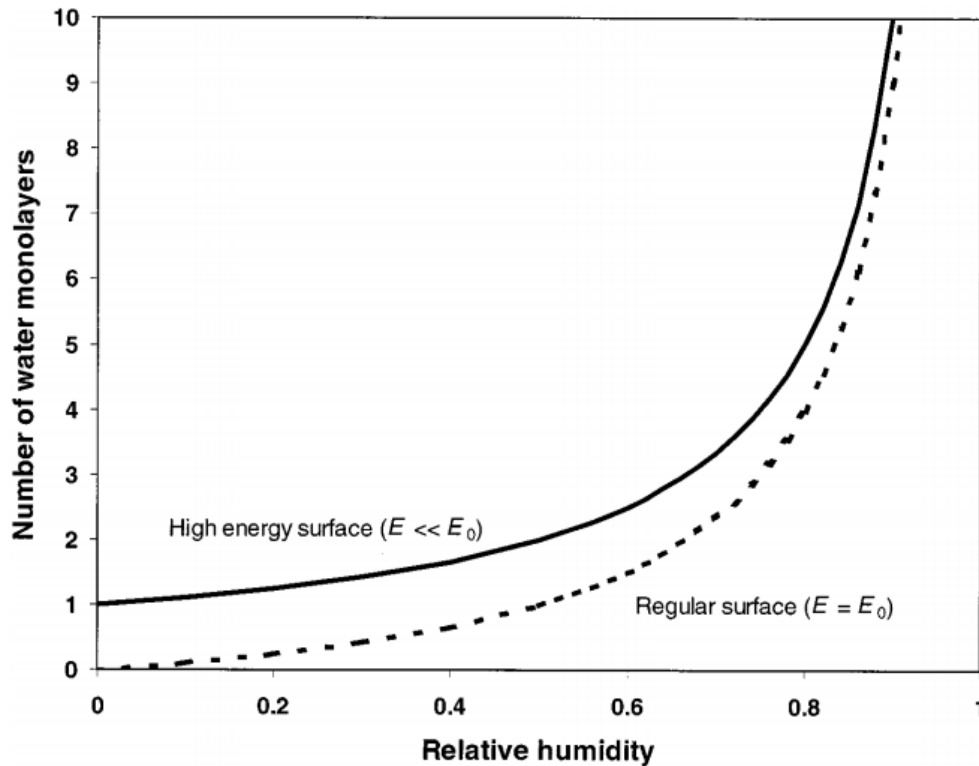
Figure 2.4 *BET equation simulated number of water monolayers as function of relative humidity, adapted from [5].*

Water condensation

At equilibrium RH level, water vapour in atmosphere condenses on cold surface at temperature below the dew point. The water film formation is dependent on the temperature difference between atmosphere and surface of PCBAs [13][14], surface chemistry [15] and surface morphology [15].

Figure 2.5 shows the temperature difference on the PCBA surface with ambient condition is kept at 25°C, while the surface is cooled down below this temperature. Water condensation took place on the surface of PCBAs at 18°C and more pronounced at 17°C under the exposed climate of 25°C, 60% RH. No significant droplet formed at 19°C and 22°C, because the temperature was higher than the dew point corresponding to 25°C, 60% RH. Results agrees with the psychrometric chart shown in **Figure 2.1**, where the humidity levels are 90% RH and 100 % RH at 19°C and 17°C respectively [13]. It is found that the water formed as droplet on the surface of PCBAs, as shown in **Figure 2.5**. The appearance of the water droplets will depend on the wettability on the surface of PCBAs.
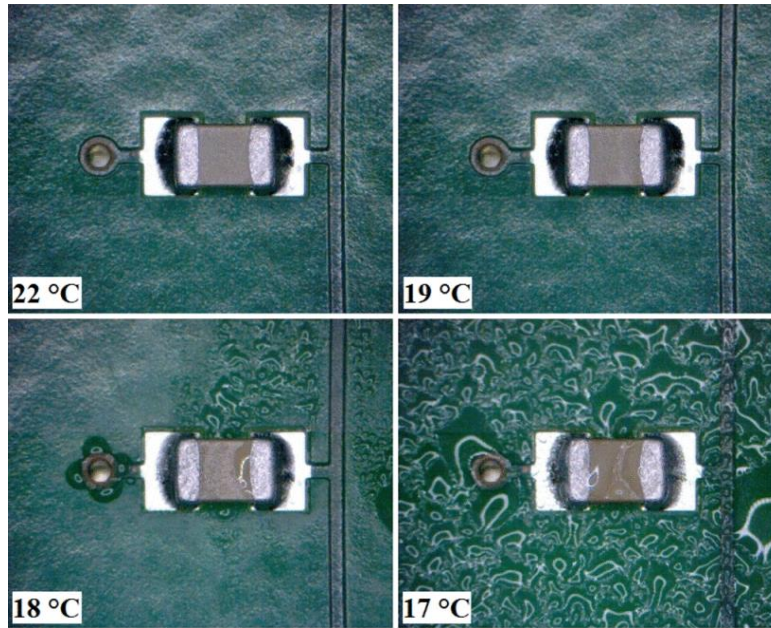
Figure 2.5 *Temperature effect on water condensation of PCBAs, adapted from [13].*

The wettability can be evaluated by measuring the contact angle of water droplet and the solid/liquid interfacial free energy. **Figure 2.6** shows that the contact angle of droplet below 90° means the hydrophilic behavior of the surface and promising wetting, whereas the contact angle of droplet higher than 90° means hydrophobic behavior and poor wettability. The interfacial tension of the liquid and smooth surface of solid can be calculated using Young's equation (**Equation 2.7**), where θ is contact angle, γ_{sv} is the sold surface tension, the γ_{sl} indicates the interfacial tension between solid and liquid, the γ_{lv} indicates the liquid surface tension [16]. Since the liquid is condensed water in all humidity interaction with the surface of PCBAs, the surface of PCBAs is the only thing that affect the appearance of water droplet under the same exposed climate. Due to the fact that the surface roughness is one of the key factors influencing the surface energy, many work was published regarding to the generalization of Young's equation for homogeneous and rough substrate [17][18].

$$\gamma_{sv} = \gamma_{sl} + \gamma_{lv}cos\theta \quad \textbf{\textit{Equation 2.7}}$$
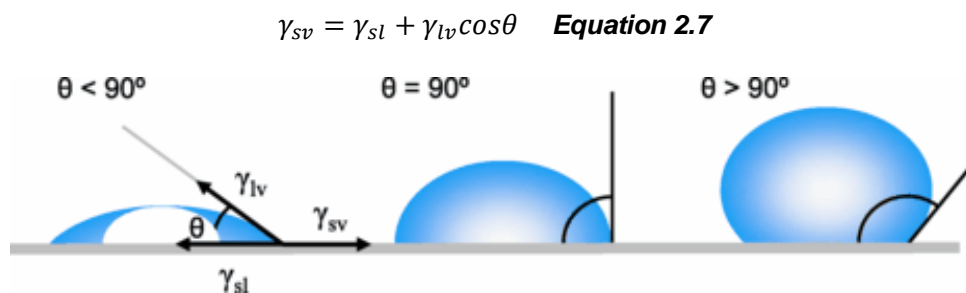
Figure 2.6 *Three types of interfacial tensions between liquid and solid surface, adapted from [16].*

Piotrowska et al. investigated the water layer formation on solder masks with various surface energy [15]. **Figure 2.7** shows the surface energy of solder mask B is much higher (showing lower contact angle) than solder mask C. **Figure 2.8** shows that the surface roughness of solder mask B is higher than solder mask C, however they have the same chemical composition. The water condensation in **Figure 2.9** shows that the water spreading and bridging tendency of solder mask B is much higher than solder mask B under the same climate exposure. Therefore, a smooth surface is preferred to avoid water connection between charged electrodes. On the other hand, the surface energy also influenced by the surface chemistry. The hydrophobic SiO_2 contained solder mask D possessed the lowest surface energy as shown in **Figure 2.7**, even though obtained a high surface roughness as shown in **Figure 2.8**. Small differences in condensation time and water droplet formation without bridging has impact on humidity effects on electronics because the condensation occurs as transient events, therefore only limited amount of water exists for a limited time interval. The leakage current would be small if the interconnection of condensation droplets can be avoided as shown in **Figure 2.9**(d)(e), and hence the humidity robustness of the PCBA can be improved.

Solder mask	Fillers	SM features
A	$BaSO_4$, SiO_2, $Mg_3Si_4O_{10}(OH)_2$, Mg-O-type	- high filler loading - very few surface defects
B	$BaSO_4$, SiO_2	- high filler amount - high amount of surface defects
C	$BaSO_4$, SiO_2	- high amount of fine filler particles and low amount of larger particles - few surface defects
D	SiO_2	- low filler content - few surface defects
E	$BaSO_4$, SiO_2, $Mg_3Si_4O_{10}(OH)_2$	- low amount of fillers - high amount of surface defects

Figure 2.7 Contact angle of water on the surface of solder masks, adapted from [15].
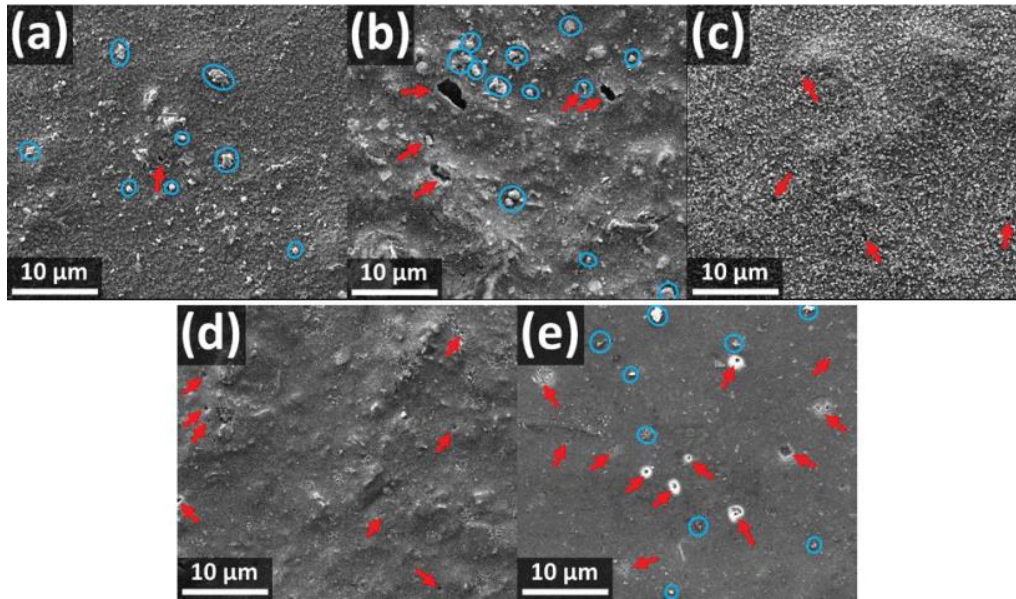
Figure 2.8 Surface morphology of five types of solder masks, adapted from [15].
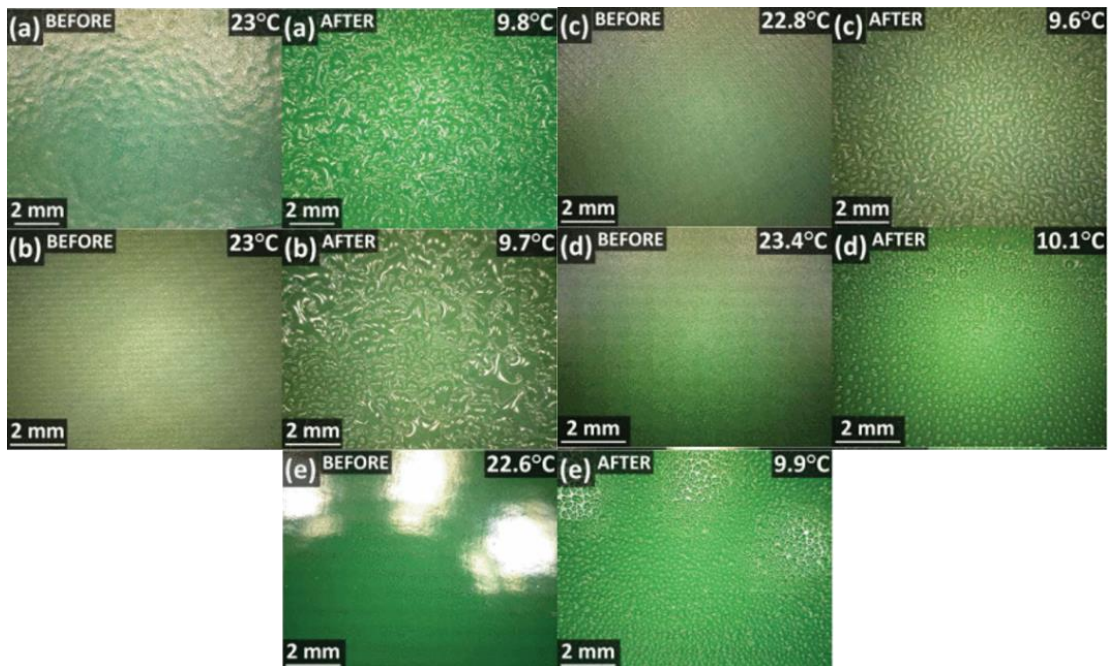
Figure 2.9 Appearance of water condensation on five types of solder masks, adapted from [15].

The surface with high roughness also contains small pores as defects as shown in **Figure 2.8**(b), which accelerate the capillary condensation. Capillary condensation is the water vapour below equilibrium relative humidity adsorbed in the pores of surface due to hydrogen bond interaction of water molecules in atmosphere and the surface of pores, as shown in **Figure 2.10**. The water condensation in porous surface can be expressed using Kelvin-Laplace equation (**Equation 2.8**,

Equation 2.9), where r represents the radius of maximum stably pore, p_l indicates the pressure in the liquid phase, R indicates ideal gas constant, T indicates the temperature in atmosphere. σ_{lg} indicates the interfacial tension between atmosphere and liquid, v_l indicates the molar volume of liquid [19]. The size of the water condensed pore is proportional to the RH level in atmosphere. Therefore, the humidity robustness of PCBAs can be improved by adjusting the surface chemistry and surface morphology.

$$r = \frac{2\sigma_{lg}v_l}{\ln(\text{RH}) \times RT} \propto -\frac{1}{\ln(\text{RH})} \quad \textit{Equation 2.8}$$

$$p_l = -\frac{RT\ln(\text{RH})}{v_l} \propto -\ln(\text{RH}) \quad \textit{Equation 2.9}$$
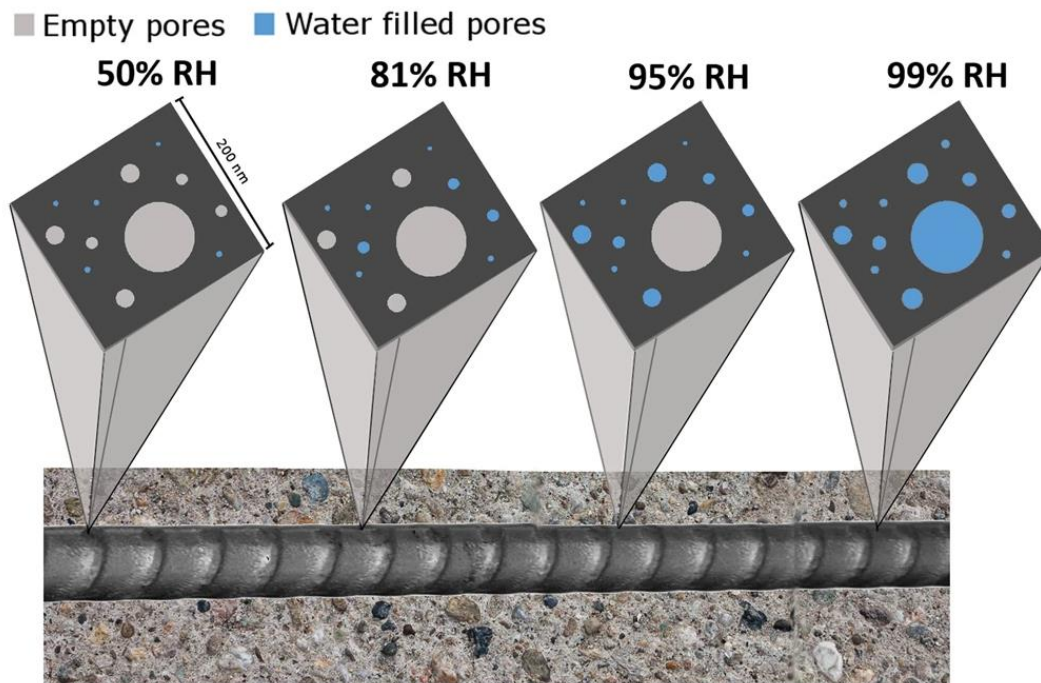
Figure 2.10 Capillary condensation in the pores under various RH value, adapted from [19].

2.2.2. Humidity interaction with contamination on PCBAs

Contamination on PCBAs

Figure 2.11 shows the list of contaminations expected on a PCBA surface from service and manufacturing processes and their origins [20][21]. The contamination from service environment depend on the place of exposure and enclosure design of the device, which determine the openings for the contaminations entered through. The contamination includes ionic airborne particles like salt, dust and dirt [22], sea salt aerosols [23], aggressive gases [21][22]. The

elemental composition of ionic particles usually contains chloride, sodium, sulphur, ammonium, calcium, magnesium etc [24]. Many of those particles are in ionic and hygroscopic nature, which reduce the relative humidity to condensation below equilibrium RH. For instance, the critical relative humidity for sodium chloride and ammonium nitrite is 75% RH and 65% RH respectively, therefore water film can build up above this humidity level due to deliquescence. Aggressive gases include SO_2, NO_x, or H_2S etc [21], which are corrosive to metals or alloys under humid conditions, while they dissolve into the water film forming aggressive acidic species.

```
Contamination
├── Service related contamination
│   ├── Forms corrosion cells / Dissolve residues
│   ├── Particles with aggressive ions e.g. Cl⁻, NH₄⁺, SO₄²⁻
│   ├── Gaseous compounds e.g. SO₂, Cl₂, NOₓ, CO₂
│   └── Hygroscopic residues e.g. salts, dust
└── Process related contamination
    ├── Polymer additives in PCB substrate e.g. curing agent surfactant
    ├── Etching & Plating chemicals e.g. chromic acids, sulfuric acids, florides
    ├── Human handling e.g. chloride, amino acids, oils
    └── Flux compounds e.g. orgainic acids, halide, polyglyclols
```

Figure 2.11 *Types contamination on PCBAs from service conditions and production process, adapted from [20].*

Another contamination source of the PCBA was the manufacturing process, which is most important for humidity related reliability issues of electronics. The contamination may come from

the bare board and component manufacturing, such as flame-proofing additives leach from insulator material [21][22], chemicals from etching and plating process [20][21][22][25], finger oil and salt from handling [26], which could be optimized by robust material selection. Nowadays, the most problematic contamination is the PCBA was from assembling process, which is due to the no-clean flux residue spreading around or trapping beneath the low stand-off height component on the PCBAs[21][20]. No-clean flux has been occupied 70-80% of electronic industry [27][28] due to the elimination of cleaning steps in electronic manufacturing, which aims at controlling the utility of the volatile organic cleaning agents and eliminate the pollutant in water [29]. The no-clean flux residue mainly comes from the liquid wave solder flux and reflow solder flux in the solder paste formulation.

Wave solder flux

No-clean wave solder flux is broadly used in the through-hole electronic manufacturing technique. The flux was applied on the bottom side of the PCBA before going through wave soldering process. During wave soldering process oxidation layer and other contaminant on the metal connections from components and the pads of PCBAs was removed by solder flux [30]. The wave solder flux acts as a media transfer the heat to joint area and properly wet the surface of joint area. During the soldering process, the wave solder flux is able to protect the joint area from re-oxidation, reduce the surface tension, and improve the wetting of melted solder alloy until the solder alloy re-solidifies [31].

Wave solder flux is a combination of solvent (alcohol, esters, water etc.), vehicles (rosin, resin), activators (carboxylic acid, amino acid etc.), surfactant, and other additives (thermal stabilizers, corrosion inhibitors etc.) [31][32]. Solvent in flux acts as a carrier to dissolve and dispense other agents. Activators in flux is to remove oxidation layer of metal. Surfactant is aim to reduce the surface tension and enhance the wetting properties during soldering process [31].

The application of no-clean wave solder flux aims to evaporate or decompose the flux substances at soldering temperature. However, acidic flux residue was also observed on PCBAs as the red colour region using pH indicator gel in **Figure 2.12** [33], and reported aggressive to corrosion of electronics [34]. The acidic flux residue contains one or several weak organic acid (WOA) flux activators, such as adipic acid, succinic acid, glutaric acid etc., which possessed the boiling temperature in arrange from 235 °C-337.5°C [29]. In practice, the soldering temperature is usually set between 230°C and 250°C to avoid the damage of components on PCBA [35][36], which is not able to decompose or evaporate the flux activators [37]. The flux residue on PCBAs was also

effected by the type and amount of flux applied [33], local temperature on PCBAs during soldering [33], soldering environment (eg. N_2, Ar gases) [37], and the configuration of PCBAs (eg. via holes) [33][38]. Therefore, significant amount of WOA residue was detected on the PCBA, which could as high as 687.33 µg/in^2 (106.54 µg/cn^2) [39].
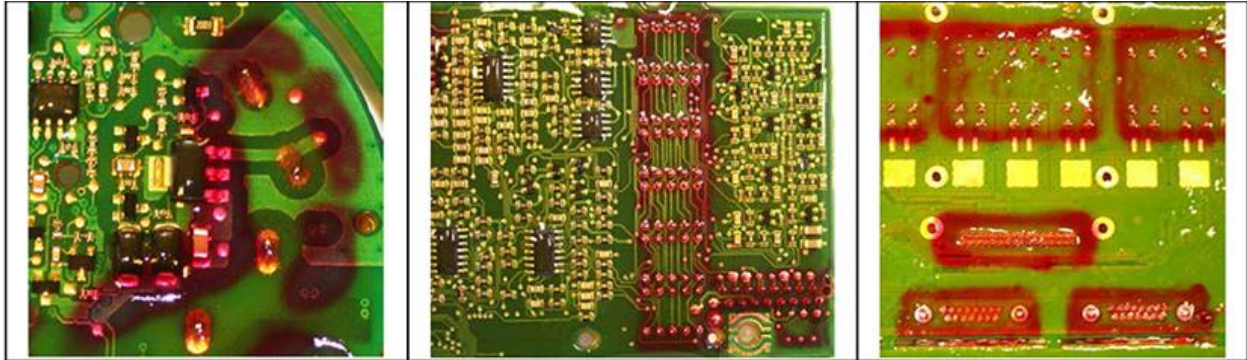
Figure 2.12 *Acid indicator presents in red colour at the region with flux residue on the wave soldered PCBAs, adapted from [33].*

Reflow flux residue

The reflow solder paste is widely used in surface-mount technology, which allows the small components to be directly mounted onto the surface of PCBAs. The reflow solder paste is a blended mixture of solder flux and powders of solder alloys, which contains resins, activators, solvents, rheological additives, and lead-free solder powders [40]. Flux activators used in reflow solder paste include 4 categories, which are organic acids, organic amines, organic halogen compounds, and organic halide salts [40]. Urethane resin, acrylic resin, and styrene-maleic acid resin etc. are the types of the commercial used resin base material for synthetic resin in the reflow flux formulation [41], which can be modified with organic acid such as abietic acid etc. [40] to obtain the function of the conventional natural rosin. During the reflow soldering process, the activator part removes the oxide film on the metal contacts to ensure the solderability of melted solder alloy. After reflow soldering process, the reflow flux residue can be distinguished as spreading around and trapping beneath the components [39][42]. The art of the reflow flux residue is to encapsulate the corrosive flux activator by the film of resin/rosin part.

Humidity interaction with the flux residue

Figure 2.13 shows the water interaction of various WOAs at 80% RH in the reduction temperature from 25℃ to 20℃, where the water condensation is the most pronounced in glutaric acid contaminated surface. Water condensation was also observed on succinic acid contaminated surface, whereas the adipic acid contaminated surface did not show any water droplet. Results

indicates the hygroscopic nature of WOAs flux residue interfere the water interaction with the surface of PCBAs. Therefore, the humidity robustness of PCBAs can be improved by the modification of flux formulation using less hygroscopic WOA flux activator.
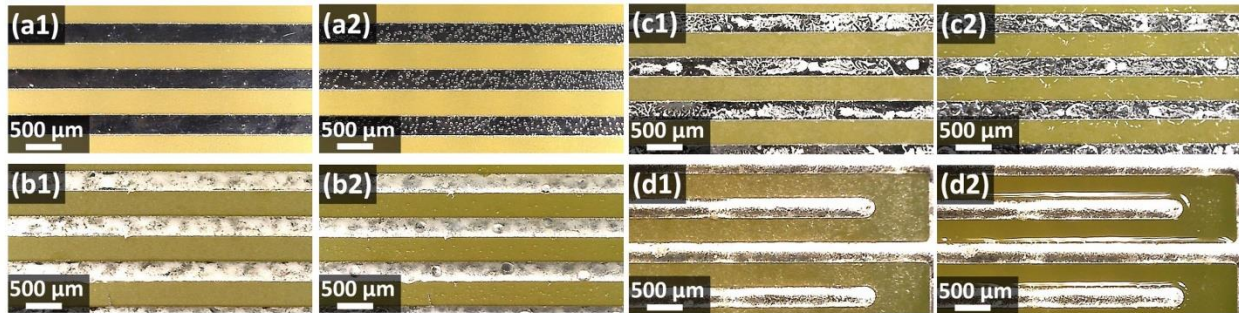
Figure 2.13 *Water condensation on PCB before (1) and after (2) the exposure of 80% RH in the reduction temperature from 25 °C to 20 °C, (a) clean surface, (b) 100 µg/cm^2 adipic acid, (c) 100 µg/cm^2 succinic acid, (d) 100 µg/cm^2 glutaric acid, adapted from [43].*

For the reflow solder flux residue, cracking and opening of film of flux residue was observed after humidity exposure, as shown in **Figure 2.14**. Consequently, the WOA activators in the resin encapsulation released to the surface of PCBA and induce the conductive electrolyte for the corrosion [44].
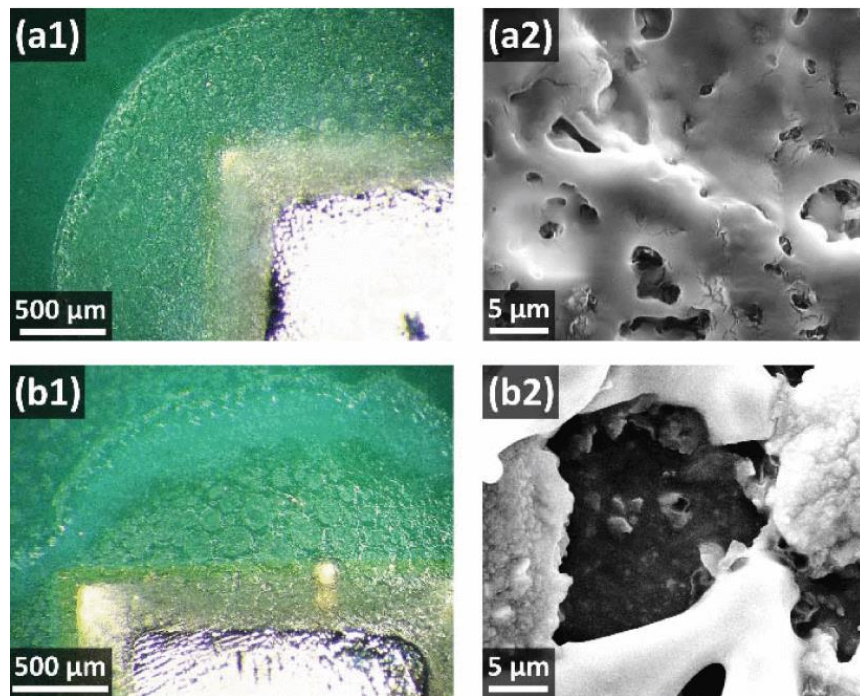
Figure 2.14 *Microscopic inspection on the cracking and opening of reflow flux residue, adapted from [44].*

Deliquescence of the flux residue

The water build up induced by the flux residue on PCBAs is due to deliquescence. Deliquescence indicates the tendency of water adsorption for crystalline substances to form aqueous solution at a relative humidity [2]. Deliquescence of crystalline substances reduced the water vapour pressue for water condensation [2]. The deliquescence interaction is expressed in **Equation 2.10**, where μ indicates the chemical potential for the interaction with humidity, μ_0 indicates the standard chemical potential, p_0 indicates vapour pressure, R represents ideal gas constant, T indicates the temperature in atmosphere [2].

$$\mu = \mu_0 + \text{RT } \ln p_0 \quad \textit{Equation 2.10}$$

The difference of chemical potential can be expressed by **Equation 2.11**, where μ_s indicates the chemical potential of solid in saturated aqueous solution, μ indicates the chemical potential of solid in water, p_s indicates vapour pressure for saturated aqueous solution, p_0 indicates vapour pressure for water. **Figure 2.15** shows the deliquescence process, where the water adsorption of the solid started in the ambient relative humidity (RH$_i$) below equilibrium relative humidity (RH$_0$), the surface of solid dissolved in to water layer and form saturated solution, the exposed solid attracted more moisture until the solid substances completely dissolved. The chemical potential of solid in water and solid in saturated aqueous solution are different.

$$\mu_s - \mu = \text{RT } \ln(p_s/p_0) \quad \textit{Equation 2.11}$$
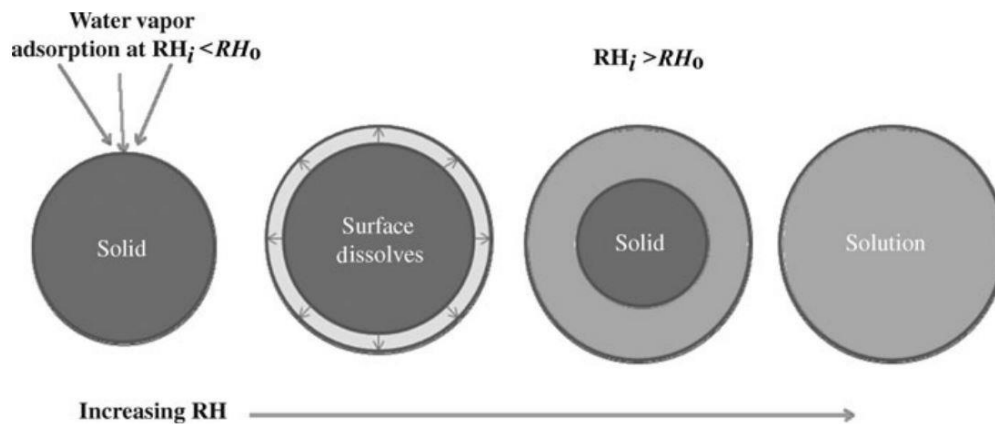
Figure 2.15 Schematic of deliquescence process for water-solid interaction, adapted from [2].

The deliquescence relative humidity of the WOAs used in no-clean flux activators for PCBA manufacturing were summarized in **Table 2.1**. The deliquescence point of WOA flux activators used in PCBA were in a range from 65-99% RH. Practically, the glutaric acid and DL-malic acid

bring the water condensation level to 78-85% RH under 25°C. However, the water condensation only occurred at 99% RH for adipic acid and succinic acid contained flux activator at 25°C. The water solubility of WOA flux activators exhibited in a range from 0.007 g/kg to 1440 g/kg, which depend upon the polarity of the molecule. Finally, the flux residue on PCBA reduced the RH level for water condensation and dissolved in the water, which formed a corrosive and conductive electrolyte layer on PCBA.

Table 2.1 The deliquescence relative humidity of commercial WOA flux activator in PCBA was summarized by Ambat et al. [21][45][46][47][48][49][50][51][52][53][54]

WOA activators	Deliquescence RH(%) at 25°C	Solubility in water (g/kg H_2O) / temperature
WOA flux activators		
Adipic acid	99.6, ≥ 99	15 / 15°C
Succinic acid	98, > 94, 98.8, ≥ 98	83.5 / 25°C
Glutaric acid	84, 83.5-85, 88-88.5, 89-99, 85±5	1400 / 25°C
DL-malic acid	86, 78	1440 / 26°C
Oxalic acid	97.3	95.2 / 20°C
Maleic acid	83±5	789 / 25°C
Malonic acid	65.2	736 / 20°C
Citric acid	79	1440 / 20°C
Suberic acid	≥90	2.43 / 25°C
Palmitic acid		0.007 / 20°C
Abietic acid		

2.3. Corrosion failures in PCBA

Corrosion is an electrochemical process, which degrade the metal or alloys into metal oxides, metal hydroxides or salts with a more chemical stable form. In electronics, WOA activator residue on PCBA promoted the water condensation due to deliquescence, which induced the corrosion cell formation on the PCBA surface. In consequence, different types of corrosion phenomena was identified on the PCBAs.

2.3.1. Galvanic corrosion

Galvanic corrosion is an electrochemical process occurred in a corrosion cell with electrolyte and two or several types of metals. The metal with higher electropotential acts as anodic material, while the metal with lower electropotential acts as cathodic material. The difference of the electropotential between anodic material and cathodic materials is the driving force for the corrosion of anodic material, whereas the cathodic material was protected during the process.

Galvanic corrosion is a typical form of corrosion found in electronic devices due to a variety of metal or alloys such as Cu, Sn, Ag, Ni, Au, Al etc. used in PCBA under water condensation or harsh climatic exposure [55]. The galvanic corrosion usually occurred at electrical contacts or the

multiple metal layer deposited region. Galvanic corrosion in wire bonding depends on the electropotential difference of Al-Au and Al-Ag couples [56]. The galvanic corrosion on the PCB with surface finish of electroless nickel/immersion gold (ENIG) depends on the types of defects. For example, galvanic corrosion of Ni was inspected when coupled Au, which is due to the defect or porosity of the Au layer on the surface [57][58]. However, when the defect presented on the whole ENIG layer, the galvanic corrosion occurred on the anodic Cu [59]. The galvanic couple also can be intermetallic compounds (IMCs) and metal, for example, the anodic Cu_9Al_4 or CuAl IMCs and cathodic Cu detected in the Cu-Al wire bonding [60]. Galvanic corrosion also occurred in the SAC solder alloys, which consist of various types of IMC phases.

SAC solder alloy and micro-galvanic corrosion

After the implementation of RoHS and WEEE legislations, SAC solder alloys became the most prominent replacement of Pb-Sn solder alloy for PCBA manufacturing due to their near eutectic composition, relative low melting temperature, and promising mechanical properties etc. [61][62]. The ternary phase diagram of SAC alloy was demonstrated in **Figure 2.16**, where the micro-constituents in the SAC alloy include pure β-Sn phase, Ag_3Sn and Cu_6Sn_5 IMCs. Moon et al. simulated the eutectic composition of SAC alloy contained 3.5 ± 0.3 wt.% Ag and 0.9 ± 0.2 wt.% Cu, which provides the eutectic melting temperature at 217.2 ± 0.2°C [63]. The simulated eutectic composition result was close to the composition of the commercialized SAC alloys such as Sn-3Ag-0.5Cu (SAC 305) in Japan, Sn-3.8Ag-0.7Cu (SAC 387) in EU and Sn-3.9Ag-0.6Cu (SAC 396) in USA [64].
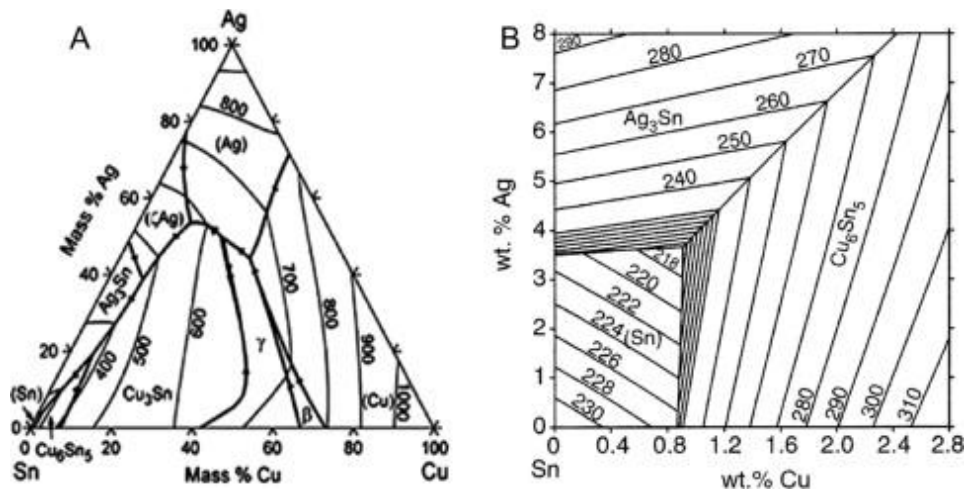
Figure 2.16 Ternary phase diagram of SAC alloy, adapted from [61].

Figure 2.17 shows the poor mechanical shock performance of SAC alloys was attributed to the formation of brittle Cu_3Sn IMC and Kirkendall voids at the interface between solder joints and Cu trace on the PCBA [65]. Consequently, additive element with various elemental composition has been used to improve the mechanical properties of SAC alloys. Ni was used as substitutional element of Cu in the SAC alloy in order to prohibit the growth of Cu_3Sn and void formation [66]. Another solution to enhance the mechanical shock resistance of PCBA is using low Ag content solder alloys [67]; however, the thermal fatigue resistance of low Ag content solder alloy was not reliable [68]. Therefore, the third generation of solder alloys with Bi and Sb additives were developed in order to cope with reliability of thermal cycling by introducing the solid solution and toughening effect [67]. However, the additive in SAC alloy may form new IMCs with different electropotential, which may influence the galvanic couplings and the corrosion properties in novel SAC alloys.
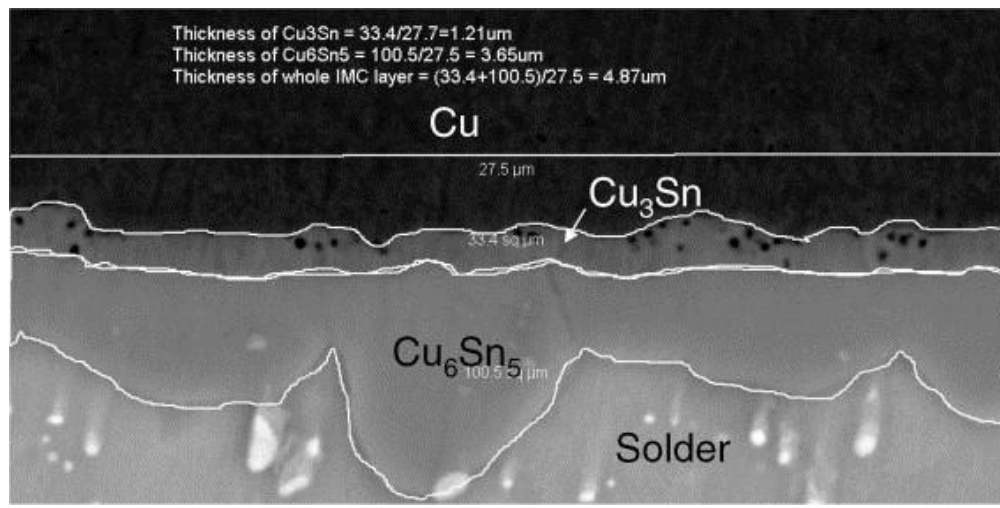
Figure 2.17 Cu_3Sn IMC and kirkendall voids formation after aging at 150°C for 100h, adapted from [65].

The corrosion behavior of SAC solder alloys was influenced by the microstructure of the solder alloy. In SAC 305 alloy, microgalvanic couple formed by anodic β-Sn phase and cathodic Ag_3Sn IMCs [69]. The corrosion performance of SAC solder alloy was influenced size and distribution of Ag_3Sn IMCs, which were controlled by adjusting cooling condition [69][70] or aging period [71]. Experiment design in the investigation mainly focused on two aspects. One aspect was to investigate the solder bulk alloy using electrochemical methods, such as electrochemical impedance spectroscopy (EIS) and potentiodynamic polarization [70] [71]. The limit of the electrochemical methods was developed for the conventional structural materials. Investigations reported the corrosion behavior by evaluating the passivation domain [72] and passivation current

density [73] etc.; however, the service condition with bias loading significantly influenced the corrosion behavior of solder alloy under humid conditions due to the breakdown of the passivation layer at high bias voltage. Therefore, another aspect for solder alloy investigation was to introduce bias voltage loading during the test, which includes thin electrolyte layer (TEL) test [74], water droplet (WD) test [75], and thermal humidity bias (THB) test using industrialized testing standard such as IEC 60068-2-14/IEC 60068-2-30 for environmental testing [76], and IPC-TM-650 2.6.3.7/IPC-TM-650 2.6.3.3 for assessing SIR and ECM performance [77][78]. The previous investigations suggested that better corrosion resistance was obtained by the solder alloys with fine and homogeneously distributed IMCs [71][79].

2.3.2. Electrolytic corrosion

Reduction of SIR and electrochemical migration

Surface insulation resistance (SIR) test is an IPC standard test designed for quantifying the deleterious effect of fabrication, process or handing residues of PCBAs under humidity conditions [80]. SIR comb pattern (test vehicle) is tested at high humidity under bias voltage loading in order to simultaneously assess leakage current induced by ionized water films, corrosion and electrochemical degradation.

The conductance of SIR is denoted as G_{SIR}, which can be expressed by **Equation 2.12** [81]:

$$G_{SIR} = \sigma t \qquad \textit{Equation 2.12}$$

Where σ indicates the conductivity of electrolyte layer, t indicates the thickness of electrolyte. The resistance of SIR comb pattern can be derived as $R_{SIR} = \frac{1}{\sigma t}$. However, the conductivity of water is very low and the thickness of water on the surface of test vehicle is 8-10 monolayers [82]. Therefore, the effect of humidity on the clean SIR comb pattern is negligible.

The key factor of the reduction of SIR is the deliquescence and solubility of WOA residue on the PCBA. According to **Table 2.1**, deliquescence occurred DL-malic acid at 75-84% RH under 25°C, whereas the deliquescence for adpic acid occurred over 98% RH. The deliquescence result of two WOAs agreed with the SIR testing results in **Table 2.2** for the SIR of adipic acid and DL-malic acid under various RH level and contamination level. The drop of SIR is obtained at 80% RH for DL-malic acid and 98 for adipic acid [83].

Table 2.2 SIR response on the adipic acid and DL-malic contaminated test SIR pattern under various RH value at 25˚C with 5 V direct current (DC) loading, adapted from [83].

Adipic acid			
Humidity	SIR (MΩ) 25μg/cm2	SIR (MΩ) 50μg/cm2	SIR (MΩ) 75μg/cm2
60% RH	5209.29	3090.50	2798.48
70% RH	4945.24	2157.70	1665.36
80% RH	2865.82	1204.58	922.45
90% RH	504.23	494.56	449.64
95% RH	209.69	263.49	293.21
98% RH	157.32	133.65	194.91
99% RH	102.78	45.73	23.79
DL-malic acid			
Humidity	SIR (MΩ) 25μg/cm2	SIR (MΩ) 50μg/cm2	SIR (MΩ) 75μg/cm2
60% RH	2902.40	1634.53	602.40
70% RH	2587.40	303.69	39.93
80% RH	2071.03	21.12	3.18
90% RH	781.92	1.58	0.42
95% RH	151.02	0.65	0.32
98% RH	30.83	0.55	0.32
99% RH	6.62	0.52	0.28

The DL-malic acid contaminated SIR pattern shows higher leakage current and form lower SIR than adipic acid contaminated SIR pattern, as shown in **Figure 2.18**(a)(b). The higher leakage current caused short circuit failure is ECM, as shown in **Figure 2.18**(c)(d). The anodic material dissolves in to electrolyte and migrates toward the cathode and deposit as a metal-hydroxide. The metal hydroxide grows back to anode as dendrite, which can reduce the gap size or bridge two biased electrodes. The actual reactions in the electrochemical cell depend on the local pH, as shown in **Figure 2.19**. The localized pH shows red colour at cathode is alkaline, whereas the pH shows purple colour at anode is acidic.
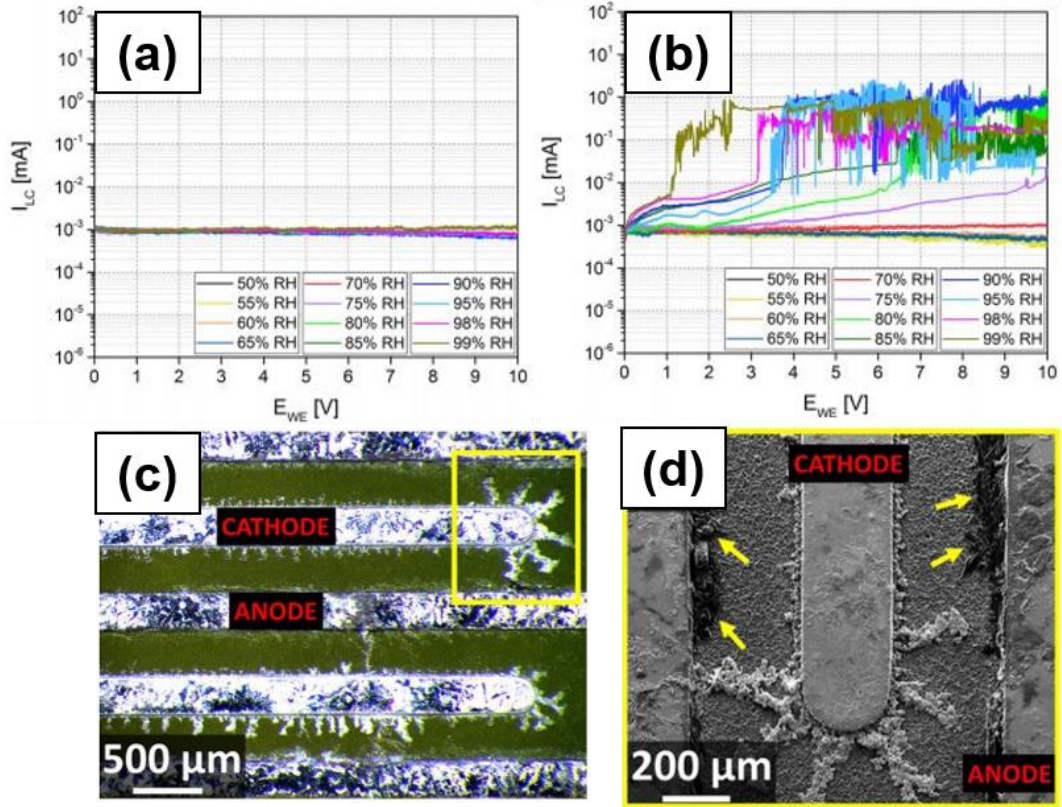
Figure 2.18 *Leakage current of SIR test vehicle with 100 µg/cm2 of (a) adipic acid, (b) DL-malic acid, (c) LOM image of ECM dendrite, (d) SEM image of ECM dendrite, adapted from* [84].
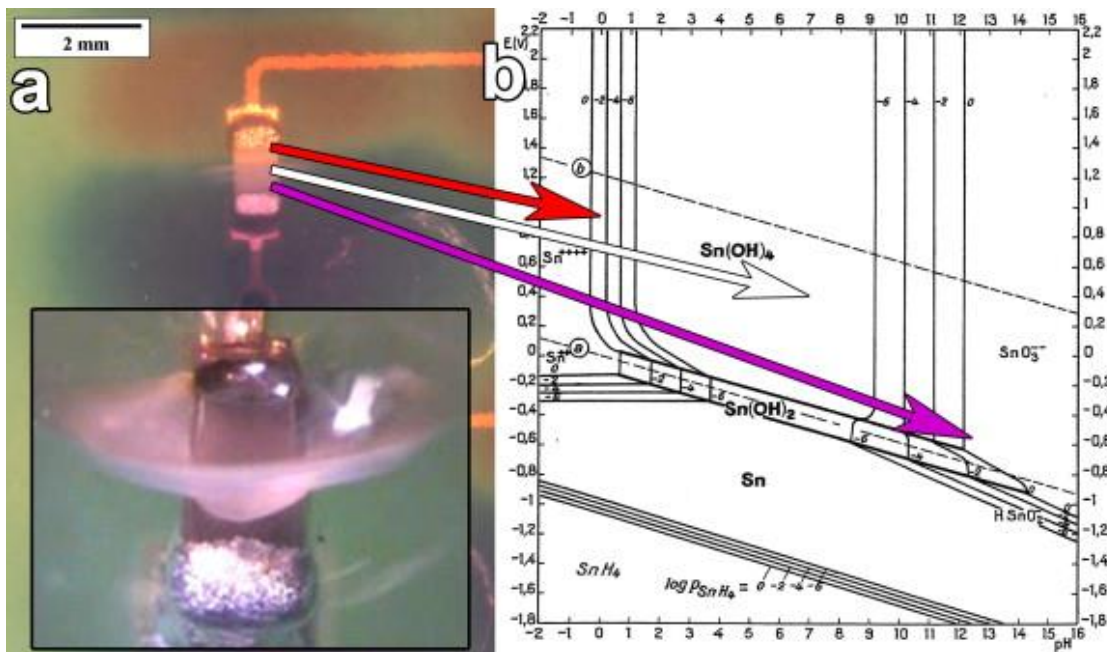
Figure 2.19 *(a) Detection of localized pH, (b) Pourbaix diagram of Tin, adapted from* [85].

The anodic reactions for Sn in the electrolyte (pH = 6.7) can be expressed as **Equation 2.13-2.15** [74]:

$$Sn \rightarrow Sn^{2+} + 2e^- \quad \textbf{\textit{Equation 2.13}}$$

$$Sn \rightarrow Sn^{4+} + 4e^- \quad \textbf{\textit{Equation 2.14}}$$

$$2H_2O \rightarrow O_2 + 4H^+ + 4e^- \quad \textbf{\textit{Equation 2.15}}$$
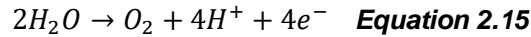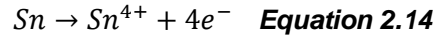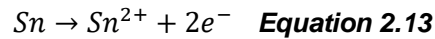
Both of the stannic ions and stannous ions present in the low pH electrolyte, and the oxidation of stannic ions could take place due to the high potential induced by the DC loading. The oxygen evolution may take place as well due to the dissociation of water [85]. Therefore, the local acid environment at anode is due to formation of H^+ at anode with the reactions as **Equation 2.16-2.17** [74]:

$$Sn^{4+} + 4H_2O \rightarrow Sn(OH)_4 + 4H^+ \quad \textbf{\textit{Equation 2.16}}$$

$$Sn + 4H_2O \rightarrow Sn(OH)_4 + 4H^+ + 4e^- \quad \textbf{\textit{Equation 2.17}}$$
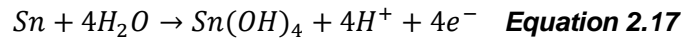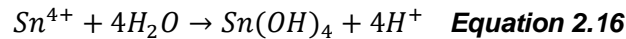
The cathodic reactions can be expressed as **Equation 2.18-2.19** [85]:

$$O_2 + 2H_2O + 4e^- \rightarrow 4OH^- \quad \textbf{\textit{Equation 2.18}}$$

$$2H_2O + 2e^- \rightarrow H_2 \uparrow + 2OH^- \quad \textbf{\textit{Equation 2.19}}$$
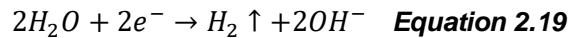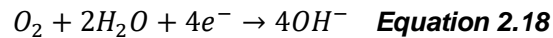
Additionally, the migration of stannic ions, stannous ions, hydroxide ions, and hydrogen ions take place in the electrolyte due to the electric filed. During the ion migration, precipitation of $Sn(OH)_4$ formed. At cathode, the localized alkaline condition could dissolve $Sn(OH)_4$ to $Sn(OH)_6{}^{2-}$, the negative charge of $Sn(OH)_6{}^{2-}$ migrate toward anode and react with H^+ in the gap to form $Sn(OH)_4$ again until bridge the two electrodes [74]. ECM was found not only in DC biased PCBAs, but also in AC biased PCBAs [86].

Degradation of laminate and conductive anodic filament formation

The Sn-Pb alloy was phased out due to toxicity according to RoHS legislation. Sn-Ag-Cu (SAC) solder alloy was utilized as alternative in electronic packaging. The highest peak temperature for Sn63Pb37 solder alloy and SAC 305 alloy are 215°C and 250°C respectively [36]. The peak soldering temperature of SAC 305 significantly exceeds the glass transition temperature of FR-4 (200°C) and interferes the cross-linking of epoxy in FR-4 due to extra thermal exposure. Therefore, the humidity absorption was detected in the PCBAs using SAC alloys [87][88][89].

The absorption of water in FR-4 laminate is by water diffusion in thermal interfered epoxy bulk. The driving force of diffusion is concentration gradient. The one dimension water diffusion can be expressed using Fickian diffusion equation (**Equation 2.20**) [87], where M_t indicate the moisture content at time t in the object, M_∞ indicates the equilibrium moisture content of object, l indicates the thickness of the object along the diffusion dimension, D represents diffusion coefficient. The effect of temperature to diffusion coefficient D can be expressed by Arrhenius equation (**Equation 2.21**) [90], where D_0 indicates Arrhenius constant for moisture diffusivity, E_d indicates activation energy of moisture diffusivity, k indicates Boltzmann's constant, T indicates temperature.

$$\frac{M_t}{M_\infty} = 1 - \sum_{n=0}^{\infty} \frac{8}{(2n+1)^2\pi^2} \exp\left(\frac{-D(2n+1)^2\pi^2 t}{4l^2}\right) \quad \textit{Equation 2.20}$$

$$D = D_0^{E_d kT} \quad \textit{Equation 2.21}$$

Many types of failures were reported according to humidity absorption in FR-4 substrate, as shown in **Figure 2.20**. For example, the water content in laminate reduces of the dielectric constant [90][91], exacerbates the polymer degradation and delamination of FR-4 substrate (**Figure 2.20**(a)) [88][92], induces differential swelling and hygroscopic stress [90], induces interface crack (popcorn cracking) under thermal stress (**Figure 2.20**(b)) [90][93][94], triggers corrosion of Cu layer [90] [95].
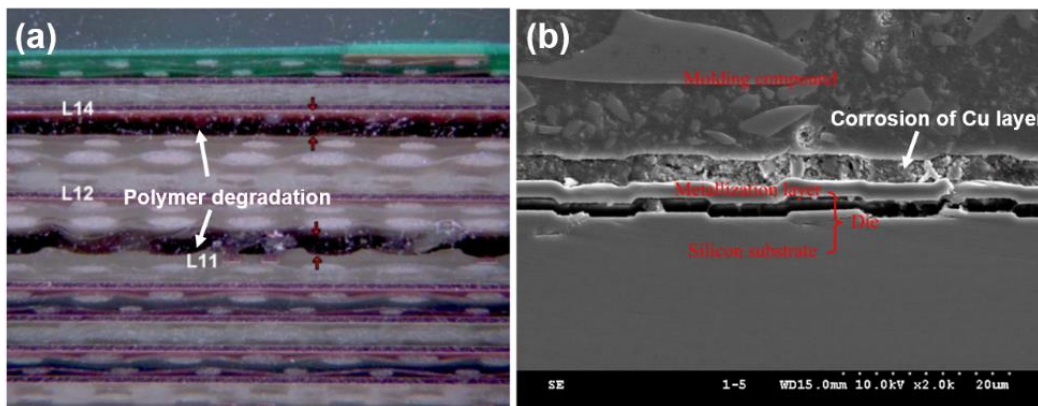
Figure 2.20 Moisture induced failure in FR-4 laminate: (a) polymer degradation, adapted from [96]*; (b) popcorn crack at polymer-metal interface, adapted from* [95].

Conductive anodic filament (CAF) is another humidity induced failure mode under DC bias voltage loading. As the humidity interaction with laminate discussed in the previous section, the delamination of substrate materials takes place under humidity exposure, which is the first stage of the CAF failure. Then, two oppositely biased copper tracks are connected by the water content

at the delaminated interface [97]. The CAF dendrite is anodic corrosion product, which grows from anodic copper track to cathodic copper track, as shown in **Figure 2.21**. The CAF failure mode is only seen in DC bias loaded PCBAs rather than alternating current (AC) bias loaded PCBAs [97]. The water soluble flux residue, mechanical stress, processing temperature, accelerated aging temperature, humidity, and the close spacing used in the configuration design of PCBAs could accelerate the CAF formation [98][99].
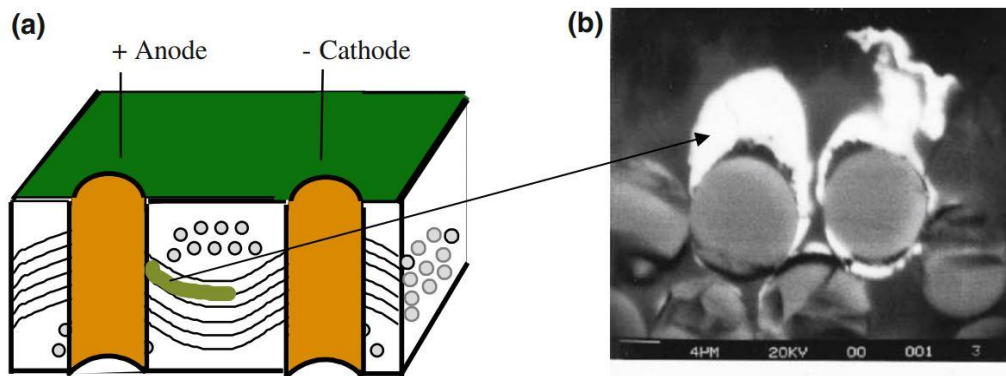
Figure 2.21 (a) Schematic of CAF formation, and (b) cross-section view of CAF failure in laminate, adapted from [100]*.*

The anodic reaction can be expressed in **Equation 2.22-2.23**, where the dissolution of Cu and electrolysis of water took place. Cu ions formed copper compounds at anode, which was pushed from anode to cathode.

$$Cu \rightarrow Cu^{n+} + ne^- \quad \textbf{\textit{Equation 2.22}}$$

$$2H_2O \rightarrow O_2 + 4H^+ + 4e^- \quad \textbf{\textit{Equation 2.23}}$$
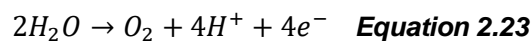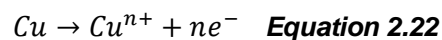
The cathodic reaction can be expressed in **Equation 2.24**, where the hydrogen gas and hydroxide ions formed as the reduction products.

$$2H_2O + 2e^- \rightarrow H_2 \uparrow + 2OH^- \quad \textbf{\textit{Equation 2.24}}$$
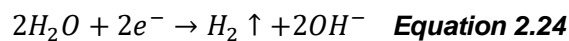
The mean time to failure (MTTF) indicate the average amount of time for a non-repairable device operate before it fails. The MTTF of CAF can be expressed by **Equation 2.25**, where C indicates the pre-exponential humidity factor, k is the Boltzman constant, T is the temperature in Kelvin, E_a indicates the activation energy of the laminate, L indicates the spacing of oppositely biased Cu track, V is the applied DC voltage [99]:

$$MTTF = C^{\frac{E_a}{kT}} + 3.84 \times 10^7 \frac{L^4}{V^2} \quad \textbf{\textit{Equation 2.25}}$$

2.4. Method of corrosion control for PCBAs

2.4.1. New flux activators with better corrosion properties

The corrosion failure of the electronics was attributed to the water condensation on the PCBA, which accelerated by the hygroscopic WOA in the flux residue. Therefore, developing new flux activators with good humidity robustness, while possessing good solderability is important. Some of the prospective organic molecules from this point of view are reviewed below, some of which are used for investigating in this thesis.

Organic amine activators

Organic amine is a Brønsted-Lowry base (accepting hydrogen from acid) and Lewis base (donate electrons for redox reaction). The copper oxide can be removed by amine under heat conditions by redox reaction, which can be expressed as **Equation 2.26-2.27**, where R represents organic radical group.

$$3CuO + 2R''NH_2 \xrightarrow{\Delta} 2Cu + R_2O + N_2 + H_2O \quad \textit{Equation 2.26}$$

$$3Cu_2O + 2RNH_2 \xrightarrow{\Delta} 6Cu + N_2 + R_2O + 2H_2O \quad \textit{Equation 2.27}$$
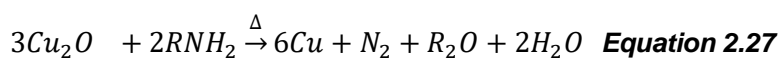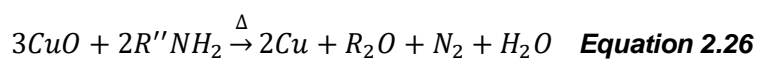
Shi et al. reported the attempt by using anonymous amines as activators, and obtained good wetting properties as shown in **Figure 2.22** [101]. The chemical reaction and by product can be variant due to the different reaction conditions such as temperature and solvent media. Cu ions are possible to form stable copper complex ligand or amine salt with amines as shown in **Figure 2.23**.
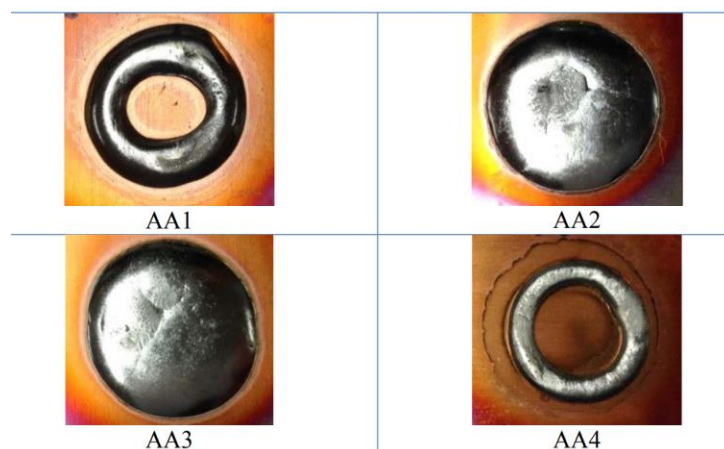
Figure 2.22 Hot plate spreading testing result of anonymous amines used as flux activators, adapted from [101].

Generally, organic amines are classified as primary amines, secondary amines and tertiary amines depending on the number of H replacement with hydrocarbyl groups. The strength of the redox activity of amine depend on the activity of the lone pair in amine group. Primary amine is a stronger base than ammonia due to the long pair in amine is pushed by the alkyl group. The aromatic amines are less basic due to the attraction of long pair from covalent π bond. The general properties of amines include [102]:

- Lone pairs of amine group is able to form hydrogen bond with water (good solubility).
- Primary and secondary amine can form hydrogen bond with themselves and other amines, which provide a higher boiling point.
- Volatile amines have strong odors.
- Smaller amines are toxic by ingestion, irritating to skin and eyes.
- The reaction with water is a protonation process, and also be able to react with acid.
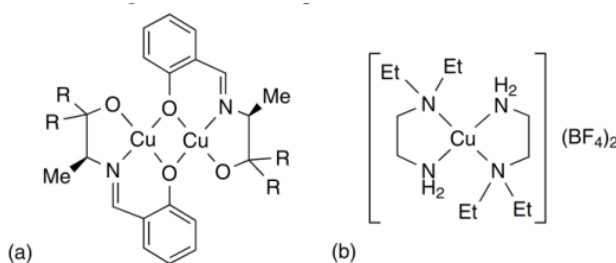
Figure 2.23 *Example of the ligand formation between copper and amines, adapted from [101].*

The screening amine candidates should follow:

- Strong lone pair in the amine group.
- Possible to form bidentate ligands with Cu or Cu ions.
- The functioning temperature and boiling is close to 250 - 255 °C (soldering temperature for WOA activators [103])
- Halogen, halide free

Blend WOA-amine activators

Amines are used in the WOA activator based flux chemistry as additives or activator to inhibit the corrosion and ECM [104]. The mixture of amines and WOAs as activator in the flux formulation is aiming to form neutralized amide by acid and base reaction. While under soldering condition, amide is expected to degrade into WOA ($RCOOH$) and amine (MNH_2HX), and hence to remove the oxides layer of metal surface independently [105]. The activators were expected to form amide

again after the soldering process to provide less hygroscopic behavior. The possible reactions can be expressed by **Equation 2.28-2.31** [105], where R and M represent organic radical group, Me represents metal :

$$RCOOH : MNH_2HX \rightarrow ROOH + MNH_2HX \quad \textbf{\textit{Equation 2.28}}$$

$$RCOOH \rightarrow ROO^- + H^+ \quad \textbf{\textit{Equation 2.29}}$$

$$MeO + 2H^+ \rightarrow H_2O + Me^{2+} \quad \textbf{\textit{Equation 2.30}}$$

$$2MNH_2HX + MeO \rightarrow MNH_2 + MeX_2 + H_2O \quad \textbf{\textit{Equation 2.31}}$$
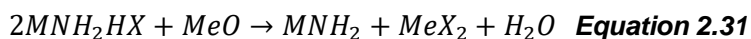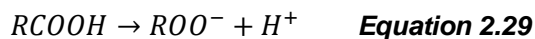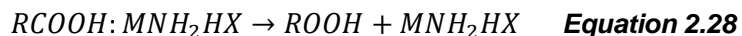
Standardized SIR test [106] and ECM test [104] were used to evaluate the humidity robustness of blend WOA-amine activators. **Figure 2.24** shows the SIR result of blend WOA-amine activator passed the threshold value of 100 MΩ for 3 types of testing kits after simulated soldering condition without cleaning. And ECM test in **Figure 2.25** did not show any dendrite formation on blend WOA-amine activator contaminated SIR pattern [104]. The corrosion performance of blend WOA-amine activator package was evaluated using standardized Cu mirror test [105]. No green/blue corrosion product was formed after test using blend WOA-amine activator contained flux (**Figure 2.26**(a)) in comparison with the pure WOA contained flux (**Figure 2.26**(b)). Therefore, blend WOA-amine can be a suitable flux activator to obtain good wetting properties, corrosion performance and humidity robustness.
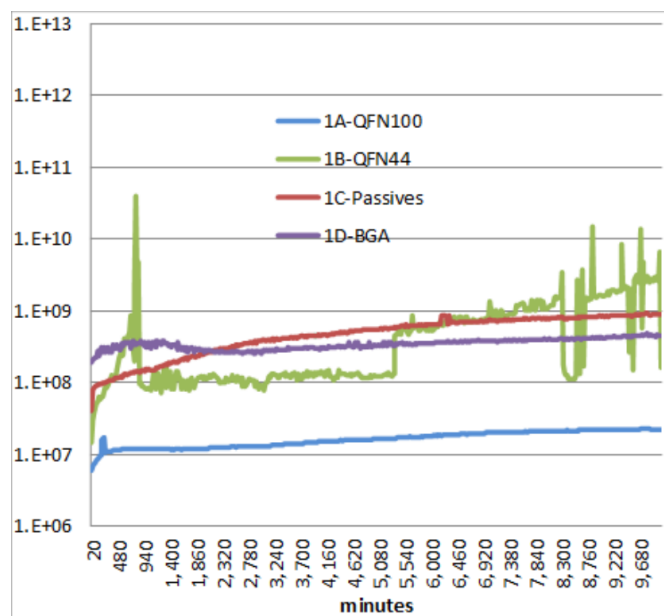
Figure 2.24 *SIR test of anonymous blend WOA-amine activator flux, adapted from [106].*
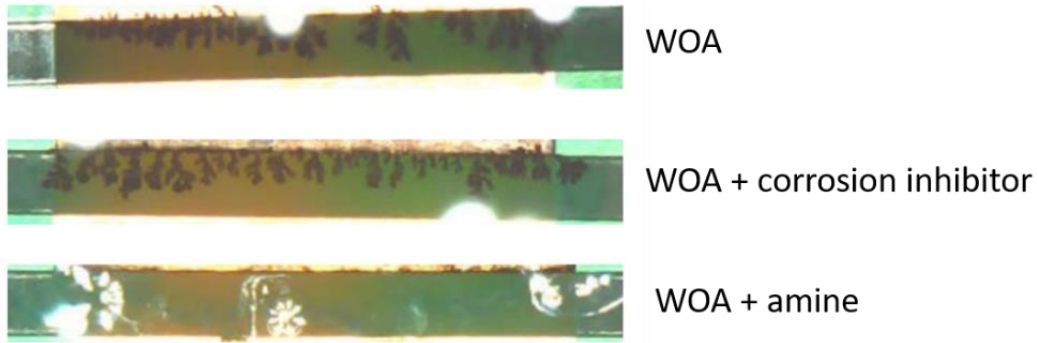
Figure 2.25 *ECM investigation with WOA, WOA + corrosion inhibitor and WOA + amine, adapted from [104].*
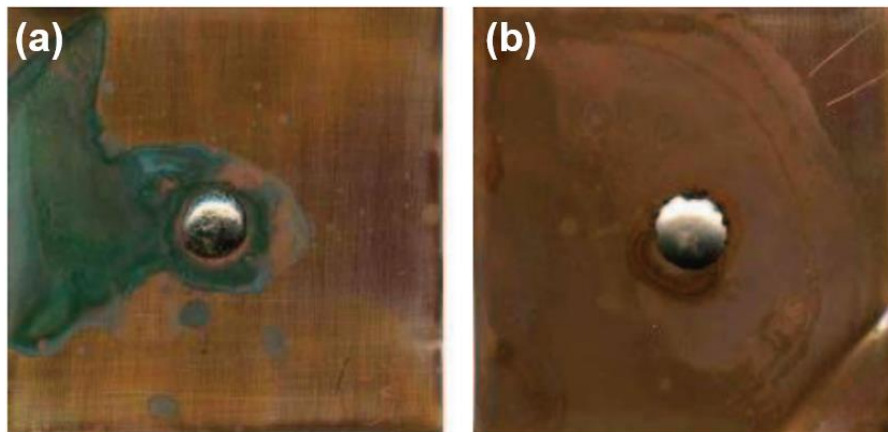
Figure 2.26 *Copper mirror test of (a) WOA based flux, (b) WOA-amine based flux, adapted from [105].*

Amino acid activators

Amino acids obtained both carboxylic group and amino group in the structure, which also generally water-soluble, mild and biodegradable [107]. According to the neutralized reaction between carboxylic group and amino group, the pH value of some amino acids could be relatively neutral. While under soldering conditions, the oxide layer can be removed by both carboxylic group and amino group. Therefore, the amino acids could be used as reliable activator candidates for the new flux formulation.

From the solderability point of view, anonymous amino acid may obtained faster wetting speed than the carboxylic acid. Koon et al. reported the amino acid is more reactive for the oxide layers

removal than carboxylic acid, which is because the oxide interaction with the positive charge group of $NH_3{}^+$, as shown in **Equation 2.32** [108].

$$2(^-OOCCH(R)NH_3{}^+) + O_2{}^{2-} \rightarrow 2(H_2CCH(R)COO)^- + H_2O \quad \textit{Equation 2.32}$$
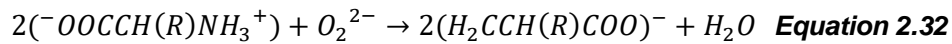
From the climatic reliability point of view, example of neutral amino acid is preferred [109]. The determination factor is isoelectronic point (pI) as shown in **Equation 2.33**, which indicates the pH that amino acid does not carry electrical charge. The pK_{a1} indicates the dissociation constant of carboxyl group, the pK_{a2} indicates the dissociation constant of amine group.

$$pI = \frac{pK_{a1} + pK_{a2}}{2} \quad \textit{Equation 2.33}$$

2.4.2. Protection of PCBAs from humidity effect using conformal coatings and PCBA cleanliness

To protect the metal/alloy material in the PCBAs, conformal coating has been broadly used on PCBAs as a barrier aiming to cope with environmental stress regimes such as airborne chemical vapours, high atmospheric humidity, corrosive gases, dust and dirt, and environmental contaminants [110]. The classification of conformal coatings is summarized in **Figure 2.27**. Six major conformal coating types includes acrylic, urethane, epoxy, fluoropolymer, silicone, and parylene [110][111]. Acrylic, urethane, epoxy, fluoropolymer, and silicone based conformal coatings are in liquid format and applied by spraying, jetting, dipping and brushing, while chemical vapour deposition (CVD) was usually used for the applying the parylene coating in a vacuum chamber. The curing mechanism of conformal coating includes solvent evaporation curing, heat curing, moisture curing, ultraviolet curing and catalyzed curing [112][113][114]. The advantages and disadvantages for each type of conformal coating are summarized in **Table 2.3**.
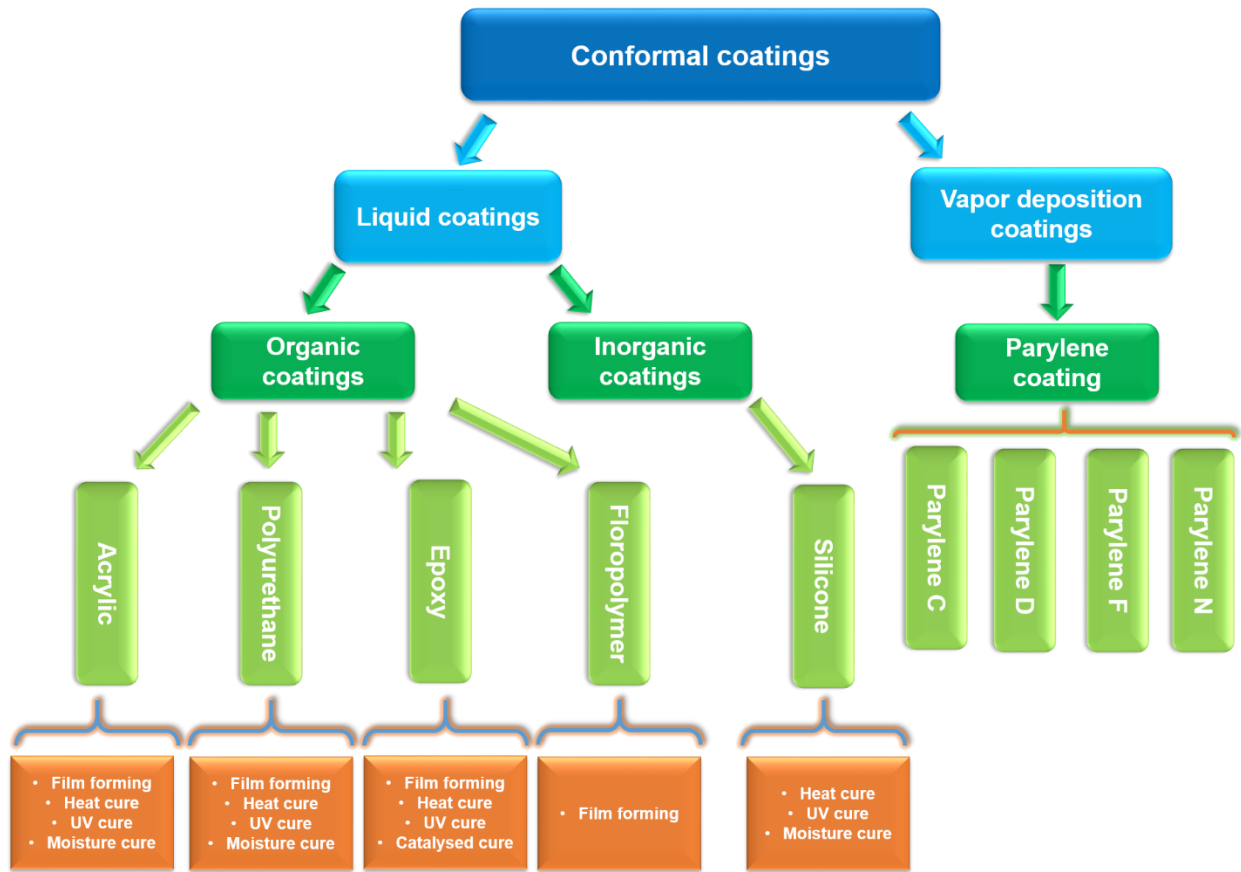
Figure 2.27 *Classification of major conformal coatings and curing methods used in electronics, adapt from [115].*

Table 2.3 *Summary of advantages and disadvantages for conformal coatings, adapted from [116][117].*

Conformal coating	Advantage	Disadvantage
Acrylic Resin (AR)	High dielectric strength Fair moisture and abrasion resistance Easy applied and removed Easy rework or repair No shrinkage during curing process Affordable option	Low chemical and solvent resistance Low abrasion resistance Not ideal for harsh environments Not ideal for high temperature applications
Urethane Resin (UR)	Great chemical resistance Great humidity resistance Great abrasion resistance	Difficult to remove Risk of peeling Long curing times Turns to brown tint using soldering iron for rework
Epoxy Resin (ER)	Great abrasion resistance Great humidity resistance Great chemical resistance Excellent performance in harsh environment	Difficult to remove Shrinkage during curing process Soldering iron required for rework or repair

Silicone Resin (SR)	Good performance in extreme temperature	Most difficult to remove
	Excellent humidity resistance	Removal requires strong chemical strippers and harsh abrasion
	Good chemical resistance Good adhesion to most PCB components and materials	Only localized repair
Parylene Resin (PR)	Best solvent resistance	Difficult to remove, must be abraded off
	Best extreme temperature resistance	Specialized equipment for chemical vapour deposition
	High dielectric strength	Not ideal for long-term exposure outdoors
	No curing required	
	Transparent and colourless	
Fluoropolymer	Easy application	Low surface protection
	A minimal amount of hydrophobicity	Thin coating with many defects and voids

The protection of conformal coating for PCBAs is based on barrier properties [118]. However, the humidity is able to diffuse through the conformal coating and reach to the conformal coating-PCBAs interface over time. The elapsed time can be estimated using **Equation 2.34**, where L indicates the thickness of the polymer layer along the diffusion path, D indicates the diffusion coefficient. The D value of silicone resin is 10^{-5} cm^2/s, while the D value of urethane and other organic resin is 10^{-6} cm^2/s [119]. Humidity is able to diffuse through the silicone resin with the thickness of 1 cm in a days, and diffuse through urethane resin with the same thickness in a week [119]. The equilibrium time of humidity for silicone resin with 1 cm thickness is 6 days, whereas for urethane resin is 1 month [5]. Since the thickness of conformal coating in application is in a range from 25 μm to 127 μm [116], the humidity can reach to the urethane-PCBAs interface within 0.4 hours and reach to silicone-PCBAs interface within 2.5 hours. The humidity in the coating is able to induce hydrolytic degradation of conformal coating [120].

$$\tau = \frac{L^2}{2D} \quad \textbf{\textit{Equation 2.34}}$$

In practice, the conformal coating is directly applied on the PCBAs without cleaning. Therefore, the adhesion of conformal coating is influenced by the no-clean flux residue at the interface of conformal coating and PCBAs. For instance, the acrylic conformal coatings are permeable to WOAs flux residue, and the WOAs are able to accelerate the degradation of the polymer [121] and trigger the loss of adhesion for conformal coating, as shown in **Figure 2.28**. In consequence, the water accumulated at interface induces the ionization of WOAs in flux residue, hence leads to corrosion of metal in the PCBAs. The ECM was also observed under the acrylic and silicone conformal coating coated SIR pattern with rosin based no-clean flux residue, as shown in **Figure 2.28**. Therefore, the effect of the flux residue to the corrosion performance of the conformal coating need to be addressed for the robust PCBA manufacturing. The ECM was also observed

under the acrylic and silicone conformal coating coated SIR pattern with rosin based no-clean flux residue, as shown in **Figure 2.29**.
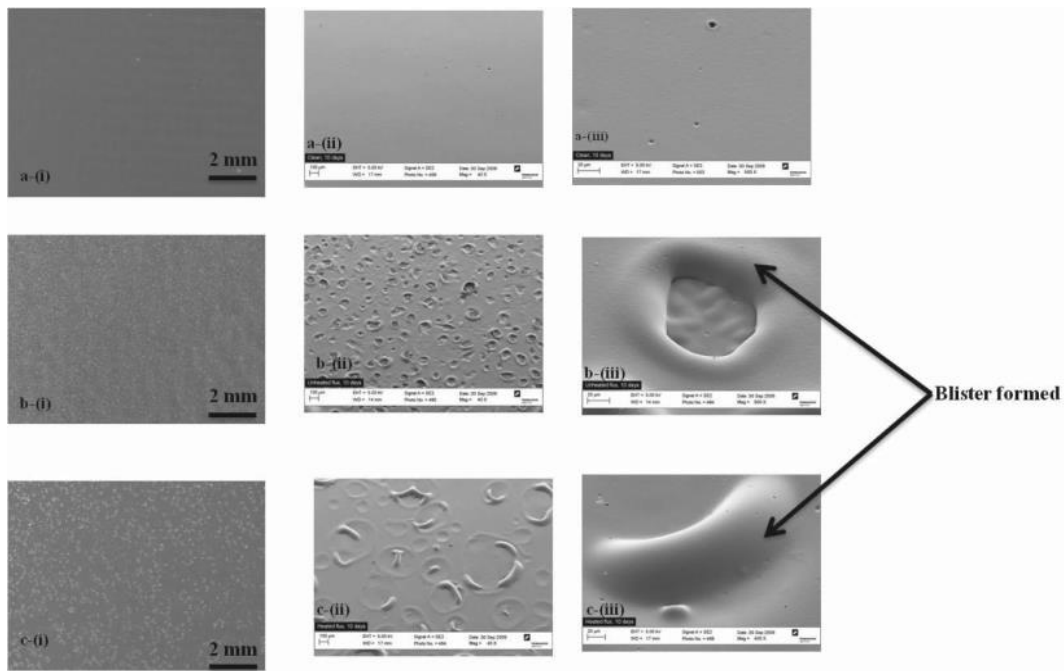
Figure 2.28 Effect of flux residue on the blister formation of acrylic conformal coating after humidity exposure, adapted from [122].
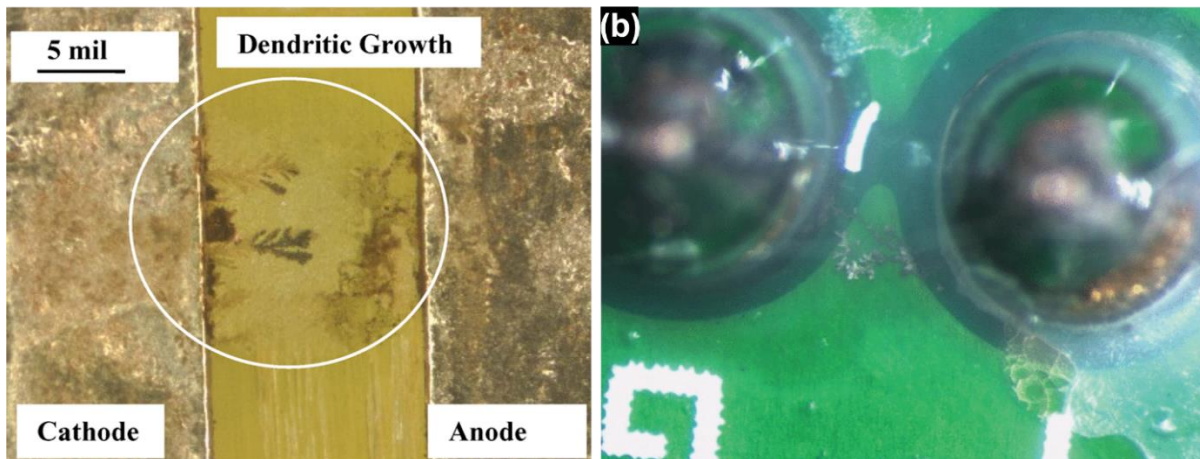
Figure 2.29 ECM on the rosin based no-clean flux contained SIR test vehicle with: (a) acrylic coating [123], (b) silicone coating [27].

2.5. Evaluation methods and techniques

The selection of the flux activator candidates mainly focused on two aspects, which are solderability and climatic reliability.

2.5.1. Solderability testing

From solderability point of view, hot plate spreading test and wetting balance test are the most commonly used evaluation method [124].

Hot plate spreading test

Hot plate spreading test (IPC-TM-650 2.4.46) was show in **Figure 2.30**. Before thermal activation, a circular solder wire formed O-ring was placed on the Cu substrate with applied flux in the center of O-ring. After preheating step and soldering step, the solder wire melted and spreaded on the Cu substrate. The wetting properties of the flux can be evaluated using contact angle of the solder alloy. The wetting properties between solder alloy and Cu substrate are determined by surface energy, and low contact angle θ indicates better wettability. **Equation 2.35** expressed the wettability can be improved when increasing γ_{SV} or decreasing γ_{SL} and γ_{LV}. Since constant volume of the solder alloy was used in the test, the wetting properties can also be evaluated using the spreading area of melted solder on the Cu susbtrate [125].

$$cos\theta = \frac{\gamma_{SV} - \gamma_{SL}}{\gamma_{LV}} \quad \textit{Equation 2.35}$$
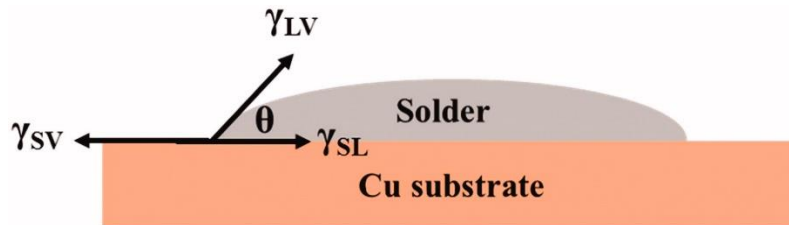
***Figure 2.30** Schematic of hot plate spreading test, adapted from [124]. Cu substrate/solder flux (γ_{SV}), melted solder alloy/Cu substrate((γ_{SL}), and melted solder alloy/solder fluxes (γ_{LV}).*

Wetting balance test

Wetting balance method (IPC-TM-650 2.4.14.2) was used to quantitatively evaluate the wetting performance of the solder flux. This method was to measure the wetting force of flux applied Cu substrate during immersion in the melted solder bath in a precisely controlled manner, as shown in **Figure 2.31**. The wetting force in negative region shows between step (a) and (b) was due to the buoyancy. The wetting of the solder alloys started from step (c) and passed the zero wetting force, and the time to reach zero wetting force was denoted as T_0. The wetting of the solder alloy kept increasing and passed the 2/3 of the maximum wetting force. The time reach to 2/3 of the maximum wetting force was denoted as $T_{2/3}$. Until step (d), the wetting force reached to the maximum level, which was denoted as F_{max}. T_0 and $T_{2/3}$ are the parameters reflecting the wetting

speed, while the F_{max} can be used to evaluate the highest wetting force obtained by each solder flux.
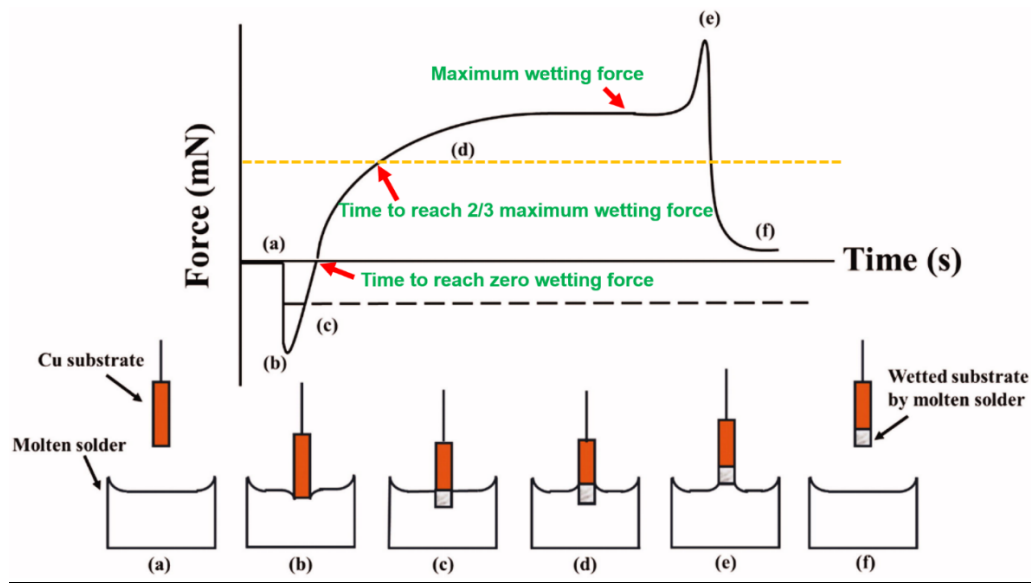
Figure 2.31 Schematic of representative steps in wetting balance test curve with the actual position of Cu substrate during each step, adapted from [124].

2.5.2. Climatic reliability testing

SIR testing

The SIR testing is a DC testing method, which has been broadly used in the electronic manufacturing society for electrical reliability control. The principle of using SIR testing is to address the corrosive and conductive effects of solder flux reside on the electrical reliability of the PCBAs. This technique measured the conductivity of the flux residue in a given area of the material by counting the movement of electrons on the surface of material, and the result can be normalized into a unit square for relative comparison [126]. If the contaminants triggered the breakdown of SIR in testing vehicle, visualization and the growth rate of ECM dendrite can be used as supplement evaluation factors [104][127]. The standardized SIR configuration of testing vehicles used in the SIR test was shown in **Figure 2.32**. The substrate of the testing vehicles is FR-4 glass fiber reinforce resin, and the electrode material is Cu [128]. The SIR testing standards was summarized in **Table 2.4**, which could be used to imitate bias loaded electronic device exposed under various harsh climatic conditions
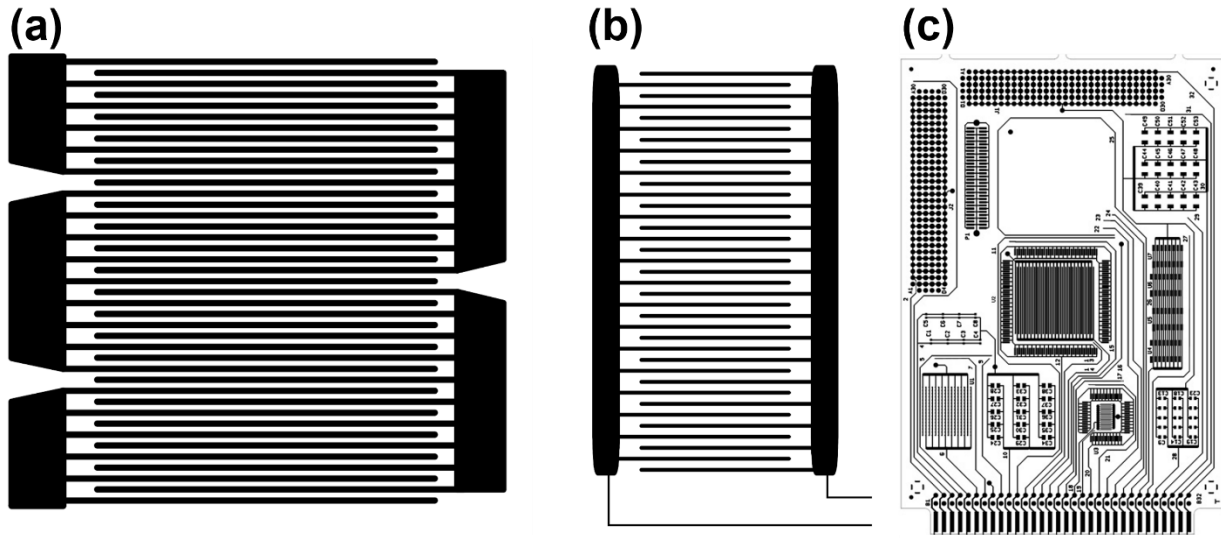
Figure 2.32 *Schematic layout of (a) IPC-B-25 SIR test pattern with line width and track spacing of 0.0125 mm [128], (b) IPC-B-24 SIR test pattern with line width of 0.4 mm and track spacing of 0.5 mm [128], (c) IPC-B-52 layout for cleanliness and residue evaluation [129].*

Table 2.4 *Summary of the SIR testing standards [78][130][13][131].*

Testing methods	IPC-TM-650 2.6.3.3	IPC-TM-650 2.6.14.1	J-STD-001	J-STD-004
Environmental testing conditions	85°C, 85% RH	40°C, 93%RH 65°C, 88%RH 85°C, 85%RH	85°C, 85% RH	35°C, 85%RH
Bias voltage (V)	45-50	10	-50	48
Measurement voltage (V)	-100	45-100	100	100
Duration (h)	168	500	168	96
Failure Criteria	<100 MΩ	ECM dendrite		Discoluoration

2.5.3. Leakage current measurement

The reason of using SIR method with high DC loading in the past was due to the technical difficulty of measuring low currents [128]. However, the resolution of the potentiostat used today can easily reach to pA level. Chronoamperometry (CA) is a DC technique, which can evaluate the leakage current level on the surface of PCBA under climatic exposure with a relative lower DC voltage in a range of 0-10 V [132][133][134]. As result, leakage current measurement is the most feasible DC method to replace conventional SIR methods to evaluate the electrical reliability for low power electronics. Consequently, qualification equipment suppliers integrated the leakage current measurement in their Auto-SIR system with the current resolution to pA level under computer control [128]. The threshold of leakage current level was defined at 1-10 μA due to the increasing

free ions by dissolution of the anodic materials and ECM dendrite formation [135][132]. A number of solder flux related investigations were conducted using leakage current measurement on IPC-B-24 SIR pattern [37] [135] [132][133], and the impact of the flux activators on the climatic reliability can be distinguished, as shown in **Figure 2.33**. High leakage current over 10 µA was observed on the SIR pattern contaminated with glutaric acid flux (**Figure 2.33**(b)), while the leakage current of adipic acid based flux located in the safety region (**Figure 2.33**(a)). Therefore, leakage current measurement can be used for the qualification of the flux residue under humidity exposure.
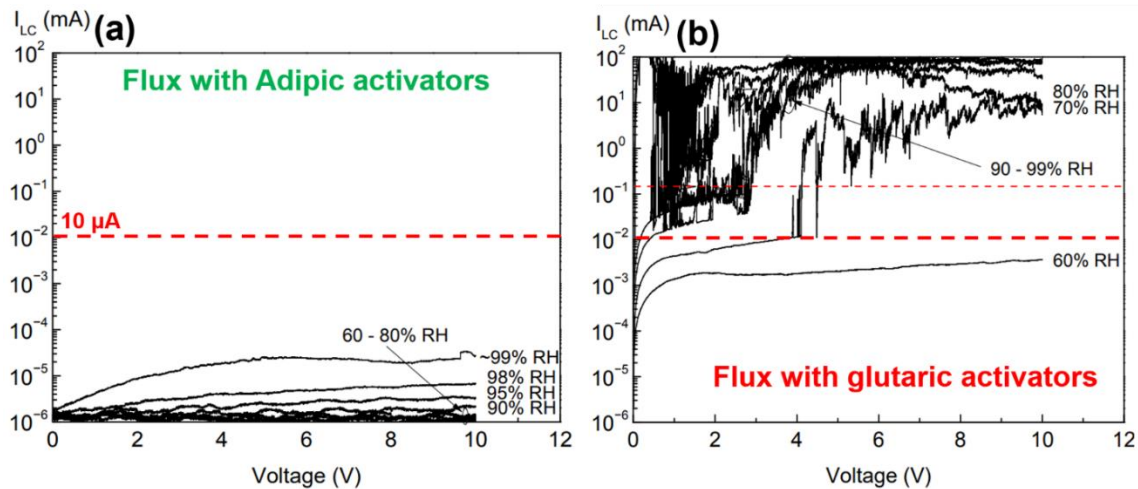
Figure 2.33 *Leakage current result of (a) Flux with adipic acid activators, (b) Flux with glutaric activators, adapted from [135].*

2.5.4. Electrochemical impedance spectroscopy testing

Electrochemical impedance spectroscopy (EIS) is an AC technique, which characterizes the impedance spectrum of an electrochemical cell by scanning in a wide range of frequencies with a small amplitude voltage [136]. Compared to the SIR testing and leakage current measurement, EIS testing is a non-destructive technique, which can provide diffusion kinetics and the evolution process of electrical signal over testing period in the electrochemical cell [137]. It has been broadly implemented in the electronic corrosion related research.

Figure 2.34 shows the kinetics of water condensation on PCB as increasing the exposed RH level, which can be monitored using EIS technique, as shown in **Figure 2.35**. The EIS equivalent circuit model of SIR interdigitated pattern was explained in **Figure 2.35**. In the dry condition, the equivalent circuit is only represented parallel connection of the surface insulation resistance (R_{SIR}) and capacitance of substrate ($C_{Substrate}$). In the water condensation condition, the equivalent circuit

represent the electrochemical process in the condensed water, where the $R_{Solution}$ represents the resistance of the solution, which can be affected by the dissolution of the flux residue. R_{ct} represents the charge transfer resistance from the electrode to the solution. Z_W represents the Warburg impedance which induced by the diffusion of ions in the solution. C_{dl} represent double layer capacitance. C_{Total} represents the total capacitance of the solution and substrate. Under water condensation condition, the parallel connection of R_{SIR} can be neglected due to its much larger value compared to other parallel components.
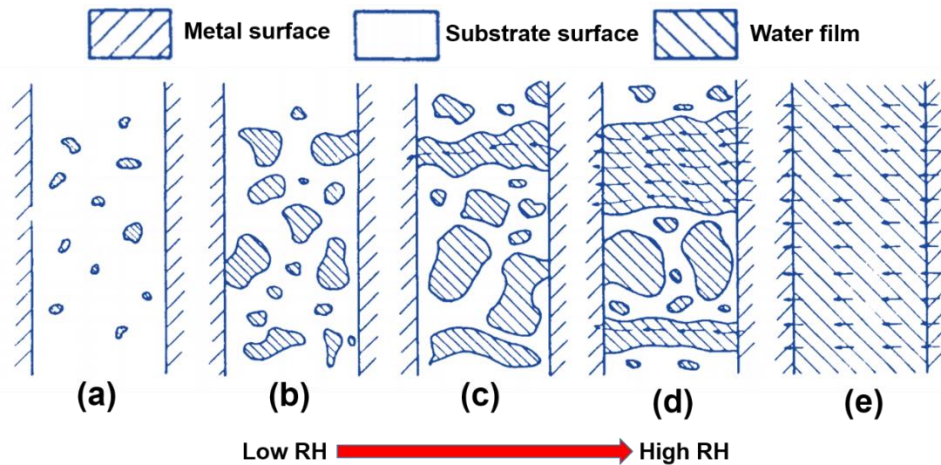
Figure 2.34 *Schematic of water condensation on a PCB surface as function of exposed RH level, adapted from [138].*
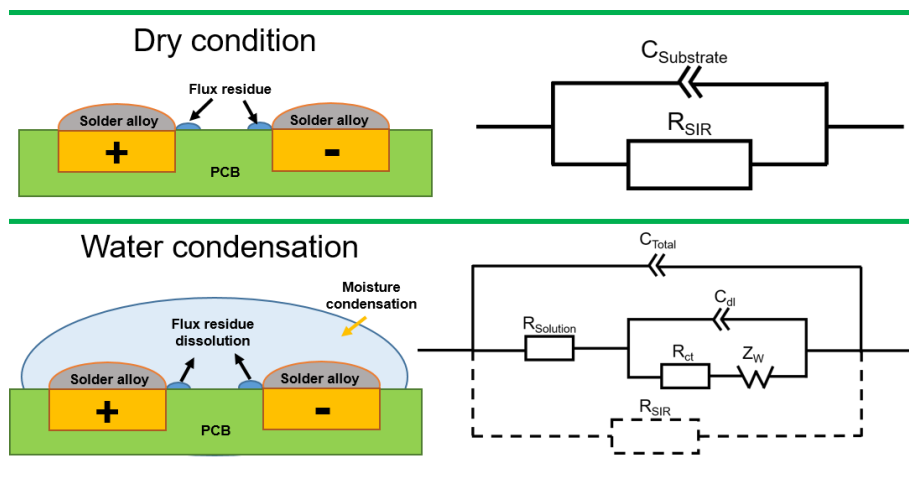
Figure 2.35 *Equivalent circuit for the flux residue contaminated SIR pattern at dry condition and water condensation condition.*

In practice, compared to the cleaned SIR pattern in **Figure 2.36**(a), the drop of the impedance value was magnificent in the flux residue contaminated SIR pattern as shown in **Figure 2.36**(b)(c),

which indicate the flux residue accelerated the water condensation process due to the hygroscopicity. In the high frequency range at 10-100 kHz, the drop of impedance for glutaric acid flux contaminated SIR pattern is more pronounced than adipic acid flux contaminated SIR pattern. The plot in **Figure 2.36**(d) shows the phase angle of glutaric acid contaminated SIR pattern shifted towards 0° compared to the adipic acid flux contaminated SIR pattern at nearly -90° under exposure of 25°C/99%RH. Phase angle results indicate the electrical property of the SIR pattern transferred from capacitive dominance to resistive dominance due to the water build up on the PCB surface and the glutaric acid flux residue dissolution.
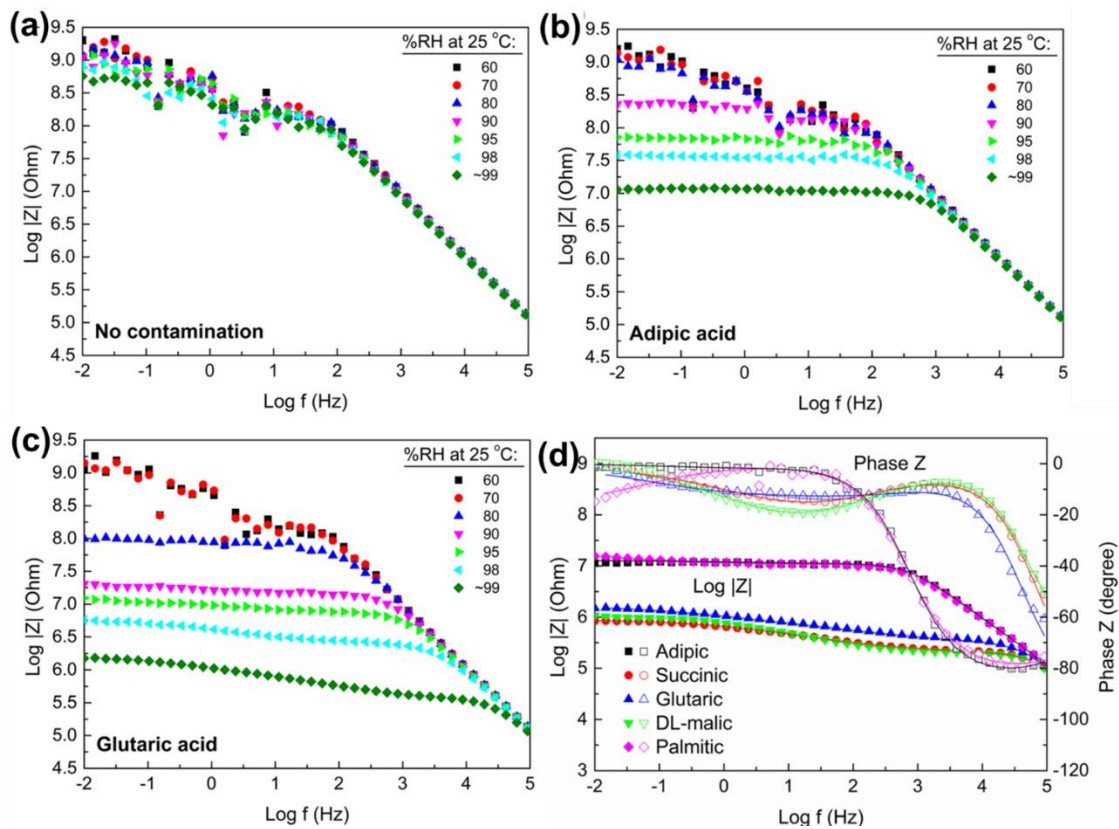
Figure 2.36 EIS response of WOA flux residue contaminated SIR interdigitated pattern: (a) no contamination, (b) adipic acid, (c) glutaric acid, (d) various flux residue contaminated SIR pattern under climatic exposure of 25°C, 99%RH, adapted from [37].

The phase transition of EIS during water condensation as function of frequency range between 10-100 kHz has been investigated by Lauser et al [139]. **Figure 2.37** shows the phase angle shifted from -90° to 0° during water condensation for the SIR with 100 µm gap size in the scanning frequency range of 10-100 kHz (**Figure 2.37**(a)), while the phase transition signal at 10 kHz is more reliable for the SIR with gap size of 300 µm (**Figure 2.37**(b)). Consequently, the single

frequency EIS scanning at 10 kHz has been applied in the humidity interaction study of WOA flux activators to evaluate climatic reliability [84][140].
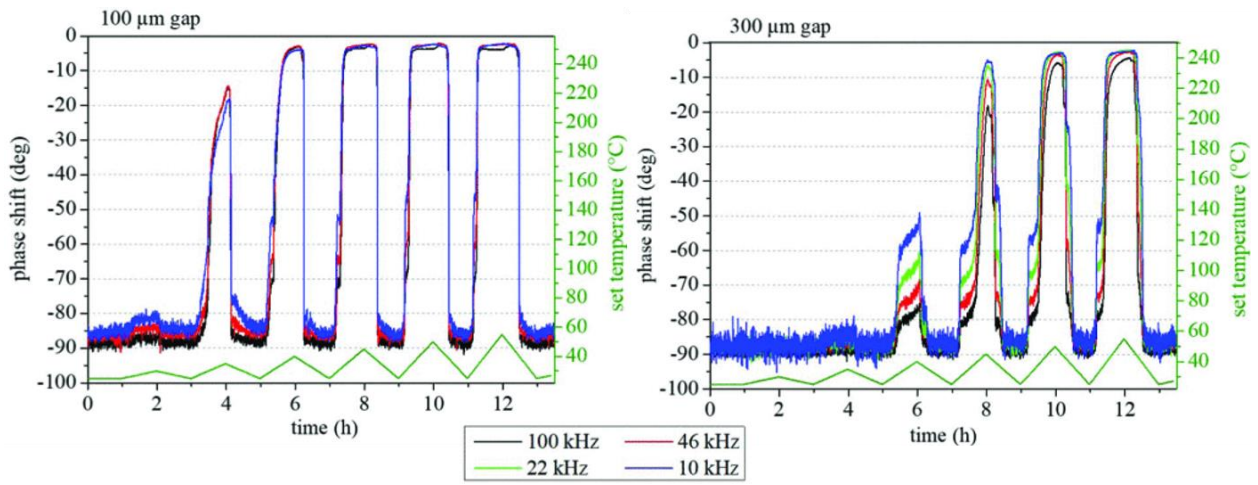
Figure 2.37 *Phase angle response of SIR pattern exposed at 97% RH with temperature ramping, adapted from [139].*

The EIS testing result is comparable to the leakage current measurement under water condensation status, shown in **Figure 2.38** [139]. The leakage current increased as the water condensation occurred as shown in **Figure 2.38**(a). Under same testing condition shown in **Figure 2.38**(b), the impedance response at frequency of 22 kHz suddenly dropped when the water condensation took place, while the phase shifted from -90° to 0°.
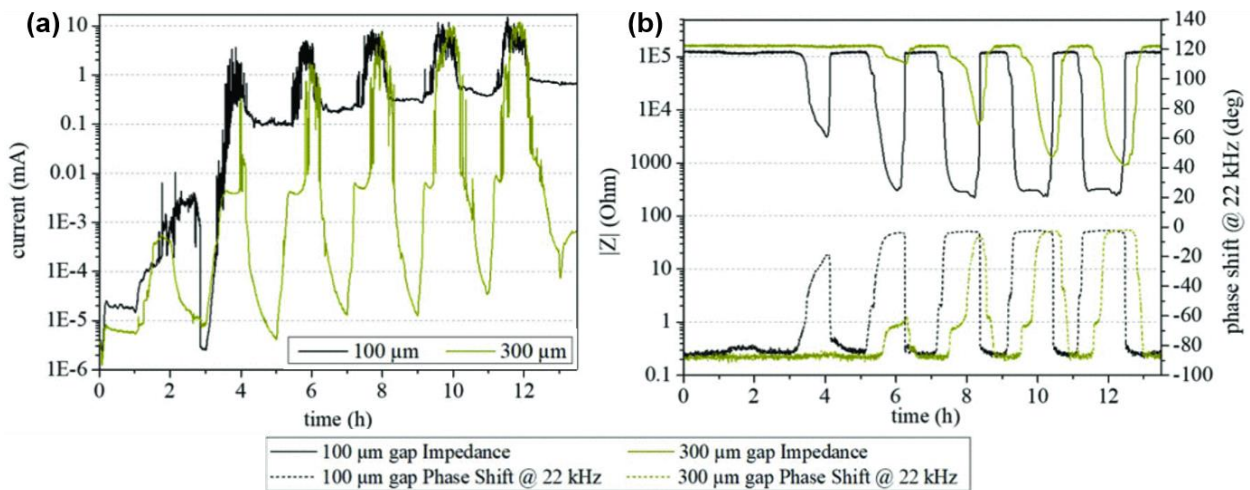
Figure 2.38 *The leakage current response and EIS response of SIR pattern under same testing condition, adapted from [139].*

2.6. Summary of the literature review and approach on PhD project

This chapter provided a fundamental review of the humidity interaction with the PCBA used in electronic devices (Chapter 2.1-2.2), the corrosion failure of PCBAs (Chapter 2.3), the corrosion control for PCBA (Chapter 2.4), the evaluation testing methods for no-clean flux (Chapter 2.5). The comprehensive understanding of the humidity related failure of electronics has brought the demands to strengthen the corrosion reliability of electronics, which agreed on the objectives of this PhD project.

The SAC solder alloys has been broadly used in PCBA to joint components. Over the years, different types of the SAC alloy with alloying additives have been developed based on the requirement of the mechanical properties, while the corrosion related investigation was limited, as described in Chapter 2.3.3. ECM (Chapter 2.3.2) susceptibility of the solder alloy is the main concern on its corrosion performance under service condition with power supply. The ECM process can be recorded either by leakage current measurement (Chapter 2.5.2), or visualization. The scope of Chapter 5 is to correlate the corrosion mechanism and ECM behavior of commercialized Sn-Ag-Cu (SAC) solder with additive element of Ni, Bi and Sb. The focus is on the electrochemical analysis of the corrosion current density in comparison with the microstructure and potential of various phases. At mean time, standardized accelerated testing was used to identify the actual electrochemical and microstructural chatacters which assisted the ECM dendrite formation.

Hygroscopic and ionic nature of the WOA flux residue induced the reduction of SIR or ECM dendrite formation (Chapter 2.3.2) as intermittent or permanent failure mode for the electronic device, which brought the demand of the optimization of no-clean flux formulation. Investigations focused on obtaining robust climatic reliability of the new activator types (Chapter 2.4.1) when maintains the solderability as WOA flux provided. In Chapter 6-8, model wave flux was formulated using amine, blend WOA-amine, and amino acid as flux activators. Thermal degradation of the flux activators can be simulated in oven and analyzed using fourier transform infrared spectroscopy (FT-IR) or thermal gravimetric analysis (TGA). The evaluation of solderability was conducted using hot plate spreading test and wetting balance method (Chapter 2.5.1). The evaluation of humidity robustness of new flux systems was conducted using leakage current measurement and EIS testing (Chapter 2.5.2). The current knowledge of WOA flux activators in Chapter 2.2.2 will be used for quality verification of the new flux activators.

The manufacturing of the surface-mounted PCBA is growing fast and has been expected to occupy 75% of the electronic market in the near future, which brought the importance of the

climatic reliability of the reflow flux residue contaminated PCBA. The impact of the flux activator plays a key role on the humidity robustness of the reflow flux residue, which may break the resin under humidity exposure (Chapter 2.2.2) and induce reduction of SIR or ECM (Chapter 2.3.2). Chapter 9 aims to explain the effect of the flux activator in reflow flux residue on the humidity robustness of PCBA and provides a solution for quality control. The cracking of flux residue and conductivity of the PCBA surface were monitored during humidity exposure. Leakage current measurement and EIS testing (Chapter 2.5.2) were exploited to understand the kinetics of the humidity interaction with different flux activators contained reflow flux residue on PCBA.

No-clean flux dominates 70-80% of the electronic manufacturing. Conformal coating was applied on the PCBA surface as the last step of manufacturing to improve the reliability of the PCBA. Investigations reported the flux residue interfered the protection performance of the conformal coating (Chapter 2.4.2) and induced ECM (Chapter 2.3.2). Therefore, it is important to understand the role that flux residue play on the failure mechanism of conformal coating protection. Chapter 10 evaluated the performance of three types of conformal coatings with two types of flux residues contaminated SIR test board. EIS testing and leakage current measurement (Chapter 2.5.2) were employed in the investigation in order to monitor the water absorption process of conformal coatings during the climatic exposure in comparison with the visualized surface morphology of the conformal coating.

References

[1]   GASPARETTO ENGINEERING, Dew point, (n.d.). https://www.gasparetto.it/en/psychrometric-chart-dew-point (accessed July 13, 2020).

[2]   L.J. Mauer, L.S. Taylor, Water-Solids Interactions: Deliquescence, Annu. Rev. Food Sci. Technol. 1 (2010) 41–63. doi:10.1146/annurev.food.080708.100915.

[3]   A. Esfandyari, S. Härter, T. Javied, J. Franke, A Lean Based Overview on Sustainability of Printed Circuit Board production assembly, Procedia CIRP. 26 (2015) 305–310. doi:10.1016/j.procir.2014.07.059.

[4]   N. Nardono, S. Caroline, Information on chemicals in electroni products, a study of needs, gaps, obstacles and solutions to provide and access information on chemicals in electronic product, Nordic Council of Ministers, Copenhagen, 2011.

[5]   M. Tencer, J.S. Moss, Humidity management of outdoor electronic equipment: methods, pitfalls, and recommendations, IEEE Trans. Components Packag. Technol. 25 (2002) 66–72. doi:10.1109/6144.991177.

[6]   V. Vadimas, J. Salil, J.M. Stendahl, A. Rajan, Analysis of surface insulation resistance related failures in electronics by circuit simulation, Circuit World. 43 (2017) 45–55. doi:10.1108/CW-09-2016-0040.

[7]   R. Ambat, S.G. Jensen, P. Møller, Corrosion Reliability of Electronic Systems, in: ECS Trans., 2008. doi:10.1149/1.2900650.

[8]   D. Minzari, M.S. Jellesen, P. Moller, P. Wahlberg, R. Ambat, Electrochemical Migration on Electronic Chip Resistors in Chloride Environments, IEEE Trans. Device Mater. Reliab. 9 (2009) 392–402. doi:10.1109/TDMR.2009.2022631.

[9]   R. Ambat, An overview on the climatic reliability issues of electronic devices, in: Proc. IMAPS Nord. Annu. Conf. 2014, 2014.

[10]   S. Sahin, G.S. Sumnu, Physical Properties of Foods, Springer, New York, NY, 2006. doi:https://doi-org.proxy.findit.dtu.dk/10.1007/0-387-30808-3.

[11]   S. Brunauer, L.E. Copeland, Physical Adsorption of Gases and Vapors on Solids, ASTM International, West Conshohocken, PA, 1963. doi:978-0-8031-6259-4.

[12]   D.J. Klinger, Humidity acceleration factor for plastic packaged electronic devices, Qual. Reliab. Eng. Int. 7 (1991) 365–370. doi:https://doi.org/10.1002/qre.4680070505.

[13]   V. Verdingovas, M.S. Jellesen, R. Ambat, Impact of NaCl contamination and climatic conditions on the reliability of printed circuit board assemblies, IEEE Trans. Device Mater. Reliab. 14 (2014) 42–51. doi:10.1109/TDMR.2013.2293792.

[14]   J. Wang, Z. Bai, K. Xiao, X. Gao, P. Yi, C. Dong, J. Wu, D. Wei, Influence of atmospheric particulates on initial corrosion behavior of printed circuit board in pollution environments, Appl. Surf. Sci. 467–468 (2019) 889–901. doi:https://doi.org/10.1016/j.apsusc.2018.10.244.

[15]   K. Piotrowska, R.U. Din, M.S. Jellesen, R. Ambat, Effect of Solder Mask Surface Chemistry and Morphology on the Water Layer Formation Under Humid Conditions, IEEE Trans. Components, Packag. Manuf. Technol. 8 (2018) 1756–1768. doi:10.1109/TCPMT.2018.2792047.

[16]   Y. Yuan, T.R. Lee, Contact Angle and Wetting Properties BT - Surface Science Techniques, in: G. Bracco, B. Holst (Eds.), Springer Berlin Heidelberg, Berlin, Heidelberg, 2013: pp. 3–34. doi:10.1007/978-3-642-34243-1_1.

[17]   X.-S. Wang, S.-W. Cui, L. Zhou, S.-H. Xu, Z.-W. Sun, R.-Z. Zhu, A generalized Young's equation for contact angles of droplets on homogeneous and rough substrates, J. Adhes. Sci. Technol. 28 (2014) 161–170. doi:10.1080/01694243.2013.833401.

[18]   G. Whyman, E. Bormashenko, T. Stein, The rigorous derivation of Young, Cassie–Baxter and Wenzel equations and the analysis of the contact angle hysteresis phenomenon, Chem. Phys. Lett. 450 (2008) 355–359. doi:https://doi.org/10.1016/j.cplett.2007.11.033.

[19]   M. Stefanoni, U.M. Angst, B. Elsener, Electrochemistry and capillary condensation theory reveal the mechanism of corrosion in dense porous media, Sci. Rep. 8 (2018) 7407. doi:10.1038/s41598-018-25794-x.

[20]   M.S. Jellesen, D. Minzari, U. Rathinavelu, P. Moller, R. Ambat, Corrosion in Electronics at Device Level, ECS Trans. 25 (2010) 1–14. doi:10.1149/1.3321952.

[21]   R. Ambat, H. Conseil-Gudla, V. Verdingovas, Corrosion in Electronics, Encycl. Interfacial Chem. Surf. Sci. Electrochem. (2018) 134–144. doi:https://doi.org/10.1016/B978-0-12-409547-2.13437-7.

[22]   S.J. Krumbein, Metallic electromigration phenomena, IEEE Trans. Components, Hybrids,

Manuf. Technol. 11 (1988) 5–15. doi:10.1109/33.2957.

[23] N.T. Lau, C.K. Chan, L.I. Chan, M. Fang, A microscopic study of the effects of particle size and composition of atmospheric aerosols on the corrosion of mild steel, Corros. Sci. 50 (2008) 2927–2933. doi:https://doi.org/10.1016/j.corsci.2008.07.009.

[24] P.-E. Tegehall, Impact of Black Pad and Intermetallic Layers on the Risk for Fractures in Solder Joints to Electroless Nickel/Immersion Gold BT - The ELFNET Book on Failure Mechanisms, Testing Methods, and Quality Issues of Lead-Free Solder Interconnects, in: G. Grossmann, C. Zardini (Eds.), Springer London, London, 2011: pp. 179–195. doi:10.1007/978-0-85729-236-0_8.

[25] M. Pecht, E.M. Bumiller, D.A. Douthit, J. Pecht, Contamination of Electronic Assemblies, Tylor & Francis Group, 2002.

[26] J.S. Vimala, M. Natesan, S. Rajendran, Corrosion and Protection of Electronic Components in Different Environmental Conditions - An Overview, Open Corros. J. 2 (2009) 105–113. doi:10.2174/1876503300902010105.

[27] P. Isaacs, T. Munson, Cleanliness Requirements: A Moving Target, in: 2019 Pan Pacific Microelectron. Symp. (Pan Pacific), 2019: pp. 1–10. doi:10.23919/PanPacific.2019.8696733.

[28] E. Bastow, The Effect of Reflow Profiling on the Electrical Reliability of No-Clean Solder Paste Flux Residues, in: IPC APEX EXPO Proc., Las Vegas, 2014.

[29] B.A. Smith, L.J. Turbini, Characterizing the weak organic acids used in low solids fluxes, J. Electron. Mater. 28 (1999) 1299–1306. doi:10.1007/s11664-999-0171-2.

[30] C.-. Huang, K. Srihari, A.J. McLenaghan, G.R. Westby, Flux activity evaluation using the wetting balance, in: Seventeenth IEEE/CPMT Int. Electron. Manuf. Technol. Symp. 'Manufacturing Technol. - Present Futur., 1995: pp. 344–350. doi:10.1109/IEMT.1995.526185.

[31] D.D.L. Chung, Materials for Electronic Packaging, Oxford: Butterworth-Heinemann, 1995.

[32] F.M. Zado, US4342607A, 1982.

[33] H. Conseil, M.S. Jellesen, R. Ambat, Contamination profile on typical printed circuit board assemblies vs soldering process, Solder. Surf. Mt. Technol. 26 (2014) 194–202. doi:10.1108/SSMT-03-2014-0007.

[34] K.S. Hansen, M.S. Jellesen, P. Moller, P.J.S. Westermann, R. Ambat, Effect of solder flux residues on corrosion of electronics, in: 2009 Annu. Reliab. Maintainab. Symp., 2009: pp. 502–508. doi:10.1109/RAMS.2009.4914727.

[35] H. M.R., V. J.H., S. H.A.H., Lead-free reflow soldering for electronics assembly, Solder. Surf. Mt. Technol. 13 (2001) 21–38. doi:10.1108/09540910110407388.

[36] P. Jianbiao, T.B. J., C. Tzu-Chien, D.W. J., The effect of reflow profile on SnPb and SnAgCu solder joint shear strength, Solder. Surf. Mt. Technol. 18 (2006) 48–56. doi:10.1108/09540910610717901.

[37] V. Verdingovas, M.S. Jellesen, R. Ambat, Solder Flux Residues and Humidity-Related Failures in Electronics: Relative Effects of Weak Organic Acids Used in No-Clean Flux Systems, J. Electron. Mater. 44 (2015) 1116–1127. doi:10.1007/s11664-014-3609-0.

[38]   K. Piotrowska, M.S. Jellesen, R. Ambat, Thermal decomposition of solder flux activators under simulated wave soldering conditions, Solder. Surf. Mt. Technol. 29 (2017) 133–143. doi:10.1108/SSMT-01-2017-0003.

[39]   P. Isaacs, T. Munson, What makes no-clean flux residue benign?, in: 2016 Pan Pacific Microelectron. Symp. (Pan Pacific), 2016: pp. 1–7. doi:10.1109/PanPacific.2016.7428404.

[40]   N.-C. Lee, 3 - Solder Paste Technology, in: N.-C.B.T.-R.S.P. Lee (Ed.), Reflow Solder. Process., Newnes, Burlington, 2001: pp. 37–55. doi:https://doi.org/10.1016/B978-075067218-4/50003-8.

[41]   M. Yamamoto, A. Takumi, K. Shiomi, M. Nakanishi, M. Watanabe, Soldering flux and solder paste composition, EP1897652A1, 2006. https://patents.google.com/patent/EP1897652A1/en.

[42]   P. Veselý, D. Bušek, O. Krammer, K. Dušek, Analysis of no-clean flux spatter during the soldering process, J. Mater. Process. Technol. 275 (2020) 116289. doi:https://doi.org/10.1016/j.jmatprotec.2019.116289.

[43]   K. Piotrowska, R. Ambat, Residue-assisted water layer build-up under transient climatic conditions and failure occurrence in electronics, IEEE Trans. Components, Packag. Manuf. Technol. (2020) 1. doi:10.1109/TCPMT.2020.3005933.

[44]   K. Piotrowska, S. Lagana, M. Jellesen, R. Ambat, Impact of Process-Related Flux Contamination on the Electronics Reliability Issues Under Detrimental Climatic Condtions, in: 2019 Pan Pacific Microelectron. Symp. (Pan Pacific), IEEE, Kauai, HI, USA, USA, 2019. doi:10.23919/PanPacific.2019.8696890.

[45]   K.M. Adams, J.E. Anderson, Y.B. Graves, Ionograph Sensitivity to Chemical Residues From 'no Clean Soldering Fluxes: Comparison Of Solvent Extract Conductivity and Surface Conductivity, Circuit World. 20 (1994) 41–44. doi:10.1108/eb046251.

[46]   C. Peng, M.N. Chan, C.K. Chan, The Hygroscopic Properties of Dicarboxylic and Multifunctional Acids: Measurements and UNIFAC Predictions, Environ. Sci. Technol. 35 (2001) 4495–4501. doi:10.1021/es0107531.

[47]   P. Saxena, L.M. Hildemann, Water Absorption by Organics: Survey of Laboratory Evidence and Evaluation of UNIFAC for Estimating Water Activity, Environ. Sci. Technol. 31 (1997) 3318–3324. doi:10.1021/es9703638.

[48]   C.N. Cruz, S.N. Pandis, Deliquescence and Hygroscopic Growth of Mixed Inorganic−Organic Atmospheric Aerosol, Environ. Sci. Technol. 34 (2000) 4313–4319. doi:10.1021/es9907109.

[49]   A. Apelblat, M. Dov, J. Wisniak, J. Zabicky, The vapour pressure of water over saturated aqueous solutions of malic, tartaric, and citric acids, at temperatures from 288 K to 323 K, J. Chem. Thermodyn. 27 (1995) 35–41. doi:https://doi.org/10.1006/jcht.1995.0004.

[50]   L. Treuel, S. Schulze, T. Leisner, R. Zellner, Deliquescence behaviour of single levitated ternary salt/carboxylic acid/water microdroplets, Faraday Discuss. 137 (2008) 265–278. doi:10.1039/B702651J.

[51]   M.N. Chan, S.M. Kreidenweis, C.K. Chan, Measurements of the Hygroscopic and Deliquescence Properties of Organic Compounds of Different Solubilities in Water and Their Relationship with Cloud Condensation Nuclei Activities, Environ. Sci. Technol. 42 (2008) 3602–3608. doi:10.1021/es7023252.

[52]   I.N. Tang, H.R. Munkelwitz, J.G. Davis, Aerosol growth studies — IV. Phase transformation of mixed salt aerosols in a moist atmosphere, J. Aerosol Sci. 9 (1978) 505–511. doi:https://doi.org/10.1016/0021-8502(78)90015-0.

[53]   S.T. Martin, Phase Transitions of Aqueous Atmospheric Particles, Chem. Rev. 100 (2000) 3403–3454. doi:10.1021/cr990034t.

[54]   J.A. Baird, R. Olayo-Valles, C. Rinaldi, L.S. Taylor, Effect of Molecular Weight, Temperature, and Additives on the Moisture Sorption Properties of Polyethylene Glycol, J. Pharm. Sci. 99 (2010) 154–168. doi:https://doi.org/10.1002/jps.21808.

[55]   M.S. Jellesen, V. Verdingovas, H. Conseil, K. Piotrowska, R. Ambat, Corrosion in electronics: Overview of failures and countermeasures, in: Proc. EuroCorr 2014, 2014.

[56]   H.A. Mustain, A.B. Lostetter, W.D. Brown, Evaluation of gold and aluminum wire bond performance for high temperature (500 /spl deg/C) silicon carbide (SiC) power modules, in: Proc. Electron. Components Technol. 2005. ECTC '05., 2005: pp. 1623-1628 Vol. 2. doi:10.1109/ECTC.2005.1442008.

[57]   Kejun Zeng, R. Stierman, D. Abbott, M. Murtuza, Root Cause of Black Pad Failure of Solder Joints with Electroless Nickel/Immersion Gold Plating, in: Therm. Thermomechanical Proc. 10th Intersoc. Conf. Phenom. Electron. Syst. 2006. ITHERM 2006., 2006: pp. 1111–1119. doi:10.1109/ITHERM.2006.1645469.

[58]   E.F. Monlevade, I.A.P. Cardoso, E.F.L. Maciel, N. Alonso-Falleiros, Galvanic corrosion of electroless nickel/immersion gold plated non-permanent electric contacts used in electronic devices–direct evidence of triggering mechanism, Eng. Fail. Anal. 96 (2019) 562–569. doi:https://doi.org/10.1016/j.engfailanal.2018.12.001.

[59]   S. Zou, X. Li, C. Dong, K. Ding, K. Xiao, Electrochemical migration, whisker formation, and corrosion behavior of printed circuit board under wet H2S environment, Electrochim. Acta. 114 (2013) 363–371. doi:https://doi.org/10.1016/j.electacta.2013.10.051.

[60]   T. Boettcher, M. Rother, S. Liedtke, M. Ullrich, M. Bollmann, A. Pinkernelle, D. Gruber, H.-J. Funke, M. Kaiser, K. Lee, M. Li, K. Leung, T. Li, M.L. Farrugia, O. O'Halloran, M. Petzold, B. März, R. Klengel, On the intermetallic corrosion of Cu-Al wire bonds, in: 2010 12th Electron. Packag. Technol. Conf., 2010: pp. 585–590. doi:10.1109/EPTC.2010.5702706.

[61]   H.R. Kotadia, P.D. Howes, S.H. Mannan, A review: On the development of low melting temperature Pb-free solders, Microelectron. Reliab. 54 (2014) 1253–1273. doi:10.1016/j.microrel.2014.02.025.

[62]   K. Suganuma, Advances in lead-free electronics soldering, Curr. Opin. Solid State Mater. Sci. 5 (2001) 55–64. doi:https://doi.org/10.1016/S1359-0286(00)00036-X.

[63]   K.-W. Moon, W.J. Boettinger, U.R. Kattner, F.S. Biancaniello, C.A. Handwerker, Experimental and thermodynamic assessment of Sn-Ag-Cu solder alloys, J. Electron. Mater. 29 (2000) 1122–1136. doi:10.1007/s11664-000-0003-x.

[64]   H. Ma, J.C. Suhling, Y. Zhang, P. Lall, M.J. Bozack, The Influence of Elevated Temperature Aging on Reliability of Lead Free Solder Joints, in: 2007 Proc. 57th Electron. Components Technol. Conf., 2007: pp. 653–668. doi:10.1109/ECTC.2007.373867.

[65]   W. Peng, E. Monlevade, M.E. Marques, Effect of thermal aging on the interfacial structure of SnAgCu solder joints on Cu, Microelectron. Reliab. 47 (2007) 2161–2168. doi:https://doi.org/10.1016/j.microrel.2006.12.006.

[66]   Y.W. Wang, C.C. Chang, C.R. Kao, Minimum effective Ni addition to SnAgCu solders for retarding Cu3Sn growth, J. Alloys Compd. 478 (2009) L1–L4. doi:10.1016/J.JALLCOM.2008.11.027.

[67]   M.N. Collins, E. Dalton, J. Punch, Microstructural influences on thermomechanical fatigue behaviour of third generation high Ag content Pb-Free solder alloys, J. Alloys Compd. 688 (2016) 164–170. doi:10.1016/j.jallcom.2016.07.191.

[68]   S. Hamasha, Y. Jaradat, A. Qasaimeh, M. Obaidat, P. Borgesen, Assessment of Solder Joint Fatigue Life Under Realistic Service Conditions, J. Electron. Mater. 43 (2014) 4472–4484. doi:10.1007/s11664-014-3436-3.

[69]   M. Wang, J. Wang, H. Feng, W. Ke, Effect of Ag3Sn intermetallic compounds on corrosion of Sn-3.0Ag-0.5Cu solder under high-temperature and high-humidity condition, Corros. Sci. 63 (2012) 20–28. doi:10.1016/J.CORSCI.2012.05.006.

[70]   G. Chen, X.H. Wang, J. Yang, W.L. Xu, Q. Lin, Effect of micromorphology on corrosion and mechanical properties of SAC305 lead-free solders, Microelectron. Reliab. 108 (2020) 113634. doi:https://doi.org/10.1016/j.microrel.2020.113634.

[71]   R.K. Kaushik, U. Batra, J.D. Sharma, Aging induced structural and electrochemical corrosion behaviour of Sn-1.0Ag-0.5Cu and Sn-3.8Ag-0.7Cu solder alloys, J. Alloys Compd. 745 (2018) 446–454. doi:10.1016/J.JALLCOM.2018.01.292.

[72]   W.R. Osório, J.E. Spinelli, C.R.M. Afonso, L.C. Peixoto, A. Garcia, Microstructure, corrosion behaviour and microhardness of a directionally solidified Sn-Cu solder alloy, Electrochim. Acta. 56 (2011) 8891–8899. doi:10.1016/j.electacta.2011.07.114.

[73]   M. FAYEKA, A.S.M.A. HASEEB, M.A. FAZAL, Electrochemical Corrosion Behaviour of Pb-free SAC 105 and SAC 305 Solder Alloys: A Comparative Study, Sains Malaysiana. 46 (2017) 295–302. doi:10.17576/jsm-2017-4602-14.

[74]   X. Zhong, G. Zhang, Y. Qiu, Z. Chen, X. Guo, Electrochemical migration of tin in thin electrolyte layer containing chloride ions, Corros. Sci. 74 (2013) 71–82. doi:10.1016/J.CORSCI.2013.04.015.

[75]   D. Minzari, M.S. Jellesen, P. Møller, R. Ambat, On the electrochemical migration mechanism of tin in electronics, Corros. Sci. 53 (2011) 3366–3379. doi:10.1016/j.corsci.2011.06.015.

[76]   B.C. Sekhar, S. Lakshminarayanan, A. Harshavardhan, An integrated seven port hybrid charger for smart home applications, in: 2016 IEEE 6th Int. Conf. Power Syst., 2016: pp. 1–5. doi:10.1109/ICPES.2016.7584150.

[77]   K. Tellefsen, SIR and ECM Testing of Soldering Materials vs. Soldering Processes, in: SMTA Int. Proc., Rosemont, IL, USA, 2015: pp. 306–309.

[78]   P. Douglas, Residues in printed wiring boards and assemblies, Circuit World. 27 (2001) 32–41. doi:10.1108/03056120110360291.

[79]   D. Li, P.P. Conway, C. Liu, Corrosion characterization of tin–lead and lead free solders in 3.5wt.% NaCl solution, Corros. Sci. 50 (2008) 995–1004. doi:https://doi.org/10.1016/j.corsci.2007.11.025.

[80]   IPC, Surface insulation resistance, IPC-TM-650 MANUAL, TEST METHODS, (n.d.). https://www.ipc.org/TM/2-6-3-7.pdf (accessed July 25, 2020).

[81]   F.N. Fuss, C.T. Hartwig, J.M. Morabito, Corrosion of solder-coated TiPdAu thin film conductors in a moist chlorine atmosphere, Thin Solid Films. 43 (1977) 189–213. doi:https://doi.org/10.1016/0040-6090(77)90385-6.

[82]   M. Tencer, Moisture ingress into nonhermetic enclosures and packages. A quasi-steady state model for diffusion and attenuation of ambient humidity variations, in: 1994 Proceedings. 44th Electron. Components Technol. Conf., 1994: pp. 196–209. doi:10.1109/ECTC.1994.367630.

[83]   S. Joshy, V. Verdingovas, M.S. Jellesen, R. Ambat, Circuit analysis to predict humidity related failures in electronics - Methodology and recommendations, Microelectron. Reliab. 93 (2019) 81–88. doi:https://doi.org/10.1016/j.microrel.2018.12.010.

[84]   K. Piotrowska, R. Ud Din, F.B. Grumsen, M.S. Jellesen, R. Ambat, Parametric Study of Solder Flux Hygroscopicity: Impact of Weak Organic Acids on Water Layer Formation and Corrosion of Electronics, J. Electron. Mater. 47 (2018) 4190–4207. doi:10.1007/s11664-018-6311-9.

[85]   D. Minzari, M.S. Jellesen, P. Møller, R. Ambat, On the electrochemical migration mechanism of tin in electronics, Corros. Sci. 53 (2011) 3366–3379. doi:10.1016/J.CORSCI.2011.06.015.

[86]   J. Kim, M. Park, D. Nam, H. Kwon, Electrochemical migration behavior of a fine-pitch IC substrate by alternating current, J. Nanosci. Nanotechnol. 14 (2014) 8258–8263. doi:10.1166/jnn.2014.9905.

[87]   B. Sood, M. Pecht, Controlling Moisture in Printed Circuit Boards, in: IPC Print. Circuit Expo, APEX Des. Summit Proc., 2011: pp. 1–53.

[88]   I. Fukuzawa, S. Ishiguro, S. Nanbu, Moisture Resistance Degradation of Plastic LSIs by Reflow Soldering, in: 23rd Int. Reliab. Phys. Symp., 1985: pp. 192–197. doi:10.1109/IRPS.1985.362097.

[89]   M. Kitano, A. Nishimura, S. Kawai, K. Nishi, Analysis of package cracking during reflow soldering process, in: 26th Annu. Proc. Reliab. Phys. Symp. 1988, 1988: pp. 90–95. doi:10.1109/RELPHY.1988.23432.

[90]   E.H. Wong, R. Rajoo, Moisture absorption and diffusion characterisation of packaging materials—advanced treatment, Microelectron. Reliab. 43 (2003) 2087–2096. doi:https://doi.org/10.1016/S0026-2714(03)00378-0.

[91]   J.-. Heinola, K.-. Latti, P. Silventoinen, J.-. Strom, M. Kettunen, A method to evaluate effects of moisture absorption on dielectric constant and dissipation factor of printed circuit board materials, in: 9th Int. Symp. Adv. Packag. Mater. Process. Prop. Interfaces (IEEE Cat. No.04TH8742). 2004 Proceedings., 2004: pp. 241–246. doi:10.1109/ISAPM.2004.1288020.

[92]   P. Alpern, K.C. Lee, Moisture-Induced Delamination in Plastic Encapsulated Microelectronic Devices: A Physics of Failure Approach, IEEE Trans. Device Mater. Reliab. 8 (2008) 478–483. doi:10.1109/TDMR.2008.2002340.

[93]   Xuejun Fan, Jiang Zhou, A. Chandra, Package structural integrity analysis considering moisture, in: 2008 58th Electron. Components Technol. Conf., 2008: pp. 1054–1066. doi:10.1109/ECTC.2008.4550106.

[94]   C. Xu, R. Kopf, J. Smetana, D. Fleming, HDPUG Pb-Free Board Materials Reliability

Project 2 moisture sensitivity and its effect on delamination, in: IPC APEX EXPO Tech. Conf., IPC - Association Connecting Electronics Industries, 2011: pp. 54–99.

[95]   Y. Chen, P. Li, The "popcorn effect" of plastic encapsulated microelectronic devices and the typical cases study, in: 2011 Int. Conf. Qual. Reliab. Risk, Maintenance, Saf. Eng., 2011: pp. 482–485. doi:10.1109/ICQR2MSE.2011.5976658.

[96]   K. O'TOOLE, B. ESSER, S. BINFIELD, C. HILLMAN, DFR SOLUTIONS, COLLEGE PARK MD, Pb-free reflow, PCB degradation, and the influence of moisture absorption, (n.d.) https://www.dfrsolutions.com/pb-free-reflow-pcb-de.

[97]   A. Caputo, L.J. Turbini, D.D. Perovic, Conductive Anodic Filament Formation Part II: Electrochemical Reactions Leading to CAF, J. Electron. Mater. 39 (2010) 92–96. doi:10.1007/s11664-009-0965-2.

[98]   A. Caputo, L.J. Turbini, D.D. Perovic, Characterization and Electrochemical Mechanism for Bromide-Containing Conductive Anodic Filament (CAF) Failure, J. Electron. Mater. 40 (2011) 1884. doi:10.1007/s11664-011-1694-x.

[99]   A. Caputo, L.J. Turbini, D.D. Perovic, Design limitations related to conductive anodic filament formation in a micro-world, Microsyst. Technol. 15 (2009) 39–44. doi:10.1007/s00542-008-0693-1.

[100]   A. Caputo, L.J. Turbini, D.D. Perovic, Conductive Anodic Filament (CAF) Formation Part I: the Influence of Water-Soluble Flux on Its Formation, J. Electron. Mater. 39 (2010) 85–91. doi:10.1007/s11664-009-0964-3.

[101]   Y. Shi, X. Wei, B. Tolla, The Role of Organic Amines in Soldering Materials, in: IPC APEX EXPO Conf. Proc., Circuit Insight, San Diego, USA, 2015.

[102]   S. College, Carboxylic Acids, Amines, and Amides, (n.d.). https://www.saddleback.edu/faculty/jzoval/mypptlectures/ch10_carb_acids_phen_amines/ chapter10_Carb_acids_phen_amines_web_current.pdf (accessed July 25, 2020).

[103]   K. Muraishi, Y. Suzuki, The thermal behaviour of dicarboxylic acids in various atmospheres, Thermochim. Acta. 232 (1994) 195–203. doi:https://doi.org/10.1016/0040-6031(94)80059-6.

[104]   B. Tolla, D. Jean, H. Bhavsar, Y. Shi, X. Wei, Reactivity of No-clean flux residues in electronic assemblies: a systematic study, in: SMTA Int., Rosemont, IL, USA, 2015.

[105]   D. Xu, X. Li, C. Wang, B. Xu, Study on wettability and corrosivity of a new no-clean flux for lead-free solder paste in electronic packaging technology, in: 2011 Second Int. Conf. Mech. Autom. Control Eng., 2011: pp. 1706–1708. doi:10.1109/MACE.2011.5987285.

[106]   M. Bixenman, D. Lober, A. Ailworth, K. Corporation, B. Tolla, D. Ph, J. Allen, D. Jean, K. Loomis, K. Corporation, Electrochemical Methods to Measure the Corrosion Potential of Flux Residues, in: IPC APEX EXPO, SMTNET, San Diego, USA, 2017.

[107]   E. B.N., Water Soluble Fluxes, their Reliability and their Usefulness as a Means of Eliminating CFC-113 Usage, Solder. Surf. Mt. Technol. 3 (1991) 16–23. doi:10.1108/eb037751.

[108]   Ooi Wan Koon, Mohd Jaffri Razai, Chan Boon Pin, Nurul Akmal Mohd Sharif, Study on IMC morphology and impact to solder joint performance for different halogen free (HF) flux in semiconductor application, in: 2010 34th IEEE/CPMT Int. Electron. Manuf. Technol.

Symp., 2010: pp. 1–6. doi:10.1109/IEMT.2010.5746722.

[109] A. Masatoshi, K. Katoh, K. Sumita, Liquid epoxy resin composition, US20070104959A1, 2006. https://patents.google.com/patent/US20070104959.

[110] Z. Kang, P. Michael, Effectiveness of conformal coatings on a PBGA subjected to unbiased high humidity, high temperature tests, Microelectron. Int. 17 (2000) 16–20. doi:10.1108/13565360010352136.

[111] M. Fridrichovsky, F. Steiner, M. Hirman, Comparison of the characteristics of PCB protective coatings, in: 2017 40th Int. Spring Semin. Electron. Technol., 2017: pp. 1–6. doi:10.1109/ISSE.2017.8000928.

[112] M. Suppa, C. Schauer, Thick film coating materials and fast conformal coating processes - a contradiction?, in: 2nd Int. IEEE Conf. Polym. Adhes. Microelectron. Photonics. POLYTRONIC 2002. Conf. Proc. (Cat. No.02EX599), 2002: pp. 165–171. doi:10.1109/POLYTR.2002.1020203.

[113] L.A. Nativi, Conformal coating systems, US4424252A, 1982.

[114] W.E. Dennis, B. VanWert, Ultraviolet curing conformal coating with dual shadow cure, US5008301A, 1989.

[115] L. Hitchens, Nexus, Classification, (n.d.). http://www.conformalcoatinghelp.com/index.php/ebook/materials/classification/ (accessed July 25, 2020).

[116] Techspray, The Essential Guide to Conformal Coating, (n.d.). https://www.techspray.com/the-essential-guide-to-conformal-coating (accessed July 25, 2020).

[117] East West, Which Type of Conformal Coating is Right for My PCB?, (n.d.). https://news.ewmfg.com/blog/which-type-conformal-coating-right-my-pcb (accessed July 25, 2020).

[118] L. Zou, C. Hunt, Test Method for Conformal Coating Protection Performance of Electronic Assembly in Harsh Environments (NPL Report DEPC MPR 060), Teddington, Middlesex, 2007.

[119] M. Tencer, Conductive aqueous layer formation at the gel-substrate interface in equilibrium with 100% RH environment, IEEE Trans. Components Packag. Technol. 23 (2000) 693–699. doi:10.1109/6144.888855.

[120] S. Manfred, Conformal coatings and their increasing importance for a safe operation of electronic assemblies, Circuit World. 33 (2007) 60–67. doi:10.1108/03056120710836954.

[121] C. Hunt, A. Mensah, A. Buxton, R. Holman, Determining conformal coating protection, Solder. Surf. Mt. Technol. 18 (2006) 38–47. doi:10.1108/09540910610717893.

[122] U. Rathinavelu, M.S. Jellesen, P. Moller, R. Ambat, Effect of No-Clean Flux Residues on the Performance of Acrylic Conformal Coating in Aggressive Environments, IEEE Trans. Components, Packag. Manuf. Technol. 2 (2012) 719–728. doi:10.1109/TCPMT.2012.2186456.

[123] S. Zhan, M.H. Azarian, M.G. Pecht, Surface insulation resistance of conformally coated printed circuit boards processed with no-clean flux, IEEE Trans. Electron. Packag. Manuf.

29 (2006) 217–223. doi:10.1109/TEPM.2006.882496.

[124] D.-H. Jung, J.-P. Jung, Review of the wettability of solder with a wetting balance test for recent advanced microelectronic packaging, Crit. Rev. Solid State Mater. Sci. 44 (2019) 324–343. doi:10.1080/10408436.2018.1490249.

[125] Y.S. Shi, X. Wei, B. Tolla, The Role of Organic Amines in Soldering Materials, (n.d.) 3–10.

[126] C. Nash, E. Bastow, Understanding SIR, in: 2011 IPC APEX EXPO Conf. Proc., 2011.

[127] Y. Zhou, L.J. Turbini, D. Ramjattan, B. Christian, M. Pritzker, Characterizing Corrosion Effects of Weak Organic Acids Using a Modified Bono Test, J. Electron. Mater. 42 (2013) 3609–3619. doi:10.1007/s11664-013-2705-x.

[128] P. Burton, P. Footner, D. Prichard, B. Richards, C. Hunt, Surface Insulation Resistance Measurements: A Review of the Various SIR Parameters (NPL REPORT CMMT (A) 48), Borehamwood, UK, 1996.

[129] Topline, Cleanliness and Residue Evaluation Test Kits Compatible IPC-B-52, (n.d.). https://www.topline.tv/952000_kit.html (accessed March 1, 2021).

[130] C. Puechagut, A. Laügt, E. Guéné, R. Anisko, Solder paste residue corrosivity assessment: Bono test, in: 2015 Eur. Microelectron. Packag. Conf., 2015: pp. 1–7.

[131] K. Tellefsen, Green Residues and Electrical Reliability, in: Proc. Int. Conf. Electron. Assem. Mater. Process Challenges, Atlanta, Georgia, USA, 1998.

[132] K. Piotrowska, M. Grzelak, R. Ambat, No-Clean Solder Flux Chemistry and Temperature Effects on Humidity-Related Reliability of Electronics, J. Electron. Mater. 48 (2019) 1207–1222. doi:10.1007/s11664-018-06862-4.

[133] V. Verdingovas, M.S. Jellesen, R. Ambat, Influence of sodium chloride and weak organic acids (flux residues) on electrochemical migration of tin on surface mount chip components, Corros. Eng. Sci. Technol. 48 (2013) 426–435. doi:10.1179/1743278213Y.0000000078.

[134] H. Conseil, V. Verdingovas, M.S. Jellesen, R. Ambat, Decomposition of no-clean solder flux systems and their effects on the corrosion reliability of electronics, J. Mater. Sci. Mater. Electron. 27 (2016) 23–32. doi:10.1007/s10854-015-3712-x.

[135] V. Verdingovas, M.S. Jellesen, R. Ambat, Relative effect of solder flux chemistry on the humidity related failures in electronics, Solder. Surf. Mt. Technol. 27 (2015) 146–156. doi:10.1108/SSMT-11-2014-0022.

[136] M. Mahdavian, M.M. Attar, Another approach in analysis of paint coatings with EIS measurement: Phase angle at high frequencies, Corros. Sci. 48 (2006) 4152–4157. doi:https://doi.org/10.1016/j.corsci.2006.03.012.

[137] R. Vlasak, I. Klueppel, G. Grundmeier, Combined EIS and FTIR–ATR study of water uptake and diffusion in polymer films on semiconducting electrodes, Electrochim. Acta. 52 (2007) 8075–8080. doi:https://doi.org/10.1016/j.electacta.2007.07.003.

[138] G.W. Warren, P. Wynblatt, M. Zamanzadeh, The role of electrochemical migration and moisture adsorption on the reliability of metallized ceramic substrates, J. Electron. Mater. 18 (1989) 339–353. doi:10.1007/BF02657426.

[139] S. Lauser, T. Richter, V. Vadimas, R. Ambat, Electrochemical Impedance Spectroscopy (EIS) for Monitoring the Water Load on PCBAs Under Cycling Condensing Conditions to

Predict Electrochemical Migration Under DC Loads, in: 2019 IEEE 69th Electron. Components Technol. Conf., 2019: pp. 515–521. doi:10.1109/ECTC.2019.00084.

[140] K. Piotrowska, V. Verdingovas, R. Ambat, Humidity-related failures in electronics: effect of binary mixtures of weak organic acid activators, J. Mater. Sci. Mater. Electron. 29 (2018) 17834–17852. doi:10.1007/s10854-018-9896-0.

3. Materials and experimental

3.1. Materials used for investigation

This chapter provide an overall summary of the materials and experimental methods used as part of the studies reported in the appended papers (Chapter 4-9). More detailed presentation of materials and experimental methods used in connection with each work can be found in individual chapters.

3.1.1. Materials use for solder alloy investigation

Five commercial SAC alloy reflow solder pastes were used in this investigation and **Table 3.1** shows the elemental compositions of the metallic particles in the pastes.

Table 3.1 *Elemental composition of five solder alloys used for the investigation.*

Solder alloy	Sn [wt%]	Ag [wt%]	Cu [wt%]	Bi [wt%]	Sb [wt%]	Ni [wt%]
SAC 305	96.5	3.0	0.5	-	-	-
SACX Plus 0307	98.95	0.3	0.7	-	-	0.05
SACX 0807	98.4	0.8	0.7	0.1	-	-
SACX Plus 0807	98.45	0.8	0.7	-	-	0.05
InnoLot	90.95	3.8	0.7	3.0	1.4	0.15

The solder alloy ingots were formed by melting commercial solder pastes under 240°C for 30 min using Pyrex® glass tube in a vacuum chamber with Ar gas protection. The melted solder alloys were cooled in water. The diameter and the height of the ingots were 1.5 cm and 1 cm respectively.

The SIR patterns shown in **Figure 3.1(a)** were made by conventional photolithography and wet etching processes using copper wire contained FR4 (fiber-glass epoxy resin) as a substrate. Five solder alloy pastes were directly coated on copper traces using stencil printing and reflow methods. The reflow soldering profile used was shown in **Figure 3.1(b).** The width of the interdigitated pattern trace on the FR4 test board is 0.4 mm, and the gap size is 0.2 mm (designed according to the IPC-B-24 test board). The dimension of the experimental testing region on the SIR pattern is 8.5 mm × 12 mm with the overlapping length of soldered trace about 7.5 mm. The total length of the 21 overlapping soldered trace is 157.5 mm, which provides oppositely biased electrodes for accelerated humidity/temperature cycling tests.

Specimens for potentiostatic pitting test were prepared by soldering a copper wire on back side of the solder alloy in order to create an electrical connection. The wire connected solder ingots were cold mounted using epoxy resin. Final surface finishing of the specimen was prepared using

50 nm neutral alumina suspension. An electrical insulation mask was applied to the surface with an exposed working area of 28.26 mm^2.

For water droplet (WD) testing, the solder alloys were cut along the diameter and copper wires were connected to two parts of alloy ingots as cathode and anode. Two electrodes were cold mounted in parallel with a gap size of 0.5 mm as shown in **Figure 3.1(c)**. The surface of WD samples was prepared using #1000 grinding paper prior to experiments.
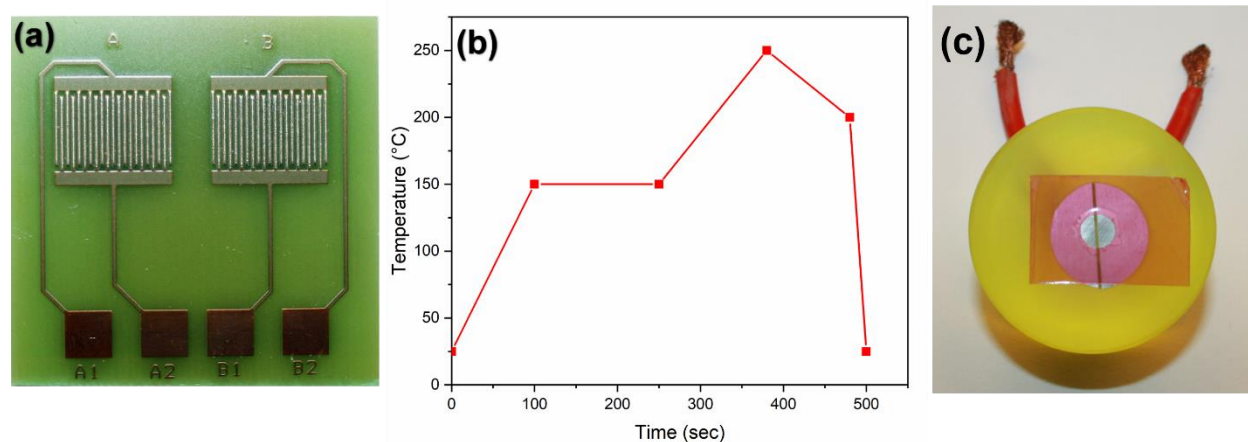
Figure 3.1 *(a) Test print circuit board (PCB) with two soldered SIR patterns, (b) reflow soldering temperature profile used for making the SIR pattern with different solder pastes, (c) epoxy mounted solder ingot sample for WD testing.*

3.1.2. Materials used for flux activator investigation

Table 3.2 shows the chemicals used for the investigations related to flux activator described in Chapter 5-7. All chemicals used are in analytical grade (Sigma Aldrich, USA). The SIR pattern shown in **Figure 3.2** was used for the electrochemical tests meant to reflect the humidity robustness of systems containing amine compounds as activators. The interdigitated pattern comprised of a hot air solder levelled (HASL) Sn-0.7Cu alloy as surface finish plated on copper tracks with an FR4 laminate as a substrate of IPC-4101/21 test board. The active testing area of the SIR pattern was 13 mm × 25 mm with a 0.3 mm pitch size and electrode width of 0.4 mm. The overlapping length of the adjacent pitch lines was 10.8 mm × 41 set, which in total provided 442.8 mm for the DC and AC tests.

Table 3.2. Chemicals used in the flux activator studies.

Alkanolmines	Amino acids	Alkyl amine	Aromatic amine	WOAs
Ethanolamine	Alanine	Tripropylamine	Naphthylamine	Succinic acid
Diethanolamine	Glutamine			Adipic acid

Triethanolamine	Glycine			Glutaric acid
Diisopropanolamine	Serine			
Triisopropanolamine				
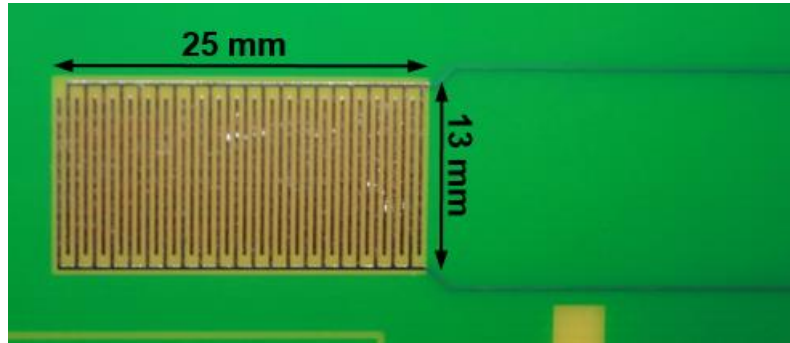
Figure 3.2 *Picture of the SIR comb pattern used for electrochemical tests.*

The contamination level of the flux activator on The SIR patterns was set at 100 µg/cm^2. In order to simulate the state and the amount of residue left on the PCBA after the wave soldering process, thermal activation of amine-contaminated SIR patterns was performed at 175℃ and 240℃ for 45 sec in a Techno HA-06 oven. The thermal activation at 240℃ aimed to simulate the proper soldering temperature existing at the interface between the PCBA and solder wave (in wave soldering process simulating bottom part of the PCBA).

Solderability assessment was conducted using a wetting balance and hot plate spreading tests. The wetting balance test was carried out using copper coupons according to the IPC-TM-650 2.4.14.2, i.e. a size of 6 mm × 25 mm × 0.5 mm prepared using electrical discharge machining. Cleaning of Cu coupons was conducted based on ISO 9455-16 international standard. For the hot plate spreading test, Cu-37Zn coupon substrate with a size of 40 mm × 75 mm × 1 mm was prepared. Cleaning of the brass coupons was conducted as described in the ISO 9455-16 standard.

3.1.3. Materials use for reflow flux investigation

Table 3.3 shows the formulation of the solder pastes used in Chapter 8. **Figure 3.3** shows the test vehicles used in the investigation. Before stencil printing, all the test vehicles was cleaned using isopropanol in ultrasonic bath for 5 min and dried in compressed air. **Figure 3.3**(a) shows the SIR interdigitated patterns with 300 µm pitch size and electrode with 400 µm width (IPC-4101/21). The SIR pattern contains the adjacent pitch lines of 10.8 mm × 41 sets in a testing area of 13 mm × 25 mm. The surface finishing of the SIR substrate is 1 µm chemical vapor deposited Sn on 35 µm Cu conductive track. Before going through reflow soldering process, the stencil with

thickness of 200 μm was used for the solder paste printing on SIR pattern. **Figure 3.3**(b) shows the open surface of SMT substrate used for flux residue characterization, which contains 9 solder points with area of 2 mm × 2 mm. The solder area of SMT substrate was printed with 250 μm thick solder paste using stencil. **Figure 3.3** (c)(d) shows the in-house test rig imitating dummy SMT component design and the electrical connection of two adjacent solder joints. Test rigs with 0.5 mm and 1 mm stand-off heights were manufactured for the investigation of stand-off height effect on the humidity robustness. The overlapping area of 2 cm × 2 cm for upper part and bottom part of SMT substrates was used for the testing. Same amount of solder paste was applied on the solder points for test rigs with both 0.5 mm stand-off height and 1 mm stand-off height using 1 mm stencil. The tested solder joints was on the adjacent position with distance of 2 mm, which were electrically connected from the back side of upper and bottom FR-4 substrates.

Table 3.3 *Formulation of the solder pastes used for Chapter 8.*

Solder paste (SP)	Resin	WOA	Solvent	Amine	Halogen	Halide	Surfactant	Solder alloy
SP1	✓	2 types	Ester, alcohol				✓	SAC 305
SP2	✓	1 type	Ester, alcohol				✓	SAC 305
SP3	✓	1 type	Ester, alcohol	✓	✓		✓	SAC 305
SP4	✓	2 types	Ester, alcohol			✓	✓	SAC 305

After stencil printing of solder paste, all the test vehicles were subjected to the reflow process in a Techno HA-06 furnace under air-static condition. During the soldering process, surface temperature of the test vehicles increased from 25℃ to 170℃ within 125 sec, then increased to peak temperature of 248℃ within 60 sec, and cooled in the oven for 60 sec.
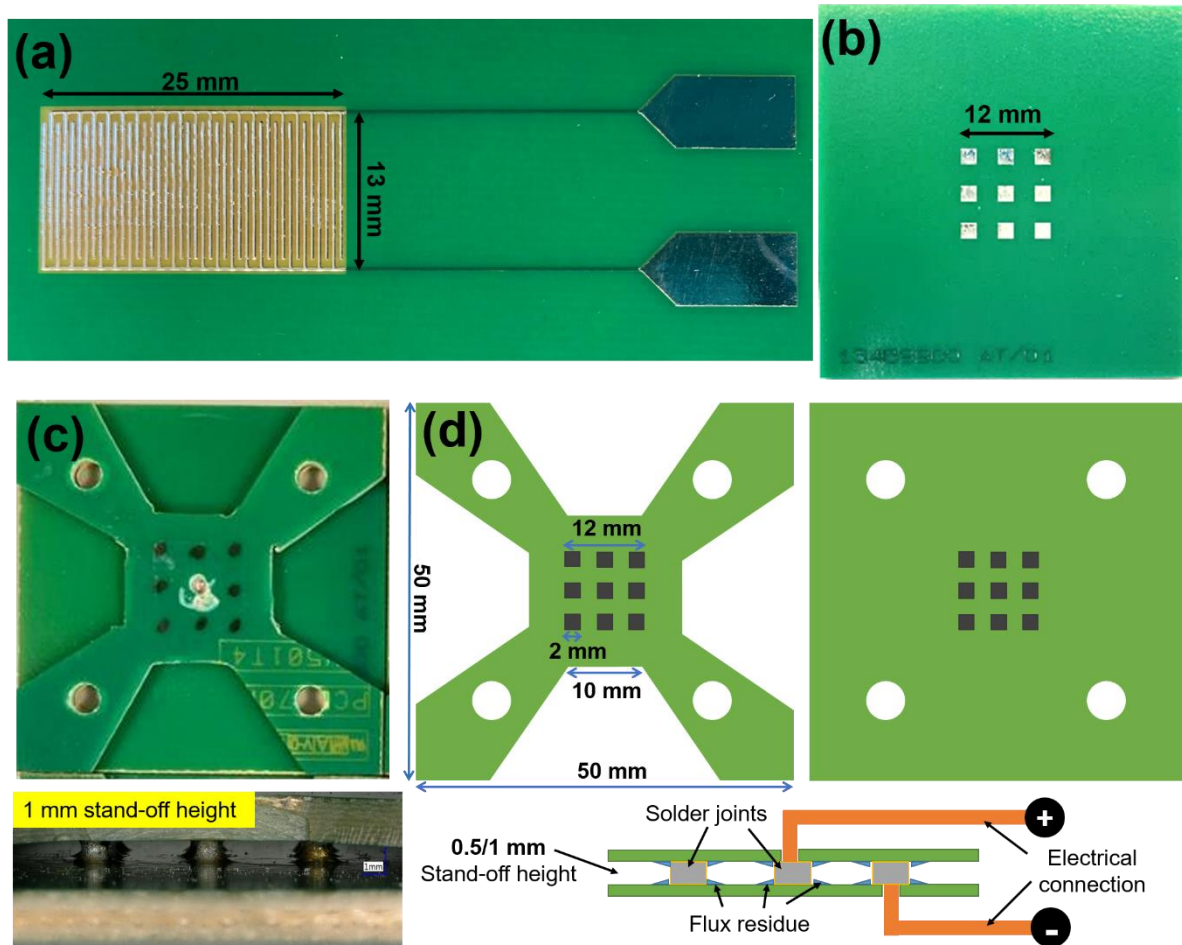
***Figure 3.3** Test vehicles used in the investigation: (a) SIR pattern with interdigitated electrodes used for printing the paste and testing, (b) an open pad imitating SMT land pattern for printing paste and subsequent residue characterization, (c) test rig imitating a dummy SMT component for stand-off height investigation after soldering, (d) schematic of the dummy SMT component in (c) showing bottom and upper part and schematic of the cross-sectional view with electrical connection made for testing.*

3.1.4. Materials use for conformal coating investigation

Figure 3.4 shows the SIR testing vehicle used for the conformal coating investigation in Chapter 9. The testing area was 13 mm × 25 mm with 0.3 mm of gap size and 0.4 mm of electrode width. The overlapping length of two electrodes was 10.8 mm × 41 sets. Surface finish for the interdigitated electrodes was hot air solder leveling using Sn-0.7Cu on the 35 µm thick Cu conductive lines. To prepare the substrate for the coating, 30 µL flux [35] was applied on isopropanol cleaned SIR pattern in order to imitate the presence of flux residue after manufacturing process. Applying 30 µL flux resulted in 162 µg/cm^2 Flux A residue and 372 µg/cm^2 Flux B residue on the SIR interdigitated pattern respectively due to different fraction of the solid

content. **Table 3.4** shows the details of the fluxes used for contamination of SIR pattern. Flux A contains adipic acid as activator, which was known as mild flux with benign corrosivity, low hygroscopicity, and less active in terms of solderability. Flux B with blend glutaric-adipic acid activator has higher solid content and acid number than Flux A, which provides better solderability, but higher hygroscopicity and corrosivity. Another set of clean test vehicles with SIR pattern were used as reference samples.
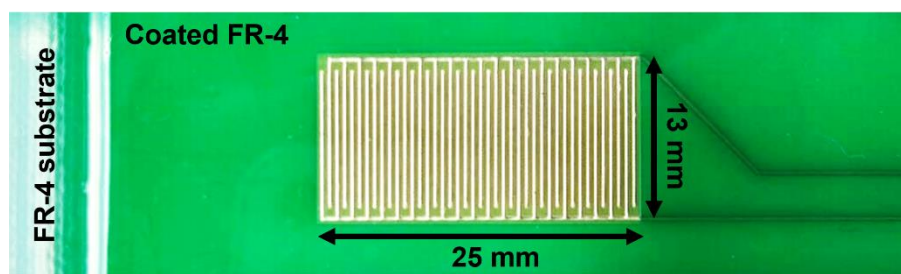
Figure 3.4 *Coated PCB board with SIR pattern for the electrochemical testing.*

Table 3.4 *Fluxes used for imitating contamination on the SIR pattern*

	IPC J-STD-004 classification	Solid content (wt.%)	Activator	Acid number (mg KOH)	Applied volume (ml)	Contamination level ($\mu g/cm^2$)
Flux A	REL0	2.2	Adipic acid	15.80	30	162
Flux B	ORM0	4.0	Glutaric acid Adipic acid	36.85	30	372

Conformal coatings used for testing:

Three types of commercial conformal coatings were used in the present work as shown in **Table 3.5**. The application solutions of coatings were based on the manuals of the actual products, including thickness, applying method and curing method etc. In parallel, another set of non-coated PCB panels were used as reference.

Table 3.5 *Details of conformal coating application used in the present research.*

Conformal coating	Thickness over electrodes (μm)	Applying method	Curing method
Synthetic rubber	60	Spray	Ambient
Elastomeric acrylate	80	Spray	Ultraviolet
Urethane/acrylate	150	Spray	Ultraviolet

3.2. Electrochemical analysis and climatic reliability assessment

3.2.1. Experimental equipment

Climatic chamber

Humidity robustness assessment was carried out in "Espec PL-3KPH" climatic chamber with a certainty of $\pm 0.3℃$ and $\pm 2.5\%$ RH of the test conditions.

Potentiostat

A multichannel Biologic VSP potentiostat was used for the electrochemical investigation.

3.2.2. Potentiodynamic polarization test

The potentiodynamic polarization tests were performed on the freshly polished surface of solder alloy with an exposed area of 0.4 cm^2 and in 100 ml of 3.5 wt.% NaCl aqueous solution. The voltage-sweep rate was set at 60 mV/min in a potential range from -200 mV to 300 mV. The reference electrode used was Ag/AgCl (aqueous saturated KCl). Each experiment was repeated five times to evaluate the standard deviation of the results. Potentiostatic pitting test was conducted to understand the micro-galvanic effect of different phases in solder alloys under DC bias loading. For the potentiostatic pittng test, a 50 mV potential over the open circuit potential was applied potentiostatically, and the test was conducted on a fine polished solder surface for 2 min after 5 min stabilization of open circuit potential.

The polarization of Cu foil was conducted using Paracell (Gamry Instruments, USA) with an exposed area of 2.85 cm^2 in 0.1 M amine or WOA aqueous solution. Open circuit potential (OCP) was record after 30 min stabilization. For the polarization, the scan range of the polarization was set from -250 mV to 1500 mV vs. OCP using Ag/AgCl electrode as reference electrode (RE). The scan rate used for the experiment was 60 mV/min. Each experiment was repeated three times with good consistency.

3.2.3. EIS measurement

EIS experiment was conducted on the two-electrodes system to investigate effect of humidity exposure on the impedance between adjacent solder joints with different stand-off height. Scanning range of frequency was set from 100 kHz to 100 mHz with the sinusoidal amplitude of 10 mV over the base potential of 0 V vs. reference electrode. EIS scan was recorded every 24 hours by EC-lab and the total duration of the experiment was 15 days.

3.2.4. Single frequency EIS measurement

Single frequency EIS at 10 kHz with the amplitude of 10 mV was applied on the flux activator contaminated SIR pattern in order to record the moisture absorption RH of flux activator during humidity ramping from 30% RH to 99% RH in 12 hours. The moisture desorption RH was measured during humidity ramping from 99% RH to 30% RH in next 12 hours. Before subjecting the single frequency EIS measurement, flux activator contaminated SIR patterns were stabilized at 30% RH in climatic chamber for 6 hours.

3.2.5. Chronoamperometry (CA) testing

CA technique was used to investigate the leakage current or ECM triggering capacity of flux activator contaminated SIR pattern under different humidity exposure conditions namely at 60% RH, 70% RH, 80% RH, 90% RH and 98% RH respectively. Before conducting the CA measurement, the flux activator contaminated SIR pattern was stabilized in the climatic chamber for 2 hour. The CA measurement for each type of flux activator contaminated SIR pattern was conducted under 10 V DC bias loads for 24 hours. Leakage current level of flux activator contaminated SIR pattern was recorded by EC-lab software.

3.3. Solderability assessment using wetting balance and hot plate test

3.3.1. Wetting balance test

Solderability tests were performed using the "Must 3 wetting balance tester" (GEN 3, UK), which allows for the measurement of the extent of wetting of molten solder on the copper coupons, which surface was initially activated by amine activators. The Cu coupon was initially immersed in the model flux solution to a depth of 10 mm and drained off the extra flux by keeping it vertically on a clean filter paper following the procedure described in IPC-TM-650 2.4.14.2. After 20 sec pre-heating of the SAC 305 solder bath incorporated in the wetting balance equipment occurred at a temperature of 270℃, which was followed by the Cu samples being dipped in the molten solder bath for 10 sec with an immersion depth of 5 mm. Both the immersion speed and withdraw speed of Cu substrate to solder bath were set to 20 mm/s.

3.3.2. Hot plate spreading test

Additional evaluation of amine solderability was conducted using the hot plate spreading test based on IPC-TM-650 2.4.46 standard using brass coupons. Solderability tests were performed using a "SD160 digital hotplate" (Stuart Equipment, UK), which allows for visual assessment of the extent of wetting of molten solder on the brass coupons, which surface was initially activated by amine activators. The source of molten solder was an O-ring of 1 cm diameter prepared from

the flux-free SAC 305 alloy and placed on the brass substrate. 50 µL of the model flux was applied at the center of an O-ring placed on the plate, and subsequently the preheating of the sample was conducted at 160℃ for 2 sec. Subsequently, the test system was transferred to another hotplate with a precisely controlled temperature of 270℃ in order to melt the solder wire and assess the solder spreading extent when the O-ring melted. The solderability level was visually assessed based on the description in the IPC-TM-650 number 2.4.46 standard.

3.4. Material characterization methods

3.4.1. Light optical microscopy (LOM)

In order to observe the corrosion of the SIR pattern, reflow flux distribution on reflow pad, solder quality, and the blisters of the conformal coating, light optical microscopy inspection was conducted using a VHX digital microscope (Keyence, Japan).

3.4.2. X-ray diffraction (XRD)

The phase analysis of SAC solder alloys was carried out using X-ray diffractometer (D8 Advance, Bruker, USA) with a molybdenum anode under the power of 40 kV and 40 mA. The scanning range was set from 10.5° to 35.6°. The increment and scan speed was set as 0.01 and 1 respectively.

3.4.3. Scanning electron microscopy (SEM) and Energy dispersive spectroscopy (EDS)

Corrosion morphology of the solder alloy surface after tests was investigated using scanning electron microscope (Quanta 200 FEG, FEI, USA) under backscattered electron (BSE) mode at 20 kV. The cross section of soldered Cu coupons, coated PCBA and corrosion product built on SIR pattern was inspected under secondary electron mode at 15 kV. The surface morphology The morphology of the climatically exposed coating samples were inspected under secondary electron mode at 3 kV. Chemical mapping analysis of the solder alloys and corrosion product was conducted using energy dispersive spectroscopy (EDS) at 15-20 kV (Oxford Instrument, UK).

3.4.4. Scanning kelvin probe force microscopy

The Volta potential mapping was performed using a Multimode 8 atomic force microscopy (AFM) (Bruker, USA) using the mode of amplitude modulation method. The AFM microscope was equipped with conductive Point Probe Plus (Nanosensors, Switzerland) electrostatic force microscopy. The silicon cantilever attached to the AFM was in a radius of 10 nm and coated with 25 nm chromium and platinum. The tip of cantilever possessed a resonance frequency in a range of 70 - 80 kHz. The dual-scan mode was used over an area of 80 µm × 80 µm of polished solder alloys with the scan rate of 0.2 Hz under the ambient condition of 25℃, 60% RH. The Volta

potential mapping result was collected by lifting the tip 50 - 100 nm above the surface in the second scan in addition to the obtained surface topography signal in the first mechanical intermittent AFM scan.

3.4.5. Thermogravimetric analysis (TGA) and differential thermal analysis (DTA)

The nature of amines subjected to varying temperatures were investigated using TGA and DTA techniques. TGA analysis was aim to investigate the liquid-gas phase transformation temperature of flux acitvator, whereas DTA analysis was employed to investigate the thermal decomposition temperature of the flux activators. Flux activators were subjected in a alumina crucible for the testing. Argon gas was used as a protection gas during the experiments. The experiment was performed with a temperature ramping rate of 20℃/min in a range from room temperature to 1000℃.

3.4.6. Fourier-transform infrared spectroscopy(FT-IR)

The flux activators and coatings were analyzed using the Nicolet iN10 MX infrared imaging microscope (Thermo Fisher Scientific, USA) with a Ge attenuated total reflectance (ATR) tip.

4. Influence of Ni, Bi, and Sb additives on the microstructure and the corrosion behavior of Sn-Ag-Cu solder alloys

Feng Li, Vadimas Verdingovas, Kai Dirscherl, Gábor Harsányi, Bálint Medgyes, Rajan Ambat

Abstract: Sn-Ag-Cu solder alloys were usually modified using trace elements to achieve various properties. This paper investigated the effect of additives of Ni, Bi, and Sb on the microstructure and corrosion behavior of SAC alloys under application condition. Investigation was carried out using both solder alloy ingots and reflow-soldered surface insulation resistance interdigitated patterns by electrochemical methods under humid and corrosive conditions. Microstructure analysis was performed using X-ray diffraction, scanning electron microscopy, energy dispersive spectroscopy etc. Volta potential distribution in the bulk of the alloy was analyzed by Scanning Kelvin Probe Force Microscopy. Results show the passivation domain of five tested solder alloys did not influence the susceptibility of electrochemical migration under 5 volt DC bias loading. Ni and Bi additives resulted in lower susceptibility of electrochemical migration due to homogeneity of the IMCs distribution in the bulk alloys. Bi precipitates in InnoLot alloy participated micro-galvanic corrosion as cathode rather than Ag containing phase as known before.

Keywords: Electronic corrosion, solder alloy, electrochemical migration, microstructure, intermetallic compound.

I.   INTRODUCTION

The Sn-Pb solder alloys have been widely implemented in the electronic industry due to their low cost, good wettability as well as excellent thermal and mechanical properties [1-2]. However, nowadays the conventional Sn-Pb solder alloys are experiencing global phase out due to the toxicity of lead. Therefore, various Sn based lead-free solder alloys are under development. Most popular lead-free solder alloy contains Sn, Ag, and Cu, also known as SAC alloy. However, there is a challenge to find optimum performance of physical, mechanical, and electrochemical properties, which suggested by alloying Bi, Zn, Sb, Cu, Ag, Ni, and other elements [3]. Since peak soldering temperature has a significant influence on the printed circuit board assemblies (PCBAs) and components due to component damaging [4], eutectic or near-eutectic alloys with a melting temperature close to Sn-37Pb alloys (Te=183°C) are favorable for electronic applications [5]. The melting temperature of Sn-Bi eutectic alloy is 139°C, which is too low for the loss of mechanical properties due to the thermal aging by the self-heating of electronic [3]. The melting temperature of Sn-Zn alloy, in contrast, is 198.5°C, which is close to the Pb-Sn alloy. At the same time, the

poor wetting properties, severe oxidation during the soldering process, and corrosion issues are problematic in manufacturing [3][6]. Sn-Sb solder alloys are promising solder alloys, but they are used usually for high temperature applications due to higher melting temperature [3]. According to the reasonable melting temperature, superior wettability and mechanical properties, the SAC alloys are more frequently used today as the most promising alternatives of Sn-Pb solder alloys for many commercial applications [1][7].

Correspondingly, there are several researchers focusing on the additives and composition effects of SAC alloys in order to enhance the performance in various aspects. Liu et al. reported the role of Bi and Ni additives in the improvement of fatigue and joint properties by the refinement of the microstructure [8].The effect of Cu content on the solidification temperature range of SAC alloy solder joint was reported by Kotadia [9]. Kanchanomai and Zhao et al. [10-11] reported the decrease in solidus temperature when increasing Bi content in SAC alloy, whereas the liquidus temperature is not sensitive to Bi content. In InnoLot alloy, substitutional Sb in β-Sn matrix provided solid solution strengthening to compensate the loss of strength by the coarsening of Ag_3Sn phase, while Bi precipitates at grain boundaries to prevent the motion of dislocations providing improved strength for the alloy [12]. Addition of Ni effectively inhibited the growth of Cu_3Sn brittle phase and improved the drop shock performance [13][14]. However, the influence of the additives to the corrosion properties of solder alloys was not well explained and the available literature connected to these aspects are presently very limited.

The corrosion investigation of SAC alloy was mainly focused on the aspects of electrochemical investigation of conventional SAC alloy bulk materials and as part of the corrosion failure of electronics under electric field conditions with humidity exposure. For the investigation of the corrosion performance of the bulk alloys, microstructure was mainly controlled by aging period and cooling rate [1][15]. Wang et al reported the microgalvanic corrosion decreased by increasing the size of Ag_3Sn [1], whereas Kaushik et al reported the fine dispersion of Ag_3Sn prohibited the localized corrosion attack [15]. However, aging and cooling rate control are not feasible in relation to electronic production and automated soldering process in actual industrial application. Rosalbino et al reported the corrosion products presented on the surface of Sn-3Ag-3Cu enhanced corrosion resistance [16], but the high Cu content alloying will increase the pastry range variation and cause other issues [17]. Therefore, many other properties of solder alloy and application requirements mentioned above must be taken into consideration when pursuing corrosion investigation.

On the other hand, some investigations focused on the corrosion failure of electronics induced by electrochemical migration (ECM). ECM is a well-known humidity induced corrosion related failure mechanism for electronics [18]. Usually on PCBAs, voltages are higher than 2 volt, which results in dissolution of metal ions and hydrolysis of water under humid exposure. The corrosion of metal at anode generates metallic ions, and hydrolysis generates hydrogen ions. Due to the close spacing between the positively and negatively biased terminals, metallic ions migrate through electrolyte layer towards cathode and deposit to form a metal dendrite between anode and cathode. Electrolysis of water also takes place at the cathode generating hydroxide ions. The mechanism of ECM is complex, which also depends on the local pH changes caused by the hydrolysis reactions. Detailed discussion of the ECM mechanism is beyond the scope of this paper, and can be found elsewhere [18]. The ECM failures on various lead free solder alloys were investigated using several testing methods under electric field and humid conditions. For example: thin electrolyte layer method [19-22], water droplet method [21-24], and climatic chamber exposure test on surface insulation resistance (SIR) pattern with chronoamperometry and electrochemical impedance spectroscopy techniques [23]. These studies mainly reported ECM susceptibility [24], dendrite morphology [20], and chemical composition of the dendrites [20][25]. However, none of these works clearly demonstrates the influence of additives on microstructure of the SAC alloy family used in the industry and their corrosion mechanism.

The present work was aim to investigate the influence of the Ni, Sb, and Bi additives on the microstructure and corrosion properties of SAC alloy under application condition. Studies were carried out based on bulk material prepared by five commercialized Ni, Sb and Bi containing SAC pastes as well as reflow-soldered institute of printed circuits (IPC) standard designed SIR interdigitated pattern. Corrosion behaviors of the alloys were investigated using electrochemical methods in bulk electrolyte, while the reflow-soldered SIR patterns were tested under humid condition adapted from the international electrotechnical commission (IEC) standard. Volta potential mapping was carried out using scanning Kelvin probe force microscopy (SKPFM) to understand the influence of Volta potential distribution of alloys on the corrosion behavior. Corrosion behavior of the alloys under application conditions was correlated to the microstructure of the alloy and electrochemical behavior.

II.   MATERIALS AND EXPERIMENTAL METHODS

Solder pastes

Five commercial SAC alloy reflow solder pastes were used in this investigation and **Table 4.1** shows the elemental compositions of the metallic particles in the pastes.

Table 4.1 Elemental composition of five solder alloys used for the investigation.

Solder alloy	Sn [wt%]	Ag [wt%]	Cu [wt%]	Bi [wt%]	Sb [wt%]	Ni [wt%]
SAC 305	96.5	3.0	0.5	-	-	-
SACX Plus 0307	98.95	0.3	0.7	-	-	0.05
SACX 0807	98.4	0.8	0.7	0.1	-	-
SACX Plus 0807	98.45	0.8	0.7	-	-	0.05
InnoLot	90.95	3.8	0.7	3.0	1.4	0.15

Solder alloy ingots

The solder alloy ingots were formed by melting commercial solder pastes under 240°C for 30 min using Pyrex® glass tube in a vacuum chamber with Ar gas protection [26]. The melted solder alloys were cooled in water. The diameter and the height of the ingots were 1.5 cm and 1 cm respectively.

Specimen preparation for potentiostatic pitting and water droplet testing

Specimens for potentiostatic pitting test were prepared by soldering a copper wire on back side of the solder alloy in order to create an electrical connection. The wire connected solder ingots were cold mounted using epoxy resin. Final surface finishing of the specimen was prepared using 50 nm neutral alumina suspension. An electrical insulation mask was applied to the surface with an exposed working area of 28.26 mm^2.

For water droplet (WD) testing, the solder alloys were cut along the diameter and copper wires were connected to two parts of alloy ingots as cathode and anode. Two electrodes were cold mounted in parallel with a gap size of 0.5 mm as shown in **Figure 4.1**. The surface of WD samples was prepared using #1000 grinding paper prior to experiments.

Printed circuit board with interdigital electrode structures using solder alloys

The SIR patterns shown in **Figure 4.2**(a) were made by conventional photolithography and wet etching processes using copper wire contained FR-4 (fiber-glass epoxy resin) as a substrate. Five solder alloy pastes were directly coated on copper traces using stencil printing and reflow methods. The reflow soldering profile used was shown in **Figure 4.2**(b). The width of the interdigitated pattern trace on the FR4 test board is 0.4 mm, and the gap size is 0.2 mm (designed according to the IPC-B-24 test board). The dimension of the experimental testing region on the SIR pattern is 8.5 mm × 12 mm with the overlapping length of soldered trace about 7.5 mm. The total length of the 21 overlapping soldered trace is 157.5 mm, which provides oppositely biased electrodes for accelerated humidity/temperature cycling tests.
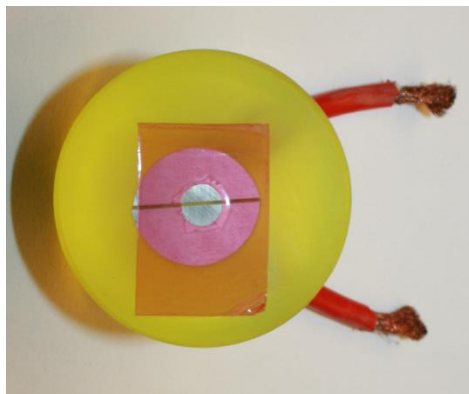
Figure 4.1 *Epoxy mounted solder ingot sample for WD testing.*
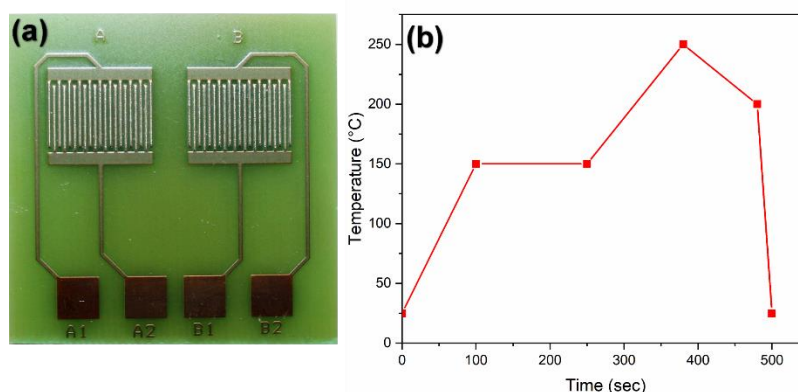
Figure 4.2 *(a) testing print circuit board (PCB) with two soldered SIR patterns, (b) reflow soldering temperature profile used for making the SIR pattern with different solder pastes.*

SIR pattern cleaning

In order to avoid the influence of acidic nature of reflow residue on SIR pattern, the flux residue on the test board was first cleaned in ultrasonic isopropanol bath for 4 hours, then 2 min brush cleaned with a commercial flux cleaning solution. The chemical composition of the cleaning solution contains 2-methylpentane (12.0–25.0 wt%), 3-methylpentane (1.0–20.0 wt%), 2,3-dimethylbutane (1.0-20.0 wt%), 2,2-dimethylbutane (1.0-20.0 wt%), n-hexane (0.1-2.0 wt%), acetone (20.0-50.0 wt%), and methanol (1.0-2.0 wt%). After immersion in isopropanol for 4 days, the soldered SIR pattern was rinsed using 98% ethanol and dried by compressing airflow prior to using for experiments.

Corrosion testing of solder alloys in bulk electrolytes

The potentiodynamic and potentiostatic tests were performed using a "Biologic VSP" multichannel potentiostat (Bio-Logic Instrument, France). The potentiodynamic polarization tests were performed on the freshly polished surface of solder alloy with an exposed area of 0.4 cm2 and in

100 ml of 3.5 wt.% NaCl aqueous solution. The voltage-sweep rate was set at 60 mV/min in a potential range from -200 mV to 300 mV. The reference electrode used was Ag/AgCl (aqueous saturated KCl). Each experiment was repeated five times to evaluate the standard deviation of the results. Potentiostatic pitting test was conducted to understand the micro-galvanic effect of different phases in solder alloys under DC bias loading. For the potentiostatic pittng test, a 50 mV potential over the open circuit potential was applied potentiostatically, and the test was conducted on a fine polished solder surface for 2 min after 5 min stabilization of open circuit potential.

Electrochemical migration behavior under water droplet testing

The experiment was conducted with chronoamperometry technique using a "Biologic VSP" multichannel potentiostat. For good statistics, 10 WD tests were conducted in parallel under different electrolyte conditions. 5 volt DC loading was applied to the specimen and the leakage current (LC) value was recorded using EC-Lab software. Unwanted surface area of the electrode was masked using electrical insulation tape with an exposed working area of 19.63 mm^2. Three types of electrolytes were used for testing namely: (i) 15 µL pure water (Millipore, Synergy UV), (ii) 20 µL of NaCl with concentration of 0.0156 g/L, and (iii) 20 µL of NaCl solution with concentration of 0.00156 g/L. The WD tests were performed at room temperature (25 ± 1°C) in a high humidity polystyrene chamber in order to control the effect of airflow and reduce the evaporation of water droplets. The experiment was in-situ recorded using an "AD7013MZT Dino-Lite" digital microscope.

Corrosion reliability testing under humid conditions using sir patterns

The accelerated humidity/temperature tests were conducted in "Espec PL-3KPH" climatic chamber with a certainty of ± 0.3°C and ± 2.5% RH. Before starting the tests, the samples were set to equilibrate with the environment in the climatic chamber at 25°C / 97% RH for 1 hour. After the stabilization period, the testing was conducted under cycling temperature between 25°C and 55°C, while the RH value was set constant at 97%. These cycling test conditions were adapted from IEC 60068-2-30 environmental testing standard. The duration of the experiment was 168 h. The temperature cycling at high RH induced transient water condensation on the surface of test board with SIR pattern, which acted as the medium for ion transport between the interdigitated electrodes. The leak current measured shows the faradaic current caused by the electrochemical process between electrodes. If this occurred on an actual electrical circuit, it could have caused reliability problem due to the interference of this leakage current with electrical functionality. Therefore, the level of leakage current and sudden increase in leakage current due to ECM are the guidelines for reliability assessment for the solder material when it is introduced on PCBAs. The condensation was more pronounced during temperature increase step from 25°C to 55°C

due to the thermal delay of the PCBAs to change the temperature from 25°C to 55°C. The bias voltage applied to the SIR pattern was set at 10 V DC using a "Biologic VSP" multichannel potentiostat. The LC values was recorded using EC-Lab software. The tests automatically stopped either when the current exceeded 20 mA or after 168 h. After the test, the dendrite formation was inspected using a Leica light optical microscope with a "Leica DFC 450 C" digital camera.

Material characterization before and after corrosion

Corrosion morphology of the alloy surface after tests was investigated using scanning electron microscope (SEM) (Inspect S, FEI, USA) with an energy dispersive spectroscopy (EDS) detector (50 mm^2 X-Max, Oxford Instrument, UK). The phase analysis was carried out using X-ray diffractometer (XRD) (D8 Advance, Bruker, USA) with a molybdenum anode. The Volta potential mapping was performed using a Multimode 8 atomic force microscopy (AFM) (Bruker, USA) using the mode of amplitude modulation method. The AFM microscope was equipped with conductive Point Probe Plus (Nanosensors, Switzerland) electrostatic force microscopy. The silicon cantilever attached to the AFM was in a radius of 10 nm and coated with 25 nm chromium and platinum. The tip of cantilever possessed a resonance frequency in a range of 70 - 80 kHz. The dual-scan mode was used over an area of 80 μm × 80 μm of polished solder alloys with the scan rate of 0.2 Hz under the ambient condition of 25°C, 60% RH. The Volta potential mapping result was collected by lifting the tip 50 - 100 nm above the surface in the second scan in addition to the obtained surface topography signal in the first mechanical intermittent AFM scan. SEM inspection was conducted after Volta potential mapping to avoid the contamination of carbon.

III.   RESULTS

Microstructure of solder alloys

The XRD results in **Figure 4.3** indicated that β-Sn, Ag$_3$Sn, and Cu$_6$Sn$_5$ presented in all five alloys. The Bi phase only presented in InnoLot alloy, while SAC 0807 did not show any Bi phase as the substitutional dissolution of trace level Bi content in β-Sn solution. InnoLot alloy also contains Sb content, however it is presented in the β-Sn solution as substitutional element. Similarly, Ni was not visible in any of the phase analysis due to the formation of solid solution with Cu, although many of the alloys tested contain small amount of Ni.
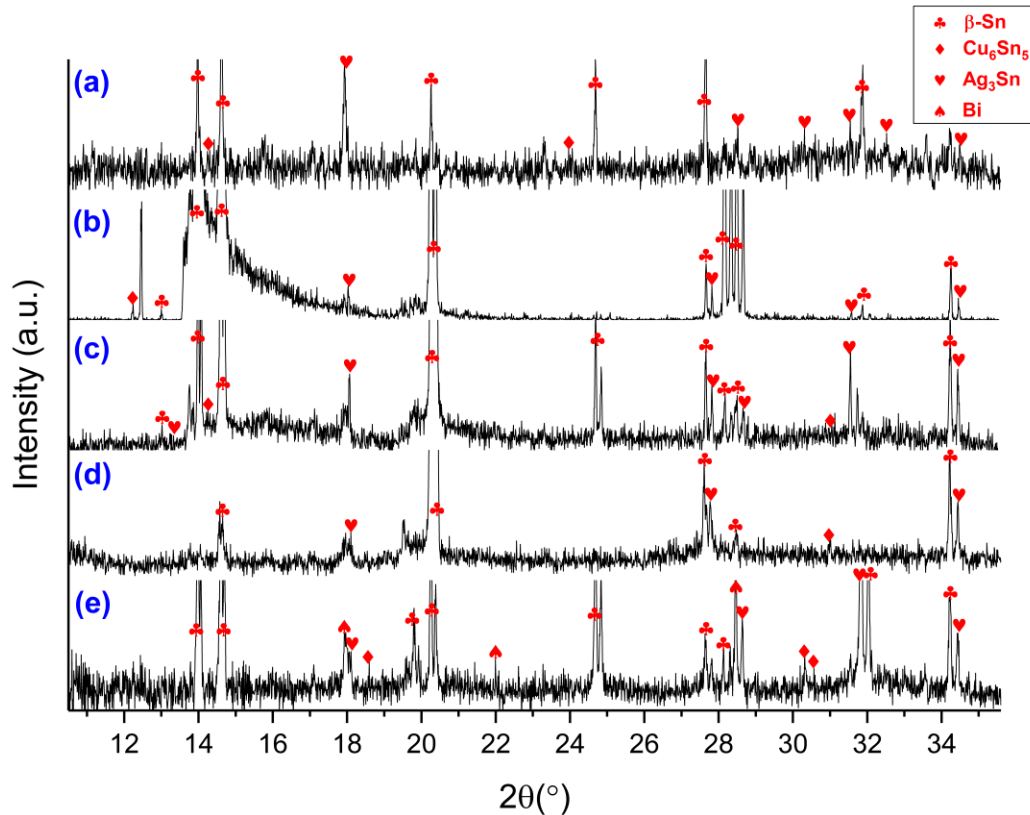
Figure 4.3 The XRD result for 5 solder alloy ingots: (a) SAC 305, (b) SACX Plus 0307, (c) SACX 0807, (d) SACX Plus 0807, (e) InnoLot.

The backscattered electron image in **Figure 4.4** shows four phases similar to the XRD result in InnoLot alloy as well as the EDS mapping result of this region. Additional elements shown in the EDS mapping is based on the comparison of the XRD results with EDS mapping, which showed the presence of different elements in the vicinity of various phases. The detailed phase analysis approach of tested SAC alloys was interfered by the low melting temperature, extremely soft surface, and extremely low elemental fraction. Thus with the slight variation in composition, the phases presented in InnoLot alloy possibly were: (Sn, Sb) solid solution region, Bi phase, Ag_3(Sn, Sb), and $(Cu, Ni)_6$(Sn, Sb)$_5$.

Figure 4.5 shows the distribution of phases in the ingots of four other alloys. Phases are marked in the backscattered electron images, which shows a general similarity to the XRD results. In SAC 305 alloy, the β-Sn phase was surrounded by the Ag_3Sn and Cu_6Sn$_5$ ternary eutectic IMCs, as shown in **Figure 4.5** (a) similar to the results from XRD. The size of the Ag_3Sn phase in this alloy was the smallest among all the five solder alloys. Compared to the size of Ag containing phases in other four alloys, Ag_3(Sn, Sb) particles in InnoLot alloy is relatively larger, as shown in **Figure**

4.4. While in the case of SACX Plux 0307 and SACX Plux 0807, some phases showed Ni as substitutional element of Cu, which might be similar to InnoLot alloy and denoted as $(Cu, Ni)_6Sn_5$. The phase constituents of these two alloys were determined as β-Sn, Ag_3Sn and $(Cu, Ni)_6Sn_5$, as shown in **Figure 4.5**(b)(d). The phase constituent of SACX 0807 alloy contains β-Sn, Ag_3Sn and Cu_6Sn_5, as shown in **Figure 4.5**(c). But no additional phase corresponding to Bi was observed in this case.
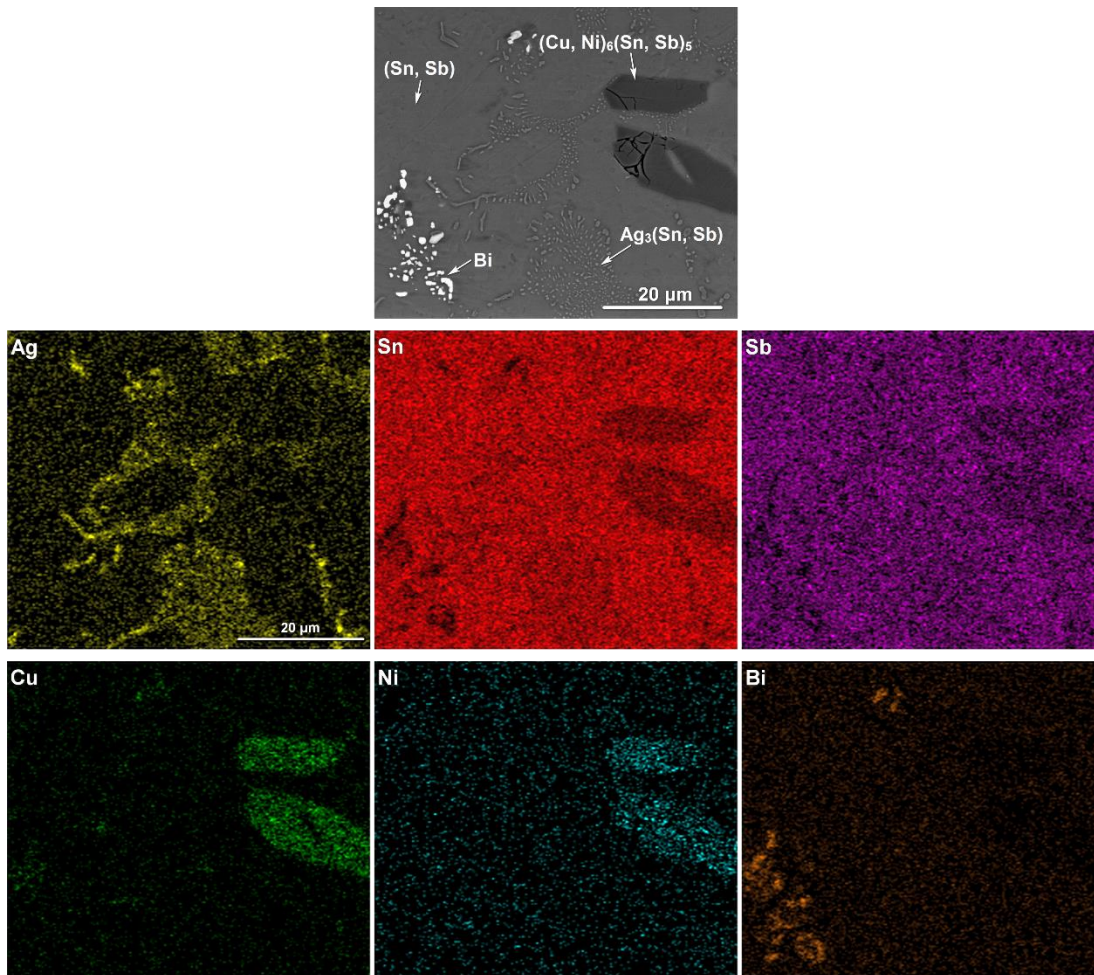
Figure 4.4 Typical EDS mapping result of InnoLot alloy. Backscattered electron image shows the area used for EDS mapping.

Since the Ag was only shown as Ag_3Sn IMCs, therefore Ag distribution also shows the distribution of Ag_3Sn IMCs. Finer Ag_3Sn IMCs was heterogeneously distributed in the SAC 305 alloy as shown in **Figure 4.6**(a). For SACX Plus 0307, distribution of Ag were locally presented in the bulk than SAC 305 alloy as shown in **Figure 4.6**(b). The Ag content was more uniformly distributed in the bulk of SACX 0807 alloys and SACX Plus 0807 alloy, as shown in **Figure 4.6**(c)(d).
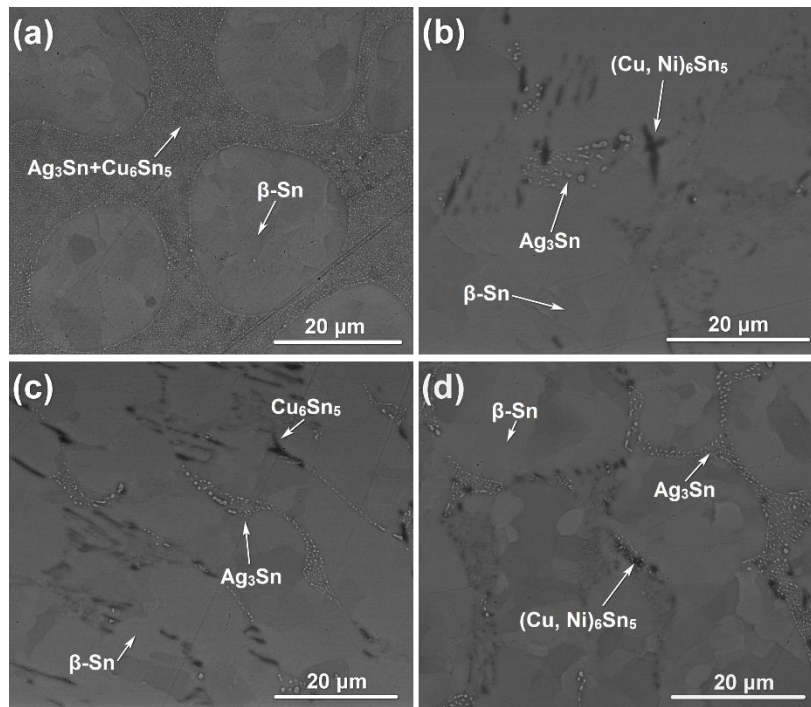
Figure 4.5 *Backscattered electron (BSE) images of solder alloys (top view of polished surface): (a) SAC 305, (b) SACX Plus 0307, (c) SACX 0807, (d) SACX Plus 0807.*
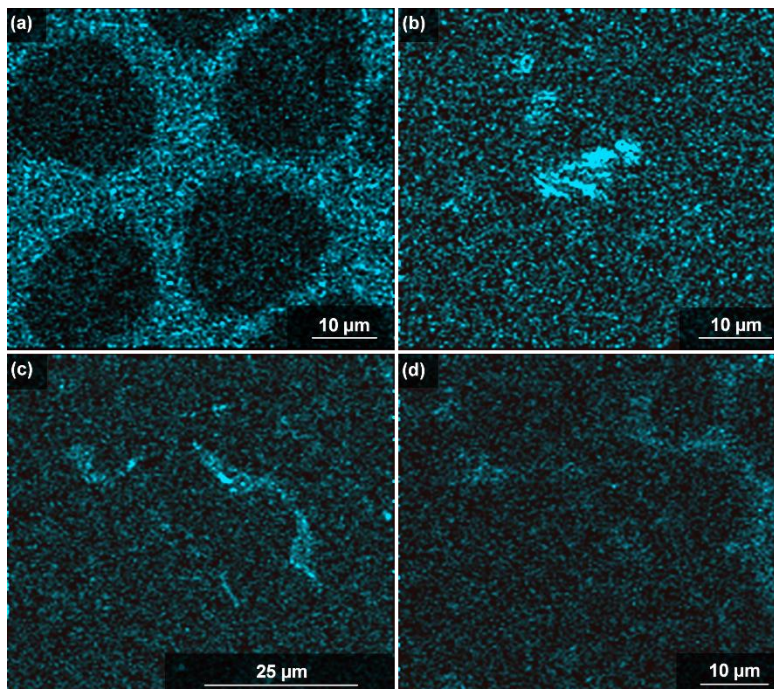
Figure 4.6 *EDS mapping of Ag element in the regions of **Figure 4.5**: (a) SAC 305 alloy, (b) SACX Plus 0307alloy, (c) SACX 0807, (d) SACX Plus 0807 alloy.*

Volta potential mapping

Volta potential mapping image in **Figure 4.7**(b) shows the potential distribution for InnoLot alloy in the same location as shown in the BSE image in **Figure 4.7**(a). The potential difference of various phases in InnoLot alloy was above 200 mV as shown in the scale bar of Volta potential in **Figure 4.7**(b). The Volta potential of Bi phase was lowest among all the phases in the alloy under ambient condition, which presented the darkest colour in **Figure 4.7**(b). While the (Sn, Sb) phase obtained the highest Volta potential in InnoLot alloy. This result confirmed pure Bi phase was more noble in contrast to the anodic (Sn, Sb) solid solution. For SACX Plus 0807 alloy shown in **Figure 4.7**(c), the potential difference of various phases was lower than 150 mV. Ag_3Sn IMCs showed noble Volta potential under ambient condition, while the β-Sn phase was more anodic.
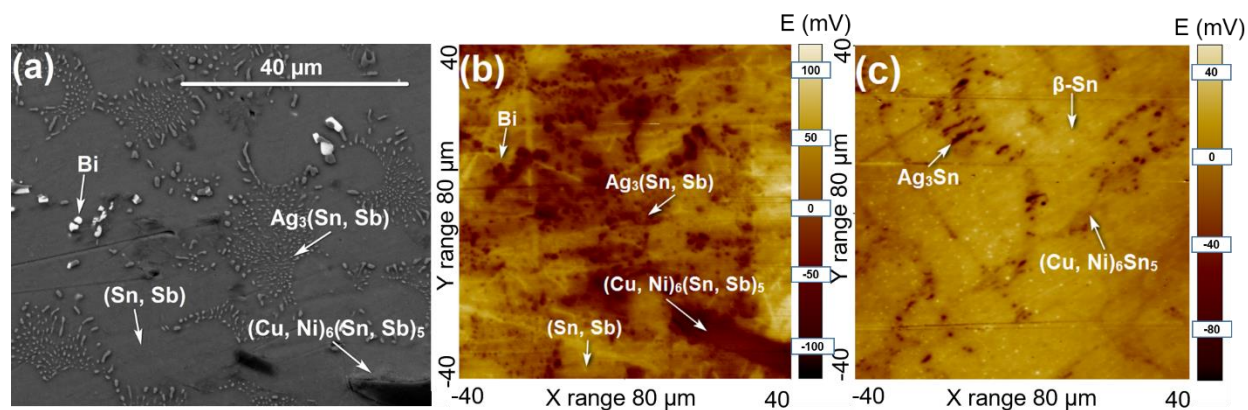
Figure 4.7 *Volta potential mapping using SKPFM in comparison with microstructure: (a) BSE image of InnoLot alloy, (b) Volta potential mapping of InnoLot alloy, (c) Volta potential mapping of SACX Plus 0807 alloy.*

Potentiodynamic/potentiostatic testing and surface morphology characterizations

The polarization curves shown in **Figure 4.8** reveal different anodic behavior, while the cathodic behavior did not show significant difference between alloys. InnoLot showed more noble potential compared other alloys with high pitting potential (more positive). SACX 0807 and SACX Plus 0807 showed similar polarization behavior with slightly more noble corrosion potential than SAC 305 and SACX Plus 0307. Due to the more active corrosion potential for SAC 305 and SACX Plus 0307, they exhibited longer passive region, while the pitting potential was higher (more positive) compared to SACX 0807 and SACX Plus 0807. The corrosion parameter summary in **Table 4.2** shows InnoLot was the most noble among all the alloys with comparatively lower corrosion current than SAC 305, SACX Plus 0307, and SACX 0807, while SACX Plus 0807 showed lowest corrosion current density.
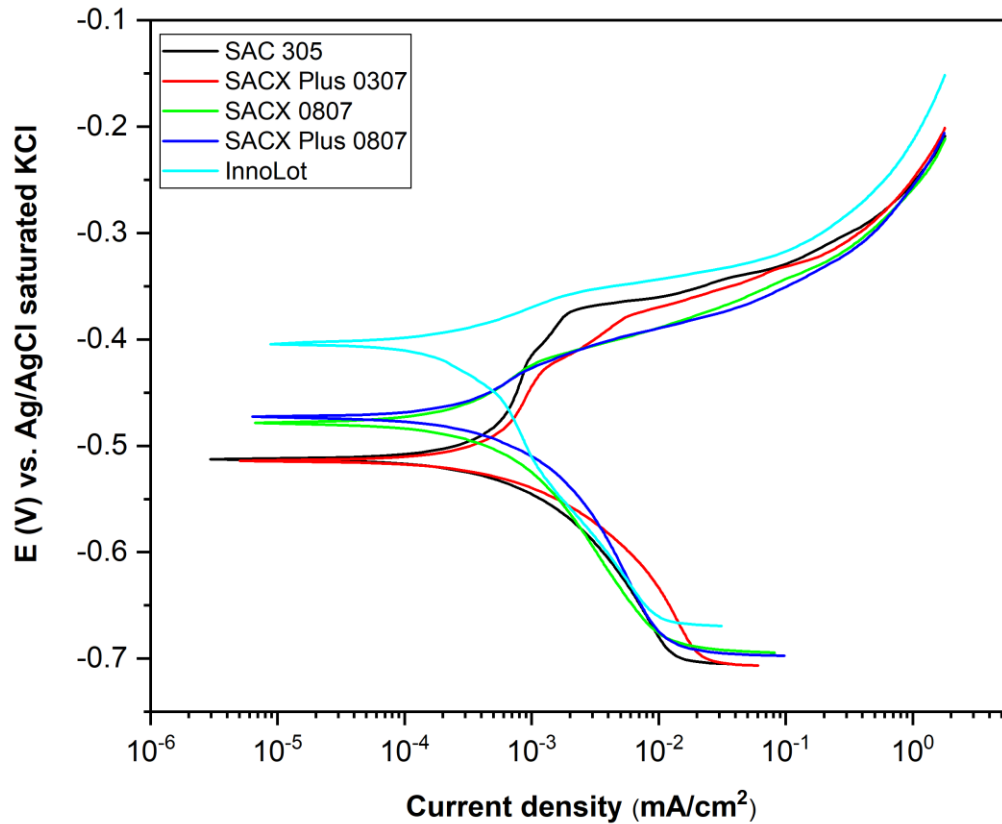
Figure 4.8 *Representative polarization curves of ingot materials of five solder alloys.*

Table 4.2 *Summary of E_{corr} and i_{corr} derived from the polarization curves for five alloys. (Each value in the table is the average value from 5 measurements shown with standard deviation.)*

Solder alloy	E_{corr} (mV vs. Ag/AgCl)	i_{corr} (μA/cm^2)
SAC 305	-505 ± 10	8.4± 2.7
SACX Plus 0307	-503 ± 26	7.6 ± 4.0
SACX 0807	-480 ± 15	5.4 ± 2.0
SACX Plus 0807	-476 ± 4	2.9 ± 0.2
InnoLot	-405 ± 8	3.3 ± 1.1

Figure 4.9 shows that surface morphology of alloy after the test. For InnoLot alloy, the pitting formed at (Sn, Sb) solid solution adjacent to the pure Bi phase as shown in **Figure 4.9**(e). For the other four alloys, the pitting formed at β-Sn phase adjacent to the Ag$_3$Sn IMCs as shown in **Figure 4.9**(a-d).
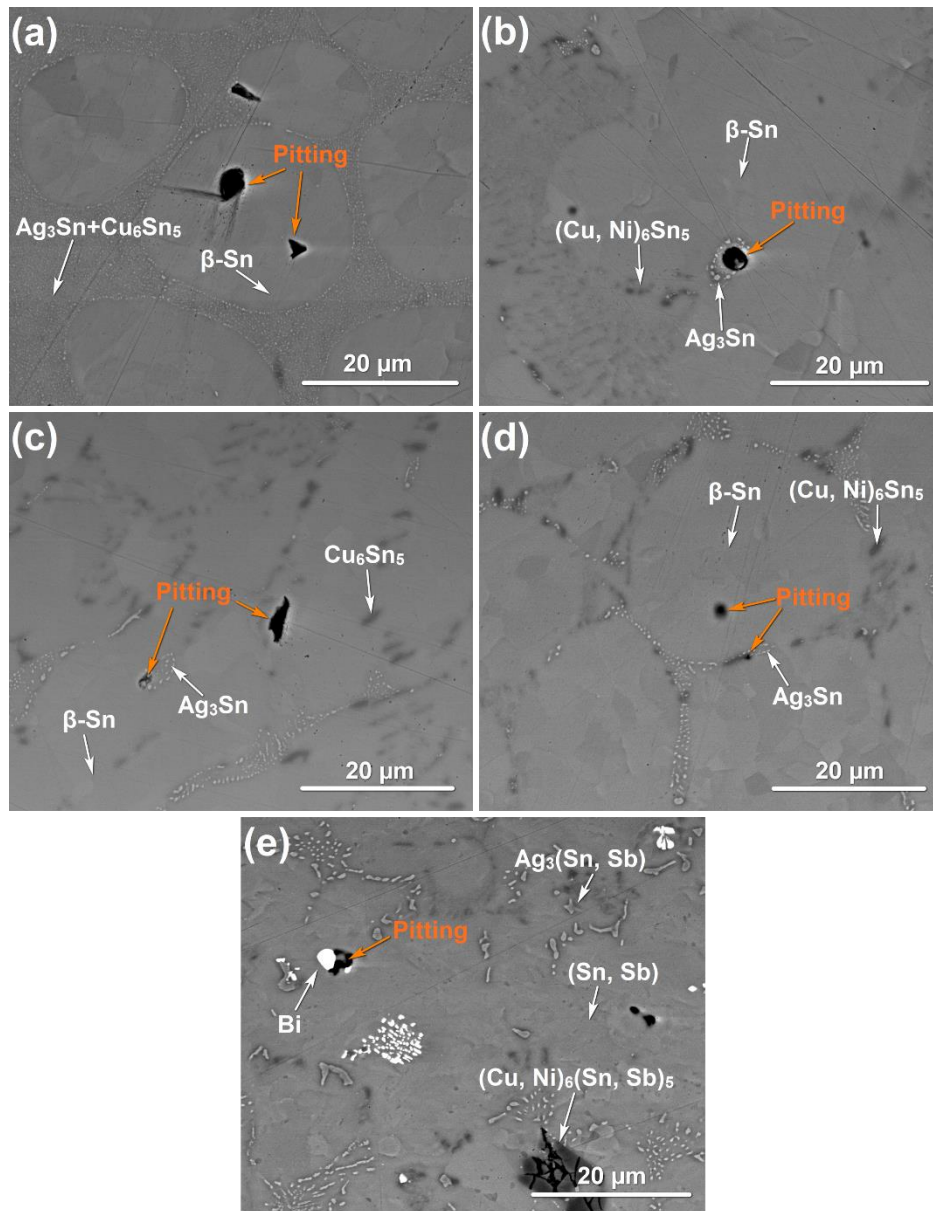
Figure 4.9 *Top view BSE of solder alloys after pitting test: (a) SAC 305, (b) SACX Plus 0307, (c) SACX 0807, (d) SACX Plus 0807, and (e) InnoLot.*

ECM susceptibility test using WD test

Typical pictures from an in-situ observation of dendrite formation over time was shown in **Figure 4.10**. During the WD test, dissolved metal ions from the anodically polarized electrode move toward the cathodically polarized electrode (under the electric filed) to deposit in the form of dendrite. Time to failure (TTF) value indicates the first observation of two electrodes bridged by dendrite. The results from WD tests were summarized in Weibull probability plots. Each point on the Weibull probability plot indicated a TTF value for one WD test. Scale parameter indicated the

time estimation at 63.2% failure rate. All the shape parameters in the present work were higher than 1, which indicates the increase of failure rate over time.

When pure water (**Figure 4.11**(a)) was used for the WD tests, the ranking of first ECM observation for each solder alloy was of the order: SAC 305 < SACX 0807 < SACX Plus 0307 < SACX Plus 0807 < InnoLot. The number of failure during WD tests for each solder alloy was of the order: SACX Plus 0807 < SACX Plus 0307 < SAC 305 < InnoLot < SACX 0807. **Figure 4.11**(c) shows the results of test using 0.0156g/L of aqueous NaCl solution. All the tests under this condition showed ECM failure. The ranking of estimated time to 63.2% failure rate for each alloy under this condition was of the order: SAC 305 < SACX Plus 0307 < SACX 0807 < SACX Plus 0807 < InnoLot. **Figure 4.11**(b) shows the result of experiments with 0.00156 mg/L aqueous NaCl solution, a similar trend was obtained as the testing results from 0.0156 mg/L NaCl solution except for the higher estimated time for 63.2% failure, which was summarized in **Table 4.3**.
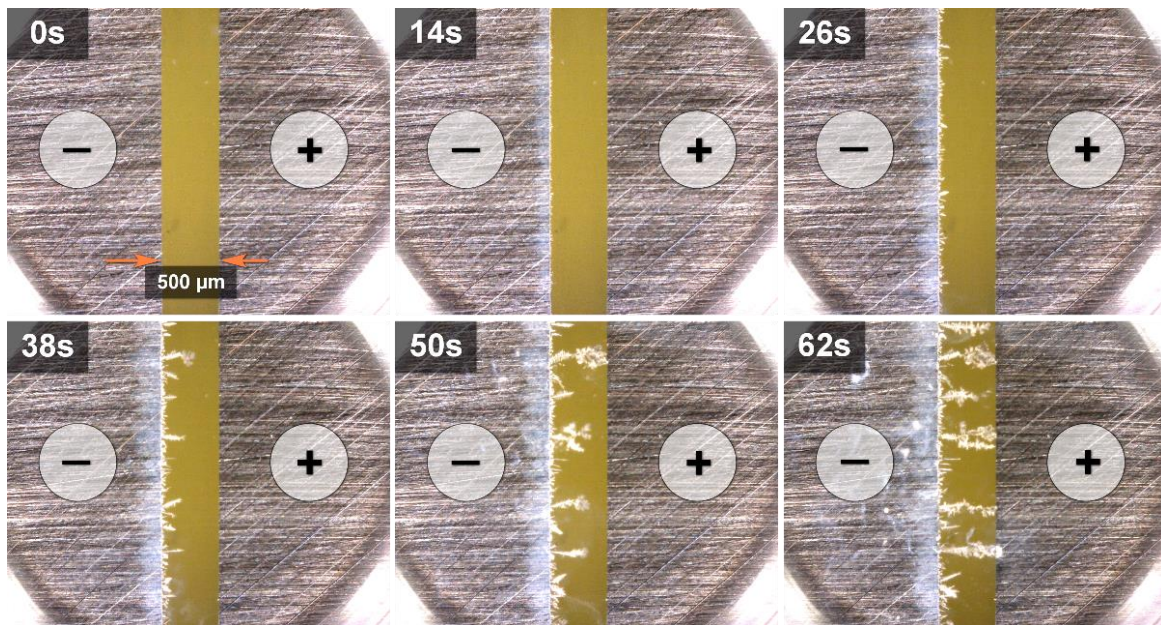
Figure 4.10 Selected pictures from in-situ observation of dendrite formation over time during WD test (SACX 0807 alloy in 0.00156mg/L aqueous NaCl solution).

For the ECM failure in pure water, due to the limited number failures, first observation of time to failure was used in the **Table 4.3**, while for the NaCl conditions, the estimated time to 63.2% failure rate was used. A significant decrease of estimated time to 63.2% failure rate for each alloy was found when increasing the concentration of NaCl solution as well as comparing the values for pure water, but the trend of the susceptibility of five alloys were the same under different concentrations of NaCl solution.
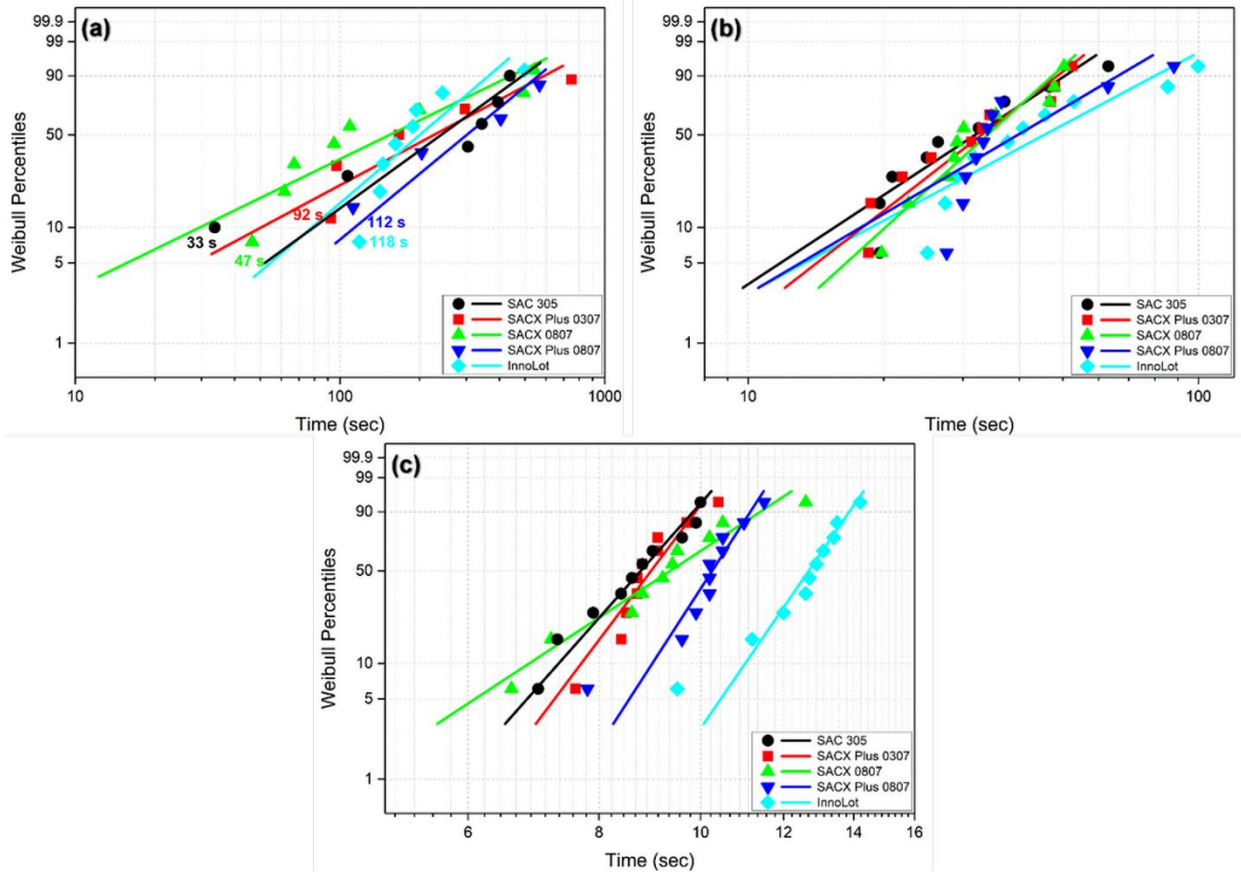
Figure 4.11 *Weibull probability analysis of TTF value under WD tests: (a) ultra-pure water, (b) 0.00156mg/L aqueous NaCl solution, (c) 0.0156mg/L aqueous NaCl solution.*

Table 4.3 *Summary of WD tests for five solder alloys under three WD test conditions showing estimated time for 63.2% failure rate.*

Estimated time to failure in different electrolytes (sec)					
	SAC 305	SACX Plus 0307	SACX 0807	SACX Plus 0807	InnoLot
Pure water	33.6	92.4	46.6	112.0	118.3
0.00156 mg/L NaCl	36.7	37.2	37.7	46.5	54.1
0.0156 mg/L NaCl	9.1	9.2	9.9	10.5	13.0

Corrosion reliability of reflow-soldered sir pattern under humid conditions

The first ECM failure of SACX Plus 0307 alloy occurred after the first round of temperature cycling as shown in **Figure 4.12**(a). The LC measurement of SACX Plus 0307 alloy stopped when the LC value exceeded 20 mA after 20 round of temperature cycles. The first ECM failure of SAC 305 was obtained after 15 temperature cycles. No failure occurred for SACX 0807, SACX Plus 0807, and InnoLot alloy (showing only constant leakage current). Based on the result of LC

measurement, the ranking of charge transferred over time **(Figure 4.12**(b)) for various alloys was: SAC 305 > SACX Plus 0307 > SACX 0807 > SACX Plus 0807 > InnoLot.

Figure 4.13 shows the dendrite formation on the interdigitated electrode made of SAC 305 and SACX Plus 0307 alloys. A number of dendrites on SAC 305 alloy soldered SIR pattern were heterogeneously distributed between electrodes, whereas SACX Plus 0307 alloy showed only few dendrites. This is in agreement with the leak current curves shown in **Figure 4.12**(a).
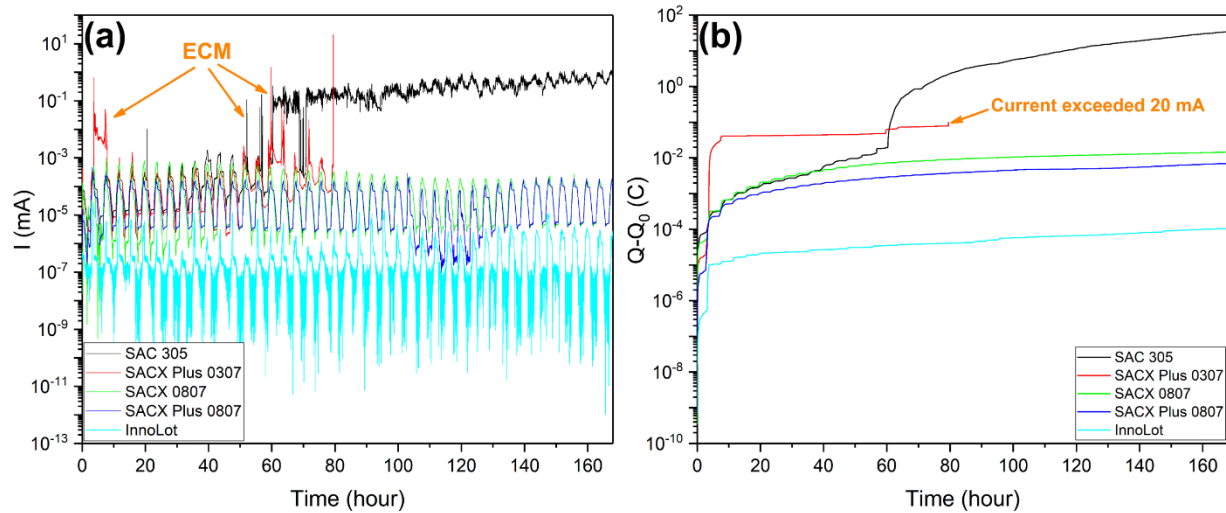
Figure 4.12 *Accelerated humidity/temperature cycling test: (a) Leakage current value, (b) Charge transferred over time calculated from the leakage current curve.*
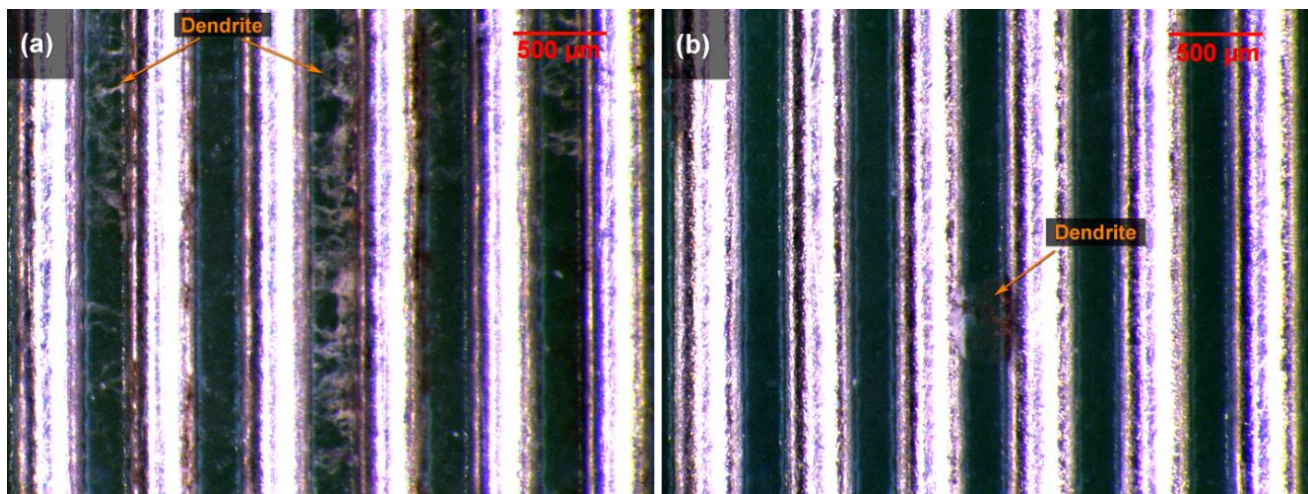
Figure 4.13 *Surface of the interdigitated electrode showing ECM formation after accelerated temperature/humidity test: (a) SAC 305 alloy soldered SIR pattern, (b) SACX Plus 0307 alloy.*

IV.   DISCUSSION

Present work shows the effect alloying elements and microstructure of SAC alloys with varying alloying addition has significant influence on the electrochemical and corrosion behavior, and therefore on the corrosion reliability when used on the surface of PCBAs. From the microstructural point of view, the distribution of silver containing phases and variation of additive alloying elements such as Bi showed significant effect on the corrosion behavior.

Role of the distribution homogeneity of Ag containing IMCs for the corrosion resistance

The Volta potential mapping result of SACX Plus 0807 alloy indicates that the noble potential of Ag_3Sn has significantly influenced the corrosion behavior of the alloys. The distribution of Ag_3Sn influenced corrosion behavior such as E_{corr} and i_{corr} values according to the surface potential homogeneity of various solder alloys. For conventional SAC 305 alloy, the corrosion attack was in correlation with the elemental and phase distribution shown in **Figure 4.4**(a) and **Figure 4.5**(a). Heterogeneously distributed Ag_3Sn IMCs in this alloy accelerated the corrosion attack in the large grain of the β-Sn phase. This is in agreement with the i_{corr} result observed for this alloy in **Table 4.2**. The SAC 305 alloy also showed highest susceptibility of ECM during WD tests, which triggers higher dissolution of Sn ions to deposit on the cathode to form dendrite. The intensity of the ECM attack was high on this SIR pattern under accelerated test as shown in **Figure 4.13**(a) with dendrites spreading all over the gaps of SIR electrodes. This result is in agreement with the report work of Medgyes et al [27], however contradictory result was reported by Medgyes et al [20] for the SACX Plus 0307 and SACX Plus 0807 alloys. Cleaning of the flux residue prior to testing was not reported in the previous work [27], which could result in different behavior due to the acidic nature of the flux residue. Piotrowska et al. reported that acidic residue resulting from the solder flux [28] can induce corrosion because of the acidic and hygroscopic nature of flux [29], which is also dependent on the type of flux residue used for reflow soldering process [30].

Between SACX Plus 0307 and SACX Plus 0807 alloy, the only difference is in the level of Ag content. Therefore, the large difference in corrosion rate might be attributed to the amount of cathodic silver containing phase distribution. For SACX Plus 0307 alloy, very localized distribution of cathodic Ag_3Sn phase resulting in localized corrosion in the β-Sn phase, as shown in **Figure 4.9**(b). The localized galvanic coupling also has resulted in higher i_{corr} result (**Table 4.2**). The higher corrosion of SACX Plus 0307 alloy soldered interdigital SIR test pattern provides more ions for ECM resulting in higher susceptibility (**Figure 4.13**(b)). On the contrary, SACX Plus 0807 alloy showed lower ECM susceptibility as shown in **Table 4.3** during the WD tests and lower corrosion

current density as shown in **Table 4.2**. This might be attributed to the relative homogeneity of the electrochemical potential distribution over the microstructure (**Figure 4.7**(c)).

Role of the Bi, Sb, and Ni additives and corrosion behavior

The precipitation of Bi phase in InnoLot alloy was attributed to the remarkable decrease of the Bi solid solubility with decrease in temperature and form Bi supersaturated Sn-rich solid solution [31]. Volta potential mapping result indicates the noble Bi phase in InnoLot alloy, as shown in **Figure 4.7**(a) and (b). The corrosion pits of InnoLot alloy were induced by galvanic effect of cathodically active Bi phase and anodic (Sn, Sb) solid solution (**Figure 4.9**(e)). ECM susceptibility and i_{corr} value of InnoLot was much lower than the conventional SAC 305 alloy, which was shown in **Table 4.2** and **Table 4.3** respectively. Since the Bi phase was confirmed as cathodically active in the Volta potential mapping as shown in **Figure 4.7**(b), the remaining Bi content in the supersaturated Sn-rich solid solution could also improve the corrosion resistance of SAC solder alloy by reducing the electrochemical heterogeneity. Although, Ag content of InnoLot and SAC 305 was similar, microstructure of InnoLot was homogeneous compared to conventional SAC 305 alloy as shown in **Figure 4.4** and **Figure 4.5**(a). This could be attributed to effect of Ni on microstructural refinement [32]. Compared to other four alloys, the dramatically decreased values of i_{corr} for InnoLot might be due to the increasing Sb content. Therefore, the best performance of corrosion resistance and ECM susceptibility for InnoLot alloy could be broadly associated with the influence of Bi, Sb, and Ni additives. While for SACX 0807 alloy, the amount of Bi and Ag was much lower. No Bi phase was observed in the bulk of SACX 0807 alloy due to the dissolution of Bi in Sn as substitutional element. The improvement of corrosion properties could be either due to better nobility of Bi content [33] or Bi addition improved the homogeneity of microstructure of the alloy by increasing melting range and prolonged the growth time of β-Sn phase [8]. The exact reason for this effect is still not clear, which requires further investigations. In the case of SACX Plus 0807 alloy, the i_{corr} value was the lowest among the five solder alloys investigated, which also in agreement of its low ECM susceptibility as shown in **Table 4.3** and low LC values as shown in **Figure 4.12**(a). The effect can be attributed to the presence of Ni, which provides more nuclei for Sn crystallization [8] and enhanced the corrosion resistance by influencing the refinement of microstructure [32]. The EDS mapping result shown in **Figure 4.6**(d) confirmed the homogeneity in the distribution of Ag_3Sn IMCs in the bulk of SACX Plus 0807 alloy, which leads to the improvement of the corrosion resistance by uniform potential on the surface of material as shown in **Figure 4.7**(c). The only difference between SACX 0807 and SACX Plux 0807 alloy is the addition of trace element of Bi and Ni. The i_{corr} result and ECM susceptibility indicate the additive of Ni performed better than Bi for corrosion resistance.

Corrosion reliability of solder alloys in connection with applications in electronics

The present work correlated corrosion properties and ECM susceptibility of tested SAC alloys. It is notice that the difference of i_{corr} value of tested alloys are very low, while the difference is significant in the results of WD and SIR tests. The minor difference in i_{corr} could be due to the small elemental composition in a relative large polarized area of 0.76 mm^2, whereas the ECM in WD tests and SIR tests took place in a much smaller region where the micro-galvanic couples located (**Figure 4.9**). However, the minor difference of i_{corr} in **Table 4.2** still fit to the results of ECM susceptibility in WD test (**Table 4.3**). The lowest passive region of InnoLot shows in **Figure 4.8** might be influenced by the higher Volta potential difference of the surface as shown in **Figure 4.7**(b), in contrast, the passive region of SACX Plus 0807 was higher than InnoLot alloy while possessed a lower Volta potential difference on the surface shown in **Figure 4.7**(c). Osório et al evaluated the corrosion resistance by analyzing passivation domain in polarization curves [6], and in the present work the passivation domain of SAC 305 alloy is much larger than SACX Plux 0807 alloy as shown in **Figure 4.8**. However, the assessment of ECM susceptibility in the present work shows better corrosion robustness of SACX Plus 0807 alloy than SAC 305 alloy. This could be due to the applied DC bias loading on PCBAs usually exceeds the passivation breakdown potential, and accelerates the corrosion process of solder alloys. Therefore, the corrosion assessment based only on the polarization curves should be used with caution. Micrograph of **Figure 4.5**(a) and (d) shows SACX Plus 0807 alloy possessed a finer Ag$_3$Sn IMCs dispersion compared to SAC 305 alloy. Correspondingly, Kaushik et al. [15] reported the fine dispersion of Ag$_3$Sn in the matrix inhibited localized corrosion attack and improved corrosion resistance. Since i_{corr} value of SACX Plus 0807 ingot was lower than SAC 305 as shown in **Table 4.2**, the corrosion rate of SAC 305 alloy was higher than SACX Plux 0807 alloy under same DC bias loading. The higher corrosion rate of SAC 305 alloy provided sufficient metallic ions in the electrolytes to form metallic hydroxide dendrites and lead to faster ECM failure compared to SACX Plus 0807. This is in agreement with the corrosion robustness of SACX Plus 0807, which is better than conventional SAC 305 alloy under both WD testing conditions and accelerated testing condition (**Table 4.3** and **Figure 4.12**). The cooling rate of the solder joint on an actual PCBA can be different due to the difference of the aging period [15][34] and cooling method [1][35]. This could be attributed to different microstructure in the bulk, for instance, the coarsening of the Ag$_3$Sn IMCs by decreasing cooling rate as reported by Wang et al. [35]. In the present study, even though the volume of the solder ingots was larger than the reflow-produced solder alloy on SIR patterns, the solder ingots were heat treated under relatively low temperature and solidified under water quench. Therefore, the difference of the microstructure for reflow processed solder alloys on SIR

patterns and alloy ingots was assumed to be negligible. The agreement between the corrosion reliability ranking (**Table 4.3**) of the reflow-soldered SIR comb patterns with i_{corr} value from the polarization result (**Table 4.2**) also shows microstructures are comparable.

V.   CONCLUSIONS

- More uniform phase distribution was obtained by the addition of Bi, Sb, and Ni in InnoLot alloy compared to conventional SAC 305 alloy. Comparing SACX Plus 0307 and SACX Plus 0807 alloy, the difference of Ag content significantly influenced the microstructure homogeneity in the low Ag content alloys. More uniform microstructure was obtained for 0.05 wt.% Ni addition rather than for 0.1 wt.% Bi addition in the matrix of Sn - 0.8 wt.% Ag - 0.7 wt.% Cu alloy.

- Volta potential mapping result under ambient condition illustrated the galvanic coupling between cathodic Bi phase and anodic (Sn, Sb) solid solution in InnoLot alloy as well as cathodic Ag_3Sn IMCs and anodic β-Sn phase in the other four alloys.

- Potentiodynamic polarization result indicated low corrosion rate of InnoLot alloy and SACX Plus 0807 compared to other solder alloys. Pitting occurred preferentially on (Sn, Sb) solid solution adjacent of Bi phase in InnoLot alloy, while on β-Sn phase adjacent to Ag_3Sn IMCs in other four alloys.

- ECM results from WD test and SIR comb pattern test confirmed the ECM failure was more related to the corrosion current density rather passivation domain of tested SAC solder alloy under 5 V DC bias loading.

VI.   REFERENCES

[1]   M. Wang, J. Wang, H. Feng, W. Ke, Effect of Ag_3Sn intermetallic compounds on corrosion of Sn-3.0Ag-0.5Cu solder under high-temperature and high-humidity condition, Corros. Sci. 63 (2012) 20–28. doi:10.1016/J.CORSCI.2012.05.006.

[2]   K. Maslinda, A.S. Anasyida, M.S. Nurulakmal, Effect of Al addition to bulk microstructure, IMC formation, wetting and mechanical properties of low-Ag SAC solder, J. Mater. Sci. Mater. Electron. 27 (2016) 489–502. doi:10.1007/s10854-015-3780-y.

[3]   K.N. Subramanian, Lead-free electronic solders: A special issue of the journal of materials science: Materials in electronics, 2007. doi:10.1007/978-0-387-48433-4.

[4]   Z. Mei, H.A. Holder, H.A. Vander Plas, Low-temperature solders, Hewlett-Packard J. 47 (1996) 91–98.

[5]   I.E. Anderson, J.C. Foley, B.A. Cook, J. Harringa, R.L. Terpstra, O. Unal, Alloying effects in near-eutectic Sn-Ag-Cu solder alloys for improved microstructural stability, J. Electron. Mater. 30 (2001) 1050–1059. doi:10.1007/s11664-001-0129-5.

[6]   W.R. Osório, J.E. Spinelli, C.R.M. Afonso, L.C. Peixoto, A. Garcia, Microstructure,

corrosion behaviour and microhardness of a directionally solidified Sn-Cu solder alloy, Electrochim. Acta. 56 (2011) 8891–8899. doi:10.1016/j.electacta.2011.07.114.

[7] K. Kanlayasiri, T. Ariga, Influence of thermal aging on microhardness and microstructure of Sn–0.3Ag–0.7Cu–xIn lead-free solders, J. Alloys Compd. 504 (2010) L5–L9. doi:10.1016/J.JALLCOM.2010.05.057.

[8] Y. Liu, F. Sun, X. Li, Effect of Ni, Bi concentration on the microstructure and shear behavior of low-Ag SAC-Bi-Ni/Cu solder joints, J. Mater. Sci. Mater. Electron. 25 (2014) 2627–2633. doi:10.1007/s10854-014-1921-3.

[9] H.R. Kotadia, P.D. Howes, S.H. Mannan, A review: On the development of low melting temperature Pb-free solders, Microelectron. Reliab. 54 (2014) 1253–1273. doi:10.1016/j.microrel.2014.02.025.

[10] C. Kanchanomai, Y. Miyashita, Y. Mutoh, Low-cycle fatigue behavior of Sn-Ag, Sn-Ag-Cu, and Sn-Ag-Cu-Bi lead-free solders, J. Electron. Mater. 31 (2002) 456–465. doi:10.1007/s11664-002-0100-0.

[11] J. Zhao, L. Qi, X.M. Wang, L. Wang, Influence of Bi on microstructures evolution and mechanical properties in Sn-Ag-Cu lead-free solder, J. Alloys Compd. 375 (2004) 196–201. doi:10.1016/j.jallcom.2003.12.005.

[12] M.N. Collins, E. Dalton, J. Punch, Microstructural influences on thermomechanical fatigue behaviour of third generation high Ag content Pb-Free solder alloys, J. Alloys Compd. 688 (2016) 164–170. doi:10.1016/j.jallcom.2016.07.191.

[13] Y.W. Wang, C.C. Chang, C.R. Kao, Minimum effective Ni addition to SnAgCu solders for retarding Cu_3Sn growth, J. Alloys Compd. 478 (2009) L1–L4. doi:10.1016/J.JALLCOM.2008.11.027.

[14] Y.W. Wang, Y.W. Lin, C.T. Tu, C.R. Kao, Effects of minor Fe, Co, and Ni additions on the reaction between SnAgCu solder and Cu, J. Alloys Compd. 478 (2009) 121–127. doi:10.1016/j.jallcom.2008.11.052.

[15] R.K. Kaushik, U. Batra, J.D. Sharma, Aging induced structural and electrochemical corrosion behaviour of Sn-1.0Ag-0.5Cu and Sn-3.8Ag-0.7Cu solder alloys, J. Alloys Compd. 745 (2018) 446–454. doi:10.1016/J.JALLCOM.2018.01.292.

[16] F. Rosalbino, E. Angelini, G. Zanicchi, R. Carlini, R. Marazza, Electrochemical corrosion study of Sn–3Ag–3Cu solder alloy in NaCl solution, Electrochim. Acta. 54 (2009) 7231–7235. doi:10.1016/J.ELECTACTA.2009.07.030.

[17] S.K. Kang, D.-Y. Shih, N.Y. Donald, W. Henderson, T. Gosselin, A. Sarkhel, N.Y. Charles Goldsmith, K.J. Puttlitz, W.K. Choi, Ag3Sn plate formation in the solidification of near-ternary eutectic Sn-Ag-Cu, JOM. 55 (2003) 61–65. doi:10.1007/s11837-003-0143-6.

[18] D. Minzari, M.S. Jellesen, P. Møller, R. Ambat, On the electrochemical migration mechanism of tin in electronics, Corros. Sci. 53 (2011) 3366–3379. doi:10.1016/J.CORSCI.2011.06.015.

[19] X. Zhong, G. Zhang, Y. Qiu, Z. Chen, X. Guo, Electrochemical migration of tin in thin electrolyte layer containing chloride ions, Corros. Sci. 74 (2013) 71–82. doi:10.1016/J.CORSCI.2013.04.015.

[20] D.Q. Yu, W. Jillek, E. Schmitt, Electrochemical migration of Sn-Pb and lead free solder

alloys under distilled water, J. Mater. Sci. Mater. Electron. 17 (2006) 219–227. doi:10.1007/s10854-006-6764-0.

[21] B. Liao, Z. Chen, Y. Qiu, G. Zhang, X. Guo, Effect of citrate ions on the electrochemical migration of tin in thin electrolyte layer containing chloride ions, Corros. Sci. 112 (2016) 393–401. doi:10.1016/J.CORSCI.2016.08.003.

[22] B. Medgyes, B. Horváth, B. Illés, T. Shinohara, A. Tahara, G. Harsányi, O. Krammer, Microstructure and elemental composition of electrochemically formed dendrites on lead-free micro-alloyed low Ag solder alloys used in electronics, Corros. Sci. 92 (2015) 43–47. doi:10.1016/J.CORSCI.2014.11.004.

[23] D. Minzari, F.B. Grumsen, M.S. Jellesen, P. Møller, R. Ambat, Electrochemical migration of tin in electronics and microstructure of the dendrites, Corros. Sci. 53 (2011) 1659–1669. doi:10.1016/J.CORSCI.2011.01.009.

[24] J.-Y. Jung, S.-B. Lee, H.-Y. Lee, Y.-C. Joo, Y.-B. Park, Effect of ionization characteristics on electrochemical migration lifetimes of Sn-3.0Ag-0.5Cu solder in NaCl and Na_2SO_4 solutions, J. Electron. Mater. 37 (2008) 1111–1118. doi:10.1007/s11664-008-0491-7.

[25] B. Medgyes, B. Illés, R. Berényi, G. Harsányi, In situ optical inspection of electrochemical migration during THB tests, J. Mater. Sci. Mater. Electron. 22 (2011) 694–700. doi:10.1007/s10854-010-0198-4.

[26] V. Verdingovas, M.S. Jellesen, R. Ambat, Solder flux residues and humidity-related failures in electronics: relative effects of weak organic acids used in no-clean flux systems, J. Electron. Mater. 44 (2015) 1116–1127. doi:10.1007/s11664-014-3609-0.

[27] V. Verdingovas, M.S. Jellesen, R. Ambat, Relative effect of solder flux chemistry on the humidity related failures in electronics, Solder. Surf. Mt. Technol. 27 (2015) 146–156. doi:10.1108/SSMT-11-2014-0022.

[28] K. Piotrowska, V. Verdingovas, R. Ambat, Humidity-related failures in electronics: effect of binary mixtures of weak organic acid activators, J. Mater. Sci. Mater. Electron. 29 (2018) 17834–17852. doi:10.1007/s10854-018-9896-0.

[29] K. Piotrowska, R. Ud Din, F.B. Grumsen, M.S. Jellesen, R. Ambat, Parametric study of solder flux hygroscopicity: impact of weak organic acids on water layer formation and corrosion of electronics, J. Electron. Mater. 47 (2018) 4190–4207. doi:10.1007/s11664-018-6311-9.

[30] K. Piotrowska, M. Grzelak, R. Ambat, No-clean solder flux chemistry and temperature effects on humidity-related reliability of electronics, J. Electron. Mater. 48 (2019) 1207–1222. doi:10.1007/s11664-018-06862-4.

[31] L. Hua, C. Yang, Corrosion behavior, whisker growth, and electrochemical migration of Sn-3.0Ag-0.5Cu solder doping with in and Zn in NaCl solution, Microelectron. Reliab. 51 (2011) 2274–2283. doi:10.1016/j.microrel.2011.06.023.

[32] G. Medgyes, Bálint; Tamási, Patrik; Hajdu, Ferenc ; Lakatos–Varsányi, Roland Murányi Magda; Gál, László; Harsányi, Corrosion investigations on lead-free micro-alloyed solder alloys used in electronics, in: Proc. Int. Spring Semin. Electron. Technol., 2015: pp. 296–299. doi:10.1109/ISSE.2015.7248009.

[33] B. Medgyes, B. Illés, G. Harsányi, Electrochemical migration of micro-alloyed low Ag solders in NaCl solution, Period. Polytech. Electr. Eng. 57 (2014) 49.

doi:10.3311/ppee.2068.

[34]   R. Piotrowska, Kamila; Lagana, Simone; Jellesen, Morten; Ambat, Impact of process-related flux contamination on the electronics reliability issues under detrimental climatic condtions, in: 2019 Pan Pacific Microelectron. Symp. (Pan Pacific), IEEE, Kauai, HI, USA, USA, 2019. doi:10.23919/PanPacific.2019.8696890.

[35]   Y. Miyazawa, T. Ariga, Influences of aging treatment on microstructure and hardness of Sn-(Ag, Bi, Zn) eutectic solder alloys, Mater. Trans. 42 (2001) 776–782. doi:10.2320/matertrans.42.776.

[36]   A.E. Hammad, Investigation of microstructure and mechanical properties of novel Sn–0.5Ag–0.7Cu solders containing small amount of Ni, Mater. Des. 50 (2013) 108–116. doi:10.1016/J.MATDES.2013.03.010.

[37]   S. Farina, C. Morando, Comparative corrosion behaviour of different Sn-based solder alloys, J. Mater. Sci. Mater. Electron. (2015) 464–471. doi:10.1007/s10854-014-2422-0.

[38]   M. Hasnine, J.C. Suhling, M.J. Bozack, Effects of high temperature aging on the microstructural evolution and mechanical behavior of SAC305 solder joints using synchrotron X-ray microdiffraction and nanoindentation, J. Mater. Sci. Mater. Electron. 28 (2017) 13496–13506. doi:10.1007/s10854-017-7189-7.

[39]   M. Wang, J. Wang, H. Feng, W. Ke, Effects of microstructure and temperature on corrosion behavior of Sn--3.0Ag--0.5Cu lead-free solder, J. Mater. Sci. Mater. Electron. 23 (2012) 148–155. doi:10.1007/s10854-011-0552-1.

5. Alkanolamines as activators in no-clean flux systems: investigation of humidity robustness and solderability

Feng Li, Kamila Piotrowska, Morten Stendahl Jellesen, Rajan Ambat

Abstract: This paper systematically investigates the humidity robustness and solderability of five alkanolamines used as activators in flux systems, and their effect was assessed along with the influence of soldering temperature. Electrochemical impedance spectroscopy and chronoamperometry techniques were used to obtain a better understanding of water adsorption, absorption, and protonation tendencies of alkanolamine candidates. Potentiodynamic polarization, hot plate spreading test, and wetting balance test were adapted for the etching ability and solderability evaluation. Thermal degradation of alkanolamine compounds was analyzed using thermogravimetric analysis (TGA) and Fourier-transform infrared spectroscopy (FT-IR). The combined results indicate a strong water absorption and protonation of diethanolamine (DEA), triethanolamine (TEA), and triisopropanolamine (TIPA), rendering them not reliable and not feasible as activators. Poor solderability of alkanolamine-based fluxes was inferred based on their thermal degradation behaviour and poor oxide removal ability under the soldering conditions.

Keywords: Alkanolamine, solder flux, electronic corrosion, humidity, reliability, solderability.

I. INTRODUCTION

No-clean fluxes were developed in 1990s in order to eliminate chlorofluorocarbons (CFCs) from the production floors according to the Montreal Protocol [1][2]. From then on, no-clean fluxes have been widely used for print circuit board assemblies (PCBAs) in electronics industry. The idea of no-clean flux systems was aimed at decomposing and evaporating their activator substances during the soldering process, and the expectation was to obtain minimal level of the residues or the residue-free PCBAs. However, in practice, significant levels of residues present on the PCBAs after the soldering process have been reported in the literature, either related to lab-scale investigations [3] or directly to the manufacturing process [4]. The amount and type of residue depend on a number of factors, including the characteristics of the PCBA, type of soldering process [4], and soldering environment (e.g. nitrogen atmosphere) [5], however, most important factors are flux chemistry and the amount of flux applied [4]. Design of the PCBA has a significant influence on trapping the residue under the low stand-off height components or around the through-hole areas [4][6].

No-clean flux residues contain various types of resin, solvents, and weak organic acids (WOAs) [5][7][8]. The typical WOAs used in commercial flux systems include succinic acid, glutaric acid, adipic acid, and malic acid [2][5]. A number of studies reported that WOA-based solder residues, arising from the use of no-clean flux systems, can induce various humidity-related reliability issues due to the electrochemical process occurring upon the residue dissolution into the water layer. This corrosion phenomenon can lead to a critical reduction of surface insulation resistance (SIR) [5][9][10] or electrochemical migration (ECM) and related short-circuit failures. In the ECM process, corrosion of e.g. Sn, Ag, and Cu takes place on the anode and the dissolved metallic ions migrate towards cathode where the metallic ions can deposit and grow back to anode in the form of metallic dendrite [11]. The corrosivity of the flux residues is directly related to the properties of WOAs remaining on the PCBAs , for example: hygroscopicity and ionic nature of various WOAs [9][12], their solubility, the amount of WOAs present on the PCBAs [10], potential bias on the PCBAs [9][13], service temperature and humidity levels [9][10][12]. The WOAs with longer carbon chain usually possess lower polarity and exhibit higher moisture absorption point (high critical relative humidity level) [9], meaning lower extent of moisture absorption and lower degree of ionization. For instance, Verdingovas et al. [13] reported that the moisture absorption relative humidity (RH) for adipic and succinic acids were 99%RH and 98%RH, respectively, while the moisture absorption point of glutaric acid was between 75%RH to 89%RH. Similar observation was made by Conseil et al. in the investigations on the flux residue and humidity interaction [3]. As shown, the chemistry of the residue strongly defines the reliability of the devices operating under humid conditions.

The type of WOAs chosen for the flux formulation is based on the WOA's strength of oxide layer etching ability that is necessary for performing a successful soldering process. This strength can be characterized by the acid dissociation constant (pKa) value describing the general strength of an acid in a solution. The WOAs with low polarity (e.g. low amount of carbon-oxygen bonds) generally exhibit low pKa values, therefore, exhibit low acid strength and low ability for oxide layer removal. However, WOAs with low pKa values show better humidity robustness due to their high moisture absorption RH level and lower dissociation possibilities [14]. In order to balance both good solderability and humidity robustness, no-clean flux system formulations use various blends of WOAs [14]. Thermodynamically, the ionic mixture shows the moisture absorption point for blends below the levels found for the individual components. Specifically, in relation with no-clean flux systems, Marcolli et al. [15] and Piotrowska et al. [14] reported that the moisture absorption RH of binary mixtures of weak organic acids shift to lower humidity range compared to the levels exhibited by any of the individual constituents. This phenomenon indicates the potential humidity-

related reliability issues for electronics occurring at lower RH levels when mixtures of activators are used in no-clean flux systems.

Recently, driven by the need for better humidity robustness of devices together with a need for good solderability of the flux formulations used for the assembling purposes, organic amines use as activators have attracted the attention of flux manufacturers [16]. Amines can remove the oxide layer from a copper surface (a common material on the printed circuit board assembly) following the Brönsted-Lowry acid base reaction as reported by Shi et al. [16]. Vaynman et al. reported the improvement of wetting properties of Cu surface using ethanolamine, diethanolamine, and triethanolamine in the solder flux system [17]. Tolla et al. reported the reduction of dendrite growth during ECM testing when amines were used as additives to the flux formulation due to the formation of complexes between amine with metallic ions [18]. The anonymous amine candidates tested as activators or as additives in activator package in these reports might show the possibility of obtaining amine-based flux systems, which can provide good humidity robustness and desired solderability properties. Corrosion reliability of these amines were further investigated using the Cu mirror test [18], surface insulation resistance (SIR) test [18], and electrochemical methods such as potentiodynamic polarization, electrochemical impedance spectroscopy (EIS), and linear polarization resistance (LPR) methods [19]. Oxidation layer removal process of WOAs and anonymous amine candidates have been investigated using potentiodynamic polarization test [20][19], hot plate spreading test [16][18] and solderability test methods [18]. The type of amines used in these investigations was not reported, while these investigations were mainly focused on the soldering aspects and direct measurements of corrosion attack, for example on the copper substrate. However, none of these studies investigated the humidity robustness and solderability aspects of amines in comparison with the commonly used WOAs in the flux systems, which is an important aspect in order to determine whether their use as activators alone or in combination with the WOAs provides better reliability. Further, the lone pair of the amino group in amine usually attracts a proton to form a conjugate acid and the hydroxide ions according to the Brønsted-Lowry acid base reaction in the condensed water, which is known as protonation behavior [21], increasing the conductivity of the electrolyte. Therefore, it is also important to investigate the moisture interaction capability of amines together with their protonation effects on electronics reliability, such as leakage current and electrochemical migration tendency, directly on the surface of PCBAs.

Present investigation focuses on a comprehensive understanding of the performance of alkanolamines as potential activators for the flux system with detailed analysis of their behavior

under humid conditions and the link to their solderability properties being relatively compared with typical WOA activators used in the industry. Potentiodynamic polarization, hot plate spreading test, and wetting balance test methods were used for understanding the ability of amines to etch the copper surface and provide good surface wettability for soldering purposes (solderability). The thermal decomposition behavior of the amines tested under soldering temperature regime was investigated using thermogravimetric (TGA) and differential thermal analysis (DTA) analysis techniques, and Fourier-transform infrared spectroscopy (FT-IR) technique. Electrochemical methods such as EIS and chronoamperometry (CA) were employed in order to evaluate the extent of humidity interaction with the alkanolamines as well as their ability to initiate electrochemical failure modes such as ECM.

II.   MATERIALS AND EXPERIMENTAL METHODS

Alkanolamine candidates used for the investigations

Five alkanolamines of analytical grade (Sigma Aldrich, USA) were tested in the present study. Molecular formula, molecular weight, melting point, boiling point, and pKa values at 25℃ are shown in **Table 5.1**. All of the amines possess hydroxyl functional groups attached to the hydrocarbon chain, and the number of these –OH groups varies between the amines. The boiling point characterizes how easy amine will vaporize/decompose during the soldering process. Due to the higher melting points of DIPA and TIPA, they are present as solids at room temperature, while EA, DEA and TEA exhibit liquid state at room temperature. The pKa-values determines the reactivity of the amines in terms of their alkaline strength, and as such can be used as an expression for their etching ability.

Table 5.1. *Physical and chemical properties of amines used in the study. Data adapted from [22].*

	Molecular formula	Molecular weight (g/mol)	Melting Point (℃)	Boiling Point (℃)	pKa at 25℃
Ethanolamine (EA)	$NH_2CH_2CH_2OH$	61.083	10.5	171	9.5
Diethanolamine (DEA)	$NH(CH_2CH_2OH)_2$	105.136	28	268.8	8.96
Triethanolamine (TEA)	$N(HOCH_2CH_2)_3$	149.188	20.5	335.4	7.76
Diisopropanolamine (DIPA)	$NH[CH_2CH(OH)CH_3]_2$	133.186	44.5	248	9.1
Triisopropanolamine (TIPA)	$N[CH_3CH(OH)CH_2]_3$	191.268	45	305	8.06

Materials preparation

a) Cu substrate for etching ability evaluation

Pure copper foil (Goodfellow, USA) was used as test substrates for the evaluation of amine etching ability. The surface of the Cu foil was polished using #4000 SiC grit paper.

b) Cu alloy substrate for solderability evaluation

Solderability assessment was conducted using a wetting balance and hot plate spreading tests. The wetting balance test was carried out using copper coupons according to the IPC-TM-650 2.4.14.2, i.e. a size of 6 mm × 25 mm × 0.5 mm prepared using electrical discharge machining. Cleaning of Cu coupons was conducted based on ISO 9455-16 international standard. For the hot plate spreading test, Cu-37Zn coupon substrate with a size of 40 mm × 75 mm × 1 mm was prepared. Cleaning of the brass coupons was conducted as described in the ISO 9455-16 standard.

c) SIR pattern for the electrochemical evaluation of humidity robustness

The SIR pattern shown in **Figure 5.1** was used for the electrochemical tests meant to reflect the humidity robustness of systems containing amine compounds as activators. The interdigitated pattern comprised of a hot air solder levelled (HASL) Sn-0.7Cu alloy as surface finish plated on copper tracks with an FR-4 laminate as a substrate of IPC-4201/21 test board. The active testing area of the SIR pattern was 13 mm × 25 mm with a 0.3 mm pitch size. The overlapping length of the adjacent pitch lines was 10.8 mm × 41 set, which in total provided 442.8 mm for the DC and AC tests. A detailed description of the pattern can be found elsewhere [23].
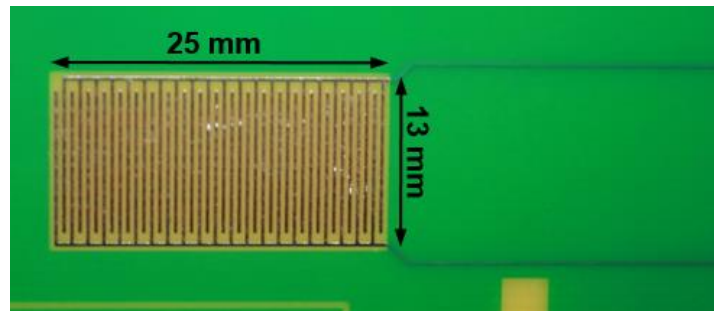
Figure 5.1 Picture of the SIR comb pattern used for electrochemical tests.

The SIR patterns were pre-contaminated with the respective alkanolamines in isopropanol solution after evaporation and the level of alkanolamine used for testing was 100 μg/cm^2. In order to simulate the state and the amount of residue left on the PCBA after the wave soldering process, thermal activation of amine-contaminated SIR patterns was performed at 175℃ and 240℃ for 45 sec in a Techno HA-06 oven. The thermal activation at 240℃ aimed to simulate the proper soldering temperature existing at the interface between the PCBA and solder wave (in wave soldering process simulating bottom part of the PCBA). Moreover, the solder flux sprayed during the wave soldering process to the bottom part of the PCBA can reach the top side through via-holes. The temperature experienced by the top side of the PCBA is approximately 170℃ [24].

Therefore, an additional thermal activation of the test boards at 175℃ was carried out in order to simulate the thermal conditions of the top side of PCBA during the soldering process [6].

Etching ability evaluation using potentiodynamic polarization test

Etching ability of five alkanolamines was evaluated by potentiodynamic polarization measurements using a "Biologic VSP" multichannel potentiostat (Bio-Logic Instruments, France). The polarization of Cu foil was conducted using Paracell (Gamry Instruments, USA) with an exposed area of 2.85 cm^2 in 0.1 M amine or WOA aqueous solution. Open circuit potential (OCP) was record after 30 min stabilization. For the polarization, the scan range of the polarization was set from -250 mV to 1500 mV vs. OCP using Ag/AgCl electrode as reference electrode (RE). The scan rate used for the experiment was 60 mV/min. Each experiment was repeated three times with good consistency.

Solderability assessment using wetting balance and hot plate test

a) Wetting balance test

Solderability tests were performed using the "Must 3 wetting balance tester" (GEN 3, UK), which allows for the measurement of the extent of wetting of molten solder on the copper coupons, which surface was initially activated by amine activators. A model flux formulation was created by mixing 4 wt.% of amine as activator and 96 wt.% isopropanol alcohol of analytical grade. The Cu coupon was initially immersed in the model flux solution to a depth of 10 mm and drained off the extra flux by keeping it vertically on a clean filter paper following the procedure described in IPC-TM-650 2.4.14.2. After 20 sec pre-heating of the SAC 305 solder bath incorporated in the wetting balance equipment occurred at a temperature of 270℃, which was followed by the Cu samples being dipped in the molten solder bath for 10 sec with an immersion depth of 5 mm. Both the immersion speed and withdraw speed of Cu substrate to solder bath were set to 20 mm/s.

Following the wetting balance test, the Cu coupons were exposed to 40℃/99% RH for 24 h in accordance with the copper mirror method (IPC-TM-650 2.3.32) in order to additionally evaluate the corrosion extent induced by the alkanolamines and WOAs based fluxes.

b) Hot plate spreading test

Additional evaluation of amine solderability was conducted using the hot plate spreading test based on IPC-TM-650 2.4.46 standard using brass coupons. Solderability tests were performed using a "SD160 digital hotplate" (Stuart Equipment, UK), which allows for visual assessment of the extent of wetting of molten solder on the brass coupons, which surface was initially activated by amine activators. The source of molten solder was an O-ring of 1 cm diameter prepared from the flux-free SAC 305 alloy and placed on the brass substrate. 50 µL of the model flux was applied at the center of an O-ring placed on the plate, and subsequently the preheating of the sample was

conducted at 160℃ for 2 sec. Subsequently, the test system was transferred to another hotplate with a precisely controlled temperature of 270℃ in order to melt the solder wire and assess the solder spreading extent when the O-ring melted. The solderability level was visually assessed based on the description in the IPC-TM-650 number 2.4.46 standard.

Analysis of corrosion products morphology and etching ability

The surface morphology of the samples subjected to solderability test and following the exposure to humidity has been examined using a VHX digital microscope (Keyence, Japan). For the assessment of the quality of amine-based model flux on etching ability, the cross section of the soldered copper coupons used for wetting balance testing and polarized samples were inspected using a Quanta 200 FEG scanning electron microscope (FEI, USA) under secondary electron mode.

Thermal decomposition behavior of amine activators

    a) **Thermal analysis using thermogravimetric analysis (TGA) and differential thermal analysis (DTA)**

The nature of amines subjected to varying temperatures were investigated using TGA and DTA techniques. TGA analysis was aim to investigate the liquid-gas phase transformation temperature of alkanolamines, whereas DTA analysis was employed to investigate the thermal decomposition temperature of the alkanolamine candidates. Pure alkanolamine candicates were subjected in a alumina crucible for the testing. Argon gas was used as a protection gas during the experiments. The experiment was performed with a temperature ramping rate of 20℃/min in a range from room temperature to 1000℃.

    b) **Structural analysis using FT-IR technique**

In order to further assess the thermal decomposition tendencies and structural changes of alkanolamines upon their exposure to soldering temperature profile, spectroscopic analysis of the aged activators was conducted after their initial thermal treatment. Thermal activation of the amines was carried out under simulated wave soldering temperatures corresponding to the top and bottom of the PCBA surface [24]. The amines were analyzed using the Nicolet iN10 MX infrared imaging microscope (Thermo Fisher Scientific, USA) with a Ge attenuated total reflectance (ATR) tip. The activation was conducted by placing respective amine compounds on a glass substrate and conducting thermal activation at 175℃ and 240℃ for 100s in the Techno HA-06 oven. 10 wt.% water in alkanolamine solution were used for water interaction analysis. Alkanolamine candidates that have not undergo a thermal exposure were used as reference in the spectral analysis.

Humidity robustness evaluation of amines using electrochemical techniques

Humidity robustness assessment was carried out in "Espec PL-3KPH" climatic chamber with a certainty of $\pm 0.3℃$ and $\pm 2.5\%$ RH of the test conditions.

a) Single frequency EIS measurement

The interdigitated two electrodes SIR pattern shown in **Figure 5.1** was used for electrochemical testing with one of the electrodes used as a reference and counter, rendering the other electrode as working electrode. EIS technique was used in order to evaluate the interaction of amine residue with water vapour under varying humidity and temperature levels. The interaction relied on the absorption of moisture by the alkanolamine and its protonation, which was manifested during the electrochemical testing, allowing for the determination of the critical RH for moisture absorption and moisture drying under various thermal activation and test temperatures.

Testing was initiated after humidity stabilization at 30% RH for 6 hours, and the EIS response was recorded at a frequency of 10 kHz over the humidity ramping from 30% RH to 99% RH in 12 hours, followed by a ramp-down to 30% RH with the same rate at a testing temperature of 25℃, 40℃, and 60℃. Testing temperatures of 25℃ and 40℃ meant to simulate the range of temperatures, at which the electronic equipment is used in different climatic locations worldwide, while 60℃ temperature was used for simulating the self-heating of the device.

A signal of a single frequency level of 10 kHz with the amplitude of 25 mV was used for impedance testing, and the level is based on the results obtained in previous investigations that used impedance technique for assessing the humidity boundaries for various flux activators [9][14][22]. Typically, the critical humidity level for moisture absorption by hygroscopic substances is called deliquescence relative humidity (DRH) and the humidity level, at which desorption of uptaken water occurs is designated as efflorescence relative humidity (ERH). Some of the amines used in these investigations are liquid at room conditions, and it is not correct to use DRH and ERH terms, therefore, the RH level for moisture absorption is designated in this paper as "moisture absorption RH" and the RH level when the water desorption occurs is termed as "moisture drying RH".

b) Chronoamperometry (CA) measurement

The CA measurements were carried out in order to understand the corrosivity of alkanolamines and their potential effect on ECM occurrence. A 5V DC potential bias was applied to the SIR pattern pre-contaminated with various amines mimicking the residue remaining on the PCBA surface, and the resulting leakage current of the SIR pattern was collected at varying RH levels of 60%, 70%, 80%, 90%, and 98%, under 25℃, 40℃, and 60℃. The initial stabilization of the test

boards was carried out for 2 hours at 30% RH. The water film build-up on the SIR pattern under various conditions and ECM occurrence were visualized in-situ using an "AD7013MZT Dino-Lite" digital microscope.

III. RESULTS

Etching ability evaluation of alkaolamines and WOAs

The amine etching ability was investigated by by anodic polarization. **Figure 5.2**(a) shows the results of etching ability testing for alkanolamines performed using the potentiodynamic polarization, and a comparison between various activators can be inferred from the anodic polarization curves for Cu. The OCP result in **Figure 5.2**(a) shows that the primary amine EA solution induced the most negative OCP of Cu, while secondary amines (DEA, DIPA) exhibited slightly higher OCP values. Tertiary amines (TEA, TIPA) exhibited the highest OCP values among the tested alkanolamines.

The electrochemical parameter leads to the dissolution of Cu was denoted as etching current density (**Figure 5.2**(b)), which was calculated by Tafel analysis from EC-Lab software. From this perspective, tertiary amines (TEA, TIPA) showed the lowest values compared to secondary amines (DIPA, DEA) or primary EA at any anodic potential level. Among the amines, the primary amine EA showed the highest current density.

The overall OCP values for copper induced by five amine solutions are more negative than the values induced by two WOAs. However, the polarization curves indicate that the anodic activity of WOAs is higher than the activity of all the tested alkanolamines over 0.2 V, which indicates high anodic dissolution rate for WOAs compared to amines over this range of voltage. The shorter glutaric acid showed higher current density during the Cu polarization over the same potential ranges compared to adipic acid.

Figure 5.3 shows the surface morphology of Cu samples after polarization in alkanolamines and glutaric acid solutions. Similarly to the etching abilities inferred from the Cu polarization curves, EA, DEA, and DIPA (**Figure 5.3**(a)-(c)) showed highly attacked copper surface (therefore, higher etching ability) compared to the surface activated by TEA and TIPA solutions (**Figure 5.3**(d) and (e)). This could be due to the higher pKa value (stronger alkalinity) of the primary and secondary amine. However, the copper sample polarized in the glutaric acid solution showed more aggressive attack of the surface (**Figure 5.3**(f)) compared to the attack observed for the amine solutions.
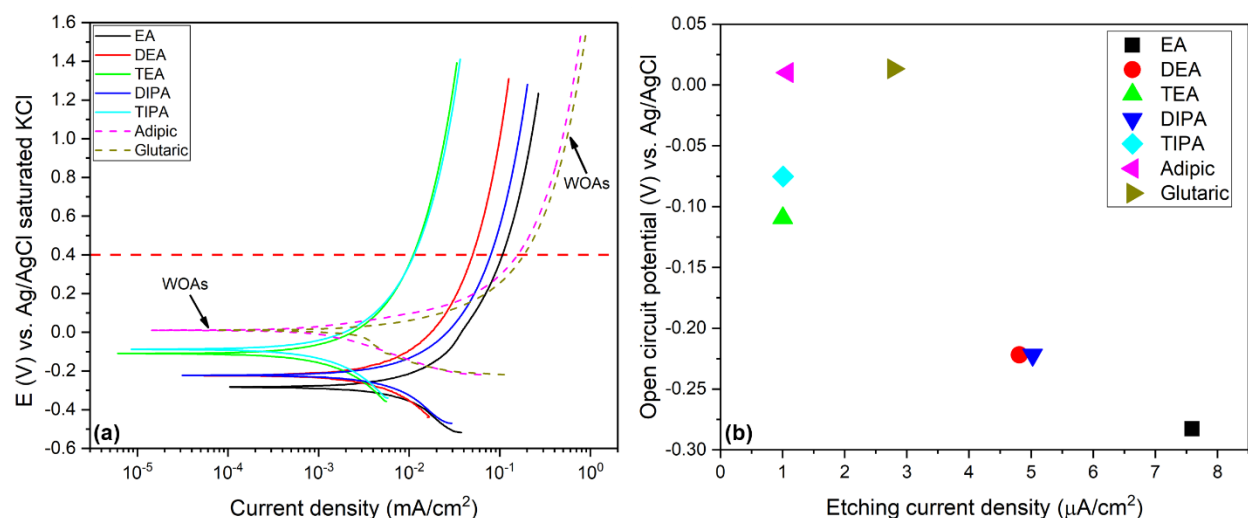
Figure 5.2 *(a) Representative polarization result for various alkanolamines and commonly used WOA activators tested using Cu substrate in 0.1 M aqueous solutions at room temperature, (b) summary of open circuit potential (OCP) and etching current density of tested solutions.*
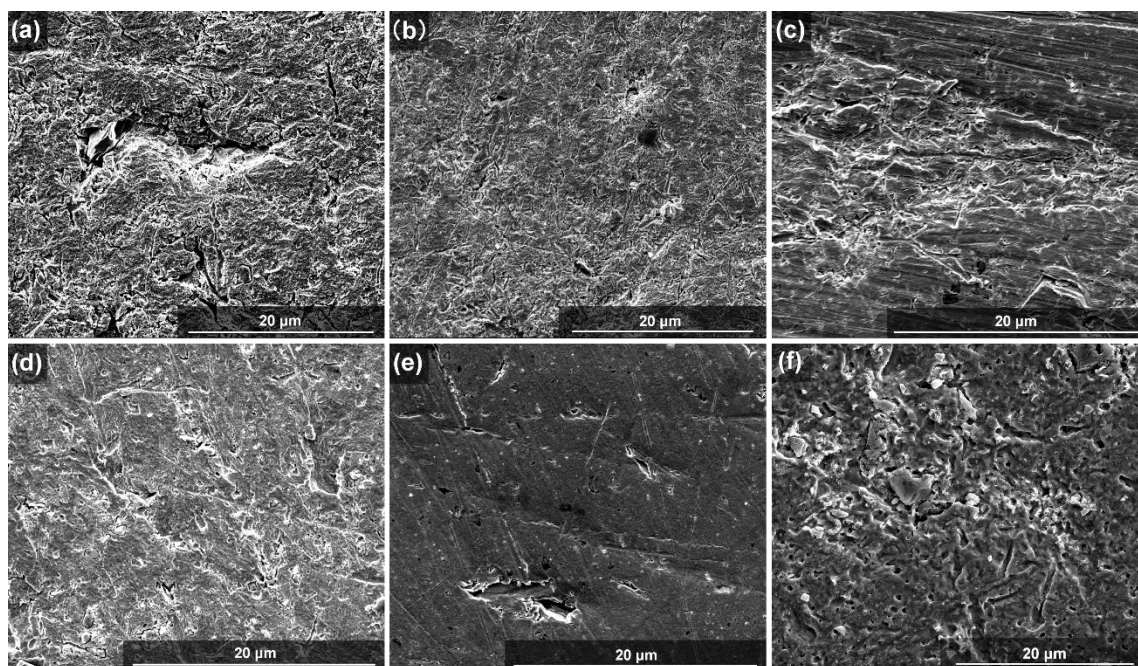
Figure 5.3 *Secondary electron (SE) images of Cu samples after polarization test in 0.1 M amine and WOA solutions; (a) EA, (b) DEA, (c) TEA, (d) DIPA, (e) TIPA, (f) glutaric acid.*

<u>Solderability assessment using amines as activators</u>

The evaluation of solderability of the surface activated by various amines was carried out using wetting balance and hot plate spreading tests.

Figure 5.4 shows the results from wetting balance testing using alkanolamines and typical WOAs based model fluxes used for surface activation of copper coupons. The wetting force of glutaric acid and adipic acid model fluxes were above 4 mN, which are significantly higher compared to the wetting force levels induced by alkanolamine model fluxes as shown in **Figure 5.4**(a). The wetting force of all the amines were below 0 N with tertiary TEA showing the highest value and primary EA the lowest among the tested amines.

The wetting length shown in **Figure 5.4**(b) was inferred by calculating an average value of the length of solder on both sides of Cu substrate along the coupon width, which also agrees with the ranking of wetting force. The wetting length of adipic acid, glutaric acid, and TEA model flux systems were higher than the immersion length of the solderability testing coupon (5 mm). The cross section SEM micrographs in **Figure 5.5**(a-e) show the thinner solder alloy exhibited on Cu substrates using all the alkanolamine fluxes compared to WOA-based fluxes (**Figure 5.5**(f-g)), which refer to poor solderability.
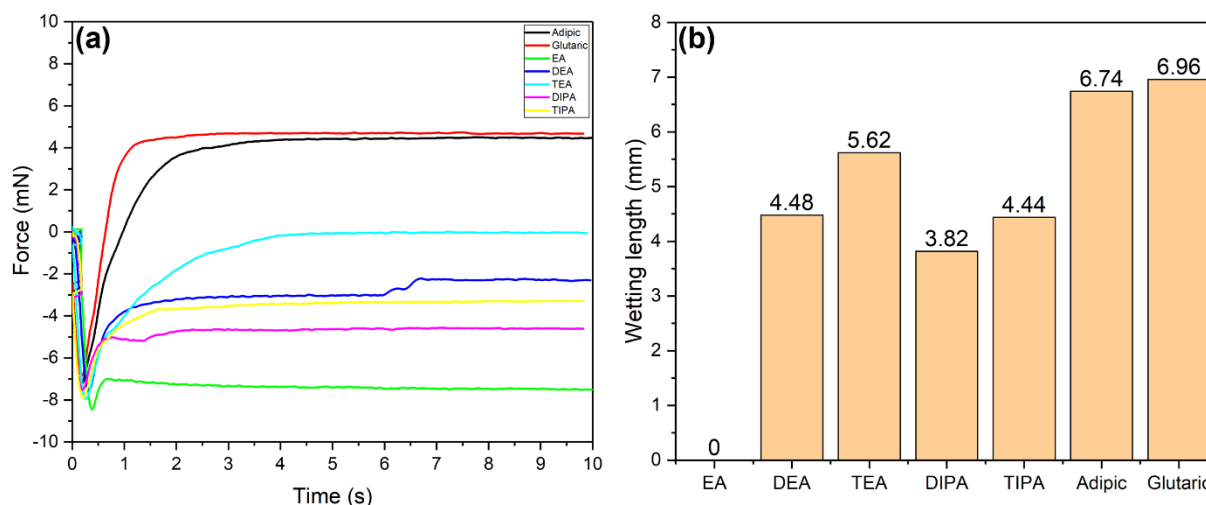
Figure 5.4 Wetting balance testing results using amines and WOAs as surface activators: (a) wetting force and (b) wetting length of solder alloy for various activators model fluxes. Results obtained for WOAs are included for comparison.

Figure 5.5 shows the visual appearance of the tested samples, which can provide an indication of the activator corrosivity in accordance with the IPC copper mirror method. Severe corrosion product formation of a green colour occurred in the case of glutaric acid and adipic acid model flux activation of the samples as shown in **Figure 5.5**(f) and (g). On the contrary, alkanolamine etched samples showed less pronounced formation of the corrosion products. Only a few

corroded spots were observed on secondary DEA and tertiary TIPA etched samples (**Figure 5.5**(b) and (e)).
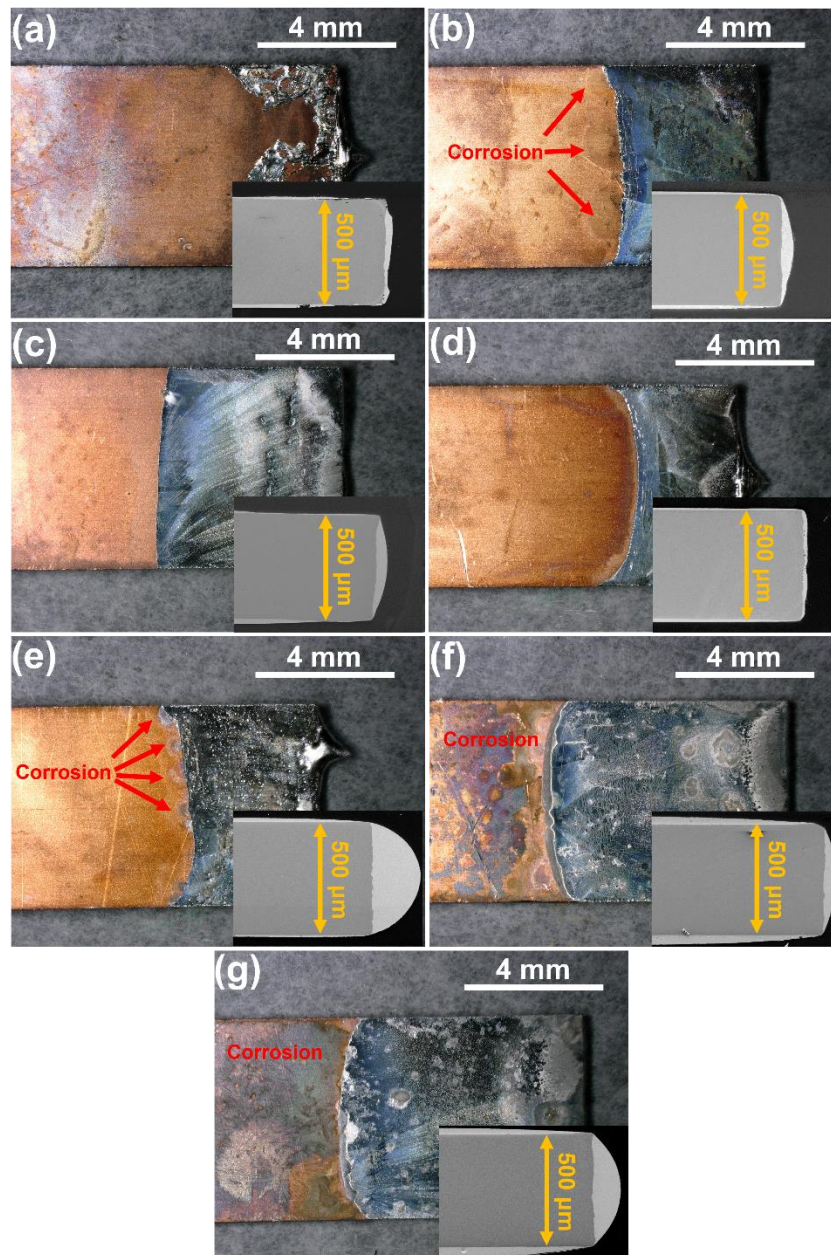
Figure 5.5 LOM inspection and cross section SEM micrographs of samples tested towards solderability assessment. Inspection performed after 24 h exposure to 40℃/99% RH: (a) EA, (b) DEA, (c) TEA, (d) DIPA, (e) TIPA, (f) Adipic acid, (g) Glutaric acid.

Figure 5.6 shows the results from the hot plate test indicating the spreading of solder material over the brass surface with different amines used as for surface activation. **Figure 5.6**(c) shows that the TEA flux provided a relatively good wettability for SAC 305 solder wire, and the best

among all amines. SAC wire partially covered the brass substrate activated by DEA flux as shown in **Figure 5.6**(b), while EA, DIPA, and TIPA fluxes were not able to activate the substrate enough to provide good wettability for SAC 305 wires (**Figure 5.6**(a)(d) and (e)).
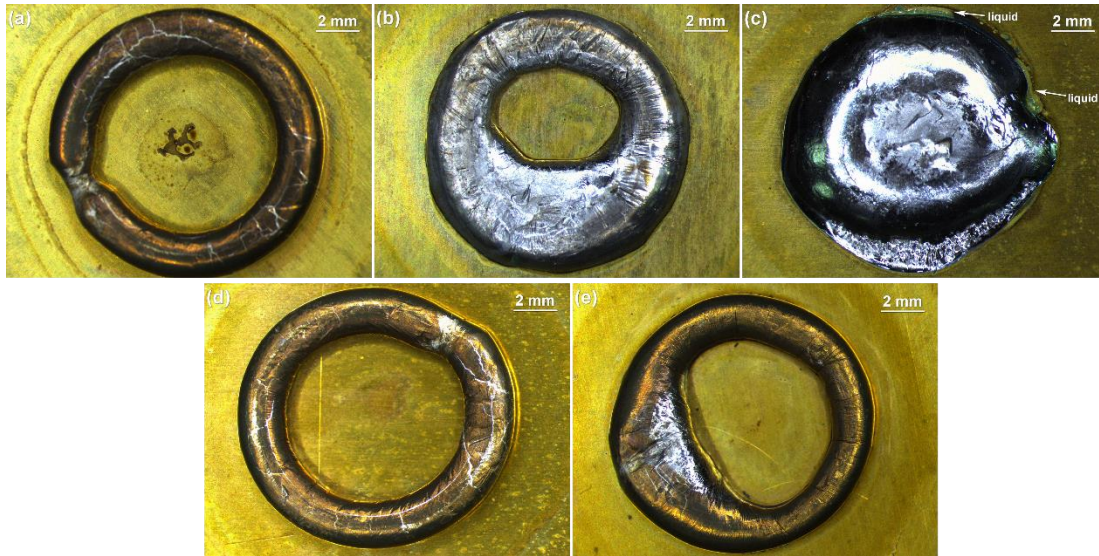
Figure 5.6 LOM micrographs of hot plate spreading tested samples: (a) EA, (b) DEA, (c) TEA, (d) DIPA, (e) TIPA.

Thermal degradation analysis of alkanolamines

Figure 5.7 shows the TGA and DTA testing results of the alkanolamines. All the TGA curves illustrated the evaporation of amines over a temperature range. The weight reduction of EA and DIPA in **Figure 5.7** (a) and (d) was initiated at 165℃ and 217℃, which is below the thermal activation temperature during a typical wave soldering process. However, the temperature, at which the weight reduction occurred for DEA, TEA, and TIPA activators was far beyond the wave soldering temperature (initiation at 244℃, 288℃, and 245℃, respectively) as shown in **Figure 5.7**(b)(c)(e). The amine evaporation for the mentioned compounds was terminated at 309℃, 406℃, and 331℃, respectively.

The DTA curves (**Figure 5.7**) showed two endothermic peaks for each amine. First peak was very broad and occurs at lower temperature range indicating a low thermal adsorption due to the stretch of molecule structure. The second peak was sharp and occurred at higher temperature range, and indicated the energy for amine evaporation. Accordingly, the difference in temperatures between the final weight loss in TGA curve and a sharp endothermic peak in DTA curve indicates that the evaporation and pyrolytic decomposition occurred under different temperatures, whereas the difference is minor.
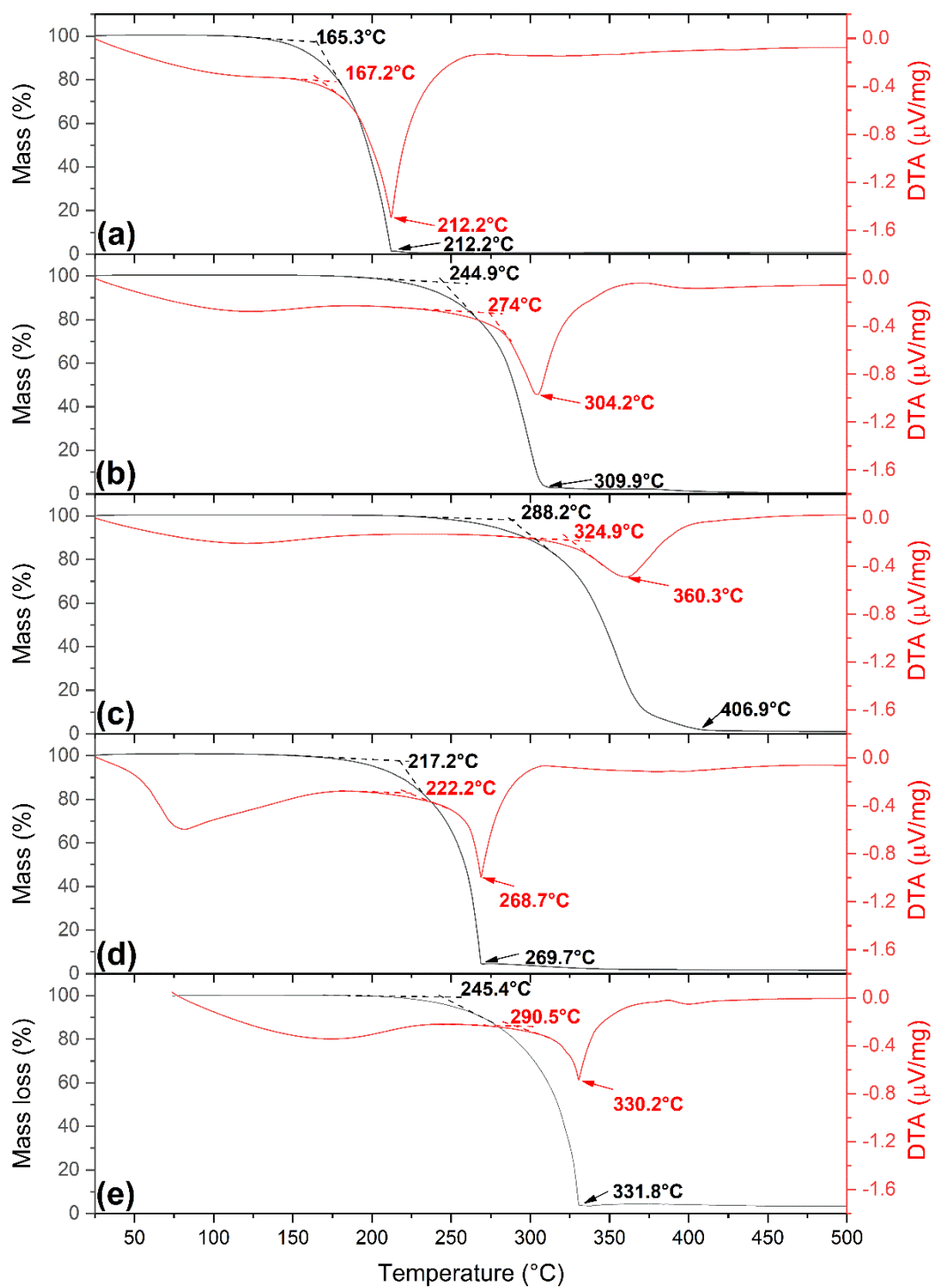
Figure 5.7 *TGA-DTA analysis of amines used in the investigations: (a) EA, (b) DEA, (c) TEA, (d) DIPA,*
(e) TIPA

In order to further assess the thermal decomposition tendencies and structural changes of alkanolamines upon their exposure to soldering temperature profile, spectroscopic analysis of the aged activators was conducted after their initial thermal treatment. **Figure 5.8** shows the FT-IR spectra of all alkanolamines after various thermal activations. It is noticed that the glass substrate did not influence the peaks in the wavenumber range between 4000-1300 cm^{-1}. Two distinct peaks [25] appeared at high frequency regions for non- and thermally-treated (175℃) samples, which suggests the appearance of N-H stretching vibration in the molecule of EA as shown in **Figure 5.8**(a). However, these two peaks disappeared after the 240℃ thermal activation. Thermal treatment did not have a significant influence on changes to the N-H stretching vibration for secondary DEA samples as shown in **Figure 5.8**(b). In case of secondary DIPA, thermal degradation of N-H bond was observed (**Figure 5.8**(d)). **Figure 5.8**(d) and (e) indicate the melting process of the solid crystals, and the transmittance increased after thermal activation, as shown in the 600-1500 cm^{-1} wavenumber region. The broadening of O-H stretch peak in the range of 3550-3680 cm^{-1} wavenumber region occurred in all the 10 wt.% water mixed alkanolamine solutions compared to pure alkanolamine candidates, as shown in **Figure 5.8**(a-e).
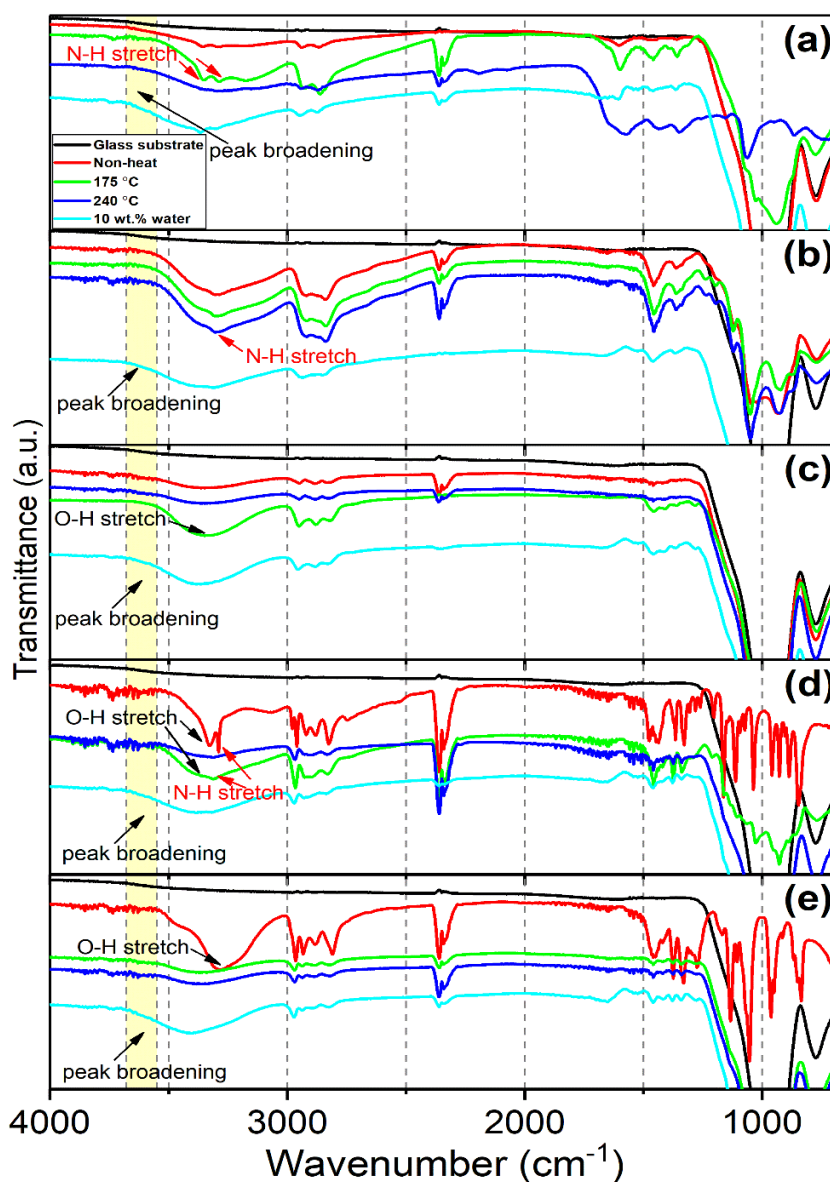
Figure 5.8 The FT-IR spectra of five alkanolamines activated at different thermal conditions: (a) EA, (b) DEA, (c) TEA, (d) DIPA, (e) TIPA

Humidity effects of amine residues on PCBA

    a) **EIS testing of amine moisture sorption behavior**

Figure 5.9 illustrates the impedance response of the SIR system pre-contaminated with amine residues, which were activated under various thermal treatments and exposed to varying humidity and temperature conditions. During the increase of RH, the impedance drop at a particular RH level corresponds to moisture absorption. The recovery point of the impedance signal upon decreasing humidity is related to drying of the dissolved residue on the SIR surface. The impedance value noted at 99% RH indicates the strength of a protonation behavior for alkanolamine candidates due to the change of solution conductivity.

In case of all amine types tested, the moisture absorption RH level is lower than the moisture drying RH showing, indicating the hysteresis behavior related to moisture intake and release. **Figure 5.9**(a) and (d) show that the EA and DIPA contaminated SIR pattern presented a high impedance response at 99% RH for all testing conditions. Thermal activation process did not influence the impedance response of the EA, TEA, and TIPA contaminated SIR patterns under the same testing conditions as shown in **Figure 5.9**(a), (c) and (e). However, the thermal activation process of DEA at 240℃ significantly shifted the critical RH level from 30% RH to approximately 75% RH under 25℃ as shown in **Figure 5.9**(b).

Test exposure to temperature and humidity has shown an influence on the behavior of five alkanolamines. **Figure 5.9**(a) and (d) show that the reduction of moisture-absorption RH, moisture-drying RH, and impedance response at 99% RH for EA and DIPA with an increase of test temperature from 25℃ to 60℃. The critical RH decreased from 94-95% RH to 86% RH upon an increase in exposure temperature, while moisture-drying RH significantly decreased from 94-95% RH to 65-66% RH. In contrast, the moisture absorption and protonation behaviors of DEA and TIPA show an opposite trend. Low impedance response was obtained at 60℃. **Figure 5.9**(b) shows the moisture absorption RH of DEA ranged from 30% RH to 88% RH and the moisture drying RH ranged from <30% RH to 81% RH under exposure temperatures of 40℃ and 60℃. While in the case of TIPA, the exposure temperature of 60℃ increased the moisture-absorption RH value and impedance value at 99% RH as shown in **Figure 5.9**(e). **Figure 5.9**(c) shows that the exposure temperature did not have any effect on the impedance response of TEA contaminated SIR pattern.
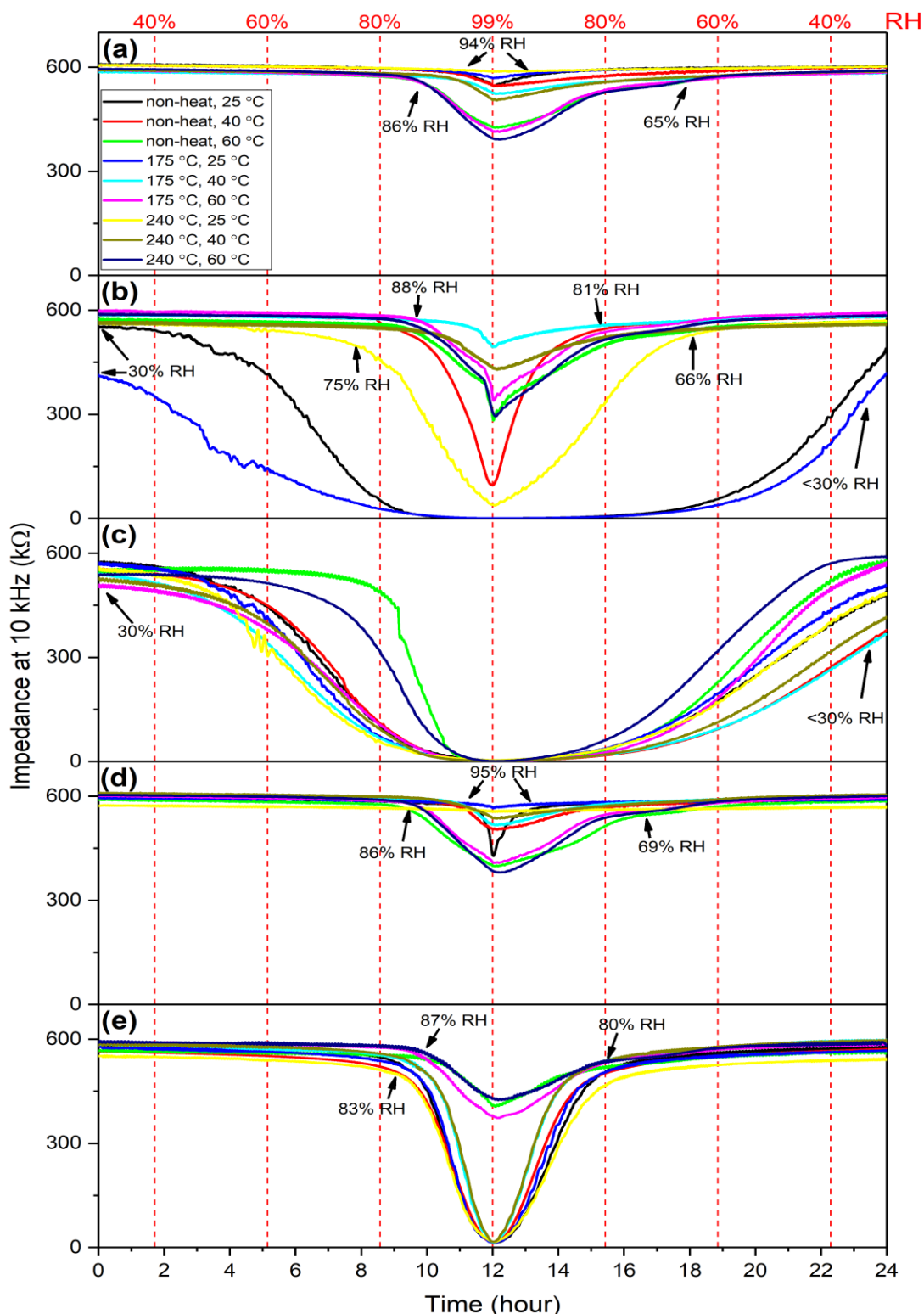
Figure 5.9 *Representative impedance result of SIR pattern pre-contaminated with amine residue under different conditions in 3 parallel tests. Signal collected at 10 KHz over humidity range for assessment of moisture sorption behavior of: (a) EA, (b) DEA, (c) TEA, (d) DIPA, (e) TIPA.*

b) CA testing of amine under different climatic conditions

Figure 5.10 shows the results of CA testing expressed as a leakage current response from the pre-contaminated SIR patterns after various thermal activation and testing conditions. Generally, the leakage current increased with an increasing relative humidity conditions for all the residues without or after thermal activation process. **Figure 5.10**(a) and (d) show that the high leakage current levels were recorded for DEA and TEA contaminated SIR patterns at low relative humidity levels, whereas EA contaminated SIR patterns maintained a low leakage current values even at high relative humidity level. **Figure 5.10**(a) and (d) show that the thermal activation reduced the leakage current of EA and DIPA contaminated SIR patterns under the same testing condition, while the leakage current remained at the similar level for DEA, TEA, and TIPA contaminated SIR patterns without or after thermal activation. The increased exposure temperature (**Figure 5.10**(a)(b)(c)) triggered a significant drop of leakage current for DEA, TEA, DIPA, and TIPA contaminated SIR patterns. For the leakage current levels of DEA and DIPA contaminated SIR patterns, the influence of the exposure temperature observed at 40℃ and 60℃ was significant, as shown in **Figure 5.10**(a)(b)(c); however, in case of TEA and TIPA, the effect was observed only at 60℃. **Figure 5.10**(a) and (b) shows the leakage current of DIPA-contaminated SIR pattern was significantly reduced at the test temperature to 40℃. However, a gradual decreasing trend of leakage current for DEA, TEA, and TIPA contaminated SIR patterns was observed from 25℃ to 60℃ as shown in **Figure 5.10**(a-c).

Figure 5.11 shows the in-situ water film development on DEA-contaminated SIR pattern and ECM failure occurrence under climatic exposure of 98% RH, 25℃ as an example of the residue behavior under humidity testing. **Figure 5.11**(a-c) show a typical view of a progressive water film build-up on the SIR pattern with DEA where no potential bias was applied. **Figure 5.11**(d-f) demonstrates the gradual corrosion of the SIR pattern manifested as a dendrite formation under bias conditions induced by the water film build–up on the contaminated surface. The application of 5 V DC load led to the formation of a small black metallic dendrite structure with its growth initiating at the cathodic pitch lines and progressing towards anodic pitch lines.
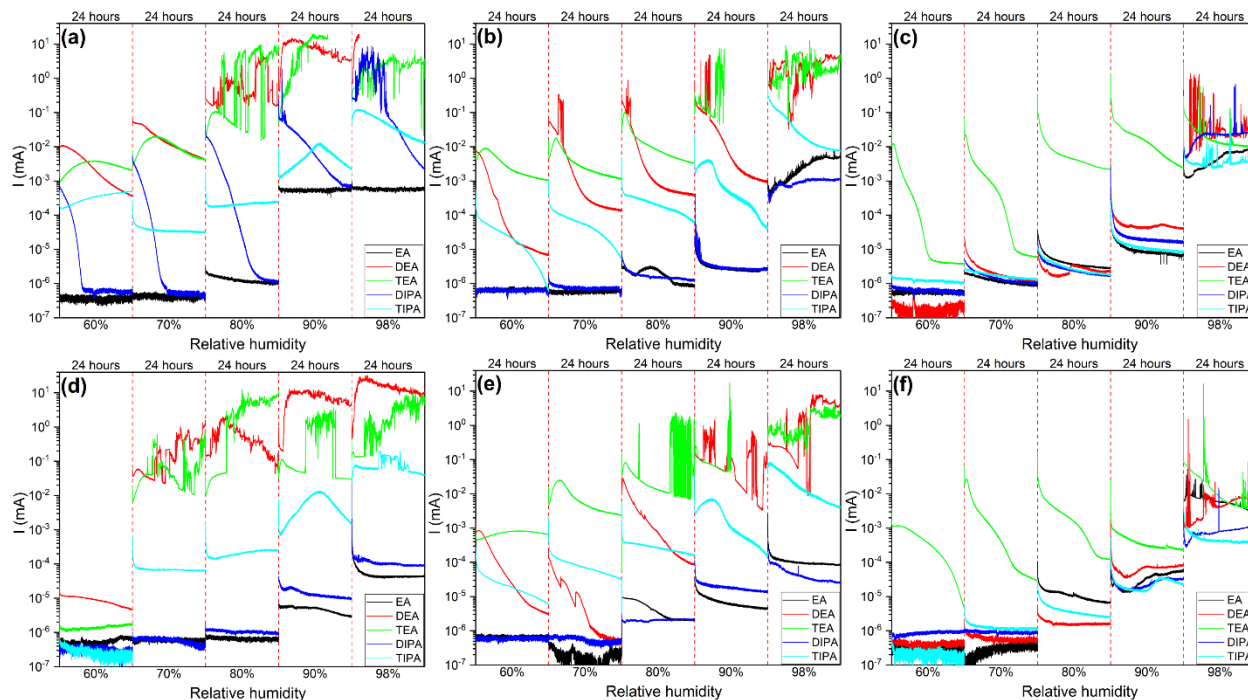
Figure 5.10 CA testing results of alkanolamine-contaminated SIR patterns tested under various testing conditions: (a) no thermal activation of amine and CA test at 25℃, (b) no thermal activation of amine and CA test at 40℃, (c) no thermal activation of amine and CA test at 60℃, (d) thermal activation at 240℃ for 45 s and CA test at 25℃, (e) thermal activation at 240℃ for 45 s and CA test at 40℃, (f) thermal activation at 240℃ for 45 s and CA test at 60℃.
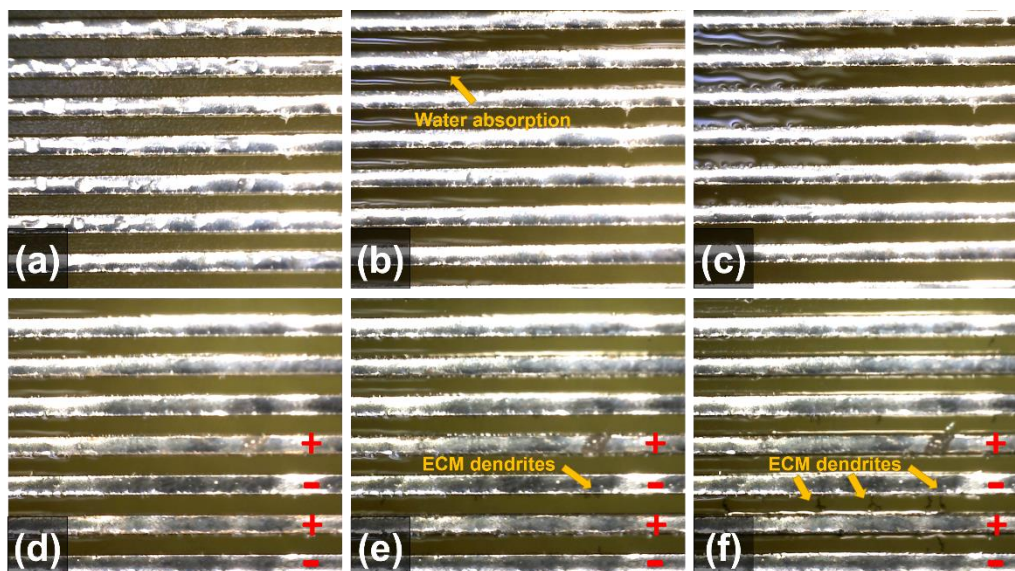
Figure 5.11 In-situ visualization of moisture absorption and ECM on DEA contaminated SIR under climatic exposure of 98% RH at 25℃: (a) 0 min 0 V, (b) 30 min 0 V, (c) 60 min 0 V, (d) 60 min 5 V, (e) 75 min 5 V, (e) 85 min 5 V.

IV.   DISCUSSION

Influence of thermal activation and exposure temperature under humidity testing on the performance of alkanolamine as flux activators

Figure 5.8(a)-(e) show that the water interaction with alkanolamine lead to the broadening of O-H stretching peak in FT-IR spectrum due to the hydrogen bond formation between hydroxyl group in water and amino groups. The humidity level triggered water interaction of alkanolamine was determined using EIS. Under exposure temperature of 25℃, as shown in **Figure 5.9**(b) and (c), the moisture absorption RH of DEA and TEA was below 30% RH, which is indicated by relatively low impedance signal at 30% RH. The protonation of amine reduced the resistance of SIR pattern to very low values under 99% RH exposure. Thermal activation did not influence the moisture absorption behavior of TEA, which might be due to the fact that the activation temperature of 240℃ was lower than the evaporation temperature of TEA of 288℃ (**Figure 5.7**(c)). However, after the thermal activation at 240℃, the moisture absorption RH of DEA increased from 30% RH to 75% RH, which is a desired effect for corrosion reliability, as the activated residue requires higher ambient humidity level for moisture absorption. This effect can be explained as a partial evaporation of the DEA as the activation temperature was close to the evaporation temperature of 244℃ (**Figure 5.7**(b)). Therefore, lower residue amount is expected from DEA than TEA if both are activated under the same soldering process.

For TIPA, the critical RH was around 83% RH (**Figure 5.9**(e)); however, the impedance testing showed large reduction of the SIR signal around this RH level, which indicates high conductivity of the electrolyte induced by the protonation behavior of TIPA. For DIPA, slight increase of impedance signal after the thermal activation at 240℃ was observed (**Figure 5.9**(d)). This might be due to the thermal activation i.e. degradation of amine occurred since the evaporation of DIPA initiates at 222℃ (**Figure 5.7**(d) and **Figure 5.8**(d)). Compared to the exposure temperature of 25℃, testing at 40℃ showed higher impedance levels of DEA-contaminated SIR pattern at 99% RH (**Figure 5.9**(b)). Under exposure temperature of 60℃, the impedance responses of DEA at 99% RH and all TIPA samples were significantly improved compared to 25℃ and 40℃ as shown in **Figure 5.9**(b) and (e). The results indicate that the water absorption and protonation behavior of alkanolamines were influenced by the exposure temperature in different ways. Patil et al. reported the effective dipoles of DEA rotate more rapidly with increasing temperature and the hydrogen bond breakage is more likely to occur at higher test temperature exposures [26]. The energy of molecule under exposure to the temperature of 40℃ could be higher than the energy of intermolecular hydrogen bond formed by water molecules attracted to the amine functional

groups and hydroxyl functional groups in DEA under exposure conditions. Amararene et al. [27] and Hinderaker et al. [28] reported a temperature of 313 K (40℃) decreased the carbonyl sulfide (COS) absorption in aqueous DEA solution. Similarly, the results in the present study show the protonation behavior of DEA was inhibited at 40℃ (**Figure 5.9**(b)). The exposure temperature of 60℃ slightly increased the moisture absorption RH of DEA and TIPA samples, which might be attributed to the increased temperature providing sufficient energy to break the hydrogen bond between water molecules and DEA/TIPA molecules. Consequently, the impedance response of non-thermally activated DEA and TIPA samples significantly increased under high humidity exposure as shown in **Figure 5.9**(b) and (e). Overall, moisture absorption RH of DEA and DIPA increased due to evaporation or degradation induced by thermal activation, while the protonation behavior of DEA and TIPA decreased upon an increase of the test temperature.

Influence of alkanolamine activators on leakage current under DC loads

Depending on different application aspects in electronic industry, 1-10 µA level of leakage current on a PCBA surface typically biased under DC conditions can be taken as the threshold for failure occurrence under humid conditions. Similar leakage current threshold value for commercial wave solder flux-contaminated SIR interdigital pattern was reported by Verdingovas et al. [13] and Piotrowska et al. [29]. Since the present work tested the same contamination level and used a similar SIR pattern as Piotrowska et al. [29], 10 µA threshold was used for a relative comparison of the results from amines.

The influence of thermal activation on leakage current under DC bias was more pronounced for EA and DIPA samples. After thermal activation at 240℃, the leakage current of EA and DIPA samples was significantly lower compared to the activators behavior that did not undergo thermal activation as shown in **Figure 5.10**(a) and (d). Comparing the activation temperature with the results of evaporation temperature and degradation temperatures from TGA/DTA in **Figure 5.7**(a) and (d), the quantity of EA and DIPA was considerably reduced after the thermal treatment at 240℃. On the other hand, the thermally-activated DEA samples (**Figure 5.10**(a) and (b)) exhibited lower leakage current levels compared to TEA samples or higher humidity level is required for the amine to reach the threshold of 10 µA compared to the non-activated samples (**Figure 5.10**(d) and (e)). This is expected to be due to the partial evaporation of DEA activator, which reduced the extent of moisture absorption behavior and protonation behavior after thermal activation.

Figure 5.10(a) and (b) shows that the TIPA fluxes required higher relative humidity level (compared to DEA and TEA) in order to induce the leakage current level over 10 µA, which indicated that, at a given RH level below or around the moisture absorption RH of TIPA, the

moisture absorption abilities of DEA and TEA samples were more pronounced compared to TIPA samples. The LC results agreed with the results of SIR impedance response testing shown in **Figure 5.9**(b), (c) and (e). Despite the protonation behavior of amino group in TIPA was strong, the decreased ability of hydroxyl group to absorb moisture led to the relatively lower leakage current levels compared to DEA and TEA samples.

Figure 5.10(a-c) show the leakage current values for DEA and TIPA samples and their reduction upon the increasing exposure temperature. This is in agreement with the impedance responses shown in **Figure 5.9**(b) and (e). In contrast, TEA samples also show similar trend of decreasing leakage current under an increasing exposure temperature; however, the impedance responses at 10 kHz (**Figure 5.9**(c)) remained at low levels under all exposure temperatures. Particularly, **Figure 5.10**(f) shows the leakage current of 240℃ activated TEA sample, which is lower than the 10 µA threshold level under the exposure temperature of 60℃, 90% RH, which does not agree with the low impedance values observed at 10 kHz under the same exposure temperature as shown in **Figure 5.9**(c). Minzari et al. [30] reported that acidic pH develops at the anode during biased conditions on an electronic component and upon the water film formation on that component due to the electrolysis of water, which leads to enhanced dissolution of Sn. In comparison with DC loading conditions, the low bias voltage level and alternative current used during the EIS testing is not able to induce hydrolysis of water and influence the local change of pH. Therefore, the conductivity of alkanolamine flux was only dependent on the extent of its moisture absorption ability and protonation behavior of alkanolamine itself during the EIS investigation. Moreover, the pH level could be the dominant factor for the DC loading investigations under various test temperatures, since the alkanolamines under test presented lower pKa and lower pH values at higher temperatures due to the breakdown of intermolecular hydrogen bond [31][32]. Pourbaix diagram of Sn in amine solution shows the presence $Sn(OH)_6^{2-}$ ions under highly alkaline conditions. When the pH value of alkanolamine electrolyte is reduced by an increasing exposure temperature, the corrosion products shift to the left side of a diagram and form $Sn(OH)_4$ [30]. Therefore, less tin ions is present in the electrolyte at higher ambient temperature, which could reduce the leakage current of alkanolamine fluxes-contaminated SIR pattern and its susceptibility to corrosion.

Comparison with the commercial used woa flux activators

The performance of five selected amine candidates under humid conditions was compared with adipic acid and glutaric acid that are typically used as commercial flux acidic activators. Among the three WOAs, Piotrowska et al. [9] reported the lowest moisture absorption point for glutaric

acid (84.7% RH, 73.9% RH, 81.5% RH under ambient temperatures of 25℃, 40℃ and 60℃, respectively). In comparison, the critical RH values of DEA, TEA, and TIPA were observed to be lower than the moisture absorption point of glutaric acid, as shown in **Figure 5.9**(b)(c)(e), whereas EA and DIPA activators showed higher humidity boundaries for moisture absorption compared to glutaric acid. Under DC loads, glutaric acid was the most aggressive one in selected WOAs, and the glutaric acid-induced leakage current of SIR pattern surpassed 10 µA level at 90% RH, 75% RH, and 85% RH at exposure temperatures of 25℃, 40℃ and 60℃, respectively [9].

In contrast, the leakage current responses from DEA and TEA contaminated samples reached the 10 µA level at lower humidity levels of 60% RH and 70% RH, respectively, as shown in **Figure 5.10**(b)(c), whereas the thermally-activated EA and DIPA samples maintained a low leakage current response even under 98% RH exposure. Therefore, EA and DIPA activators represent a couple of benign flux residue types in terms of their influence on ECM and corrosion point of view compared to the commercial used WOAs activators.

In order to compare the IPC copper mirror testing results of amines versus some of the acidic activators, **Figure 5.5**(a)-(e) shows that the amount of corrosion products induced by alkanolamines was qualitatively lower compared to the amount of corrosion products induced by adipic and glutraric acids (**Figure 5.5**(f) and (g)). Similar corrosion appearance was reported by Tolla et al. [18]. Combined with the EIS and CA results discussed previously, lower amount of blue corrosion product does not directly have less influence on the reduction of SIR or leakage current values. Thus, the copper mirror method (IPC-TM-650 No. 2.3.32) was evaluated as generally not suitable for understanding the actual leak current response from the alkanolamine contaminated system under humid conditions. Therefore, in order to deduce the humidity effects of residues on the PCBA surface, LC or impedance tests are needed, since these show how the electrical property of the residue solution is degraded and related to changing solubility due to the moisture absorption by flux residues or an increased humidity and temperature levels.

In order to explain the corrosion mechanisms of WOA and alkanolamine fluxes on Cu, Pourbaix diagram was simulated for a temperature of 25℃ using HSC software as shown in **Figure 5.12**. For WOA fluxes, the electrolyte formed on Cu substrate is acidic. Based on the potential and pH, Cu^{2+} ions was formed on the surface according to Pourbaix diagram in **Figure 5.12**(a). Under humidity exposure, Cu^{2+} on the copper substrate formed Cu_2O, $Cu(OH)_2$ and Cu contained organic salt [33] appeared as blue/green colour [1]. While Pourbaix diagram of Cu-alkanolamine in **Figure 5.12**(b) shows that Cu substrate formed $Cu(NH_3)^+$ and $Cu(OH)_4^{2-}$ ions under aqueous alkaline conditions at very low potential range. In consequence, the polarization results in **Figure**

5.2 also agreed that the OCP values of alkanolamines are significantly lower than WOAs. Casassas et al. [34] reported that the ligands of EA and DEA bond to the Cu^{2+} through N atoms of amine groups, and this is followed by deprotonation of hydroxyl groups and chelation of hydroxyl group with Cu^{2+}, whereas the complexes of Cu^{2+} formed with one or two ligand molecules of TEA depend on the concentrations of TEA. These complexes of non-thermally-degraded amine candidates, such as $Cu(EA)_2^{2+}$, $Cu(EA)_4^{2+}$, $Cu(DEA)_3^{2+}$ and $Cu(TEA)_2^{2+}$ etc. [35][36], which were the corrosion products on the substrate of Cu, are less identifiable by color compared to glutaric acid soldered samples shown in **Figure 5.5**. Even though the alkanolamines were able to form ionic complexes with the free metallic ions, the ECM dendrites still were formed between two electrodes and induced the short circuit failures as shown in **Figure 5.11**(d)-(f).

Qu et al. evaluated the oxide removal kinetics exhibited by WOAs and amines using a corrosion current density and corrosion potential values obtained through the potentiodynamic polarization testing [20]. However, the polarization results in **Figure 5.2** indicate that the corrosion current density and corrosion potential values did not match the amine ranking of solderability as shown in **Figure 5.4**(a). This is due to the fact that the electrochemical investigation was conducted in water-based electrolyte at ambient conditions instead of the soldering temperature. Hence, the interaction of alkanolamines and WOAs with Cu oxides is different in the electrolyte conditions compared to the soldering process conditions with no electrolyte present. Therefore, the electrochemical investigations cannot be used as a sole activator screening method; however, they require an additional investigation in order to evaluate the activator effect at the soldering process conditions.

In case of WOAs, the wetting balance testing results agreed with the polarization testing results, where the oxides removal ability of WOAs followed the trend: glutaric acid > adipic acid. This is due to the occurrence of the same complexation (**Equation 5.1**) and disproportionation (**Equation 5.2**) [19] reactions of Cu oxides and WOAs in both soldering and electrolyte conditions.

$$CuO + 2RCOOH = Cu(RCOO)_2 + H_2O \quad \textit{Equation 5.1}$$

$$Cu_2O + 2RCOOH = Cu(RCOO)_2 + Cu + H_2O \quad \textit{Equation 5.2}$$
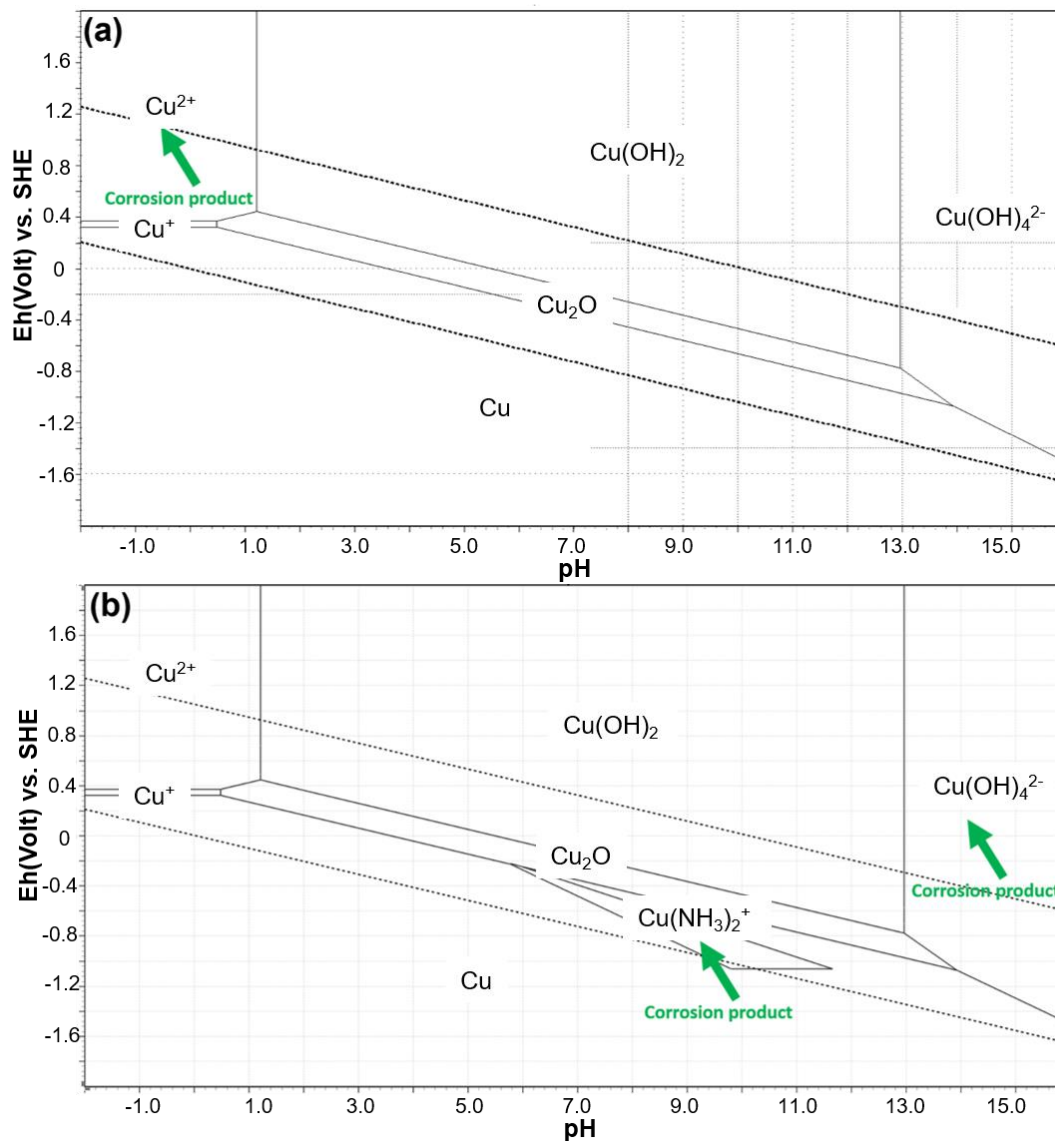
Figure 5.12 Pourbaix diagrams of Cu simulated at 25℃ with 1 mol/L concentration of N and Cu respectively: (a) Pourbaix diagram of Cu-WOA-water system, (b) Pourbaix diagram of Cu-alkanoamine-water system.

On the other hand, Cu oxides removal mechanism exhibited by the alkanolamines in electrolyte conditions occurs through the protonation (**Equation 5.4**) and complex formation mechanisms (**Equation 5.3** and **Equation 5.4**). However, under soldering conditions, redox reactions take place between the Cu oxides and amine activators as shown in **Equation 5.5** and **Equation 5.6**, where Cu is reduced from +II to 0 and N is oxidized from –III to 0. Since the reaction mechanism of amines and Cu are different in electrolyte and under dry soldering process, it is not possible to analyze the oxide removal kinetics using the electrochemical methods for amine based flux

systems. Moreover, the electrochemical testing was conducted at room temperature, which cannot assess the thermal degradation process of amine activators. For example, EA and DIPA possess good oxides removal abilities in the electrolyte, but cannot provide good solderability at soldering conditions as shown in **Figure 5.6**(a) and (d).

$$CuO + 4RNH_2 + H_2O = Cu(RNH_2)_4^{2+} + 2OH^- \quad \textit{Equation 5.3}$$

$$Cu_2O + 4RNH_2 + H_2O = Cu(RNH_2)_4^{2+} + Cu + 2OH^- \quad \textit{Equation 5.4}$$

$$3CuO + 2RNH_2 = 2Cu + R_2O + N_2 + 2H_2O \quad \textit{Equation 5.5}$$

$$3Cu_2O + 2RNH_2 = 6Cu + R_2O + N_2 + 2H_2O \quad \textit{Equation 5.6}$$
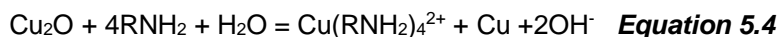
Additionally, the hot plate spreading testing confirmed the large spreading area of TEA model flux as shown in **Figure 5.6**(c), which agreed with the spreading appearance of two anonymous amines from the study of Shi et al. [16]. However, the result of wetting balance indicates the wetting force and wetting length of TEA model flux were much lower compared to the results obtained for adipic and glutaric acids as shown in **Figure 5.4**(b). Therefore, the hot plate spreading test can only be used as a flux qualitative comparison for amine based flux system and a wetting balance provides quantitative information from the solderability perspective.

V.   CONCLUSIONS

- The dynamic polarization results show that five alkanolamine candidates obtain higher etching current density on Cu compared to WOAs at low potential range in aqueous medium; however, the etching ability of WOAs is higher than alkanolamine candidates at a potential range over 0.2 V vs. Ag/AgCl. The ranking of etching ability for alkanolamine candidates in aqueous condition at room temperature is: EA > DIPA > DEA > TEA > TIPA, which renders EA to be the most effective among the tested amines.

- TGA results show that the evaporation of EA, DEA and DIPA from the surface can occur at 240℃, whereas the thermal degradation temperatures of DEA, TEA and TIPA are much higher than the typical soldering temperature range. Thermal degradation of amine groups in EA and DIPA under the soldering conditions was confirmed by FT-IR results.

- Hot plate spreading test qualitatively shows good wettability for TEA model flux, while EA, DIPA and TIPA model fluxes did not wet the surface of brass substrates under the testing temperature of 270℃. Solderability testing results show lower wetting properties of five alkanolamines compared to the tested WOAs. The ranking of solderability for tested WOAs and alkanolamines is: glutaric acid > adipic acid > TEA > DEA > TIPA > DIPA > EA.

- High leakage current levels and ECM occurrence were induced by the thermal activated DEA and TEA contaminated SIR patterns at 25℃/70% RH, whereas the leakage current remained below 10^{-4} mA after thermal activation at 240℃ for the EA and DIPA contaminated SIR patterns. The reduction of leakage current levels for DEA, TEA, and TIPA contaminated SIR patterns were obtained by increasing the testing temperature from 25℃ to 60℃.

- EIS results indicate that the moisture absorption of DEA, TEA, and TIPA is initiated at low RH range (30 - 86% RH) compared to the critical RH levels exhibited by WOAs activators (84.7 – 99% RH) at room temperature, while EA- and DIPA-contaminated SIR maintained the high impedance values at 99% RH under all the testing temperatures. The increased testing temperature from 25℃ to 60℃ significantly inhibited the moisture absorption behavior (increasing the moisture absorption RH) of DEA and TIPA, while reduced the moisture absorption RH from 95% RH to 86% RH for EA and DEA.

VI.   REFERENCES

[1]   C. Ramirez, K. -S. Lei, Evaluation of the Reliability and Corrosivity of VOC-free, No-clean Fluxesusing Standard, Modified and Electrochemical Methods*, Solder. & Surf. Mt. Technol. 8 (1996) 6–9. doi:10.1108/09540919610777555.

[2]   K.M. Adams, J.E. Anderson, Y.B. Graves, Ionograph Sensitivity to Chemical Residues From 'no Clean Soldering Fluxes: Comparison Of Solvent Extract Conductivity and Surface Conductivity, Circuit World. 20 (1994) 41–44. doi:10.1108/eb046251.

[3]   H. Conseil, V. Verdingovas, M.S. Jellesen, R. Ambat, Decomposition of no-clean solder flux systems and their effects on the corrosion reliability of electronics, J. Mater. Sci. Mater. Electron. 27 (2016) 23–32. doi:10.1007/s10854-015-3712-x.

[4]   H. Conseil, M.S. Jellesen, R. Ambat, Contamination profile on typical printed circuit board assemblies vs soldering process, Solder. Surf. Mt. Technol. 26 (2014) 194–202. doi:10.1108/SSMT-03-2014-0007.

[5]   V. Verdingovas, M.S. Jellesen, R. Ambat, Solder Flux Residues and Humidity-Related Failures in Electronics: Relative Effects of Weak Organic Acids Used in No-Clean Flux Systems, J. Electron. Mater. 44 (2015) 1116–1127. doi:10.1007/s11664-014-3609-0.

[6]   K. Piotrowska, M.S. Jellesen, R. Ambat, Thermal decomposition of solder flux activators under simulated wave soldering conditions, Solder. Surf. Mt. Technol. 29 (2017) 133–143. doi:10.1108/SSMT-01-2017-0003.

[7]   B.A. Smith, L.J. Turbini, Characterizing the weak organic acids used in low solids fluxes, J. Electron. Mater. 28 (1999) 1299–1306. doi:10.1007/s11664-999-0171-2.

[8]   S. Zhan, M.H. Azarian, M. Pecht, Reliability of printed circuit boards processed using no-clean flux technology in temperature-humidity-bias conditions, IEEE Trans. Device Mater. Reliab. 8 (2008) 426–434. doi:10.1109/TDMR.2008.922908.

[9]   K. Piotrowska, R. Ud Din, F.B. Grumsen, M.S. Jellesen, R. Ambat, Parametric Study of Solder Flux Hygroscopicity: Impact of Weak Organic Acids on Water Layer Formation and Corrosion of Electronics, J. Electron. Mater. 47 (2018) 4190–4207. doi:10.1007/s11664-018-6311-9.

[10]   C. Hunt, L. Zou, The impact of temperature and humidity conditions on surface insulation resistance values for various fluxes, Solder. Surf. Mt. Technol. 11 (1999) 36–43.

[11]   X. Zhong, S. Yu, L. Chen, J. Hu, Z. Zhang, Test methods for electrochemical migration: a review, J. Mater. Sci. Mater. Electron. 28 (2017) 2279–2289. doi:10.1007/s10854-016-5713-9.

[12]   J.E. Sohn, U. Ray, Weak Organic Acids and Surface Insulation Resistance, Circuit World. 21 (1995) 22–26. doi:10.1108/eb044046.

[13]   V. Verdingovas, M.S. Jellesen, R. Ambat, Relative effect of solder flux chemistry on the humidity related failures in electronics, Solder. Surf. Mt. Technol. 27 (2015) 146–156. doi:10.1108/SSMT-11-2014-0022.

[14]   K. Piotrowska, V. Verdingovas, R. Ambat, Humidity-related failures in electronics: effect of binary mixtures of weak organic acid activators, J. Mater. Sci. Mater. Electron. 29 (2018) 17834–17852. doi:10.1007/s10854-018-9896-0.

[15]   C. Marcolli, B. Luo, T. Peter, Mixing of the Organic Aerosol Fractions: Liquids as the Thermodynamically Stable Phases, J. Phys. Chem. A. 108 (2004) 2216–2224. doi:10.1021/jp036080l.

[16]   Y. Shi, X. Wei, B. Tolla, The Role of Organic Amines in Soldering Materials, in: IPC APEX EXPO Conf. Proc., Circuit Insight, San Diego, USA, 2015.

[17]   S. Vaynman, M.E. Fine, Flux development for lead-free solders containing zinc, J. Electron. Mater. 29 (2000) 1160–1163. doi:10.1007/s11664-000-0007-6.

[18]   B. Tolla, D. Jean, H. Bhavsar, Y. Shi, X. Wei, Reactivity of No-clean flux residues in electronic assemblies: a systematic study, in: SMTA Int., Rosemont, IL, USA, 2015.

[19]   M. Bixenman, D. Lober, A. Ailworth, K. Corporation, B. Tolla, D. Ph, J. Allen, D. Jean, K. Loomis, K. Corporation, Electrochemical Methods to Measure the Corrosion Potential of Flux Residues, in: IPC APEX EXPO, SMTNET, San Diego, USA, 2017.

[20]   G. Qu, Activity of Halide-Free Flux at Copper and Tin Surfaces, Louisiana State University, 2013. http://etd.lsu.edu/docs/available/etd-04102013-085656/.

[21]   C. Went, Organic Acids and Bases, in: Ion. Org. Mech., Macmillan Education UK, London, 1986: pp. 58–78. doi:10.1007/978-1-349-07964-3_4.

[22]   D.R. et al. Lide, CRC Handbook of Chemistry and Physics, 2009−2010, 90th ed. CRC Handbook of Chemistry and Physics, 2009−2010, 90th ed . Edited by David R. Lide , Editor-in-Chief, and W. M. "Mickey" Haynes , Associate Editor (National Institute of Standards and Technology, J. Am. Chem. Soc. 131 (2009) 12862–12862. doi:10.1021/ja906434c.

[23]   V. Verdingovas, M.S. Jellesen, R. Ambat, Impact of NaCl contamination and climatic conditions on the reliability of printed circuit board assemblies, IEEE Trans. Device Mater. Reliab. 14 (2014) 42–51. doi:10.1109/TDMR.2013.2293792.

[24]   K.S. Hansen, M.S. Jellesen, P. Moller, P.J.S. Westermann, R. Ambat, Effect of solder flux

residues on corrosion of electronics, in: 2009 Annu. Reliab. Maintainab. Symp., 2009: pp. 502–508. doi:10.1109/RAMS.2009.4914727.

[25] R.M. Silverstein, F.X. Webster, D.J. Kiemle, D.L. Bryce, Spectrometric Identification of Organic Compounds, 8th Edition, Wiley, 2014.

[26] A. V. Patil, G.N. Shinde, V.P. Pawar, Dielectric relaxation study of hydrogen bonded structures in ethanolamine with diethanolamine using TDR technique, J. Mol. Liq. 168 (2012) 42–46. doi:10.1016/j.molliq.2012.01.017.

[27] F. Amararene, C. Bouallou, Kinetics of carbonyl sulfide (COS) absorption with aqueous solutions of diethanolamine and methyldiethanolamine, Ind. Eng. Chem. Res. 43 (2004) 6136–6141. doi:10.1021/ie030540f.

[28] G. Hinderaker, O.C. Sandall, Absorption of carbonyl sulfide in aqueous diethanolamine, Chem. Eng. Sci. 55 (2000) 5813–5818. doi:10.1016/S0009-2509(00)00420-6.

[29] K. Piotrowska, M. Grzelak, R. Ambat, No-Clean Solder Flux Chemistry and Temperature Effects on Humidity-Related Reliability of Electronics, J. Electron. Mater. 48 (2019) 1207–1222. doi:10.1007/s11664-018-06862-4.

[30] D. Minzari, M.S. Jellesen, P. Møller, R. Ambat, On the electrochemical migration mechanism of tin in electronics, Corros. Sci. 53 (2011) 3366–3379. doi:10.1016/j.corsci.2011.06.015.

[31] F. Khalili, A. Henni, A.L.L. East, pKa Values of Some Piperazines at (298, 303, 313, and 323) K, J. Chem. Eng. Data. 54 (2009) 2914–2917. doi:10.1021/je900005c.

[32] R.J. LIttel, M. Bos, G.J. Knoop, Dissociation Constants of Some Alkanolamines at 293, 303, 318, and 333 K, J. Chem. Eng. Data. 35 (1990) 276–277. doi:10.1021/je00061a014.

[33] E. Cano, C.L. Torres, J.M. Bastidas, An XPS study of copper corrosion originated by formic acid vapour at 40% and 80% relative humidity, Werkstoffe Und Korrosion. 52 (2001) 667–676. doi:10.1002/1521-4176(200109)52:9<667::aid-maco667>3.3.co;2-8.

[34] E. Casassas, L.L. Gustems, R. Tauler, Spectrophotometric study of complex formation in copper(II) mono-, di-, and tri-ethanolamine systems, J. Chem. Soc. Dalt. Trans. (1989) 569–573. doi:10.1039/DT9890000569.

[35] D.M. Puente-Siller, J.C. Fuentes-Aceituno, F. Nava-Alonso, An analysis of the efficiency and sustainability of the thiosulfate-copper-ammonia-monoethanolamine system for the recovery of silver as an alternative to cyanidation, Hydrometallurgy. 169 (2017) 16–25. doi:10.1016/j.hydromet.2016.12.003.

[36] C. Kwang Ko, W.G. Lee, Dissolution of copper oxide by the ethanolamine and ammonium fluoride in aqueous solution, Surf. Interface Anal. 44 (2012) 94–97. doi:10.1002/sia.3777.

6. Amino acids as activators for wave solder flux systems: investigation of solderability and humidity effects

Feng Li, *Ioannis Mantis, Morten Stendahl Jellesen, Rajan Ambat*

Abstract: Flux activators in flux formulation is to remove oxides from metal surface, hence allow the formation of metallurgical bond between metal substrate and solder alloy. However, flux activator in the no-clean flux residue on printed circuit board assemblies affects the climatic reliability due to its hygroscopic and ionic behavior under humidity exposure. This paper systematically investigated the solderability of four amino acids wave flux activators using wetting balance test and microscopy inspection, and the humidity effects of four amino acids was analyzed using electrochemical impedance spectroscopy (EIS) and chronoamperometry under various testing conditions. Water absorption and thermal degradation were analyzed using gravimetric method and Fourier-transform infrared spectroscopy (FT-IR). Combined results indicate glutamine based model flux obtained superior solderability for 96.5Sn-3Ag-0.5Cu (SAC 305) alloy due to suitable melting and activation temperature of amino group for the oxides removal. The robust humidity reliability of amino acids was dependent upon relative high deliquescence point and low moisture absorption under harsh climatic conditions.

Keywords: Amino acid, solder flux, electronic corrosion, humidity, reliability, solderability.

I.   INTRODUCTION

The miniaturization of electronic packaging tendency brought the cheaper, multifunctional capability, and portability of electronic devices to our daily life. However, miniaturization of the devices with close distances on the Printed Circuit Board (PCBA) assembly also cause higher electrical field [1], which in combination with other factors results in the reduction of surface insulation resistance (SIR) between oppositely biased electrode terminals under humid conditions [2][3] and higher leakage current [4][5]. The ionic and hygroscopic contaminants on PCBAs reduce the humidity boundary for water condensation [5] due to their electrolyte properties and increase the risk of intermittent or permeant failures [1].

No-clean flux residue is one of the most representative intrinsic contamination source on the PCBA surface since 70-80% production of electronics today use no-clean flux chemistry [6]. It was designed with the idea that during the soldering process, content of the flux system evaporate or degrade, therefore leave minimal residues [4][7] to save cleaning steps in the manufacturing

process [6]. However, due to sluggish kinetics of evaporation and decomposition depending on the thermal conditions on the PCBA surface, considerable amount of flux residue will be presented after the soldering process [6][8]. Such flux residue mainly contains weak organic acids (WOAs) activators and the rosin/resin component of the flux system [4][9][10]. On the component side of selective wave soldered PCBAs, residue levels of WOAs up to ~687μg/in^2 has been reported [6]. The most frequently used WOAs in the flux formulation today include glutaric acid, succinic acid, adipic acid etc. [7][11][12]. The deliquescence relative humidity level of WOAs are in a range of 78-99% [4], therefore at least for the WOAs with lower level humidity boundaries develops the risk of water condensation on PCBAs at lower humidity levels. The dissolution of WOAs to the water film will reduce the pH of the electrolyte layer on the PCBA surface, while the dissolution provides good conductivity and some WOAs can accelerate the corrosion of the metallic terminals under biased conditions on the PCBA surface [13][14][15]. The electrochemical process on the biased surface, and dissolved metallic ions from anodic terminals further induce high leakage current and possibly end up with the electrochemical migration (ECM) and short circuit [16].

One criteria for selection of no-clean flux activators for the flux systems are based on the removal ability of the oxide layer and evaporation temperature, while partially on corrosion reliability. For instance, adipic acid has lower hygroscopicity and lower acidic dissociation constant (pKa) value than glutaric acid, which indicates good corrosion reliability of adipic acid [9], whereas the solderability for adipic acid based flux is lower than glutaric acid based flux. Therefore, many flux manufacturers use multiple WOAs in flux chemistry to obtain both solderability and corrosion reliability [7][17], although one WOA type can dominate. Thermodynamically, mixing of ionic component reduce DRH compared to the individual components [18] due to the lowering effect of deliquescent stability [19]. On the other hand, organic amines were reported as an effective additive to improve the corrosion reliability of the flux systems though leaving flux residue on the PCBAs after soldering process [20][21][22]. Organic amines are weakly alkaline [23], which can neutralize the WOAs residues if there are present together in a flux system. Additionally, investigations shows that the growth of ECM dendrite was inhibited by forming stable Cu complex compounds with amines [22].

Amino acids are generally water-soluble, mild and biodegradable [24], which can be suitable flux activators compared to WOAs [25]. Recently, anonymous amino acid candidates were tested in the formulation of wave solder fluxes [26] and reflow solder pastes [27]. Reported results indicate amino acid contained flux formulation obtained better assembly with minimum defects compared

to WOA contained solder paste in low temperature soldering application [27]. These investigations on anonymous amino acid activators were mainly focused on the printability and solderability aspects and the interpretation of the corrosion reliability assessment is limited. Kiani et al. reported the corrosion inhibition performance of cysteine, methionine, and alanine on Pb-bearing solder alloy [28]; while Yang et al. reported the good solderability of glutamic acid in halogen containing fluxes [29]. However, the available literature specifically focused on amino acid as additives to the halogen containing flux systems and lead based solder alloys instead of the presently employed no-clean flux systems [30][31] and lead free solder alloys [32]. Patents suggested isoleucine, glycine, alanine, serine, arginine, glutamine etc. can be used flux activators in both wave solder flux and solder paste [25][33], while the performance of these activators on solderability, humidity robustness and corrosion reliability are not clarified in literature. Therefore, it is important to understand the moisture interaction capability of amino acid residue and the corrosion reliability aspects, such as leakage current and electrochemical migration on the surface of PCBAs.

The present investigation focused on understanding the corrosion reliability of four types of amino acids when used as flux activators, and if they are present as residues, while the solderability of these activators are investigated together. An interdigitated SIR pattern was used as the test vehicle for investigations. Electrochemical impedance spectroscopy (EIS) was used to understand the humidity interaction with amino acid residues. ECM susceptibility of amino acids contaminated SIR pattern was evaluated using chronoamperometry (CA). Wetting balance was used to investigate the solderability of amino acid model fluxes. The degradation production of amino acid residue was analyzed using fourier-transform infrared spectroscopy (FT-IR).

II.   MATERIALS AND EXPERIMENTAL METHODS

Amino acids used for the investigation

Table 6.1 shows the physical and chemical properties of four amino acids with relatively neutral pH value. As the **Table 6.1** shows, the molecular weight of the amino acid vary from approximately 75 – 146 g/mol, while the melting point varies from low melting point of 185 to 314°C. Melting point is an important parameter in connection with use as flux activator. Isoelectronic point (pI) indicates the pH that amino acid does not carry electrical charge. It can be expressed by **Equation 6.1**, where pK_{a1} is the dissociation constant of carboxyl group, pK_{a2} is the dissociation constant of amino group. For investigations, model fluxes were mixed using 4 wt.% of amino acid and 96 wt.% ultra pure water in ultrasonic bath for 30 mins. Ultra pure water source was adapted from Milipore water purification system (Synergy UV, Germany).

$$pI = \frac{pK_{a1}+pK_{a2}}{2} \qquad \textbf{\textit{Equation 6.1}}$$

Table 6.1 *Properties of the amino acids used in the investigation.*

	Molecular Structure	Molecular Weight (g/mol)	Melting Point (°C)	pK$_{a1}$ (carboxyl)	pK$_{a2}$ (amino)	pI
Alanine		89.09	314	2.34	9.69	6.00
Glutamine		146.14	185	2.17	9.13	5.65
Glycine		75.07	233	2.34	9.6	5.97
Serine		105.09	246	2.21	9.15	5.68
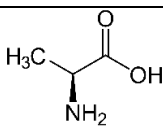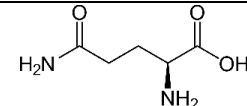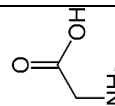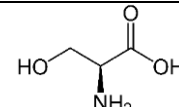
Solderability testing

Cu coupons in a size of 6 mm × 25 mm × 0.5 mm were prepared using electrical discharge machining based on the requirements from IPC-TM-650 no.2.4.14.2 for solderability testing. Cu coupons were cleaned using ISO 9455-16 soft soldering fluxes standard before each test. The solderability test was performed in an air-static condition. Molten bath of SAC 305 solder alloy was controlled at 270°C using a Must 3 wetting balance (GEN 3, UK). Model flux was applied on the Cu coupons by dipping for 2 sec. After 20 sec preheating at the position of 1 cm above the molten solder bath, Cu coupons were immersed in the solder bath for 10 sec to a depth of 5 mm. The speed of immersion and withdraw of Cu coupons was 20 mm/s. As reference, model WOA fluxes with 4 wt.% adipic acid and succinic acid in isopropanol alcohol was used.

Evaluation of humidity effects of amino acids using EIS and CA methods

Humidity exposure experiments were conducted in a climatic chamber (Espec PL-3KPH, Japan) with the accuracy of ± 0.3°C and ± 2.5% relative humidity (RH) using a five-channel potentiostat (Biologic VSP, France). Issacs et al. reported the localized contamination level of WOA on wave soldered PCBA can be as high as 687μg/in^2 (106.5 μg/cm^2) [6]. Therefore, the contamination level of the amino acid on the SIR testing area was determined at 100 μg/cm^2. To imitate the soldering process, some of the SIR test board was thermally activated at 240°C for 45 sec in a

Techno HA-06 furnace. For three electrode electrochemical experiments, one electrode of the SIR interdigitated pattern was used as reference and counter, the other was used as working electrode, imitating positive and negative bias points on a PCBA surface.

EIS technique was used to investigate the deliquescence relative humidity (DRH) and efflorescence relative humidity (ERH) of amino acid candidates. DRH indicates the humidity level triggering water absorption by amino acids, and ERH indicates the lower humidity level required for the release of water from the amino acids. In previous work, scanning frequency of 1-10 KHz in EIS was confirmed to provide the information of the transformation from capacitive dominant behavior to resistive dominant behavior of SIR components during water condensation process [18][34]. Therefore, scanning frequency was set at 10 KHz in the amplitude of 25 mV in order to record the impedance response of amino acid contaminated SIR interdigitated pattern during the 24 hours under linear humidity ramping from 30% RH to 99% RH, and then ramped back to 30% RH. To understand the influence of the service temperature on the water absorption and desorption behavior, tests were conducted at 25℃, 40℃, and 60℃ respectively. All test boards were dried in the climatic chamber at 30% RH for 6 hours before the EIS measurement started.

CA technique was used to understand the leakage current and ECM induced by amino acid residue on the SIR interdigitated pattern under humid conditions. For this purpose, a 5 V DC bias was applied on the SIR test board during the test. Prior to the data recording, test boards were stabilized at the testing climate for 4 hours. Leakage current value of the test boards was recorded at relative humidity level of 80%, 90%, and 98% over 24 hours at testing temperature of 25℃, 40℃, and 60℃ respectively.

Test vehicle for electrochemical testing

Test PCB board with SIR interdigitated patterns (IPC-4201/21) shown in **Figure 6.1** was used as test vehicle in the present work. The surface finish of the PCB was hot air solder leveling using SN100C alloy on the 35 µm thick Cu trace. The width of the conductive lines and the pitch distance are 0.3 mm. Testing area of the SIR pattern was 13 mm × 25 mm and the overlapping length of electrodes was 442.8 mm in 41 sets. Test PCBs were initially cleaned with isopropanol alcohol and dried under compressing air before each test.
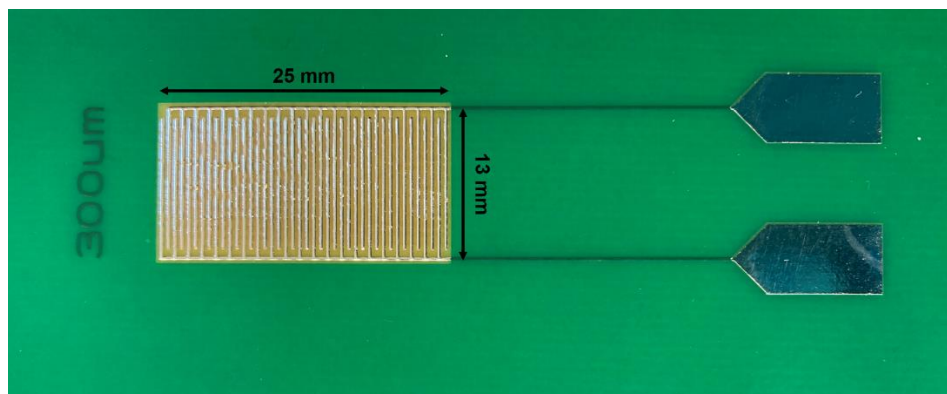
Figure 6.1 *Test PCB board with SIR interdigitated pattern used for investigations.*

Quantification of water absorption and test objects characterization

Water absorption behavior of amino acids and two commercial used activators as reference (adipic acid, succinic acids) were evaluated using a Vsorp gravimetric analyzer (ProUmid, Germany) under the RH stages of 85%, 90%, and 95% respectively at room temperature until the water absorption reaches the equilibrium condition. The tested samples of amino acids and WOs were stabilized at 25℃, 30% RH for 620 hours before water absorption test.

The surface morphology of Cu coupons used for solderability testing was inspected using a light optical microscope (LOM) (Keyence VHX, Japan). The cross section of soldered Cu coupons and corrosion product built on SIR pattern was further evaluated using scanning electron microscopy (SEM) (FEI Quanta 200 FEG, USA) under secondary electron mode at 15 kV. The chemistry of the corrosion product on the SIR pattern was analyzed using a 50 mm^2 X-Max EDS detector (Oxford Instrument, UK). The thermal degradation product of tested amino acids were analyzed using a Nicolet iN10 MX FT-IR (Thermo Fisher Scientific, USA) after thermal activation under 240℃ for 100 sec in a Techno HA-06 oven.

III.   RESULTS

Solderability assessment of amino acid candidates

Figure 6.2 shows the wetting force of six types of model fluxes containing individual amino acids and two WOAs as reference. The highest maximum wetting force was obtained by succinic acid at 3.99 mN, followed by glutamine at 3.76 mN and adipic acid at 3.65 mN. Wetting force for glutamine is slightly higher than the commercially used adipic acid. However, the time reach to zero wetting force and the time reach two third wetting force of glutamine is slightly higher than adipic acid and succinic acid. Serine also shows positive maximum wetting force at 2.82 mN, while the maximum wetting force is lower than for adipic acid and the wetting took 2.36 sec to

reach to zero wetting force, which is much higher than 0.88 sec for adipic acid and 0.95 sec for succinic acid. The wetting force of alanine and glycine were in negative value, which indicate the fluxes were not able to etch the surface of Cu coupons during soldering process. The rank of the time to zero wetting force and time reach two third wetting force are the same, which were : serine > glutamine > succinic acid > adipic acid >> glycine/alanine. The rank of the solderability values were: succinic acid > glutamine > adipic acid > serine > glycine > alanine.
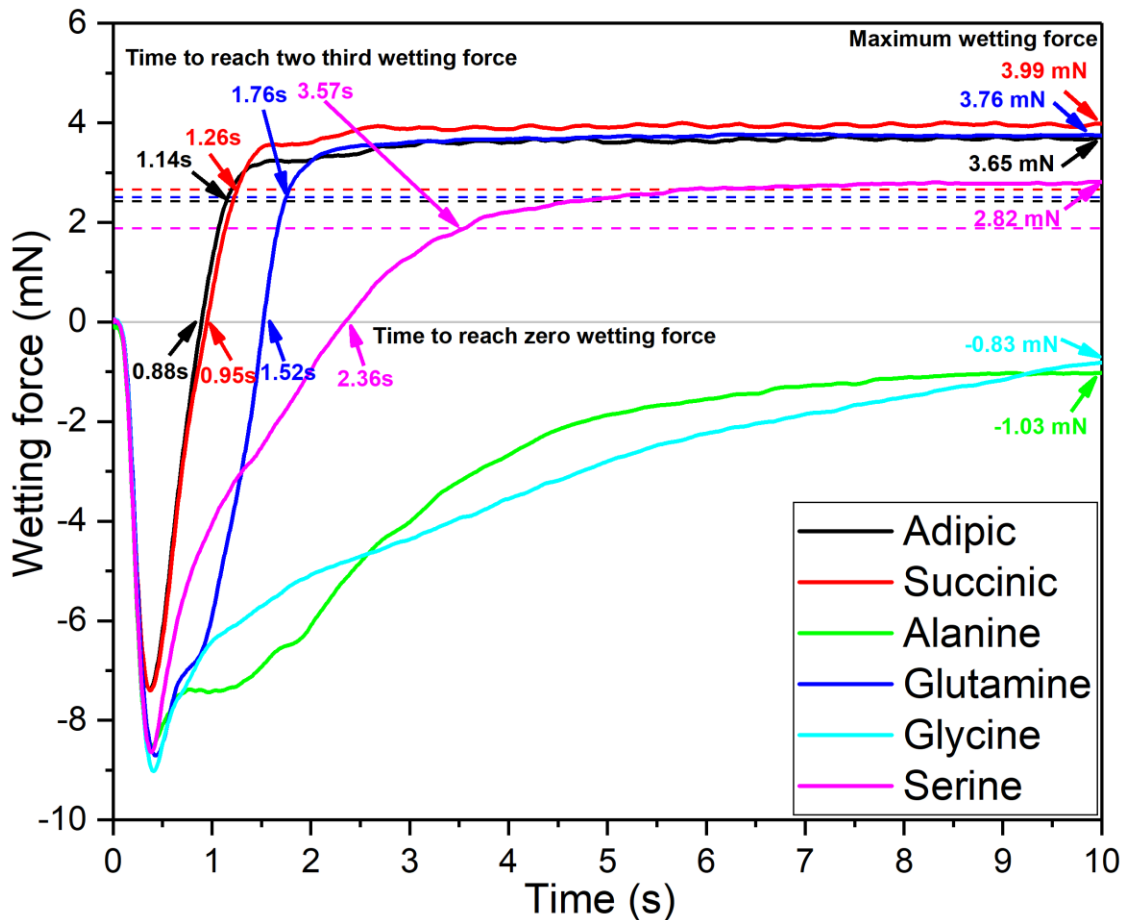
Figure 6.2 Wetting balance results of amino acids and reference WOA model fluxes.

Figure 6.3 shows the surface appearance and defects of the soldered Cu coupons using four amino acid model fluxes. LOM images and SEM images in **Figure 6.3**(a) and (c) shows the poor wetting properties of alanine and glycine fluxes. Interface defects were observed in the cross-section of the exposed Cu area without the coverage of solder alloy. The wetting appearance of serine flux shown in **Figure 6.3**(d) was better than alanine and glycine, however, the cross section image also shows many interface defects and solder material dripping at the tip of the Cu coupon.

Figure 6.3(b) shows the good wetting appearance using glutamine model flux, and the solder alloy homogeneously covered the Cu substrate without any defects.
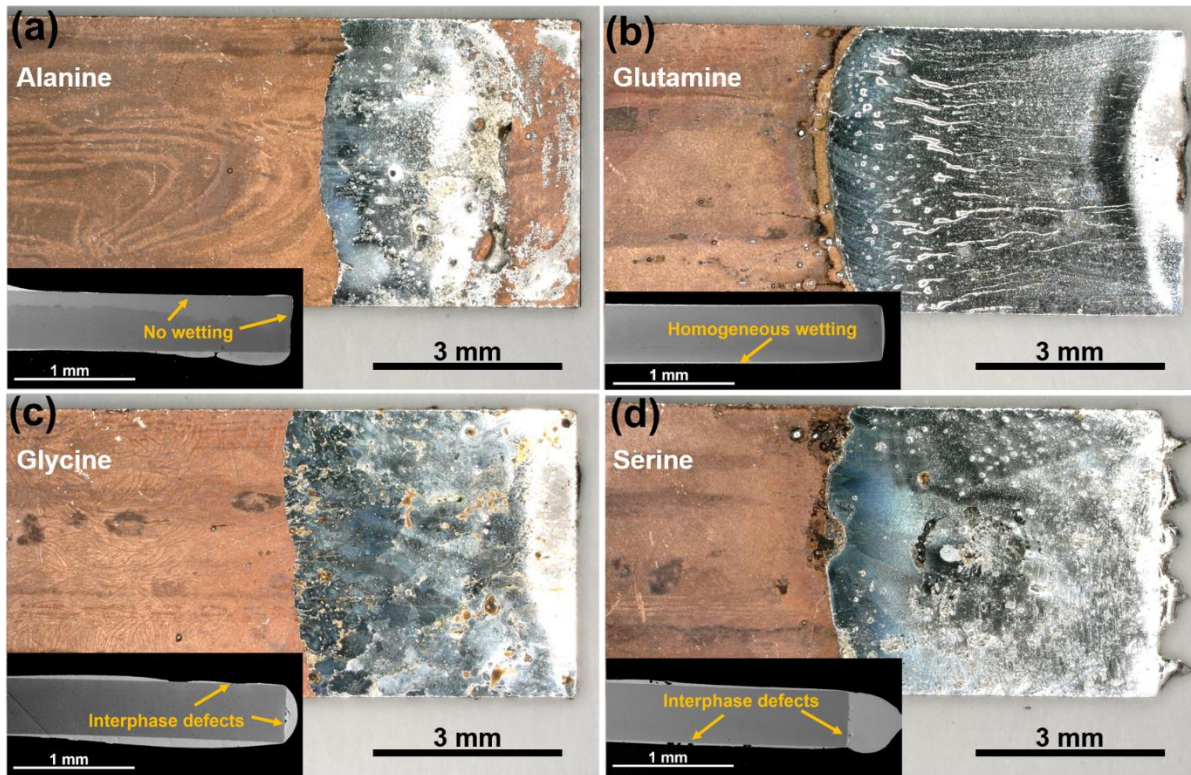
Figure 6.3 *LOM images of solder wetted Cu coupons after testing using amino acids model fluxes (cross-sectional image is shown in inset): (a) alanine, (b) glutamine, (c) glycine, and (d) serine.*

Humidity behavior of amino acids as activators

a) Water absorption behavior using gravimetric method

Figure 6.4 shows the water weight gain of amino acids and WOAs under three stages of humidity exposure. An higher increase of weight gain was shown by succinic acid and alanine close to 85% RH, which indicates the lower DRH of succinic acid and alanine. The weight gain of glycine and serine maintained at lowest level of 0.1% under 90% RH exposure; however, the weight gain of serine suddenly increased to the highest level over 20.0% among all the tested samples when the humidity level increased to 95% RH. Water weight gain of adipic acid and glutamine increased from 0.15% to 0.35% as increasing RH level from 85% to 95%; however, the water absorption induced weight gain of adipic acid and glutamine still maintained the lowest level among all test samples under humidity exposure of 95% RH.
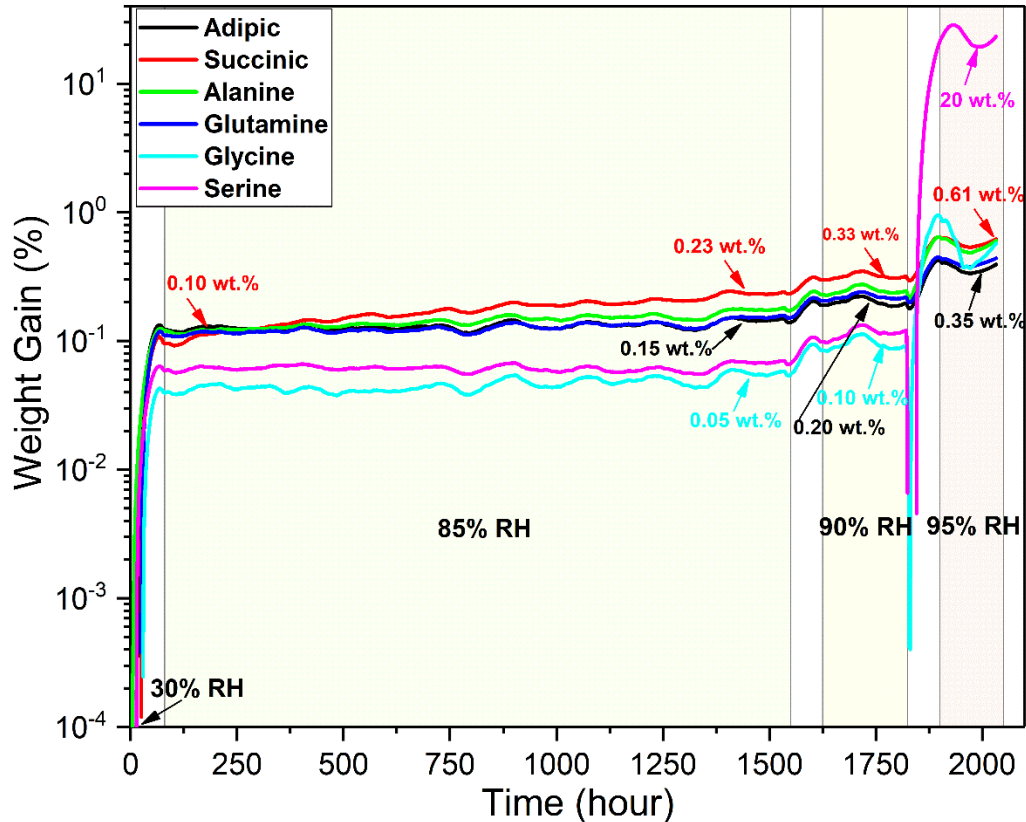
Figure 6.4 Water absorption of the amino acids and WOAs under humidity exposure.

b) Deliquescence behavior of amino acids candidate using single frequency EIS measurement

Figure 6.5 shows the impedance response of the amino acid contaminated SIR test boards under various testing conditions. During the humidity ramping from 30% RH to 99% RH, the RH value induced sudden drop of the impedance representing the DRH or water absorption behavior of amino acids, whereas RH triggered the abrupt increase of impedance over the ramping from 99% RH to 30 % RH represents ERH or water drying. Impedance response at high humidity exposure indicate the ionization behavior of amino acids. Generally, moisture hysteresis behavior of tested amino acids was observed, which indicates the lower ERH value compared to DRH value for all tested amino acids. The increased testing temperature triggered the decrease of the DRH and ERH level of amino acids, which is highest for the 60°C. The reduction of the impedance response of amino acids is pronounced with increase in testing temperature. Regarding the influence of the thermal activation of the SIR prior to testing, the DRH and ERH level of thermal activated glutamine contaminated SIR pattern was slightly higher than non-thermal activated samples under all testing temperature, whereas the thermal activation reduced the DRH and ERH levels for the other three amino acids.
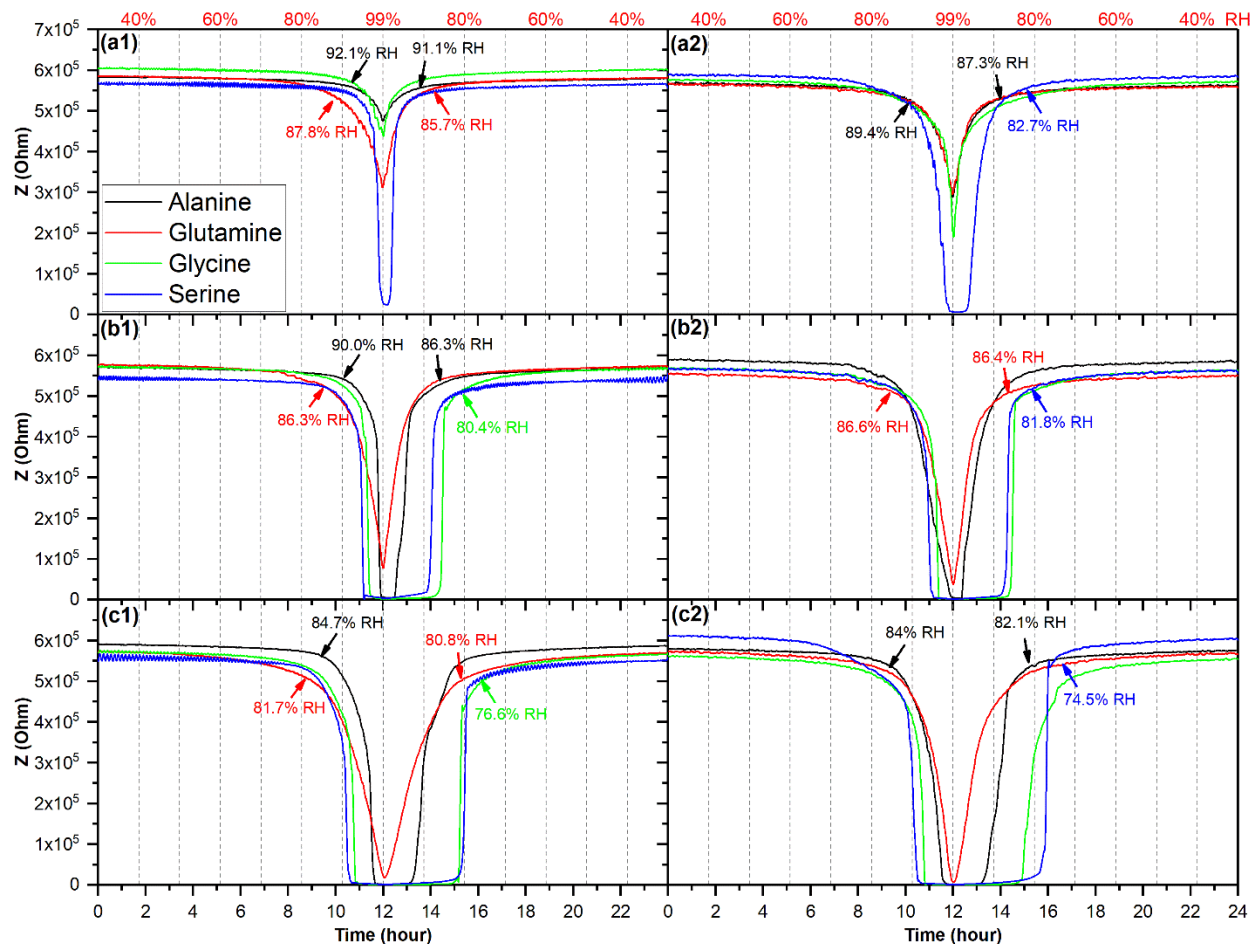
Figure 6.5 *Impedance response at 10 KHz of (1) non-thermal activated, (2) 240℃ activated, amino acids contaminated SIR test boards under various testing temperature: (a) 25℃, (b) 40℃, (c) 60℃.*

Table 6.2 summarized the DRH value and ERH value from the EIS response at 10 kHz. In general, thermal activation at 240℃ induced slight reduction of DRH and ERH value for alanine, glycine and serine samples, whereas the DRH and ERH value of glutamine slight increased after thermal activation. Under testing temperature of 25℃, the reduction of impedance respons was observed serine contaminated SIR pattern at 92.1% RH as shown in **Figure 6.5**(a1), while the impedance response of alanine, glycine and glutamine was maintained at relative high level under 99% RH exposure as shown in **Figure 6.5**(a1)(a2). Under the testing temperature of 40℃, DRH level of alanine dramatically decreased from 90% RH to 81.9% RH after thermal activation (**Table 6.2**), whereas less than 3% reduction of DRH values were obtained by glycine and serine. When the testing temperature increased to 60℃ as shown in **Figure 6.5**(c1)(c2), the increase of the DRH level of glutamine was observed from 81.7% RH to approximately 85% RH after thermal activation , which obtained highest DRH value after thermal activation. According to **Figure 6.5**

and **Table 6.2**, the ranking of the corrosion reliability from the deliquescence and ionization point of view is: glutamine > alanine > glycine > serine.

Table 6.2 Summary of DRH and ERH value for tested amino acid and representative WOA activators [9] *at various testing conditions.*

Testing temperature	DRH (% RH)						ERH (% RH)					
	25℃		40℃		60℃		25℃		40℃		60℃	
Thermal activation	Non-heat	240℃	Non-heat	240℃	Non-heat	240℃	Non-heat	240℃	Non-heat	240℃	Non-heat	240℃
Alanine	92.1 ± 1.5	89.4 ± 1.2	90.0 ± 1.5	81.9 ± 1.5	84.7 ± 1.1	84.0 ± 1.8	91.1 ± 0.9	87.3 ± 1.4	86.3 ± 1.5	82.3 ± 0.5	78.7 ± 1.5	82.1 ± 1.6
Glutamine	87.8 ± 1.4	90.6 ± 1.5	86.3 ± 0.9	86.6 ± 0.7	81.7 ± 2.1	84.9 ± 3.5	85.7 ± 1.4	88.0 ± 0.8	87.8 ± 0.8	86.4 ± 0.7	80.8 ± 0.4	81.1 ± 2.4
Glycine	91.3 ± 1.8	91.1 ± 0.6	90.6 ± 0.9	88.0 ± 1.6	82.9 ± 1.3	81,7 ± 1,8	91.0 ± 0.4	89.8 ± 1.9	80.4 ± 1.9	82.6 ± 0.6	76.6 ± 0.8	70.9 ± 1.5
Serine	92.0 ± 0.6	88.7 ± 1.3	84.5 ± 2.9	83.1 ± 1.1	81.9 ± 1.1	76.3 ± 4.5	91.3 ± 1.2	82.7 ± 1.0	83.3 ± 1.3	81.8 ± 0.9	77.7 ± 1.5	74.5 ± 1.2
Adipic acid	97.4 ± 1.1		91.5 ± 0.8		83.2 ± 0.7				81.1 ± 3.4		60.9 ± 1.4	
Succinic acid	94.2 ± 0.4		91.3 ± 1.2		82.2 ± 1.5		91.3 ± 0.6		81.6 ± 2.6		61.7 ± 2.5	

c) <u>Leakage currents for amino acids under humidity exposure</u>

Figure 6.6 shows the leakage current response of the activated and non-activated amino acids at three different humidity levels close to their DRH and at three testing temperature levels. An increase of leakage current was obtained by increasing the testing temperature for amino acids. At 25℃, the leakage current of alanine and glutamine contaminated SIR test board maintained below 1 μA at 98% RH (**Figure 6.6**(a1)(b1)), whereas high leakage current was obtained from the glycine and serine contaminated SIR test boards at 98% RH (**Figure 6.6**(c1)(d1)). At 40℃, critical RH of serine decreased from 98% RH to 90% RH (**Figure 6.6**(d2)), whereas alanine, glutamine and glycine contaminated SIR testing board still maintained low leakage current below 1 μA at 90% RH(**Figure 6.6**(a2)(b2)(c2)). At testing temperature of 60℃, the critical RH value of glycine and serine declined to 90% RH as shown in **Figure 6.6**(c3)(d3). In many cases as shown in **Figure 6.6**(a3)(c2)(c3)(d2) under these conditions, leakage current exceeded 20 mA at the beginning of the bias loading and induced short circuit failures.
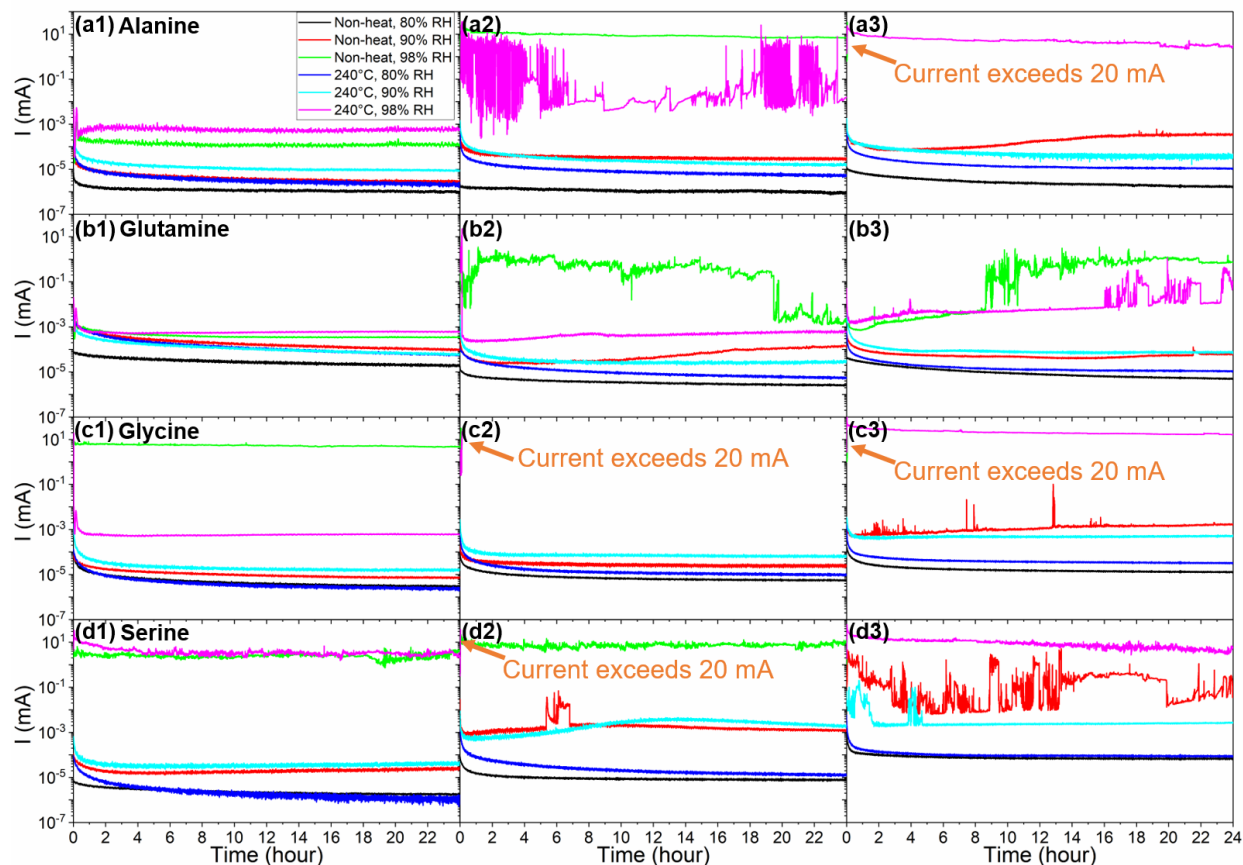
Figure 6.6 *Leakage current response of (a) alanine, (b) glutamine, (c) glycine, (d) serine contaminated SIR testing board at testing temperature of : (1) 25℃, (2) 40℃, (3) 60℃.*

Figure 6.7 presents the appearance of the amino acids contaminated SIR interdigitated pattern after leakage current measurement at 40℃, 98% RH. The plate like corrosion product was observed on glutamine, glycine and serine contaminated SIR pattern and deposited between two electrodes (**Figure 6.7**(b)(c)(d)). After CA testing at 40℃, 98% RH℃, while the dendritic corrosion product was observed on the alanine contaminated SIR pattern as shown **Figure 6.7**(a). The EDS mapping result in **Figure 6.7**(e)(f) indicates the corrosion product was in consist of Sn and O element.
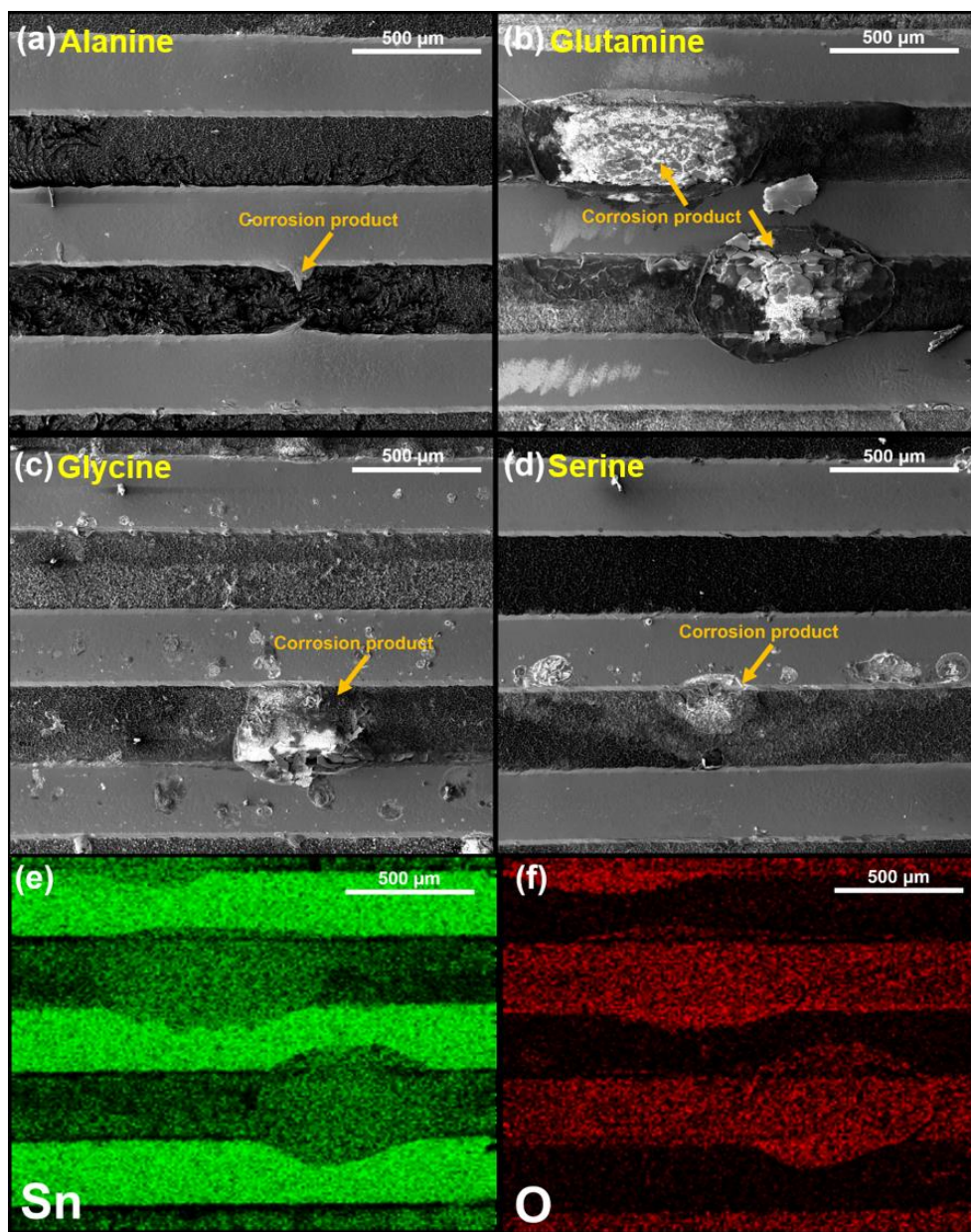
Figure 6.7 SEM images of non-thermal activated amino acids contaminated the SIR interdigitated pattern after CA testing at 40℃, 98% RH: (a) alanine, (b) glutamine, (c) glycine, (d) serine, and EDS mapping result of glutamine contaminated SIR board: (e) Sn, (f) O.

Evaluation of structural degradation of amino acids during thermal activation

Figure 6.8 shows the influence of thermal activation temperature of 240℃ on the degradation behavior of 4 tested amino acids. **Figure 6.8**(b) shows that the O-H peak at 3402 cm^{-1} and four N-H stretch peaks in a range between 3170-3308 cm^{-1} for glutamine disappeared after thermal activation at 240℃, while the C=O peak at 1648 cm^{-1} and C-O stretch peak at 1217 cm^{-1} are still remained in the degradation product. **Figure 6.8**(d) shows that O-H stretch peak, N-H stretch

peaks, and C-H stretch peaks disappeared in serine after thermal activation, while presented C=O and C-O stretch peaks in the degradation product. The thermal activation did not influence the structure of alanine, glycine, as shown in **Figure 6.8**(a)(c).
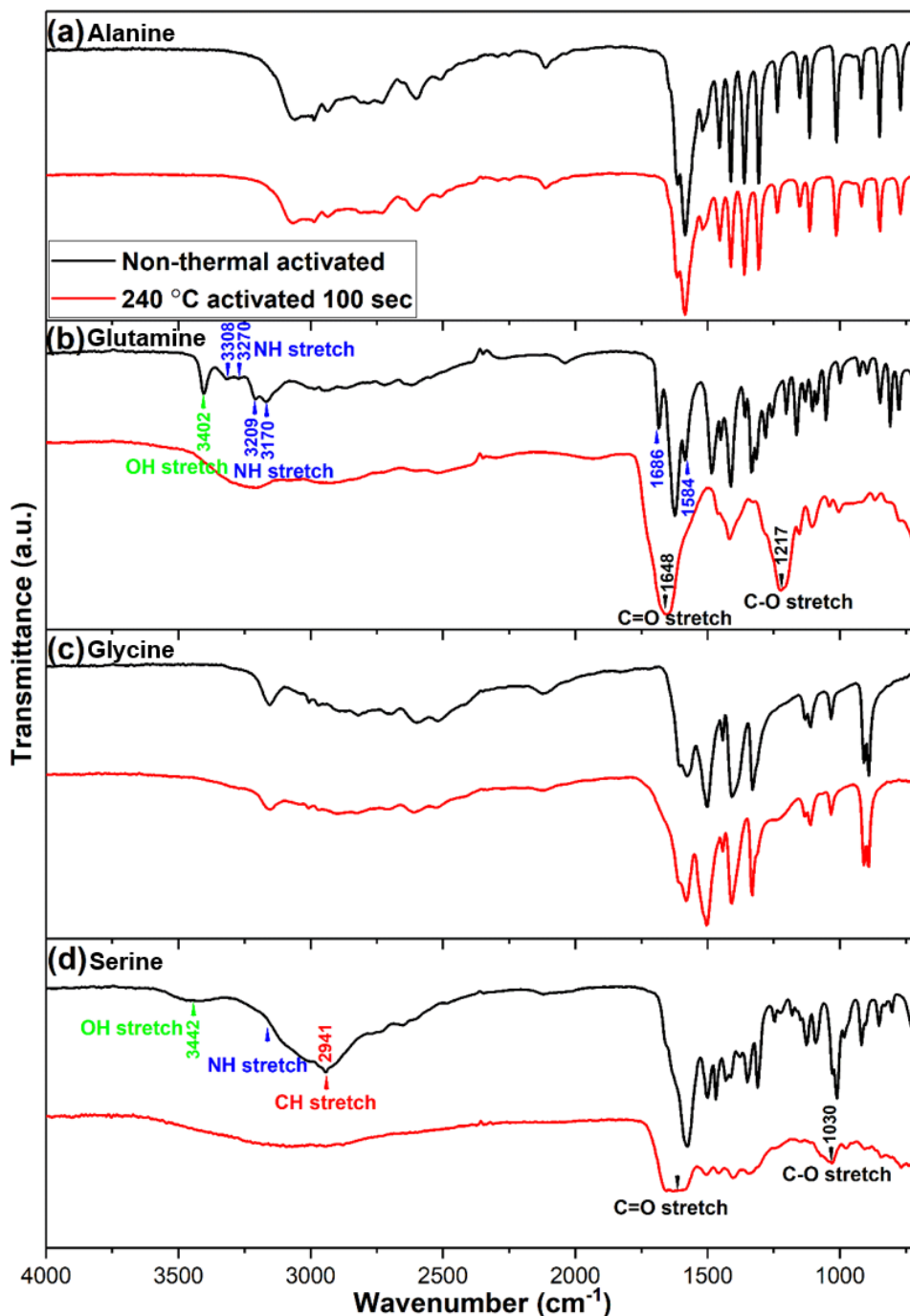
Figure 6.8 *FT-IR analysis of 4 tested amino acids after thermal activation at 240℃: (a) alanine, (b) glutamine, (c) glycine, (d) serine.*

IV.   DISCUSSION

Present study investigated the solderability and corrosion reliability of four amino acid as candidates for solder flux activators. When dissolved in water, all of them has pH close to neutral value. The solderability of flux depends upon the activator type [35], melting temperature of flux activator [36], and flux formulation temperature [35]. The interesting character of amino acid as activator is that the oxide removal function of amino acids on copper can be obtained by both carboxyl group and amino group. The oxide removal action of carboxyl group is through complexation and dispropotionation [21], whereas the oxide removal action of amino group is through redox reaction [37].

However, on the other hand, the corrosion reliability of the activator residue under humid conditions is dependent upon the hygroscopicity and ionization behavior when water layer is present. The hygroscopicity indicate the water absorption ability, which is determined by the DRH [9][38], while the water retention ability is indicated by ERH. The ionization behavior is related to the dissociation constant of the compound, which in terms of corrosion reliability changes the conductivity of the water layer formed on the PCBA surface [16][38]. The results obtained in this work suggest good solderability and corrosion reliability using glutamine as flux activator. Even though the corrosion robustness of glycine and alanine was confirmed by single frequency EIS and CA techniques, the solderability performance of these two candidates is inferior to the commercial used WOAs. The differences between DRH and ERH level of amino acid candidates indicate the hysteresis from water uptake and release, which is similar to commercially used WOAs [9]. After thermal activation, the reduction of the DRH and ERH value for alanine, glycine and serine could be due to the degradation of the carboxyl group, which induced higher hygroscopic anhydride species [3].

Solderability assessment of amino acids and the commercially used WOA flux activators

The solderability of amino acid depends on the activity of the carboxyl group and amino group at soldering temperature unlike for WOAs, which contain only carboxyl groups. It is known that the pK_{a1} value cannot interpret the activities of carboxyl group in amino acids and WOAs under soldering condition since the pK_{a1} value only represent the activities of carboxyl group in water. However, it is noticed that the wetting force of succinic acid is higher than adipic acid as shown in **Figure 6.2**, which indicate the activity of two carboxyl groups in succinic acid is higher than adipic acid under soldering temperature of 270℃. This compares with the behavior of the pK_{a1} value for succinic acid (4.21) which is higher than adipic acid (4.44) [9]. Amino acids used in the present investigation contain one carboxyl group and one amino group. The ranking of wetting

force for amino acid agreed with the ranking of pK$_{a1}$ value as shown in **Table 6.1**, where the pK$_{a1}$ value of glutamine is the highest, followed by serine, glycine and alanine from high to low. Based on this, one could use pK$_{a1}$ value as a screening factor for identifying the solderability for the selection of flux activators from the same chemical category.

The effect of melting temperature also influence the wetting force of flux activators used the in present work. Flux activators with low melting temperature provide a liquid barrier between metal and atmosphere to avoid re-oxidation. For instance, the melting temperatures of glutamine, succinic acid, and adipic acid are 185℃, 185℃, and 151.5℃ respectively [4][35], which provide relative good solderability compared to the other three tested amino acids with higher melting temperatures as shown in **Figure 6.3**(a)(c)(d). From the results of wetting force in **Figure 6.2**, it can be seen that the flux activators with melting temperature below 185℃ is able to protect the Cu surface from re-oxidation and maintain wettability at the soldering temperature of 270℃, whereas the glycine flux activators with melting temperature beyond 233℃ cannot maintain the solderability. Additionally, the wetting force obtained by serine flux is higher than the glycine although the melting temperature of serine (246℃) is higher than glycine (233℃) as shown in **Figure 6.2**. However, the pk$_{a1}$ value of serine (2.21) is higher than glycine (2.34), which agrees with the result of wetting force. It indicates that the melting temperature is not the only the important factor affecting the solderability, but also the activity of the carboxyl group. Amino group in glutamine and glycine degrade under temperature of 240℃ shown in **Figure 6.8**(b)(d), which resulted in redox reaction with Cu oxide [23]. The higher maximum wetting force obtained by glutamine could be attributed to the higher amount of zwitterions since glutamine is the only tested candidate which possesses two amino group in chemical structure. The zwitterions resulted in a more reactive positive charge group of -NH$_3$$^+$ when applied on metal oxides, which is more effective in oxide removal and ready for the oxides reaction in most of time during soldering process [26], as shown in the **Equation 6.2**.

$$2[R - CH(NH_3^+) - COO^-] + O^{2-} = 2[R - CH(NH_2) - COO]^- + H_2O \quad \textit{Equation 6.2}$$
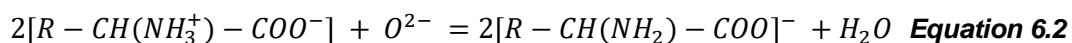
Humidity interaction assessment of amino acids and the commercial used WOA flux activators

Humidity interaction with flux activators plays the key role in the corrosion related failure of electronics when they are used in flux and residues remain. Water absorption behavior of various WOA activators were investigated using single frequency EIS method [9][7] and gravimetric method [18]. In **Table 6.2**, results from previous EIS investigations reported the DRH values of succinic acid are 94.2% RH, 91.3% RH, 82.2% RH at 25℃, 40℃, 60℃ respectively [9]. While for

adipic acid, the DRH values are 97.4% RH, 91.5% RH, and 83.2% RH at 25℃, 40℃, 60℃ respectively [9]. Compared to the summarized DRH value in **Table 6.2**, the DRH level of tested amino acids was lower compared to adipic acid and succinic acid, whereas the ERH levels of tested amino acids were slightly higher than succinic acid under all testing temperatures. Even though the DRH level of glutamine (86.3% RH at 25℃, 86.6 at 40℃) is lower than adipic acid and succinic acid, the glutamine obtained higher DRH value compared to adipic acid and succinic under testing temperature of 60℃.

The thermal activation effect on serine shows the reduction of DRH and ERH level, which is similar to the thermal activation effect on commercial used WOA flux activators. For commercially used WOA activators, the thermal effect on the reduction of the DRH and ERH value is due to the formation of the anhydride-like degradation products with higher affinity to water absorption [3]. While for serine, the influence of the thermal degradation product could be the reason induced higher hygroscopicity. **Figure 6.8**(d) shows a wide peak of C=O stretch in a range of 1600-1700 cm^{-1} and C-O stretch peak, which could be from the anhydride. Yablokov et al. reported thermal decomposition of serine took place at 30-50℃ below melting temperature and induced degradation product such as short-chain WOAs and short-chain amides [40], which obtained the deliquescent properties [41]. In contrast, the thermal degradation product of glutamine possessed lower hygroscopic behavior than glutamine, this could be due to the relative larger size and length of the side chains in the degradation product [9][42]. For alanine and glycine, stable molecule structure as shown in **Figure 6.8**(a)(c) resulted the minimal change of DRH and ERH after thermal activation.

In the present study, the gravimetric results of water absorption for tested WOAs and amino acids shown in **Figure 6.4** agreed with the results of single frequency EIS testing as shown in **Table 6.2**. The highest water gain rate was shown by succinic acid at 85-90% RH, whereas the water gain rate of serine surpassed the succinic acid at 95% RH. Nonetheless, EIS testing and gravimetric testing of flux activators revealed humidity interaction from different perspectives. For instance, DRH level obtained from EIS testing shows the sudden effect of the water absorption under humidity exposure, which is 94.2% RH for succinic acid at 25℃ [9]. However, gravimetric result in **Figure 6.4** demonstrates the water absorption behavior of succinic acid started at a much lower RH range (≤85% RH) than DRH in a low growth rate. This gravimetric testing confirmed the effect of the flux residue on water condensation layer, but the amount of water also depends on the kinetics under constant humidity exposure. Therefore, adipic acid and glutamine obtained the

best humidity robustness due to their lowest water gain rate among all tested activators based on constant humidity exposure.

Influence of amino acid activators on leakage current under DC load

The threshold value of leakage current in this study was determined as 10 µA according to the previous DC investigation on WOA based wave flux contaminated SIR interdigital pattern [7][36]. It is noticed that the leakage current value of glutamine contaminated SIR pattern under 98% RH reduced after thermal activation as shown in **Figure 6.5**(b2)(b3), while the thermal activation of 240℃ did not influence the leakage current of alanine, glycine and serine contaminated SIR pattern under humidity exposure. Weiss et al. reported that the degradation of glutamine took place at 185℃ and form H_2O and NH_3 [37], while the thermal degradation temperature of alanine, glycine, and serine was 309℃, 240℃, and 222℃ respectively [38]. Therefore, the reduction of the leakage current response of glutamine could be due to less ionic residue presented on the SIR pattern. However, the effect of testing temperature on the leakage current values is more pronounced for alanine, glycine and serine. This could be due to the increased temperature, which enhances of the mobility of the molecules and induces the formation of thicker water layer on PCBA surface [7], which raises the solubility of the amino acid residue on the SIR pattern and triggers higher leakage current [9].

The hygroscopic and ionic nature of flux activator candidates played a key role on the leakage current values of SIR pattern under DC load [9][36]. The leakage current measurements comply with the water absorption results as shown in **Figure 6.4**. Water absorption of serine is the highest (> 1.0 wt. %) in all the tested candidates under 95% RH, 25℃ as shown in **Figure 6.4**. The highest water absorption triggered the ionization of the serine on the SIR pattern and lead to the highest reduction of the impedance as shown in **Figure 6.5**(a1)(a2) and highest leakage current (**Figure 6.6**(d1)) under same climatic condition. The critical RH level indicates the RH level induced leakage current exceeding the threshold leakage current of 1 µA. Piotrowska et al. reported the critical RH values of adipic acid and succinic acid are 98% RH and 95% RH under 60℃ [9]. In the present work, the crucial RH of serine induced higher leakage current decreased from 98% to 90% RH as the testing temperature increased from 25℃ to 60℃. Coinciding with this, the water weight gain values of serine and glycine are much higher compared to succinic acid and adipic acid obtained under high humidity exposure as shown in **Figure 6.4**. On the contrary, the water weight gain of glutamine is the lowest (0.35 wt.%) in all tested flux activators under 60℃ as shown in **Figure 6.4**, and possessed the lowest leakage current as shown in **Figure 6.6**(b1). Water absorption results confirmed that the glutamine absorbed similar water level as adipic acid, and

alanine absorbed similar water level as succinic acid (**Figure 6.4**). This is in agreement the low leakage current values of glutamine and alanine under exposure of 98% RH at 25℃ and 40℃ (**Figure 6.6**(b1-3)(a1-3)). Piotrowska et al. [9] reported the leakage current values of 100 µg/cm^2 adipic acid and succinic acid comtaminated SIR pattern (IPC-4201/21) were below 1 µA at 99% RH under testing temperature of 25℃, whereas exceeded 1 µA at 98% RH under testing temperature of 40℃ and 60℃. The alanine or glutamine contaminated SIR pattern tested in present investigation also demonstrates the occurrence of high leakage current failure at 98% RH under 40℃ and 60℃, as shown in **Figure 6.6**(a2-3)(b2-3). However, **Figure 6.6**(b2) shows the leakage current level of 240℃ activated glutamine contaminated SIR pattern was below 1 µA at 98% RH/40℃, which indicates the better humidity robustness of glutamine as flux activator in comparison with adipic acid and succinic acid.

The occurrence of deteriorative leakage current was due to the conductive corrosion product formation, which bridged the adjacent oppositely biased electrodes under DC load [39]. The morphology of the corrosion product in **Figure 6.7**(b) confirmed that the corrosion product induced by glutamine is not like the ECM dendrites with structures of main-branches and side-branches [40][41]. Additionally, ECM dendrites are in the form of metal or in combination with hydroxide [39] [41] agreed with the EDS mapping result as shown in **Figure 6.7**(e)(f).

V.   CONCLUSIONS

- Solderability testing results shows that the wetting force of glutamine model flux is located between the wetting forces of commercial used adipic acid and succinic acid model fluxes, and homogeneous wetting appearance was obtained after using glutamine model flux under wave soldering temperature of 270℃. However, the wetting forces of alanine, glycine and serine model fluxes are much lower than adipic acid model flux.

- Water absorption test shows that the water weight gain rate of glutamine and adipic acid are the lowest in all 6 tested flux activator candidate under constant humidity exposure at 25℃, 95% RH, whereas water weight gain rate of serine and glycine are much higher than succinic acid. However, the water weight gain rate of serine and glycine are the lowest when exposed under humidity level below 90% RH at 25℃

- EIS results indicates the DRH and ERH levels of 240℃ activated glutamine are the highest in all tested amino acid candidates under same testing temperature, and glutamine contaminated SIR pattern possessed highest impedance response under 99% RH humidity exposure. Thermal activation decreased the DRH and ERH level of alanine, glycine and serine in a rate

of 1-5%, whereas an improvement of DRH and ERH level has been found on glutamine after thermal activation. Increased testing temperature decreased the DRH and ERH levels of all tested amino acids.

- A significant reduction of the leakage current has been observed on the glutamine contaminated after 240℃ thermal activation when exposed under 98% RH at 40℃ and 60℃. Critical RH value of serine contaminated SIR pattern decreased from 99% RH to 90% RH after increasing test temperature from 25℃ to 60℃. Higher baseline of leakage current of serine and glycine was obtained as increasing test temperature, whereas glutamine and glycine remained at the same level under exposed humidity level below 90% RH.

VI.   REFERENCES

[1]   S. Zhan, M.H. Azarian, M. Pecht, Reliability of printed circuit boards processed using no-clean flux technology in temperature-humidity-bias conditions, IEEE Trans. Device Mater. Reliab. 8 (2008) 426–434. doi:10.1109/TDMR.2008.922908.

[2]   C. Hunt, L. Zou, The impact of temperature and humidity conditions on surface insulation resistance values for various fluxes, Solder. Surf. Mt. Technol. 11 (1999) 36–43.

[3]   K. Piotrowska, M.S. Jellesen, R. Ambat, Thermal decomposition of solder flux activators under simulated wave soldering conditions, Solder. Surf. Mt. Technol. 29 (2017) 133–143. doi:10.1108/SSMT-01-2017-0003.

[4]   V. Verdingovas, M.S. Jellesen, R. Ambat, Solder Flux Residues and Humidity-Related Failures in Electronics: Relative Effects of Weak Organic Acids Used in No-Clean Flux Systems, J. Electron. Mater. 44 (2015) 1116–1127. doi:10.1007/s11664-014-3609-0.

[5]   R. Ambat, H. Conseil-Gudla, V. Verdingovas, Corrosion in Electronics, Encycl. Interfacial Chem. Surf. Sci. Electrochem. (2018) 134–144. doi:https://doi.org/10.1016/B978-0-12-409547-2.13437-7.

[6]   P. Isaacs, T. Munson, What makes no-clean flux residue benign?, in: 2016 Pan Pacific Microelectron. Symp. (Pan Pacific), 2016: pp. 1–7. doi:10.1109/PanPacific.2016.7428404.

[7]   K. Piotrowska, M. Grzelak, R. Ambat, No-Clean Solder Flux Chemistry and Temperature Effects on Humidity-Related Reliability of Electronics, J. Electron. Mater. 48 (2019) 1207–1222. doi:10.1007/s11664-018-06862-4.

[8]   C. Helene, S.J. Morten, A. Rajan, Contamination profile on typical printed circuit board assemblies vs soldering process, Solder. Surf. Mt. Technol. 26 (2014) 194–202. doi:10.1108/SSMT-03-2014-0007.

[9]   K. Piotrowska, R. Ud Din, F.B. Grumsen, M.S. Jellesen, R. Ambat, Parametric Study of Solder Flux Hygroscopicity: Impact of Weak Organic Acids on Water Layer Formation and Corrosion of Electronics, J. Electron. Mater. 47 (2018) 4190–4207. doi:10.1007/s11664-018-6311-9.

[10]   K. Piotrowska, R. Ambat, Residue-assisted water layer build-up under transient climatic

conditions and failure occurrence in electronics, IEEE Trans. Components, Packag. Manuf. Technol. (2020) 1. doi:10.1109/TCPMT.2020.3005933.

[11]   B.A. Smith, L.J. Turbini, Characterizing the weak organic acids used in low solids fluxes, J. Electron. Mater. 28 (1999) 1299–1306. doi:10.1007/s11664-999-0171-2.

[12]   K. Piotrowska, L. Feng, R. Ambat, Thermal decomposition of binary mixtures of organic activators used in no-clean fluxes and impact on PCBA corrosion reliability, Solder. Surf. Mt. Technol. 32 (2019) 93–103. doi:10.1108/SSMT-05-2019-0020.

[13]   H. Conseil, V. Verdingovas, M.S. Jellesen, R. Ambat, Decomposition of no-clean solder flux systems and their effects on the corrosion reliability of electronics, J. Mater. Sci. Mater. Electron. 27 (2016) 23–32. doi:10.1007/s10854-015-3712-x.

[14]   K.S. Hansen, M.S. Jellesen, P. Moller, P.J.S. Westermann, R. Ambat, Effect of solder flux residues on corrosion of electronics, in: 2009 Annu. Reliab. Maintainab. Symp., 2009: pp. 502–508. doi:10.1109/RAMS.2009.4914727.

[15]   M.S. Jellesen, D. Minzari, U. Rathinavelu, P. Møller, R. Ambat, Corrosion failure due to flux residues in an electronic add-on device, Eng. Fail. Anal. 17 (2010) 1263–1272. doi:10.1016/j.engfailanal.2010.02.010.

[16]   V. Verdingovas, M.S. Jellesen, R. Ambat, Influence of sodium chloride and weak organic acids (flux residues) on electrochemical migration of tin on surface mount chip components, Corros. Eng. Sci. Technol. 48 (2013) 426–435. doi:10.1179/1743278213Y.0000000078.

[17]   B. Alan, Z. Ling, C. Hunt, Development of New Solderability Test Fluxes, NPL Report MATC(A)122, 2002.

[18]   K. Piotrowska, V. Verdingovas, R. Ambat, Humidity-related failures in electronics: effect of binary mixtures of weak organic acid activators, J. Mater. Sci. Mater. Electron. 29 (2018) 17834–17852. doi:10.1007/s10854-018-9896-0.

[19]   A.K. Salameh, L.S. Taylor, Role of Deliquescence Lowering in Enhancing Chemical Reactivity in Physical Mixtures, J. Phys. Chem. B. 110 (2006) 10190–10196. doi:10.1021/jp0612376.

[20]   D. Xu, X. Li, C. Wang, B. Xu, Study on wettability and corrosivity of a new no-clean flux for lead-free solder paste in electronic packaging technology, in: 2011 Second Int. Conf. Mech. Autom. Control Eng., 2011: pp. 1706–1708. doi:10.1109/MACE.2011.5987285.

[21]   M. Bixenman, D. Lober, A. Ailworth, K. Corporation, B. Tolla, D. Ph, J. Allen, D. Jean, K. Loomis, K. Corporation, Electrochemical Methods to Measure the Corrosion Potential of Flux Residues, in: IPC APEX EXPO, SMTNET, San Diego, USA, 2017.

[22]   B. Tolla, D. Jean, H. Bhavsar, Y. Shi, X. Wei, Reactivity of No-clean flux residues in electronic assemblies: a systematic study, in: SMTA Int., Rosemont, IL, USA, 2015.

[23]   Y. Shi, X. Wei, B. Tolla, The Role of Organic Amines in Soldering Materials, in: IPC APEX EXPO Conf. Proc., Circuit Insight, San Diego, USA, 2015.

[24]   E. B.N., Water Soluble Fluxes, their Reliability and their Usefulness as a Means of Eliminating CFC-113 Usage, Solder. Surf. Mt. Technol. 3 (1991) 16–23. doi:10.1108/eb037751.

[25]   A. Masatoshi, K. Katoh, K. Sumita, Liquid epoxy resin composition, US20070104959A1, 2006. https://patents.google.com/patent/US20070104959.

[26]   Ooi Wan Koon, Mohd Jaffri Razai, Chan Boon Pin, Nurul Akmal Mohd Sharif, Study on IMC morphology and impact to solder joint performance for different halogen free (HF) flux in semiconductor application, in: 2010 34th IEEE/CPMT Int. Electron. Manuf. Technol. Symp., 2010: pp. 1–6. doi:10.1109/IEMT.2010.5746722.

[27]   H. V. Ramakrishna, H.S. Harish, J. Manjuvani, V. Bhaskar, R. Kumar, V. Patil, S. Sarkar, Engineered flux for low temperature solders, in: Proc. SMTA Int., Rosemont, IL, USA, 2018: pp. 1–7. https://www.circuitinsight.com/pdf/engineered_flux_flow_temperature_solders_smta.pdf.

[28]   M.A. Kiani, M.F. Mousavi, S. Ghasemi, M. Shamsipur, S.H. Kazemi, Inhibitory effect of some amino acids on corrosion of Pb–Ca–Sn alloy in sulfuric acid solution, Corros. Sci. 50 (2008) 1035–1045. doi:https://doi.org/10.1016/j.corsci.2007.11.031.

[29]   Min Yang, Tao Zhang, Xiuzhong Liu, Songming He, Water-soluble fluxes for Sn-4Zn-0.89Cu-3.5Bi-0.3Re alloy lead-free solder, in: 2009 16th IEEE Int. Symp. Phys. Fail. Anal. Integr. Circuits, 2009: pp. 785–789. doi:10.1109/IPFA.2009.5232724.

[30]   R. C., Evaluation of the Reliability and Corrosivity of VOC-free, No-clean Fluxesusing Standard, Modified and Electrochemical Methods*, Solder. & Surf. Mt. Technol. 8 (1996) 6–9. doi:10.1108/09540919610777555.

[31]   K.M. Adams, J.E. Anderson, Y.B. Graves, Ionograph Sensitivity to Chemical Residues From 'no Clean Soldering Fluxes: Comparison Of Solvent Extract Conductivity and Surface Conductivity, Circuit World. 20 (1994) 41–44. doi:10.1108/eb046251.

[32]   C. Idnani, Impact of New Materials and Processes on Manufacturing: Green (Pb and halide free), RoHS experience, in: 2007 32nd IEEE/CPMT Int. Electron. Manuf. Technol. Symp., 2007: pp. 332–334. doi:10.1109/IEMT.2007.4417084.

[33]   M. Yamamoto, T. Shiomi, K. Nakanishi, M. Watanabe, M. Aihara, Soldering flux and solder paste composition, EP1897652A1, 2008.

[34]   L. D'Angelo, V. Verdingovas, L. Ferrero, E. Bolzacchini, R. Ambat, On the Effects of Atmospheric Particles Contamination and Humidity on Tin Corrosion, IEEE Trans. Device Mater. Reliab. 17 (2017) 746–757. doi:10.1109/TDMR.2017.2771505.

[35]   M. Stogniew, L.A. Geelhaar, P.S. Callery, Synthesis of deuterium enriched L-glutamine and 4-aminobutanamide from pyridazinones, J. Label. Compd. Radiopharm. 18 (1981) 897–903. doi:https://doi.org/10.1002/jlcr.2580180615.

[36]   V. Verdingovas, M.S. Jellesen, R. Ambat, Relative effect of solder flux chemistry on the humidity related failures in electronics, Solder. Surf. Mt. Technol. 27 (2015) 146–156. doi:10.1108/SSMT-11-2014-0022.

[37]   I.M. Weiss, C. Muth, R. Drumm, H.O.K. Kirchner, Thermal decomposition of the amino acids glycine, cysteine, aspartic acid, asparagine, glutamic acid, glutamine, arginine and histidine, BMC Biophys. 11 (2018) 2. doi:10.1186/s13628-018-0042-4.

[38]   V.Y. Yablokov, I.L. Smel'tsova, I.A. Zelyaev, S. V Mitrofanova, Studies of the rates of thermal decomposition of glycine, alanine, and serine, Russ. J. Gen. Chem. 79 (2009) 1704–1706. doi:10.1134/S1070363209080209.

[39]   D. Minzari, M.S. Jellesen, P. Møller, R. Ambat, On the electrochemical migration mechanism of tin in electronics, Corros. Sci. 53 (2011) 3366–3379. doi:10.1016/J.CORSCI.2011.06.015.

[40]   D. Minzari, F.B. Grumsen, M.S. Jellesen, P. Møller, R. Ambat, Electrochemical migration of tin in electronics and microstructure of the dendrites, Corros. Sci. 53 (2011) 1659–1669. doi:10.1016/J.CORSCI.2011.01.009.

[41]   B. Medgyes, B. Horváth, B. Illés, T. Shinohara, A. Tahara, G. Harsányi, O. Krammer, Microstructure and elemental composition of electrochemically formed dendrites on lead-free micro-alloyed low Ag solder alloys used in electronics, Corros. Sci. 92 (2015) 43–47. doi:10.1016/J.CORSCI.2014.11.004.

7. Comparative study of tripropylamine and naphthylamine as additives in wave solder flux: investigation of solderability and humidity effects

Feng Li, *Morten Stendahl Jellesen, Rajan Ambat*

Abstract: Dicarboxylic acid flux activators are used in no-clean wave solder flux formulation for activating the solder surfaces on Printed Circuit Board Assembly (PCBA) during the soldering process. However, flux residues containing dicarboxylic acid components on PCBA can cause adverse corrosion issues under humid conditions due to its hygroscopic and acidic nature. This paper systematically investigated tripropylamine and naphthylamine as additives together with dicarboxylic acid activators on the solderability performance and humidity robustness. Evaluation of the solderability was assessed using hot plate spreading test and wetting balance methods, while thermal degradation was investigated using Fourier-transform infrared spectroscopy. The moisture interaction behavior of activator chemistry was investigated using electrochemical impedance spectroscopy and chronoamperometry techniques. Results showed improvement of wetting ability using tripropylamine additive in succinic acid based fluxes, while tripropylamine additive increased the maximum wetting force for adipic acid based flux activators. Significant reduction of leakage current value was obtained using tripropylamine and naphthylamine additives in succinic acid based fluxes under 98% RH/40°C.

Keywords: Amine, solder flux, electronic corrosion, humidity, reliability, solderability.

I.   INTRODUCTION

Due to the green manufacturing trends in the electronic industry, halogenated cleaning solvents for printed circuit board assembly (PCBA) and leaded solders were phased out based on Montreal Protocol [1] and Waste Electrical and Electronic Equipment (WEEE) [2]. Hence, elimination of cleaning steps in electronic manufacturing became the trend in order to decrease the utility of the volatile organic cleaning agents[3]. Consequently, no-clean flux formulation with weak organic acid (WOA) as activator was broadly implemented over 70% of the electronic industry [4][5]. Commercially used WOA based flux system today use activators such as adipic acid, succinic acid, glutaric acid etc. [3], which possess boiling temperature at 337.5°C, 234°C and 273°C respectively [6]. In practice, the soldering temperature is usually set between 230°C and 250°C to avoid the damage of components on PCBA [7][8]. Even though the soldering temperature may degrade succinic acid and form degradation product (succinic anhydride), the degradation product

will present on PCBA due to the higher boiling point [3]. Therefore, significant amount of WOA contained flux residue was detected in many electronic devices after soldering process [9][10][11], and the localized contamination level of WOA can be as high as 687µg/in^2 (106.5 µg/cm^2) [11].

A number of investigations reported that the WOA contained flux residue on PCBA surface can trigger corrosion related failures such as reduction of the surface insulation resistance (SIR) [12][13][14], parasitic leakage issue under low stand-off components [11], and electrochemical migration (ECM) [15][16]. ECM is one the most detrimental failure mode for the electronic corrosion, and the failure rate of ECM in electronic devices can be as high as 1-4% [17]. For a PCBA under exposure to humidity, corrosion cell forms when water layer connects between oppositely biased electrodes. Bias on the electrodes and electrochemical process, trigger metal dissolution at the anode, which migrate towards the cathode and deposit forming conductor bridge and short circuit [18][19]. Under humidity exposure, the hygroscopic behavior of WOA activators in the flux residue changes the humidity level for condensed water layer formation, due to the difference in the critical relative humidity (cRH) [20][21]. Acidity of WOA also changes the pH of the solution and ionization causes increased conductivity, while both of these asepcts will favor ECM dendrite formation [22]. The solderability and corrosivity of WOA activators depend on the acid dissociation constant (pKa), which is affected by the polarity of the WOA. The PCBA contaminated by WOA with shorter carbon chain (such as glutaric acid) is more aggressive for ECM [23], although the glutaric acid provides better solderability [24]. Glutaric acid also have lower cRH leading to water layer formation on PCBA under lower humidity level when exposed to humidity.

In order to balance the corrosion effect and solderability of the no-clean flux, blended WOA activators [23], blended WOA-amine activators [25][26], and corrosion inhibitors [25] were introduced to the flux formulation. Piotrowska et al. reported the binary blended WOAs as activator resulting in a lower cRH than the individual WOA, which indicates the water condensation and corrosion can occur at even lower RH value [27]. Tolla et al. reported the inhibition of ECM dendrite growth obtained by blended anonymous organic amine and WOA, and corrosion inhibitor used in the study was not as good as organic amine candidates [25]. Xu et al. reported that the blended WOA and triethanolamine (TEA) exhibited better solderability and minor corrosion by Cu mirror test [28]; however, in the study, low deliquescence RH of TEA (below 30% RH) was attributed to humidity interaction with hydroxyl group of TEA, which induced ECM dendrites formation under 5 volts DC load at 70% RH/25°C [24]. The humidity robustness of the organic amine activator candidates in flux formulation also depend on the protonation strength of the lone

pair in amino group, which could induce the water dissociation for the formation of negatively charged hydroxide ions [29]. The protonation behavior of amine activator residues could be influenced by the environmental temperature, for example, the protonation of diethanolamine (DEA), TEA and triisopropanolamine (TIPA) was significantly prohibited by increasing testing temperature from 25°C to 60°C [24]. Moreover, strong water absorption behavior was obtained by alkanolamine due to the intermolecular hydrogen bond formation between hydroxyl group in alkanolamine and hydrogen in water molecule, which accelerated the ECM failure in electronics [24]. Therefore, it is important to understand the behavior other amine categories such as aromatic and alkyl-amine types on their performance of solderability and humditiy related effects.

Tripropylamine and naphthyamine were tested for the present investigation as the representative materials for alkyl-amine and aromatic amine. The present study systematically investigated the amine additives in WOA activator based flux formulation on the solderability and climatic reliability. SIR interdigitated pattern (IPC-4201/21) was used as vehicle for electrochemical tests. Chronoamperometry was used to investigate the leakage current level and ECM susceptibility induced by the flux residue. Electrochemical impedance spectroscopy (EIS) was used to understand the critical relative humidity for model flux with/without organic amine additives. The solderability of organic amine modified flux formulation was investigated using wetting balance. The degradation product of flux residue was analyzed using fourier-transform infrared spectroscopy (FT-IR).

II.   MATERIALS AND EXPERIMENTAL METHODS

<u>Materials preparation</u>

a) <u>Model flux formulation used in the investigation</u>

Table 7.1 shows physical and chemical properties of two organic amines and two WOAs used for the investigations. All chemicals used are in analytical grade (Sigma Aldrich, USA). The melting point indicates the temperature at which the chemical become liquid and protected the soldering region from re-oxidation. Due to the low melting point of tripropylamine at -93.5°C, it presents as liquid state at room temperature. Naphthylamine, succinic acid, and adipic acid require higher temperatures to melt. The boiling point demonstrates the temperature for the evaporation of chemicals, which directly influence the soldering function. The acidic dissociation constant (pKa) determines the solubility of chemicals in water and the strength for the oxides dissolution during soldering condition. Low pKa value of chemicals indicates higher acidity. **Table 7.2** shows the flux formulation and the codename of the model fluxes used in the investigation. The fraction of the

WOA activators was maintained at 4 wt.%, whereas organic amine additives were set at 0.2 wt.% and 0.4 wt.%. The flux activator and amine additive was dissolved in insopropanol alcohol by 30 min by ultra-sonic bath mixing.

Table 7.1 Properties of the WOAs and organic amines used in the investigation.

	Molecular structure	Molecular weight(g/mol)	Melting point (°C)	Boiling Point (°C)	pKa1	pKa2
Tripropylamine		143.27	-93.5	156	10.65	-
Naphthylamine		143.18	49.2	300.8	3.92	-
Succinic acid		118.09	188	235	4.21	5.64
Adipic acid		146.14	153.2	337.5	4.43	5.41
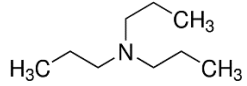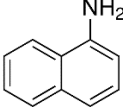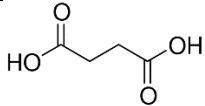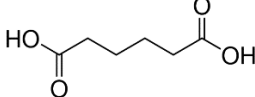
Table 7.2 Model flux formulation used in the investigation.

Model flux	Model flux formulation (Solvent: isopropanol alcohol)
A	4 wt.% Adipic acid
S	4 wt.% Succinic acid
AT02	4 wt.% Adipic acid, 0.2 wt% Tripropylamine
AT04	4 wt.% Adipic acid, 0.4 wt% Tripropylamine
AN02	4 wt.% Adipic acid, 0.2 wt% Naphthylamine
AN04	4 wt.% Adipic acid, 0.4 wt% Naphthylamine
ST02	4 wt.% Succinic acid, 0.2 wt% Tripropylamine
ST04	4 wt.% Succinic acid, 0.4 wt% Tripropylamine
SN02	4 wt.% Succinic acid, 0.2 wt% Naphthylamine
SN04	4 wt.% Succinic acid, 0.4 wt% Naphthylamine

b) Cu alloy substrates for solderability analysis

For the wetting balance tests (IPC-TM-650 2.4.14.2), the ETP grade Cu substrates with dimension of 6 mm × 25 mm × 0.5 mm were prepared using electronic discharge machining. For the hot plate spreading tests (IPC-TM-650 2.4.46), Cu63/Zn37 brass substrates with dimension of 40 mm

× 75 mm × 1 mm were prepared. Cleaning of the test substrate was carried out based on ISO 9455-16 standard.

c) Test vehicle for humidity robustness evaluation using electrochemical methods

Test boards with SIR interdigitate comb pattern (IPC-4201/21) were used for the electrochemical study, as shown in **Figure 7.1**. The surface finish of the SIR pattern was using hot air solder leveled (HASL) Sn-0.7Cu alloy on 35 µm Cu trace. In the total testing area of 25 mm × 13 mm, the entire overlapping length of conductive lines is 442.8 mm with 41 adjacent sets of electrodes. The pitch size of the conductive lines is 300 µm. Before subjecting the electrochemical tests, the testing region of SIR pattern was contaminated to the level of 100 µg/cm^2 flux residue to imitate the localized contamination after soldering process. Amount of flux applied was simulating the flux applied during actual soldering application. Thermal effect of the soldering process on flux residue was simulated using a Techno HA-06 oven for a thermal treatment at 240°C for 45 sec. Flux activator contaminated SIR patterns without subjecting to thermal exposure were used as reference for the electrochemical tests.
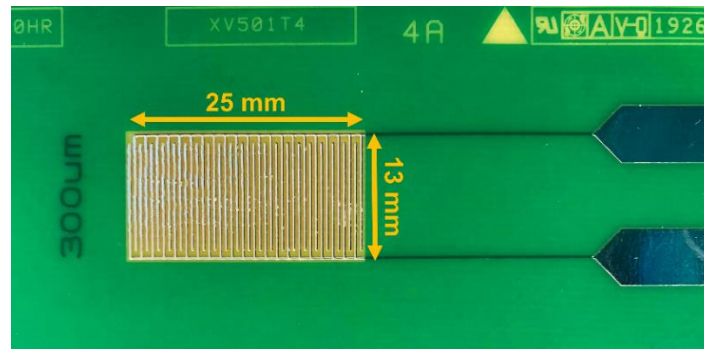
Figure 7.1 Test boards with SIR interdigitated pattern used for electrochemical study.

Solderability evaluation using hot plate spreading testing and wetting balance

a) Hot plate spreading test

Hot plate spreading tests were conducted using two SD160 digital hotplates (Stuart, UK). An O-ring in diameter of 1 cm was prepared using flux-free 96.5Sn-3Ag-0.5Cu (SAC 305) solder alloy. Before testing, 50 µL of the model flux was applied in the center of the solder O-ring on the Cu63/Zn37 substrate. After 4 sec preheat treatment at 160°C, the sample was subjected on another hot plate with a temperature of 270°C until the solder O-ring melted. The spreading of the melted solder alloy was visualized using a light optical microscope (LOM) (Keyence VHX, Japan).

b) Wetting balance test

Investigation of the solderability of the model fluxes was carried out using the Must 3 wetting balance (GEN3, UK) at an air-static environment, which provided the wetting force of the SAC 305 solder alloy on the flux activated Cu substrates during wave soldering process. To apply the flux, the tested side of cleaned Cu substrate was vertically immersed in the model flux to a depth of 10 mm and cleaned the extra flux using a filter paper as described in the procedure of IPC-TM 650 2.4.14.2. The temperature of SAC 305 solder bath in the wetting balance was precisely controlled at 270°C, which provides the heat source for the preheat treatment of Cu samples. After 20 sec preheat treatment of the Cu substrate by placing on the solder bath with the distance of 10 mm, the tested side of Cu substrate was immersed in the solder bath for 10 sec with the immersion depth of 5 mm in the speed of 20 mm/s. After soldering process, the interphase quality between the SAC 305 alloy layer and the Cu substrate was evaluated by the cross section inspection using the Quanta 200 FEG scanning electron microscope (FEI, USA) under secondary electron mode at 15 kV.

Thermal decomposition analysis of model flux activators using FT-IR

In order to obtain the structural elucidation of flux activators after soldering process, spectroscopic analysis was carried out using the Nicolet iN10 MX infrared imaging microscope (Thermo Fisher Scientific, USA) equipped with a Ge attenuated total reflectance (ATR) tip. Model flux were placed on the glass substrate and dried in the fume hood, which only leaves the flux activators on the glass substrate. The thermal treatment was carried out on this by placing it in the Techno HA-06 oven at 240°C for 100 sec to simulate the thermal input of flux activators during wave soldering condition. Flux activators without subjecting to thermal exposure was used as reference for the FT-IR analysis.

Humidity robustness analysis of flux activators using electrochemical techniques

Climatic exposure of the flux activator contaminated SIR interdigitate pattern was conducted in the Espec PL-3KPH climatic chamber (Espec, Japan) with a certainty of ± 0.3 ℃ and ± 2.5% relative humidity (RH). Electrochemical tests on the SIR interdigitate pattern were performed using the multi-channel Biologic VSP potentiostat (Biologic, France). Three-electrode electrochemical system were used to imitate positive and negative bias on the surface of the PCBA. One electrode of the SIR interdigitated pattern was used as counter and reference electrodes, while the other electrode was used as working electrode. Electrochemical tests were conducted at testing temperature of 25℃, 40℃ and 60℃ in order to imitate different service condition of electronic device. For instance, 25℃ and 40℃ were used to imitate the environmental temperature, while 60℃ was used to imitate the self-heating of the devices.

a) Single frequency EIS measurement

Single frequency EIS technique was used to investigate the level of relative humidity (RH) triggering moisture absorption and moisture release from the flux residue contaminated SIR pattern. Moisture absorption of the flux activator contaminated SIR pattern was determined by deliquescence relative humidity (DRH) of the flux activator package, while the moisture release behavior was determined by efflorescence relative humidity (ERH). During water condensation on the PCBA, the phase angle of SIR components shifted from -90° to 0° at high frequency range between 10 and 100 kHz [30][31], which indicates the transition of electrical property from capacitance dominant behavior to resistance dominant behavior. Consequently, the EIS measurement at such frequency is able to roughly estimate the DRH and ERH [20][27][32]. Single frequency EIS at 10 kHz with the amplitude of 10 mV was applied on the flux activator contaminated SIR pattern in order to record the DRH value of flux activator during humidity ramping from 30% RH to 99% RH in 12 hours. The ERH value was measured during humidity ramping from 99% RH to 30% RH in next 12 hours. Before subjecting the single frequency EIS measurement, flux activator contaminated SIR patterns were stabilized at 30% RH in climatic chamber for 6 hours.

b) Chronoamperometry (CA) testing

CA technique was used to investigate the leakage current or ECM triggering capacity of flux activator contaminated SIR pattern under different humidity exposure conditions namely at 60% RH, 70% RH, 80% RH, 90% RH and 98% RH respectively. Before conducting the CA measurement, the flux activator contaminated SIR pattern was stabilized in the climatic chamber for 1 hour. The CA measurement for each type of flux activator contaminated SIR pattern was conducted under 10 V DC bias loads for 3 hours. Leakage current level of flux activator contaminated SIR pattern was recorded by EC-lab software. The threshold value of leakage current value was defined at 10 µA based on the previous investigation of flux contamination using IPC-4201/21 SIR pattern [23][32].

III.   RESULTS

Evaluation of solderability for model fluxes

Figure 7.2 shows the spreading of the SAC 305 alloy when using different model fluxes after hot plate spreading test. **Figure 7.2**(a2-3)(b2-3) shows the tripropylamine additive in adipic acid and succinic acid contained model fluxes increased the spreading area of the SAC 305 alloy compared to pure adipic acid and succinic model flux etched sample shown in **Figure 7.2**(a1)(b1). **Figure 7.2**(a5)(b5) indicate that the spreading area of SAC 305 alloy decreased using 0.4 wt.%

naphthylamine additive in activator package. **Figure 7.2**(a2)(a3) shows the tripropylanine addtive in adipic acid flux expanded the spreading area towards center of the O-ring, however, for the for tripropylamine modified succinic acid fluxes, spreading tendency was opposite as shown in **Figure 7.2**(b2)(b3).
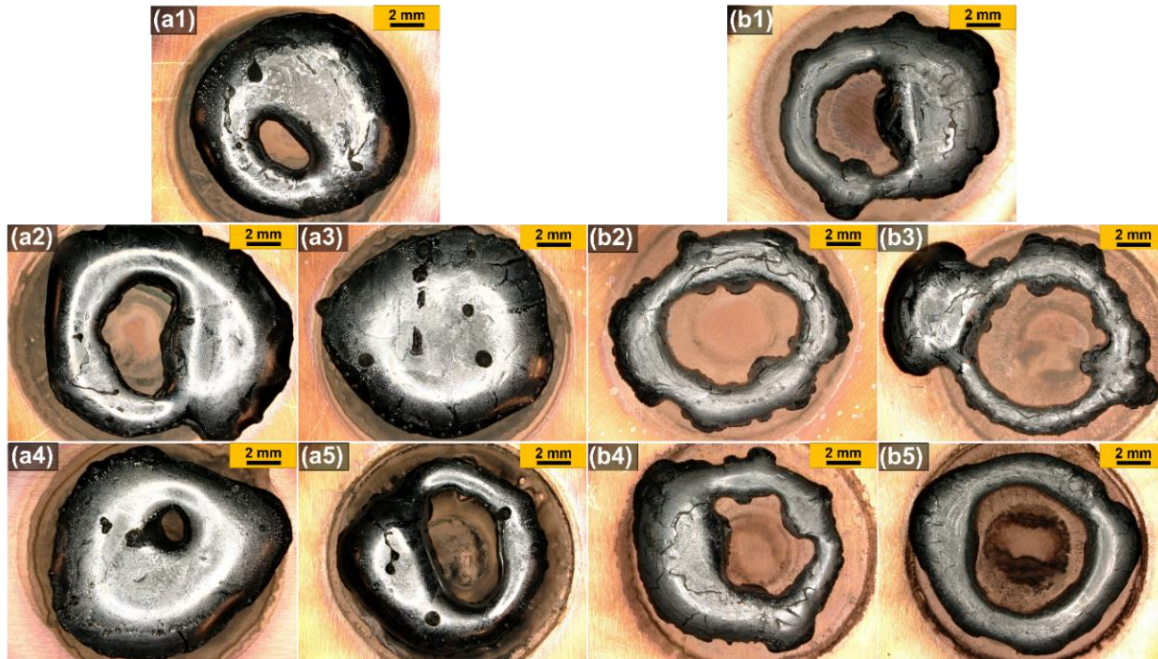
Figure 7.2 *LOM photographs of specimens after hot plate spreading test using various model fluxes: (a1) A, (a2) AT02, (a3) AT04, (a4) AN02, (a5) AN04, (b1) S, (b2) ST02, (b3) ST04, (b4) SN02, (b5) SN04.*

Figure 7.3 shows the curves of wetting force induced by the model fluxes during wetting balance testing. Time to reach zero wetting force (T_0), time to two thirds maximum wetting force ($T_{2/3}$), and maximum wetting force (F_{max}) were summarized in **Table 7.3**. T_0 and $T_{2/3}$ parameters demonstrate the speed of wetting, while the F_{max} parameter demonstrates the solderability. The effect of amine additives on F_{max} was more pronounced on adipic acid contained flux formulations, as shown in **Figure 7.3**(a). Compared to 3.69 mN obtained by pure adipic acid model flux (**Figure 7.3**(b)), the F_{max} was improved using ST02, ST04 and SN02 model fluxes, which were 4.11 mN, 4.08 mN and 3.92 mN respectively. However, the F_{max} of AN04 model flux decreased to the level of 3.49 mN. In comparison, the F_{max} was slightly reduced when using amine additive in succinic acid contained flux formulation. The SN02 and SN04 model fluxes induced slightly lower F_{max} at 3.73 mN compared to ST02 model flux at 3.98 mN and ST04 model flux at 3.89 mN. Generally, the wetting speed of 4 amine additive modified succinic acid model fluxes was faster than 4 amine additive modified adipic acid model fluxes. **Figure 7.3**(a) illustrates the wetting speed for adipic contained

model flux was significantly influenced by amine additives. The $T_{2/3}$ of AT04 model flux decreased to 1.18 sec in comparison with pure adipic acid model flux for 1.32 sec, whereas larger T_0 and $T_{2/3}$ were obtained when using AT02, AN02 and AN04 model fluxes, as shown in **Table 7.3**. In contrast, the amine additives in succunic acid fluxes reduced the T_0 to approximate 0.74-0.79 sec, and the $T_{2/3}$ values for amine additive modified succinic acid model flux were approximate 0.96-1.01 sec.
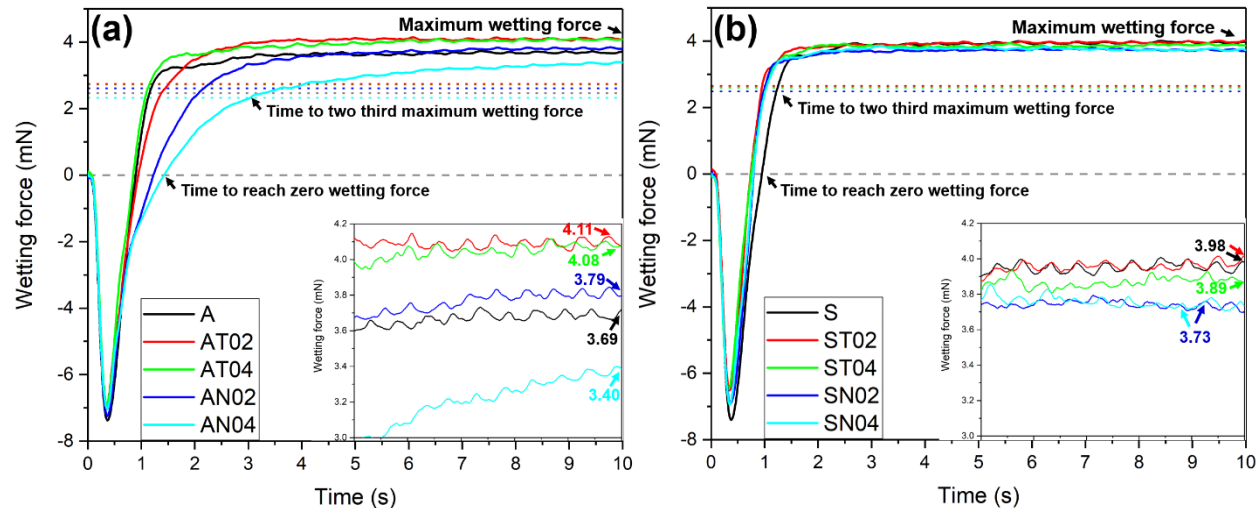
Figure 7.3 *Wetting balance test result using various model fluxes for surface activation: (a) model fluxes with adipic acid as main activators, (b) model fluxes with succinic acid as main activators.*

Table 7.3 *Summary of qualification parameters in wetting balance result from 3 parallel tests.*

	Time to reach Zero Wetting force (sec)	Time to two thirds maximum wetting force (sec)	Maximum Wetting force (mN)
Adipic acid	0.94 ± 0.09	1.32 ± 0.23	3.69 ± 0.03
AT02	0.97 ± 0.06	1.55 ± 0.06	4.11 ± 0.02
AT04	0.89 ± 0.05	1.18 ± 0.03	4.08 ± 0.03
AN02	1.18 ± 0.05	2.18 ± 0.06	3.92 ± 0.04
AN04	1.38 ± 0.04	2.77 ± 0.20	3.49 ± 0.10
Succinic acid	1,00 ± 0.06	1.34± 0.08	3.97 ± 0.04
ST02	0.74 ± 0.03	0.96 ± 0.02	3.98 ± 0.03
ST04	0.75 ± 0.02	1.01 ± 0.02	3.89 ± 0.02
SN02	0.79 ± 0.03	0.99 ± 0.02	3.73 ± 0.03
SN04	0.79 ± 0.01	1.00 ± 0.02	3.73 ± 0.03

Figure 7.4 shows the cross-section of the wetting balance tested samples indicating the quality of SAC 305 layer on Cu substrates when various fluxes are used. Some defect was observed on the tip of Cu substrate activated using pure adipic acid model flux, as shown in **Figure 7.4**(a1),

while **Figure 7.4**(a2-5) shows perfect coverage of SAC 305 layer was observed when using tripropylamine and naphtylamine modified model fluxes for the test, although the thickness of the SAC 305 layer was different. Compared to pure adipic acid model flux activated sample in **Figure 7.4**(a1), **Figure 7.4**(a5)(a4) shows that the 0.4 wt.% and 0.2 wt.% naphthylamine additive in adipic acid contained model flux reduced the maximum thickness of the SAC 305 layer from 41 μm to 38 μm and 28 μm respectively. However, **Figure 7.4**(a3) indicates that the maximum thickness of SAC 305 layer in AT04 sample was slightly higher than pure adipic acid model flux activated Cu sample. For the model fluxes with succinic acid as activators, the 0.4 wt.% and 0.2 wt.% naphthylamine additive increased the maximum thickness of SAC 305 layer from 12 μm to 69 μm and 37 μm respectively, as shown in **Figure 7.4**(b1)(b5)(b4). Higher maximum thickness of SAC 305 layer at 42 μm was obtained using ST04 model flux in comparison with 13 μm SAC 305 layer using ST02 model flux.
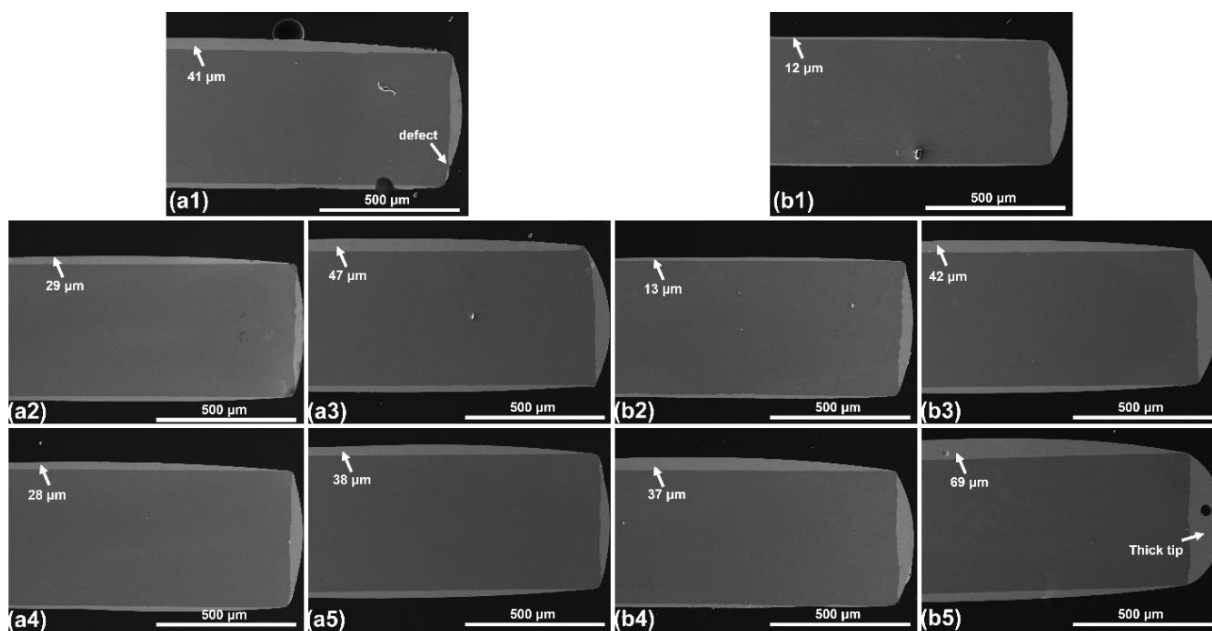
Figure 7.4 *Secondary electron micrograph of the SAC 305 coated Cu substrates in the view of cross section after wetting balance testing: (a1) A, (a2) AT02, (a3) AT04, (a4) AN02, (a5) AN04, (b1) S, (b2) ST02, (b3) ST04, (b4) SN02, (b5) SN04.*

Evaluation of structural degradation of flux activator packages after thermal activation

Figure 7.5 illustrates the effect of simulated soldering temperature on the thermal degradation of the tested flux activator packages. Generally, the amide formation was detected in model fluxes with succinic acid activators as shown in **Figure 7.5**(c); while none of the amide peak was detected in the model fluxes with adipic acid as activators as shown in **Figure 7.5**(a). After adding

amine additive in model flux with succinic acid activator as shown in **Figure 7.5**(c), the C=O bond at 1685 cm^{-1} split into two peaks which located at 1685 cm^{-1} and 1725 cm^{-1}. The C=O stretching bond at 1685 cm^{-1} belongs to carboxylic acid, while the C=O stretching peak at 1725 cm^{-1} belongs to the newly formed amide. The peak of C-N stretching bond in amide group was detected at 1106 cm^{-1}. **Figure 7.5**(d) shows the degradation of the amide in the model flux with succinic acid activator occurred after thermal activation at 240℃. The carboxylic acid C=O stretching bond still presented at 1685 cm^{-1} for pure succinic acid model flux. In the amine additive contained succinic acid fluxes, the amide C=O stretching bond at 1725 cm^{-1} disappeared and the peak of carboxylic C=O stretching bond shifted to left in a range between 1692-1696 cm^{-1}. After thermal activation, no significant difference was observed in the spectra of adipic acid based model fluxes in comparison with the non-thermal activated one, as shown in **Figure 7.5**(a)(b).
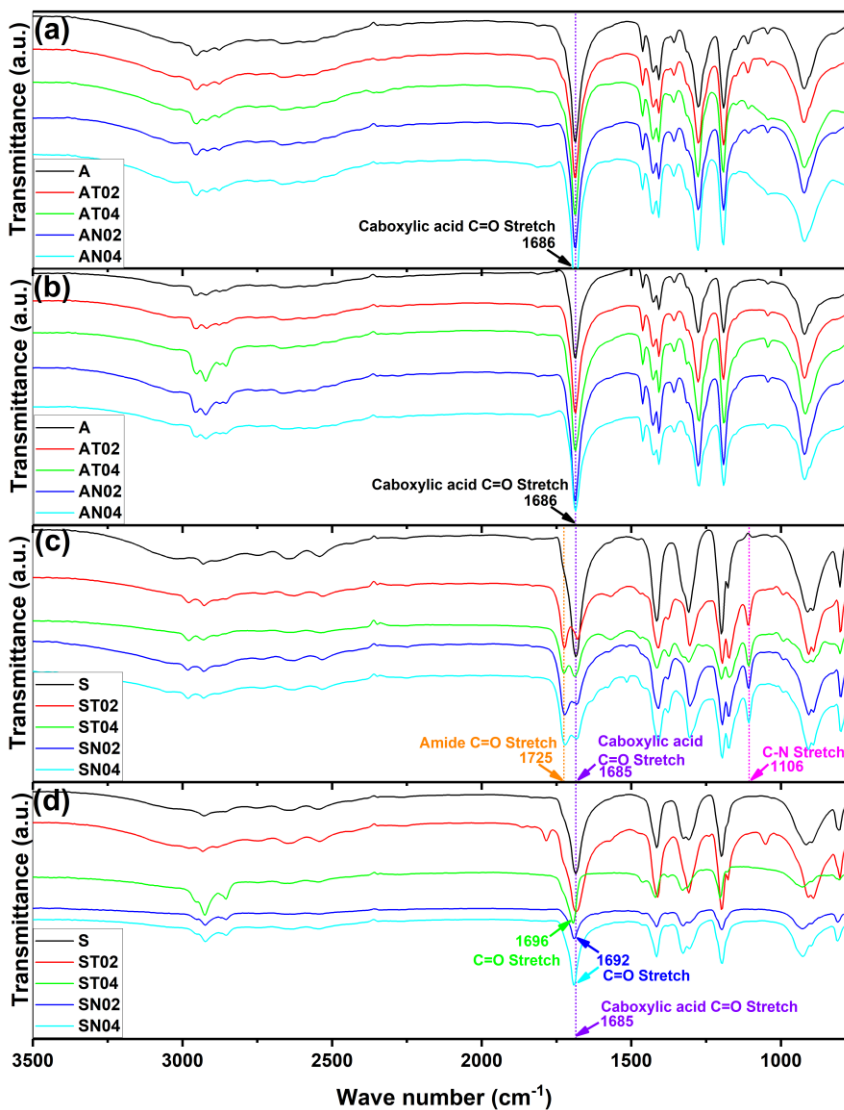
Figure 7.5 *The FT-IR spectra of tested flux activators with/without thermal treatment: (a) adipic acid contained activator packages with no thermal activation, (b) adipic acid contained activator packages after thermal treatment at 240℃ for 100 sec, (c) succinic acid contained activator packages with no thermal activation, (d) succinic acid contained activator packages after thermal treatment at 240℃ for 100 sec.*

Electrochemical investigation of model fluxes

a) Deliquescence assessment of model fluxes using single frequency EIS
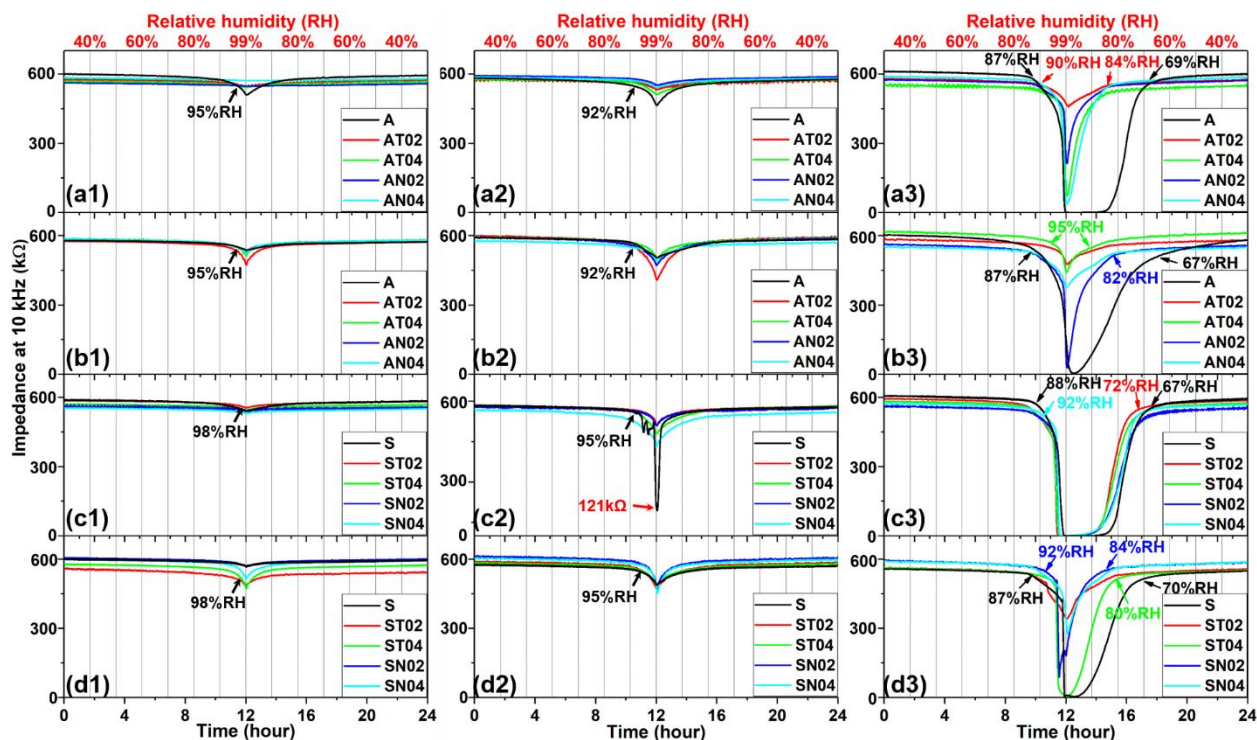
Figure 7.6 *Impedance response at 10 kHz of SIR pattern contaminated with: (a) non-thermal activated adipic acid model fluxes, (b) 240℃ activated adipic acid model fluxes, (c) non-thermal activated succinic acid model fluxes, (d) 240℃ activated succinic acid model fluxes; under testing temperature of (1) 25℃, (2) 40℃, (3) 60℃.*

Figure 7.6 demonstrates the impedance response of model fluxes contaminated SIR patterns tested under various climatic condition. In general, the reduction of DRH was obtained for all tested model flux activators when increasing the testing temperature from 25℃ to 60℃. Under testing temperature of 25℃, DRH value of all the tested activator package was beyond 95% RH, and impedance response at 99% RH for all the activator packages was maintained above 500 kΩ. Under testing temperature of 40℃, significant drop of impedance was obtained by non-thermal activated pure succinic acid contaminated SIR pattern as shown in **Figure 7.6**(c2). In contrast, the non-thermal activated amine additive contained succinic acid fluxes exhibited high impedance level above 450 kΩ under 99% RH. After thermal activation at 240℃ (**Figure 7.6**(d2)), the high level of impedance was obtained again by pure succinic acid activator contaminated SIR pattern under 99% RH. **Figure 7.6**(a3)(b3)(c3)(d3) shows that the DRH values of pure adipic acid and pure succinic acid fluxes are within 87-88% RH under the testing temperature of 60℃, which were higher than ERH value obtained between 67-70% RH. In the non-thermal activated adipic

acid contained model fluxes shown In **Figure 7.6**(a3), amine additives slightly improved the DRH and ERH value of activator packages to 90% RH and 84% RH respectively. Compared to the pure adipic acid sample, amine additives significantly improved the impedance response of adipic acid fluxes at 99% RH. However, amine additives did not influence the impedance response of the non-thermal activated succinic acid fluxes under 99% RH exposure, as shown in **Figure 7.6**(c3). Under testing temperature of 60℃, significant improvement of the ERH value and the impedance response at 99% RH was obtained by fluxes with amine additives after thermal activation at 240℃, as shown in **Figure 7.6**(b3)(d3).

b) <u>Leakage current for model fluxes under humidity exposure</u>

Figure 7.7 shows the leakage current response of model flux activator contaminated SIR pattern under various climatic testing conditions. In general, leakage current value increased for all tested model flux residues with increasing RH for testing. Under the same testing condition, **Figure 7.7**(b1-b3) indicates that the thermal-activated adipic acid contained model fluxes contaminated SIR patterns exhibited the same leakage current values as no thermal activated sample shown in **Figure 7.7**(a1-a3). High leakage current exceeding 10 μA occurred at 98% RH/60℃ for all five adipic acid model fluxes contaminated SIR patterns (shown in **Figure 7.7**(a3)(b3)). **Figure 7.7**(a1-a3) demonstrates the amine additives did not influence the leakage current level of model fluxes with adipic acid activators under same testing condition. However, thermal activation significantly influenced the leakage current level of succinic acid contained model fluxes in different ways. Under testing temperature of 25℃, thermal activated pure succinic acid induced high leakage current failure at 98% RH, whereas the leakage current level of none thermal activated pure succinic acid was below 1 μA. Under testing temperature of 40℃, compared to the high leakage current failure of SIR pattern induced by all five non-thermal activated succinic acid fluxes shown in **Figure 7.7**(c2), thermal activation at 240℃ for amine modified succinic acid model fluxes suppressed the leakage current level SIR pattern under 98% RH exposure (**Figure 7.7**(d2)).
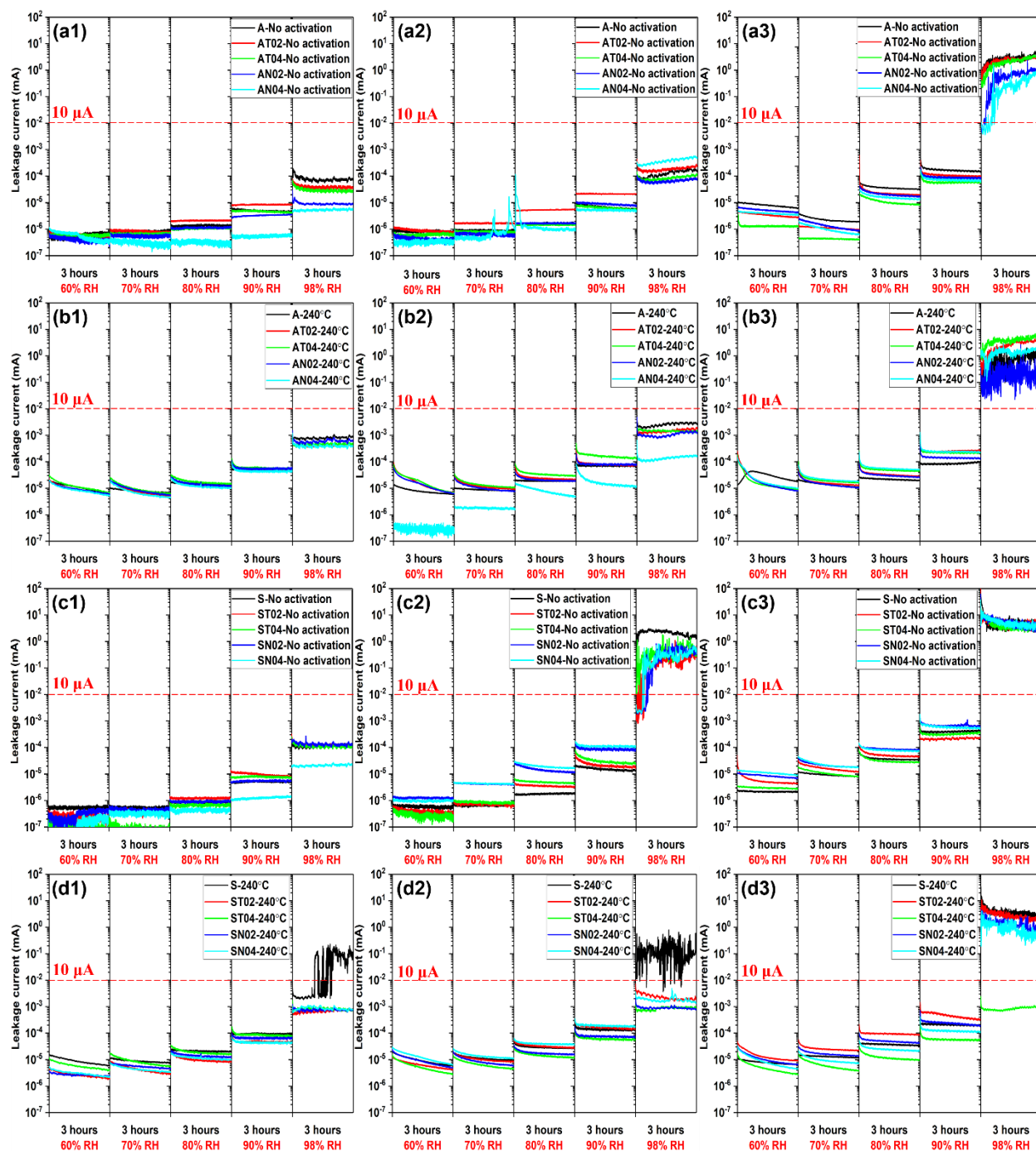
Figure 7.7 *Leakage current results of the model fluxes contaminated SIR pattern under various testing condition: (a) non-thermal activated adipic acid model fluxes, (b) 240℃ activated adipic acid model fluxes, (c) non-thermal activated succinic acid model fluxes, (d) 240℃ activated succinic acid model fluxes; under testing temperature of (1) 25℃, (2) 40℃, (3) 60℃.*

IV.   DISCUSSION

Present investigation demonstrates the effect of tripropylamine and naphthylamine additives on the solderability and climatic reiliability of commercial used WOA activator residue on PCBA after simulated wave soldering condition. The Cu oxide removal mechanism using WOA activators was achieved through the complexation (**Equation 7.1**) and disproportionation (**Equation 7.2**) reactions [26], where the R in carboxylic acid represents as an organic radical [33].

$$CuO + 2RCOOH = Cu(RCOO)_2 + H_2O \quad \textbf{Equation 7.1}$$

$$Cu_2O + 2RCOOH = Cu(RCOO)_2 + Cu + H_2O \quad \textbf{Equation 7.2}$$

The succinic acid with shorter organic carbon chain shows high polarity and lower pKa values in comparison with adipic acid, as shown in **Table 7.1**. From the solderability point view, result in **Table 7.3** demonstrates that the succinic acid possessed higher maximum wetting force value compared to adipic acid. However, the higher ionization strength of succinic acid also lead to higher leakage current [6] and ECM failure [20] under humidity exposure with 10 V DC bias loading, while the leakage current value induced by adipic acid was located in the safety range below 10 µA under 25℃ and 40℃ [20]. Present study exhibited the improvement of the leakage current performance and the wetting speed of succinic acid model flux after addition of tripropylamine. On the other hand, after addition of 0.4 wt.% tripropylamine in adipic acid model flux, the F_{max} and wetting speed of AT04 flux was improved in comparison with pure adipic acid and pure succinic acid model fluxes. At the same time, the leakage current value of the tripropylamine additive modified adipic acid model fluxes maintained at safe level below 10 µA as pure adipic acid model flux, as shown in **Figure 7.7**(b1-b3).

Influence of amine additives in WOA model fluxes on the performance of solderability

Tripropylamine and naphthylamine additives exhibit different influences on the wetting properties of adipic acid and succnic acid based fluxes. Reaction between WOA and amine can be consider as Brønsted–Lowry acid base reaction shown in **Equation 7.3**, where R' and R'' represent organic radicals.

$$R'COOH + R''NH_2 = R' - CO(NH) - R'' + H_2O \quad \textbf{Equation 7.3}$$
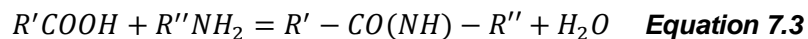
In the case of succinic acid based model fluxes, significant improvement of the wetting speed was obtained by the tripropylamine and naphthylamine modified flux formulation as shown in **Table 7.3**; however, the maximum wetting forces of all the amine modified fluxes did not exceed the pure succinic acid model flux. The wetting speed and F_{max} were influenced by the oxides removal

mechanism of amine modified succinic acid based fluxes. **Figure 7.5**(c)(d) demonstrates C=O stretching bond at 1725 cm^{-1} and C-N stretching bond at 1106 cm^{-1} for amide disappeared after simulated wave soldering process at 240℃. The degradation of amide triggered the formation of the more reactive positive charge group $(R'CO)^+$ and negative charge group $(R''NH)^-$ at the initial thermal activation stage during soldering process as demonstration in **Equation 7.4**. The oxides removal reaction between CuO and the degradation product of amide was demonstrated as **Equation 7.5**. In comparison with relative higher T_0 and $T_{2/3}$ values obtained by pure succinic acid fluxes, the faster wetting speed of amine additive modified succinic fluxes could be due to the reaction between CuO and the more reactive $(R'CO)^+$ as well as $(R''NH)^-$ charge groups during soldering process. As a result, the localized spreading appearance was obtained using amine modified succinic acid fluxes, as shown in **Figure 7.2**(b2-5). After simulated soldering process, the shift of the carboxylic acid C=O stretching bond for ST04, SN02 and SN04 model fluxes in **Figure 7.5**(d) indicates active carboxylic group of succinic acid was consumed by amine additives to form amide, which reduced the number of carboxylic group in participation of the oxide removal during soldering process. In consequence, the reduction of F_{max} was more pronounced for the 0.4 wt.% amine additive modified succinic based model fluxes shown **Table 7.3**, and the thicker layer of SAC 305 alloy was observed on Cu substrate compared to pure succinic acid flux (**Figure 7.4**(b1)(b3)). Significant reduction of F_{max} was obtained by naththylamine modified succinic acid. This could be attributed to the covalent π bond of benzene ring in naphthylamine re-allocated the electron density in amide molecule, hence reduced the polarity of the carboxylic group. Therefore, the activation of the carboxylic group in the amide formed by naphthylamine and succinic acid was prohibited during soldering process, which triggered thicker layer of the SAC 305 alloy coated on the Cu substrate as shown in **Figure 7.4**(b4)(b5).

$$R' - CO(NH) - R'' = (R'CO)^+ + (R''NH)^- \quad \textbf{\textit{Equation 7.4}}$$

$$2(R'CO)^+ + 2(R''NH)^- + 4CuO = Cu(R'COO)_2 + 3Cu + R''_2O + N_2 + H_2O \quad \textbf{\textit{Equation 7.5}}$$
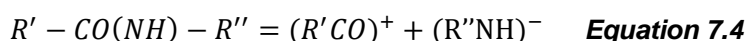
However, amide bond was not detected in the flux formulation with amine additive and adipic acid, as shown in **Figure 7.5**(a). Therefore, the oxide removal reaction by adipic acid and amine additives were subjected in parallel during soldering process. Apart from the oxide removal process of by adipic acid, the increase of F_{max} for tripropylamine modified adipic acid based flux was attributed to the redox reaction between tripropylamine and CuO during soldering process, which is demonstrated in **Equation 7.6**. As result, larger spreading area of the SAC 305 alloy was obtained by AT02 and AT04 in comparison with pure adipic acid flux, shown in **Figure 7.2**(a1-3). Compared to tripropylamine modified adipic acid fluxes, significant increase of T_0 and $T_{2/3}$ values

was obtained using naphthylamine additive in adipic acid model fluxes, shown in **Table 7.3**. The covalent π bond in naphthylamine additive may prohibit the activity of carboxyl group in adipic acid, which required more energy and longer time for the complexation reaction to take palce between carboxylic groups in adipic acid and the oxides on the metal surface. In consequence, 0.4 wt.% naphthylamine additive modified adipic acid flux (AN04) required longer time to reach to maximum wetting force in comparison with 0.2 wt.% naphthylamine modified adipic acid flux (AN02). Therefore, the increasing trend of wetting force for AN04 was still visible at 10 sec asshown in **Figure 7.3**(a).

$$3CuO + 2R''NH_2 = 2Cu + R_2O + N_2 + H_2O \quad \textit{Equation 7.6}$$
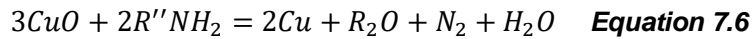
Influence of amine additives on the humidity interaction and leakage current response

Humidity interaction of the WOA activator residue on PCBA was dependent upon the hygroscopicity of the WOA or its degradation products after soldering process, which triggered the moisture adsorption and absorption from the environment [6]. The hygroscopicity of the flux residue on SIR interdigitated pattern was roughly estimated by single frequency EIS measurement in previous work [20][27][32]. **Table 7.4** shows the DRH value of adipic acid and succinic acid from the literature under testing temperature of 25℃, 40℃ and 60℃ respectively, which were comparable with the single frequency EIS measured DRH values for the tested WOAs in the present work. After water condensation triggered by WOA at lower RH value, the solubility of WOA and dissociation constant of carboxyl groups played the key role on the conductivity and corrosivity of the electrolyte formed on the surface of PCBA. Under testing temperature of 25℃, low solubility for adipic acid (0.17 mol/L) and succinic acid (0.69 mol/L) resulted in high impedance response of pure WOA contaminated SIR pattern under 99% RH exposure, as shown in **Figure 7.6**(a1)(c1). As a consequence, low leakage current was observed due to less ionization of WOA on the surface of PCBA (**Figure 7.7**(a1)(c1)). When the testing temperature increased to 40℃, the drop of impedance for pure succinic acid model flux contaminated SIR pattern shown in **Figure 7.6**(c2) was attributed to the much higher solubility of 1.16 mol/L in comparison with 0.33 mol/L for adipic acid. As a result, the leakage current of succinic acid comtaminated SIR pattern exceeded 10 μA under 98% RH/40℃ (**Figure 7.7**(a1)), while the leakage current level of adipic acid contaminated SIR pattern remained at safety range (**Figure 7.7**(c1)). Solubility of adipic acid and succinic acid significantly increased under testing temperature 60℃, which resulted the reduction of impedance (**Figure 7.6**(a3)(c3)) and high leakage current exceeding safety range (**Figure 7.7**(a3)(c3)). Since the WOA induced failures were more pronounced at high testing temperature and high RH, the influences of amine additives on the humidity interaction of WOA

activators would be more representative under the testing temperature of 60℃ for adipic acid based flux, and above 40℃ for succinic acid based flux, as shown in **Figure 7.7**(b3)(d3).

Table 7.4 *Summary of DRH values [20], and solubility [34] of tested WOA in literature with measured DRH in present work.*

	DRH in literature / Measured DRH(% RH)			Solubility (mol/L)		
Temperature	25°C	40°C	60°C	25°C	40°C	60°C
Adipic acid	97.4 / 95	91.5 / 92	83.2 / 87	0.17	0.33	1.05
Succinic acid	94.2 / 98	91.3 / 95	82.2 / 88	0.69	1.16	2.22

The role of the amine additives played in succinic acid based fluxes and adipic acid based fluxes were different, which resulted different performances of humidity interaction under testing temperature of 60℃. FT-IR result in **Figure 7.5**(a) shows the independent presence of the adipic acid and amine additive in flux residue. The ionization of the adipic acid and the protonation of amine additive simultaneously occurred in the condensed water. As result, intermolecular hydrogen bond formed by dipole-dipole interaction between carboxylic group and amino group [35] as shown in **Equation 7.7**. The intermolecular hydrogen bond formed between adipic acid and amine additive could re-distribute the electron density of the polarized carboxyl group and amino group, which might reduce the polarity of adipic acid. Therefore, ERH of amine modified adipic acid flux shown in **Figure 7.6**(a3) significantly increased to 84% RH in comparison with 69% RH obtained by pure adipic acid at 60℃. Moreover, the Van der Waals force of intermolecular hydrogen bond between adipic acid and amine additives might reduce the number of the free ions in the electrolyte. Therefore, the impedance response of amine modified adipic acid is much better than pure adipic acid as shown in **Figure 7.6**(a3). While for succinic acid based model fluxes with amine additives, amide formation was confirmed by FT-IR analysis, as shown in **Figure 7.5**(c). Amide group appeared to be polar since oxygen and nitrogen can form hydrogen bond with water in atmosphere [36]. Therefore, minimal improvement of DRH and ERH was obtained by the amine additive modified succinic acid fluxes, as shown in **Figure 7.6**(c3).

$$R'COOH + R''NH_2 = R'COOH \cdots NH_2R'' \qquad \textbf{\textit{Equation 7.7}}$$

Thermal activation played a vital role on the humidity robustness of the amine modified model fluxes. In the case of adipic acid based fluxes, the DRH and ERH value of tripropylamine additive modified fluxes increased from 90% RH and 84% RH to 95% RH and 95% RH after thermal activation, which might be attributed to the thermal degradation product of tripropylamine. However, the mechanism required further chemical analysis. In comparison, the soldering

temperature of 240℃ is not able to evaporate or degrade naphthylamine due to its higher boiling temperature at 300.8℃. As result, the DRH and ERH value of naphtylamine modified fluxes did not change after thermal activation. For the succinic acid based fluxes, significant improvement of ERH was obtained after thermal activation, which is due to the thermal degradation of the amide, as shown in **Figure 7.5**(d). The carboxylic acid C=O stretching peak at 1685 cm^{-1} shifted towards amide C=O stretching peak after thermal activation, which indicates the presence of limited amount of amide group in flux residue. After thermal activation, the 0.4 wt.% tripropylamine modified succinic acid flux (ST04) obtained the largest shift C=O stretching peak, as shown in **Figure 7.5**(d). In consequence, moisture desorption behavior of ST04 is slightly worse compared to naphthylamine modified succinic acid fluxes (**Figure 7.6**(d3)). Under 10 V DC bias loading, the degradation of amide reduced the polarity of the flux reside and coherently triggered the lower moisture absorption under testing condition of 98% RH/40℃, which lead to the significant reduction of the leakage current response shown in **Figure 7.7**(d2).

V.   CONCLUSIONS

- FT-IR results indicate both tripropylamine and naphthylamine are able to form amides with succinic acids after flux formulation, while the adipic acid and amine additives did not. Thermal degradation of the amide C=O stretching bond was detected in the amine additive modified succinic acid based fluxes.

- Solderability testing showed improvement of the wetting speed using tripropylamine and naphthylamine additive in succinic acid based model fluxes, however, the maximum wetting force was reduced by tripropylamine and naphthylamine additive. The 0.2-0.4 wt.% tripropylamine additive in adipic acid based model fluxes significantly increased the maximum wetting force.

- Single frequency EIS results show the tripropylamine and naphthylamine additives in adipic acid based model fluxes significantly increased the ERH and DRH in comparison with pure adipic acid flux under testing temperature of 60℃. Thermal activation at 240℃ significantly increased ERH of two amine additives modified succinic acid based fluxes and adipic acid based fluxes.

- Leakage current testing results indicate the tripropylamine and naphthylamine additive in succinic acid model fluxes significantly decreased the leakage current level below threshold value of 10 μA under testing condition of 98% RH/25℃ and 98% RH/40℃ after simulated soldering process.

VI.   REFERENCES

[1]   B. N. Ellis, Contamination Control and the Montreal Protocol, Circuit World. 15 (1989) 43–46. doi:10.1108/eb043988.

[2]   S. Menon, E. George, M. Osterman, M. Pecht, High lead solder (over 85 %) solder in the electronics industry: RoHS exemptions and alternatives, J. Mater. Sci. Mater. Electron. 26 (2015) 4021–4030. doi:10.1007/s10854-015-2940-4.

[3]   B.A. Smith, L.J. Turbini, Characterizing the weak organic acids used in low solids fluxes, J. Electron. Mater. 28 (1999) 1299–1306. doi:10.1007/s11664-999-0171-2.

[4]   K.N. Subramanian, Lead-free electronic solders: A special issue of the journal of materials science: Materials in electronics, 2007. doi:10.1007/978-0-387-48433-4.

[5]   E. Bastow, The Effect of Reflow Profiling on the Electrical Reliability of No-Clean Solder Paste Flux Residues, in: IPC APEX EXPO Proc., Las Vegas, 2014.

[6]   V. Verdingovas, M.S. Jellesen, R. Ambat, Solder Flux Residues and Humidity-Related Failures in Electronics: Relative Effects of Weak Organic Acids Used in No-Clean Flux Systems, J. Electron. Mater. 44 (2015) 1116–1127. doi:10.1007/s11664-014-3609-0.

[7]   H. M.R., V. J.H., S. H.A.H., Lead-free reflow soldering for electronics assembly, Solder. Surf. Mt. Technol. 13 (2001) 21–38. doi:10.1108/09540910110407388.

[8]   P. Jianbiao, T.B. J., C. Tzu-Chien, D.W. J., The effect of reflow profile on SnPb and SnAgCu solder joint shear strength, Solder. Surf. Mt. Technol. 18 (2006) 48–56. doi:10.1108/09540910610717901.

[9]   K.S. Hansen, M.S. Jellesen, P. Moller, P.J.S. Westermann, R. Ambat, Effect of solder flux residues on corrosion of electronics, in: 2009 Annu. Reliab. Maintainab. Symp., 2009: pp. 502–508. doi:10.1109/RAMS.2009.4914727.

[10]   C. Helene, S.J. Morten, A. Rajan, Contamination profile on typical printed circuit board assemblies vs soldering process, Solder. Surf. Mt. Technol. 26 (2014) 194–202. doi:10.1108/SSMT-03-2014-0007.

[11]   P. Isaacs, T. Munson, What makes no-clean flux residue benign?, in: 2016 Pan Pacific Microelectron. Symp. (Pan Pacific), 2016: pp. 1–7. doi:10.1109/PanPacific.2016.7428404.

[12]   S. Zhan, M.H. Azarian, M.G. Pecht, Surface Insulation Resistance of Conformally Coated Printed Circuit Boards Processed With No-Clean Flux, IEEE Trans. Electron. Packag. Manuf. 29 (2006) 217–223. doi:10.1109/TEPM.2006.882496.

[13]   V. Vadimas, J. Salil, J.M. Stendahl, A. Rajan, Analysis of surface insulation resistance related failures in electronics by circuit simulation, Circuit World. 43 (2017) 45–55. doi:10.1108/CW-09-2016-0040.

[14]   P.-E. Tegehall, Impact of Humidity and Contamination on Surface Insulation Resistance and Electrochemical Migration, in: G. Grossmann, C. Zardini (Eds.), ELFNET B. Fail. Mech. Test. Methods, Qual. Issues Lead-Free Solder Interconnects, Springer London, London, 2011: pp. 227–253. doi:10.1007/978-0-85729-236-0_10.

[15]   V. Verdingovas, M.S. Jellesen, R. Ambat, Influence of sodium chloride and weak organic acids (flux residues) on electrochemical migration of tin on surface mount chip components, Corros. Eng. Sci. Technol. 48 (2013) 426–435. doi:10.1179/1743278213Y.0000000078.

[16] S. Joshy, V. Verdingovas, M.S. Jellesen, R. Ambat, Circuit analysis to predict humidity related failures in electronics - Methodology and recommendations, Microelectron. Reliab. 93 (2019) 81–88. doi:https://doi.org/10.1016/j.microrel.2018.12.010.

[17] P. Isaacs, T. Munson, Cleanliness Requirements: A Moving Target, in: 2019 Pan Pacific Microelectron. Symp. (Pan Pacific), 2019: pp. 1–10. doi:10.23919/PanPacific.2019.8696733.

[18] D. Minzari, F.B. Grumsen, M.S. Jellesen, P. Møller, R. Ambat, Electrochemical migration of tin in electronics and microstructure of the dendrites, Corros. Sci. 53 (2011) 1659–1669. doi:10.1016/J.CORSCI.2011.01.009.

[19] V.A. Online, X. Zhong, L. Chen, Z. Zhang, S. Gao, Electrochemical migration of Sn and Sn solder alloys : a review, RSC Adv. Soc. Chem. 7 (2017) 28186–28206. doi:10.1039/c7ra04368f.

[20] K. Piotrowska, R. Ud Din, F.B. Grumsen, M.S. Jellesen, R. Ambat, Parametric Study of Solder Flux Hygroscopicity: Impact of Weak Organic Acids on Water Layer Formation and Corrosion of Electronics, J. Electron. Mater. 47 (2018) 4190–4207. doi:10.1007/s11664-018-6311-9.

[21] K. Piotrowska, R. Ambat, Residue-Assisted Water Layer Build-Up Under Transient Climatic Conditions and Failure Occurrences in Electronics, IEEE Trans. Components, Packag. Manuf. Technol. 10 (2020) 1617–1635. doi:10.1109/TCPMT.2020.3005933.

[22] D. Minzari, M.S. Jellesen, P. Møller, R. Ambat, On the electrochemical migration mechanism of tin in electronics, Corros. Sci. 53 (2011) 3366–3379. doi:10.1016/J.CORSCI.2011.06.015.

[23] V. Verdingovas, M.S. Jellesen, R. Ambat, Relative effect of solder flux chemistry on the humidity related failures in electronics, Solder. Surf. Mt. Technol. 27 (2015) 146–156. doi:10.1108/SSMT-11-2014-0022.

[24] F. Li, K. Piotrowska, M.S. Jellesen, R. Ambat, Alkanolamines as activators in no-clean flux systems: investigation of humidity robustness and solderability, J. Mater. Sci. Mater. Electron. (2021). doi:10.1007/s10854-020-05235-0.

[25] B. Tolla, D. Jean, H. Bhavsar, Y. Shi, X. Wei, Reactivity of No-clean flux residues in electronic assemblies: a systematic study, in: SMTA Int., Rosemont, IL, USA, 2015.

[26] M. Bixenman, D. Lober, A. Ailworth, K. Corporation, B. Tolla, D. Ph, J. Allen, D. Jean, K. Loomis, K. Corporation, Electrochemical Methods to Measure the Corrosion Potential of Flux Residues, in: IPC APEX EXPO, SMTNET, San Diego, USA, 2017.

[27] K. Piotrowska, V. Verdingovas, R. Ambat, Humidity-related failures in electronics: effect of binary mixtures of weak organic acid activators, J. Mater. Sci. Mater. Electron. 29 (2018) 17834–17852. doi:10.1007/s10854-018-9896-0.

[28] D. Xu, X. Li, C. Wang, B. Xu, Study on wettability and corrosivity of a new no-clean flux for lead-free solder paste in electronic packaging technology, in: 2011 Second Int. Conf. Mech. Autom. Control Eng., 2011: pp. 1706–1708. doi:10.1109/MACE.2011.5987285.

[29] Y. Shi, X. Wei, B. Tolla, The Role of Organic Amines in Soldering Materials, in: IPC APEX EXPO Conf. Proc., Circuit Insight, San Diego, USA, 2015.

[30] L. D'Angelo, V. Verdingovas, L. Ferrero, E. Bolzacchini, R. Ambat, On the Effects of

Atmospheric Particles Contamination and Humidity on Tin Corrosion, IEEE Trans. Device Mater. Reliab. 17 (2017) 746–757. doi:10.1109/TDMR.2017.2771505.

[31] S. Lauser, T. Richter, V. Vadimas, R. Ambat, Electrochemical Impedance Spectroscopy (EIS) for Monitoring the Water Load on PCBAs Under Cycling Condensing Conditions to Predict Electrochemical Migration Under DC Loads, in: 2019 IEEE 69th Electron. Components Technol. Conf., 2019: pp. 515–521. doi:10.1109/ECTC.2019.00084.

[32] K. Piotrowska, M. Grzelak, R. Ambat, No-Clean Solder Flux Chemistry and Temperature Effects on Humidity-Related Reliability of Electronics, J. Electron. Mater. 48 (2019) 1207–1222. doi:10.1007/s11664-018-06862-4.

[33] B.A. Smith, L.J. Turbini, Characterizing the weak organic acids used in low solids fluxes, J. Electron. Mater. 28 (1999) 1299–1306. doi:10.1007/s11664-999-0171-2.

[34] A. Apelblat, E. Manzurola, Solubility of oxalic, malonic, succinic, adipic, maleic, malic, citric, and tartaric acids in water from 278.15 to 338.15 K, J. Chem. Thermodyn. 19 (1987) 317–320. doi:https://doi.org/10.1016/0021-9614(87)90139-X.

[35] Y.K. Hong, W.H. Hong, D.H. Han, Application of reactive extraction to recovery of carboxylic acids, Biotechnol. Bioprocess Eng. 6 (2001) 386–394. doi:10.1007/BF02932319.

[36] O.D. Bonner, S.C. Young, Water—amide interaction, Spectrochim. Acta Part A Mol. Spectrosc. 31 (1975) 1975–1979. doi:https://doi.org/10.1016/0584-8539(75)80255-8.

8. Effect of reflow process related flux residue on the climatic reliability of surface-mount electronic devices

Feng Li, Anish Rao Lakkaraju, Morten Stendahl Jellesen, Rajan Ambat

Abstract: This paper investigated the effect reflow flux residue on the humidity related failure of electronic devices by experimentally simulating the surface mount component soldering process, residue trapping, and its behavior under humidity. Standardized accelerated climatic test on surface insulation resistance (SIR) interdigitated pattern was performed to benchmark the humidity interaction of the tested flux formulations. The influence of stand-off height for the surface-mount component on the humidity robustness was analyzed using an in-house designed dummy test rig and electrochemical impedance spectroscopy (EIS). Scanning electron microscopy (SEM) and conductivity measurement was used to understand the hydrolytic degradation of the flux residue and the release of the conductive ionic residues during climatic exposure. Results indicate the spreading area and the hydrolytic degradation behavior of the flux residue were influenced by the type of flux activators used in flux formulation. The climatic reliability was influenced by the combined effect of the aggressiveness of flux activator and the spreading of the flux residue. However, result also shows that the climatic reliability of the surface-mount device can be improved by increasing the stand-off height of the components together with selected flux formulation.

Keywords: SMT, BGA, solder flux, electronic corrosion, climatic reliability.

I.   INTRODUCTION

Driven by the continuous trend in the miniaturization of electronic devices, surface-mount technology (SMT) was widely implemented in the electronic industry due the compact size with smaller SMT components. SMT market was expected with a compound annual growth rate of 7.46% until 2025 [1], and was estimated to occupy 75% of the electronic production [2]. However, the highly compact system raised the challenge of repair and rework process with high cost due to the difficulty of heat dissipation from smaller area [3]. Moreover, electronic manufacturers may devoted as high as 40% of their time to identify the failures and fixing the problems [4]. In order to save the cost, many companies replaces replace printed circuit board assembly (PCBA) instead of repairing of the dysfunctional PCBAs, which incur high cost.

Corrosion of electronic became a significant issue along with the growing implementation of the miniaturized electronic devices in a variety of humid service environment. During humidity

exposure, the localized corrosion cells are easily formed on miniaturized PCBA due to water condensation between adjacent oppositely biased terminals [5]. Electrochemical migration (ECM) is one of the most severe corrosion related short-circuiting failure mode for electronic device [6], and the failure rate of ECM in electronic devices can be as high as 1-4% [7]. No-clean flux has been occupied 70-80% of electronic industry [7][8] for which no cleaning is involved after the soldering process. Numerous investigations have reported that the soldering condition is not sufficient to completely evaporate or decompose the flux substances [9][10] and significant level of no-clean flux residue was observed on the PCBA surface [9][11][12]. Particularly, the flux activator (linear dicarboxylic acids) in the flux residue was reported as the most aggressive process-related contamination, which accelerates the moisture sorption and corrosion related issues [13][14][15][16]. The hygroscopic nature of flux activators reduce the relative humidity (RH) level for water condensation, and the ionization behavior increased the conductivity of the electrolyte layer [11][14][15] [17][18][19]. In consequence, the process-related flux residue plays a vital role on the corrosion of electronics, which lead to the intermittent failures such as ECM dendrite formation and the reduction of surface insulation resistance (SIR) [5][13][17]. Most of these previous investigations were conducted using no-clean wave solder flux for through-hole technology, however, limited investigations was reported based on the reflow solder flux for SMT assemblies although the ECM failure was reported on SMT component due to no-clean flux residue [7][11].

The no-clean reflow flux residue was reported spreading around or trapping beneath the low stand-off height component on the SMT PCBAs after the reflow soldering process [12][20]. This residue mainly contains a base resin/rosin and activators. The base resin/rosin functions as a carrier and binder for the flux activators on the metal surface [21]. Flux activators used in reflow solder paste include 4 categories, which are organic acids, organic amines, organic halogen compounds, and organic halide salts [22]. During the reflow soldering process, the activator part removes the oxide film on the metal contacts to ensure the solderability of melted solder alloy. After soldering process, the corrosive activator residue can be encapsulated by the film of resin/rosin part and hence to achieve the purpose of "no-clean" from the process related contamination point of view. Nowadays, synthetic resin is widely used in the reflow flux formulation to replace natural rosin due to lower residue attack [22]. Urethane resin, acrylic resin, and styrene-maleic acid resin etc. are the types of the commercial used resin base material for synthetic resin in the reflow flux formulation [21], which can be modified with organic acid such as abietic acid etc. [22] to obtain the function of the conventional natural rosin. It has been reported that the hydrolytic degradation of the abietic acid modified urethane based polymers occurred at glass

transition temperature of 60 - 90 ℃ [23], which is incidentally close to the service conditions of electronics in automotive industry [24] and many other standardized testing methods [14][25][26]. Therefore, the fact is that the encapsulation film of flux residue may degrade and lead to the release of the flux activators due to humidity interaction [27]. As a result, the released flux activator from the encapsulation film triggers the corrosion of solder joints and the reduction of SIR under prolonged high temperature and humid exposure [24][27]. Since the SMT will dominate the miniaturized electronic manufacturing in future, it is important to understand effect of reflow process related flux residue on the humidity robustness of electronics.

This paper systematically investigated the influence of four types of reflow paste flux residues with different flux activators on the climatic reliability of PCBA after SMT processing. Test vehicles used in this work are reflow soldered SIR pattern and an in-house designed dummy test rig imitating an SMT component. The conductivity of reflow flux residues as a function of humidity exposure was measured along with the surface morphology evolution acquired by scanning electron microscopy (SEM). Kinetics of humidity interaction with reflow flux residue was analyzed using electrochemical impedance spectroscopy (EIS). The ECM susceptibility of reflow flux residue was analyzed using chronoamperometry under accelerated climate condition. Effect of stand-off height for the dummy component on PCBA surface was investigated to understand the effect of humidity when the flux residue was trapped imitating the actual condition of an SMT component with different stand-off height.

II.   MATERIALS AND EXPERIMENTAL METHODS

Solder pastes used for the investigation

Table 8.1 Formulation of the solder pastes used for the investigation.

Solder paste (SP)	Resin	WOA	Solvent	Amine	Halogen	Halide	Surfactant	Solder alloy
SP1	✓	2 types	Ester, alcohol				✓	SAC 305
SP2	✓	1 type	Ester, alcohol				✓	SAC 305
SP3	✓	1 type	Ester, alcohol	✓	✓		✓	SAC 305
SP4	✓	2 types	Ester, alcohol			✓	✓	SAC 305

Table 8.1 shows the formulation of the solder pastes used in the present investigation. The amount and type of resin, solvent, surfactant, and alloy in the formulation are the same. Ester and alcohol were used as solvent and SAC 305 alloy was used as solder alloy. For SP1, 2 types of WOAs were used as activator package in the flux formulation. Only 1 type of WOA was used in

SP2. 1 type of WOA, 1 type of amine and 1type of halogen were used as activator package in SP3. Two types of WOAs and 1 type of halide were used as activator package in SP4.

Preparation of test vehicles

Figure 8.1 shows the test vehicles used in the investigation. Before stencil printing, all the test vehicles was cleaned using isopropanol in ultrasonic bath for 5 min and dried in compressed air. **Figure 8.1**(a) shows the SIR interdigitated patterns with 300 μm pitch size and line width (IPC-4201/21). The SIR pattern contains the adjacent pitch lines of 10.8 mm × 41 sets in a testing area of 13 mm × 25 mm. The surface finishing of the SIR substrate is 1 μm chemical vapor deposited Sn on 35 μm Cu conductive track. Before going through reflow soldering process, the stencil with thickness of 200 μm was used for the solder paste printing on SIR pattern. **Figure 8.1**(b) shows the open surface of SMT substrate used for flux residue characterization, which contains 9 solder points with area of 2 mm × 2 mm. The solder area of SMT substrate was printed with 250 μm thick solder paste using stencil. **Figure 8.1**(c)(d) shows the in-house test rig imitating dummy SMT component design and the electrical connection of two adjacent solder joints. Test rigs with 0.5 mm and 1 mm stand-off heights were manufactured for the investigation of stand-off height effect on the humidity robustness. The overlapping area of 2 cm × 2 cm for upper part and bottom part of SMT substrates was used for the testing. Same amount of solder paste was applied on the solder points for test rigs with both 0.5 mm stand-off height and 1 mm stand-off height using 1 mm stencil. The tested solder joints was on the adjacent position with distance of 2 mm, which were electrically connected from the back side of upper and bottom FR-4 substrates.

After stencil printing of solder paste, all the test vehicles were subjected to the reflow process in a Techno HA-06 furnace under air-static condition. During the soldering process, surface temperature of the test vehicles increased from 25℃ to 170℃ within 125 sec, then increased to peak temperature of 248 ℃ within 60 sec, and cooled in the oven for 60 sec.

Climatic exposure for electrochemical testing

In order to analyze the corrosion reliability of four solder pastes, accelerated climatic tests were carried out in an "Espec PL-3KPH" climatic chamber with the tolerance of ± 0.3°C and ± 2.5% relative humidity (RH). The accelerated testing condition was adapted from IEC 60068-2-30 environmental testing standard. The testing was conducted under a cycling temperature between 40°C and 60°C under 98% RH for 120 hours (30 cycles). One cycle of temperature at high RH during the test acts as a duration of a water condensation and evaporation process. Due to the thermal delay, the surface temperature of SIR board was lower than ambient temperature during

1 hour ramping step from 40°C to 60°C, which induced transient water condensation on the surface of SIR pattern.

The dummy SMT components with 2 stand-off heights are exposed in an "Espec PL-3KPH" climatic chamber under constant climatic conditions of 60°C, 98% RH for the study of water interaction kinetic with flux residue.
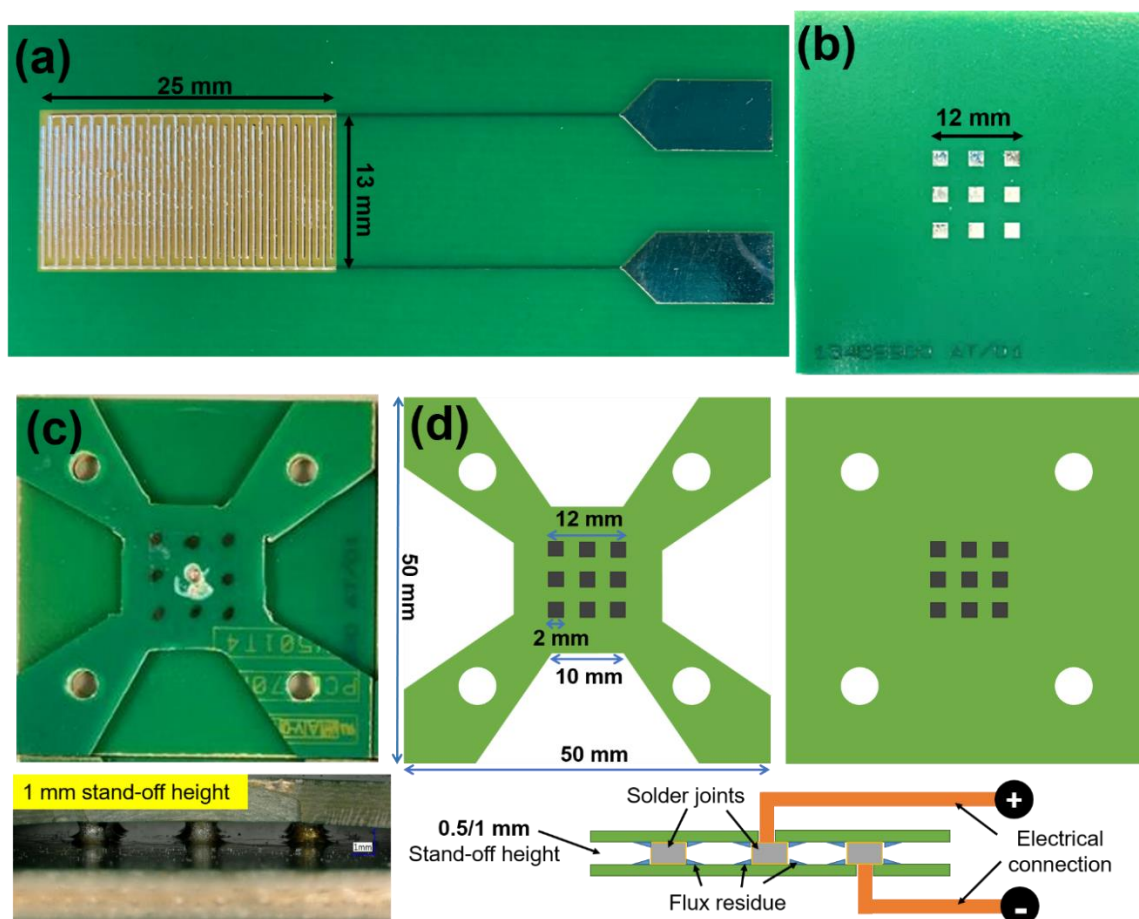
Figure 8.1 *Test vehicles used in the investigation: (a) SIR pattern with interdigitated electrodes used for printing the paste and testing, (b) an open pad imitating SMT land pattern for printing paste and subsequent residue characterization, (c) test rig imitating a dummy SMT component for stand-off height investigation after soldering, (d) schematic of the dummy SMT component in (c) showing bottom and upper part and schematic of the cross-sectional view with electrical connection made for testing.*

Electrochemical testing methods

Under climatic exposure, chronoamperometric technique was used to understand the leakage current induced by the flux residue. A 10 V DC bias was applied to the SIR pattern using a multi-channel potentiostat (Biologic VSP, France) during accelerated climatic testing. The condensed water layer formed between oppositely biased electrodes acted as a media for ion transportation,

which resulted in leakage current and ECM due to electrochemical process. The leakage current was recorded using EC-lab software. After accelerated climatic testing, flux residue and ECM dendrite formation on SIR patterns were inspected using light optical microscopy (LOM) (Keyebce VHX, Japan).

To understand the water interaction kinetic with relow flux residue, EIS experiment was conducted using a "Biologic VSP" potentiostat on the two-electrodes system to investigate effect of humidity exposure on the impedance between adjacent solder joints with different stand-off height. Scanning range of frequency was set from 100 kHz to 100 mHz with the sinusoidal amplitude of 10 mV over the base potential of 0 V vs. reference electrode. EIS scan was recorded every 24 hours by EC-lab and the total duration of the experiment was 15 days. The spreading of flux residue on tested samples was inspected using LOM.

Flux residue morphology changes and activator release during humidity exposure

In order to evaluate the opening up of the residue and release of the activator component from residue during humidity exposure, 3 sets of SMT substrates (test vehicle shown in **Figure** 8.1(b)) reflowed using four solder pastes were used. Samples were exposed in an "Espec PL-3KPH" climatic chamber under 60°C, 98% RH for 5, 10, 15 days respectively. To study the thermal effect during humidity exposure, a set of the reflow soldered SMT substrates was exposed under 60°C, 30% RH. A set of samples without climatic exposure was used as reference. To extract the released conductive substances from the flux residue, 200 µL Millipore water ((Synergy UV, Germany) was applied on one solder joint for 3 min. 3 extraction tests were conducted on one reflow soldered SMT substrate for good statistics. The conductivity of the extracted solution was measured using a SevenCompact S230 conductivity meter (Mettler Toledo, USA).

The surface morphology of the flux residue on the soldered SMT substrate was inspected using a scanning electron microscope (SEM) (FEI Quanta 200 FEG, USA) under secondary electron mode at 3 kV. The spreading of the flux residue was visualized using LOM before and after climatic exposure.

III.   RESULTS

Corrosion reliability of reflow soldered SIR pattern under accelerated climatic condition

Figure 8.2(a) shows leak current resulting from the SIR interdigitated pattern during exposure to cyclic humidity conditions, while **Figure 8.2**(b) shows the total charge transfer between the SIR electrodes deduced from **Figure 8.2**(a) for easy comparison. In general, the peak of the leakage current curve (**Figure 8.2**(a)) during one climatic cycle refer to the water condensation during the

stage of increasing temperature from 40°C to 60°C and the valley of the leakage current curve refer to the water release stage when the testing temperature ramped from 60°C to 40°C. The difference of leakage current level of SP1 and SP2 was minimal under water releasing stage. While under water condensation stage during climatic test, the leakage current level of SP2 reflow soldered SIR pattern is much higher than SP1 reflow soldered SIR pattern, which exceeded the 1 µA. The highest leakage current (LC) value was observed for SP4 soldered SIR pattern as shown in **Figure 8.2**(a), which was observed almost from the beginning of the testing. The SP2 soldered SIR pattern showed second highest LC value, which exceeded 10 µA at the first cycle. For SP1 and SP3 soldered SIR patterns, the maximum LC value was below 1 µA. The charge transfer values shown in **Figure 8.2**(b) match with this exhibiting similar trends. Overall, the ranking from the charge transfer curves over 120 hours for various solder pastes was: SP4 > SP2 > SP1 > SP3.
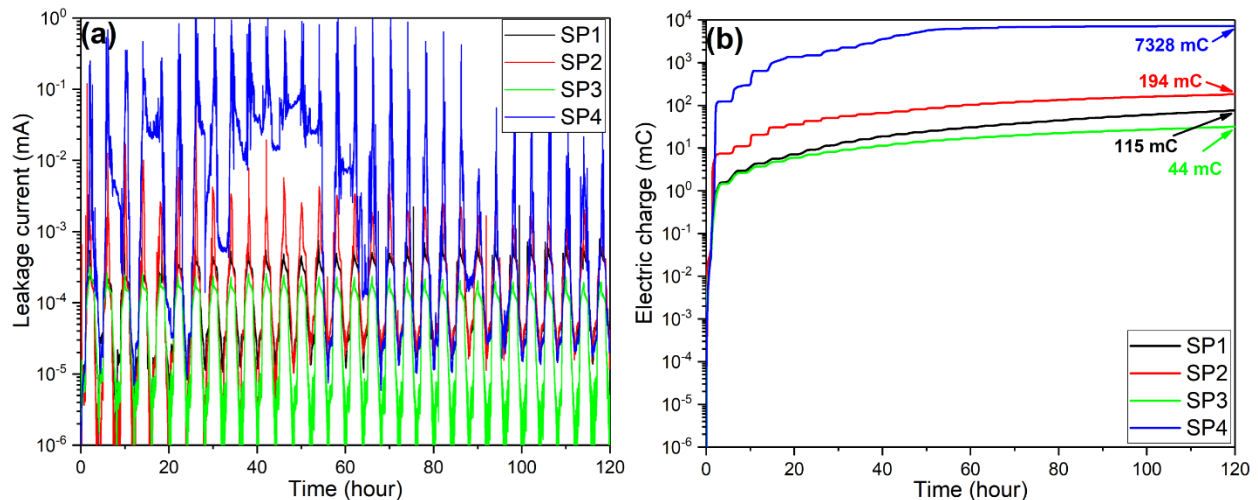
Figure 8.2 *Results of accelerated humidity testing using the reflowed SIR interdigitated pattern: (a) leakage current under 10 V, (b) Charge transferred vs time for various cases in (a).*

Figure 8.3 shows optical micrographs of the SIR test PCB surface after accelerated climatic testing. The variation in the distribution of the flux residue depending of the type of solder activators. More flux residues free area was observed in SP1 soldered SIR pattern, as shown in **Figure 8.3**(a). For SP2 and SP4, the distribution of flux residue was not uniform on the PCBA, which was denoted as "low flux region" and "high flux region" as shown in **Figure 8.3**(b)(d). The flux residue from SP3 uniformly distributed on SIR interdigitated region after soldering process, as shown in **Figure 8.3**(c). ECM dendrite formation was observed on SP4 reflow soldered SIR test board, particularly in the high flux region as shown in **Figure 8.3**(d), whereas no significant corrosion was found for SP1, SP2 and SP3.
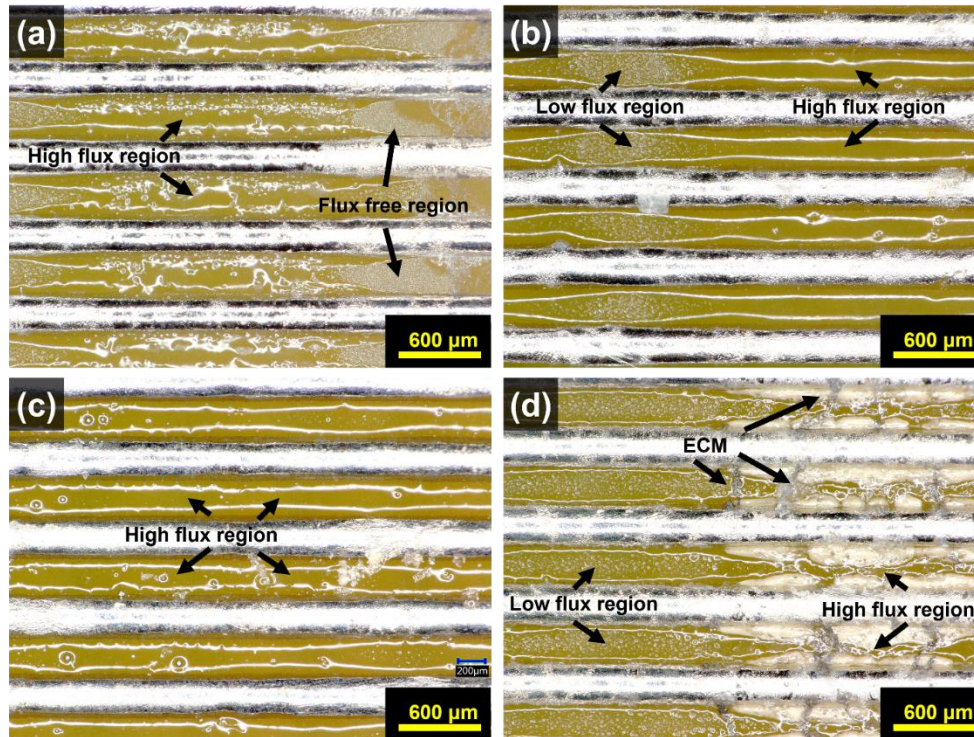
Figure 8.3 *Surface morphology of the SIR interdigitated pattern after cyclic humidity testing: (a) SP1, (b) SP2, (c) SP3, (d) SP4.*

Evolution of flux residue under constant humidity exposure

Figure 8.4 shows the conductivity of the ionic substance released from flux residue after exposing the humidity for different exposure time. After reflow soldering process, conductivity values for the solution extracted from the pads was approximately 5 µS/cm for all four pastes. The conductivity value of the extract for SP4 flux residue increased to 75 µS/cm after 15 days exposure at 60°C, 98% RH. While the conductivity value of SP2 flux residue was at 45 µS/cm, which was the lowest among all 4 types of flux residues. Significant increase of the conductivity value for SP2 was found after first 5 days humidity exposure and maintained similar conductivity level until 15 days. The conductivity values of SP1 and SP3 are in similar level at 60 µS/cm. In comparison, no significant change of the conductivity values for all 4 types of flux residue was found after 15 days exposure under 60°C, however using lower humidity value of 30% RH.

Figure 8.5 shows the spreading effect of the flux residue before and after climatic exposure at 60°C, 98% RH for 15 days. After reflow soldering process, the spreading area of the flux residue on SP2 and SP3 substrates was larger than SP1 and SP4 substrates, as shown in **Figure 8.5**(b1)(c1). After climatic exposure, the spreading area of SP3 substrates significantly increased, as shown in **Figure 8.5**(b3). Whereas for SP1 and SP4 substrate shown in **Figure 8.5**(a2)(d2), the spreading area remained in the same level as before climatic exposure.
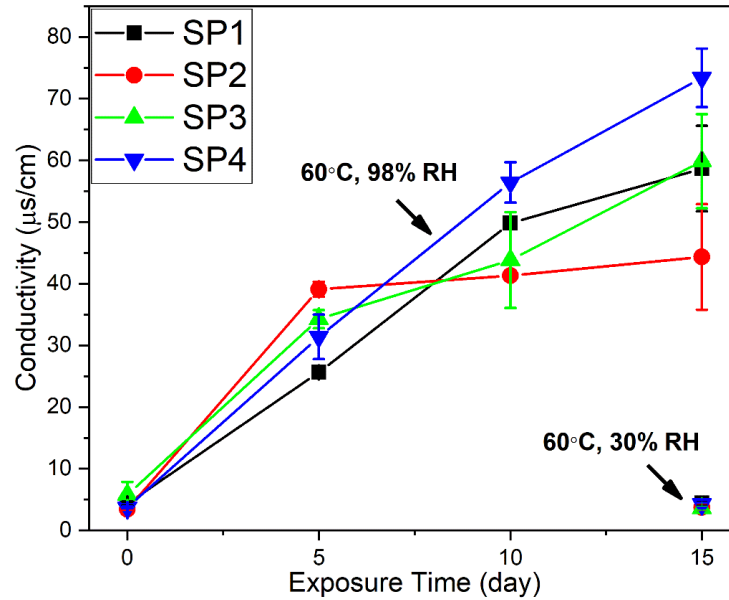
Figure 8.4 *Conductivity measurement of water extracted ionic substance from flux residue after humidity exposure.*
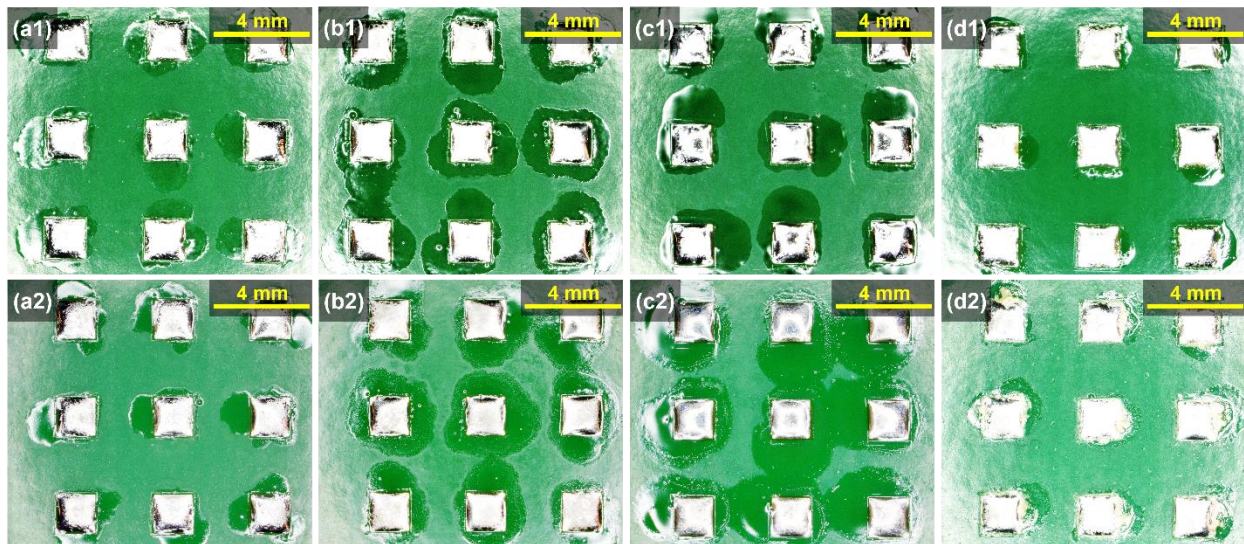
Figure 8.5 *LOM inspection of the flux residue spreading on reflow soldered SMT substrates using 4 types of solder pastes: (a) SP1, (b) SP2, (c) SP3, (d) SP4; (1) non-climatic exposure, (2) exposed at 60°C, 98% RH for 15 days.*

Figure 8.6 shows the surface morphology evolution of 4 types of flux residue during climatic exposure under 60°C, 98% RH. After 5 days exposure, blisters were observed on the flux residue of SP1, SP2 and SP4 as shown in **Figure 8.6**(a2)(b2)(c2). Surface of the SP2 residue did not show significant change until 15 days climatic exposure. After 10 days climatic exposure, openings were observed on the flux residue of SP1 and SP4, as shown in **Figure 8.6**(a3)(d3).

Figure 8.6(a4) and (d4) show the size of the blisters in the flux residue of SP1 and SP4 increased during the climatic exposure; however, **Figure 8.6**(b2)(b3)(b4) show that the change of the surface morphology for the SP2 flux residue was minimal when extending climatic exposure period until 15 days. SP4 showed significantly different morphology after 15 days of exposure compared to SP1 and SP3 with a flowery type of surface morphology different from lower exposure time, while SP2 and SP3 did not show significant change.
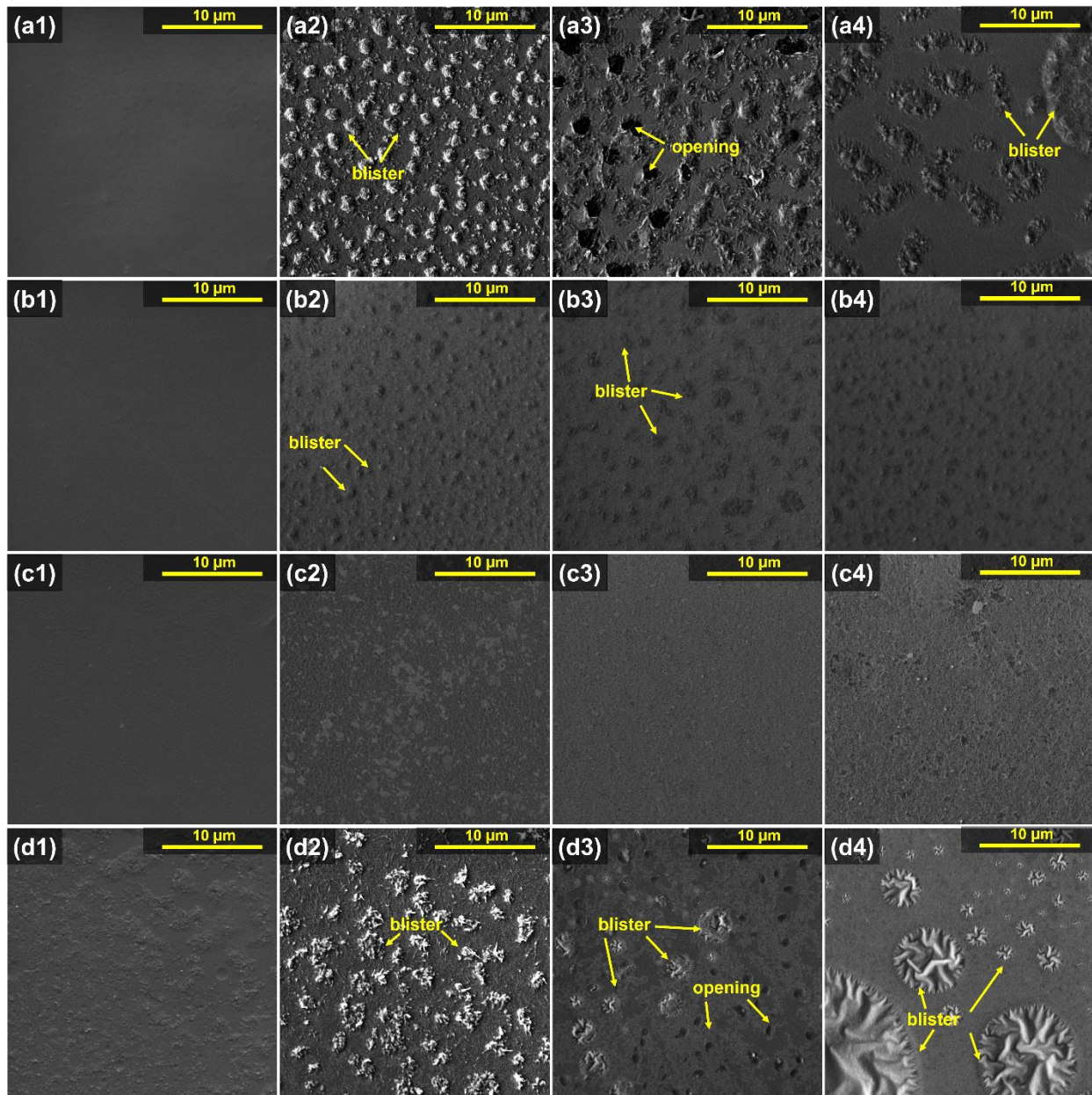
Figure 8.6 *SEM images of the surface morphology evolution for the four types of flux residues: (a) SP1, (b) SP2, (c) SP3, (d) SP4; (1) non-climatic exposure, (2) exposed at 60°C, 98% RH for 5 days, (3) exposed at 60°C, 98% RH for 10 days, (4) exposed at 60°C, 98% RH for 15 days.*

Evaluation of reflow soldered dummy smt component using EIS

The dummy SMT component shown in **Figure 8.1**(c) after the soldering process was subjected to humidity exposure to investigate the evolution of the residue in the gap. Change in electrical characteristics due to residue changes (similar to the effect shown in **Figure 8.5** and **Figure 8.6** and release of activator components was monitored using electrochemical impedance spectroscopy. **Figure 8.7** shows the full impedance spectra at various exposure times for 4 pastes with 2 different stand-off heights exposed at constant 60°C, 98% RH. In general, the component with stand-off height of 1 mm obtained higher impedance value at frequency from 10^{-1} Hz to 10^3 Hz, as shown in **Figure 8.7**(a). Compared to the non-exposed EIS results, significant reduction of the impedance values for SP1, SP2, and SP4 were observed on the dummy components with 0.5 mm stand-off height after 7 days climatic exposure (**Figure 8.7**(b)). For SP2 and SP3, significant reduction of the impedance was also observed on the dummy components with 1 mm stand-off height. The EIS characteristics of SP2 and SP3 in the shaded area transformed from capacitance behavior to resistance behavior (looking at the corresponding phase angle results, which is not shown). The reduction of the impedance value for dummy component with 1mm stand-off height shown in **Figure 8.7**(b) was pronounced in the frequency range from 10^{-1} Hz to 10^4 Hz, which is broader than the dummy components with 0.5 mm stand-off height. After 14 days climatic exposure (**Figure 8.7**(c)), an increased impedance value was observed in the SP3 reflowed soldered dummy component with 1 mm stand-off height, whereas the change of impedance values for other dummy components were minimal compared to the impedance values collected after 7 days exposure.
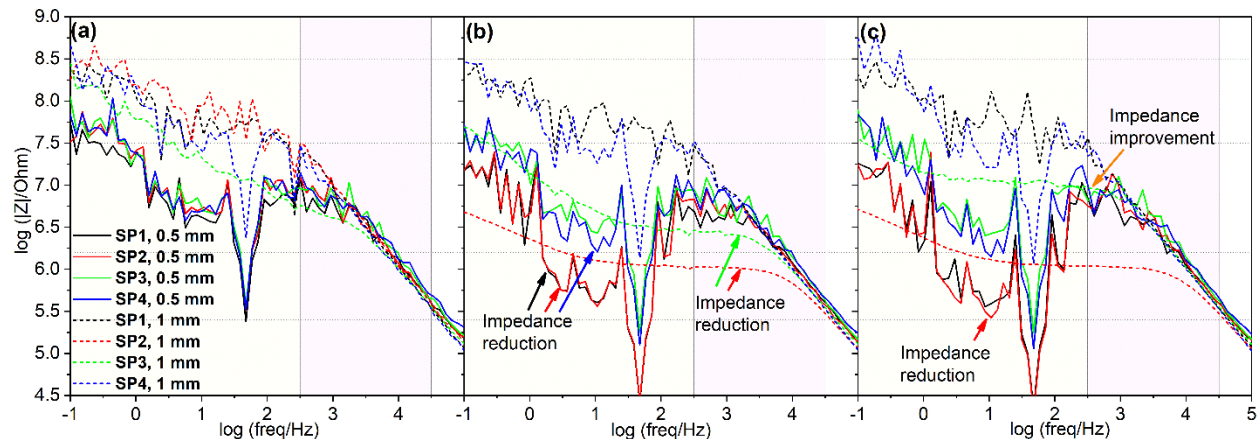
Figure 8.7 *Impedance value of reflow soldered dummy SMT component with different stand-off height during climatic exposure at 60°C, 98% RH: (a) non-exposure, (b) 7 days exposure, (c) 14 days exposure.*

The dummy components were opened up after humidity exposure for the analysis of nature of residue. **Figure 8.8** shows the flux residue distribution between the gap after humidity exposure

with two different stand-off heights after 14 days exposure under 60°C, 98% RH. For the 0.5 mm stand-off height dummy components, the adjacent solder joints were connected by all four types of reflow-process related flux residue, as shown in **Figure 8.8**(a1)(b1)(c1)(d1). For the 1 mm stand-off height components, the adjacent solder joints were connected by the flux residue of SP2, SP3, as shown in **Figure 8.8**(b2)(c2). However, the flux residue of SP1 abd SP4 beneath the 1 mm stand-off height component did not spread after climatic exposure, which resulted the flux free region demonstrated between solder joints as shown in **Figure 8.8**(a2)(d2).
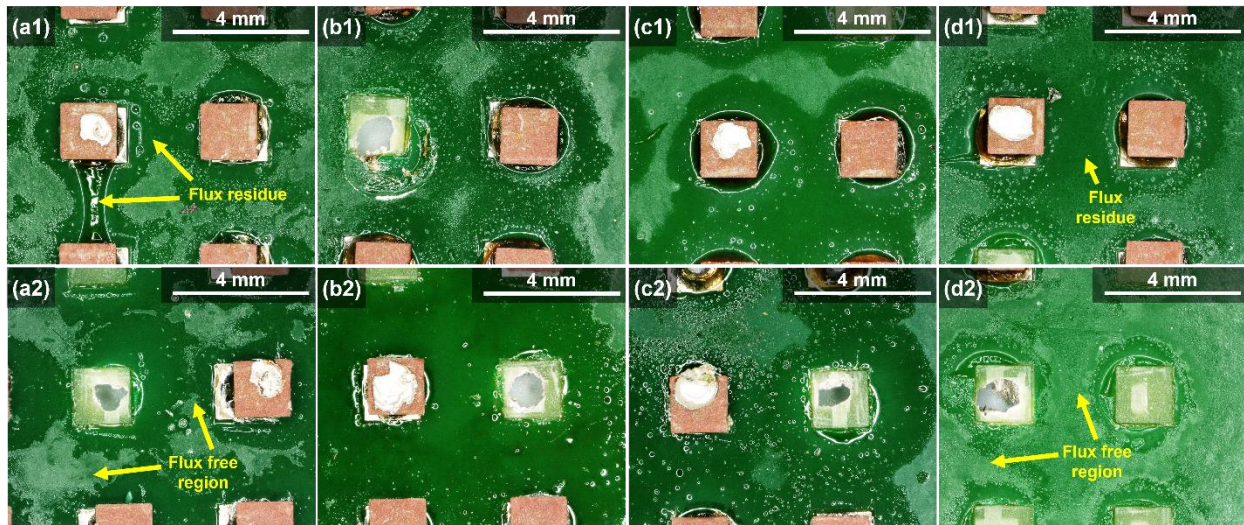
Figure 8.8 *LOM image of flux residue distribution under the dummy components after 14 days climatic exposure at 60°C, 98% RH: (a) SP1, (b) SP2, (c) SP3, (d) SP4; (1) 0.5 mm stand-off height. (2) 1 mm stand-off height.*

IV.   DISCUSSION

The present investigation focused on understanding the effect of activator chemistry in the reflow paste with similar composition of other parts of the flux formulation. The concealed nature of reflow residue from the soldering process has been reported earlier [27]. It showed that the reflow residue consists of the hardened resin part in which the residues of the activator components are embedded. It has also been reported that the concealed residue open up under humidity exposure possibly due to the hydrolysis of the resin components leaving activators exposed to the humidity and water film causing reliability issues. However, morphological changes to the concealed residue can be not only due to the interaction of the resin with humidity, but also the hygroscopic nature of the activator component can change the behavior. Therefore, in this work similar resin system was used with different activator components in order to understand the relative effects on the morphological changes during humidity exposure. Overall, the result shows that the

morphological change to the concealed residue depends on the activator package in the flux system. The humidity interaction with flux residues triggered the failure of the resin encapsulation and spreading of the flux residue on the surface of PCBAs, which could affect reliability on a PCBA surface. Effect was found to be a function of the stand-off height of the component.

Effect of humidity on paste residues and effect of activator chemistry

The morphology changes to the flux residue was affected by humidity interaction with flux activators during the climatic exposure at 60°C, 98% RH as shown in **Figure 8.6**. Opening and blisters observed on the flux residue of SP4 and SP1 could be accelerated by hygroscopic flux activators in flux residue. The deliquescence relative humidity (DRH) of halide used in solder flux formulation usually show much lower deliquescent point, which could be in a range of 65-78% RH [28][29]. As result, significant amount of blisters and opening with largest size formed on the flux residue of SP4 after climatic exposure (**Figure 8.6**(d2-d4)). In comparison, the WOA activators possessed higher DRH than halides at room temperature [5], which is in a range between 84% RH (glutaric acid) to 99% RH (adipic acid) [14][15]. Hence, limited blister formation and opening was obtained when flux contains single WOA as for SP2 and SP3 (**Figure 8.6**(b4)(c4)). Practically, the binary blended WOA activators used in flux formulation is aiming at balancing the solderability during soldering process and maintain humidity robustness under harsh climatic exposure [30]. However, the binary blended WOAs activators resulted reduction of the DRH level than any of the individual WOA in the mixture [16]. Therefore, numerous blisters and openings were found on the binary blended WOA flux residue of SP1 after humidity exposure (**Figure 8.6**(a2-a4)).

The opening effect of flux residue during climatic exposure resulted in the release of conductive substances such as flux activators. As a result, the conductivity of the extracted solution for flux residue increased during climatic exposure period as shown in **Figure 8.4**. The evolution of the measured conductivity of SP1, SP2, and SP4 agreed with the opening and blister formed on the flux residue surface during climatic exposure as in **Figure 8.6**. The conductivity value of extracted solution for SP1 and SP4 value significantly increased during exposure period at 60°C, 98% RH, which is due to the opening and blister formation as shown **Figure 8.6**(a2-a4)(d2-d4). The highest conductivity obtained for SP4 was attributed to the dissolution of halide content [31], which released by forming big blisters. For SP2 shown in **Figure 8.6**(b2-b4), similar surface morphology of flux residue was observed after 5 days, 10 days, and 15 days climatic exposure resulted in the similar conductivity value for extracted solution as shown **Figure 8.4**. The conductivity value of extracted solution for SP3 was in the same level as SP1; however, no significant change of surface morphology has been observed on SP3 flux residue. The increased conductivity level of

SP3 flux residue could be due to the spreading of flux residue after climatic exposure as shown in **Figure 8.5**(c2), which resulted a much larger contact area for the exposure of conductive substances.

Impact of residues from pastes on the leak current during SIR testing

Humidity interaction with reflow-process related flux residue significantly influenced the leakage current of the reflow soldered SIR pattern as shown in **Figure 8.2**. The presence of the free halide ions is extremely detrimental on the corrosion of metals or metal oxides in the electronics [5]. For SP4 soldered SIR pattern, halide dissolution caused strong ionization behavior under water condensation stage during climatic accelerating test. As a result, the leakage current value of SP4 exceeded the critical value of 10 µA [19] due to the halide ions induced ECM dendrites formation [32] exhibited in **Figure 8.3**(d), which lead to the highest charge transfer as shown in **Figure 8.2**(b).

Figure 8.2 shows the leakage current value of SP2 is much higher than SP1, which did not agree with the result of the higher conductivity level of SP1 shown in **Figure 8.4**. However, **Figure 8.3**(b) and **Figure 8.5**(b1) show that higher spreading area was obtained by SP2 flux residue after soldering process. The flux residue took up moisture during water condensation stage, which could triggered the ionization of the carboxyl group in WOA flux activator and acted as a conductive media between oppositely biased electrodes. Therefore, the charge transfer value of SP2 reflow solder SIR pattern is higher than SP1 reflow soldered SIR pattern (**Figure 8.2**(b)) due to larger coverage area over oppositely biased electrodes.

Compared to SP2 reflow soldered SIR pattern, although the spreading area of SP3 is larger after soldering process (**Figure 8.3**(c)) and climatic exposure (**Figure 8.5**(c2)), the SP3 reflow soldered SIR pattern obtained a much lower leakage current value. Xu et al. [33] reported the wettability of the flux activators can be improved by organic amine, which agree to the larger spreading area of the flux residue in the present study. Meanwhile, the organic amine content in the flux formulation provided a robust anti-corrosion performance due to the neutralized Brønsted-Lowry acid base reaction [34] between the amino group in organic amine and carboxyl group WOA. As result, the ionization of the carboxyl group in WOA is diminished during water condensation stage and hence the relative high conductivity value of SP3 flux residue shown in **Figure 8.3** did not result in higher corrosion. Consequently, the blended WOA-amine provide high corrosion resistance [35] and inhibition of the ECM dendrite formation [36]. Therefore, the flux residue of SP3 behaved as a poor corrosive media for charge transfer as shown in **Figure 8.2**(b).

Impact of the stand-off height of component on the climatic reliability of SMT device

The same amount of the solder pastes used in the production of dummy SMT component with different stand-off height. Results from the stand-off height testing shows that the effect of reflow flux residue under humid conditions changes due to the hygroscopicity of the flux activator and the spreading area of flux residue. The impedance value between adjacent solder joints of the dummy SMT component was affected by reflow-process related flux residue under climatic exposure at 60°C, 98% RH, as shown in **Figure 8.7**. The spreading of the flux residue is more pronounced beneath the SMT dummy components with 0.5 mm stand-off height (**Figure 8.8**(a1)(b1)(c1)(d1)), which resulted the hygroscopic and ionic media between solder joints in SP1, SP2 and SP4 samples. In consequence, the reduction of the impedance value was observed for SP1, SP2 and SP4 samples with 0.5 mm stand-off height after 7 days and 14 days climatic exposure (**Figure 8.7**(b)(c)). Since the blended WOA-amine activator contained flux residue in SP3 samples is less corrosive, therefore the impedance value of SP3 sample with 0.5 mm stand-off height maintained at a higher level.

Generally, the impedance value of the SMT component increased when increasing the stand-off height from 0.5 mm to 1 mm. The larger space induced the more heat transfer through air, which might activated more flux activator for the oxides removal during soldering process. On the other hand, the increased stand-off height of SMT component eliminated of capillary force at the component-PCB interface, which affected the distribution area of the flux residue with the nature of less spreading such as SP1 and SP4. As result, the absence of the hygroscopic flux residue was found between solder joints of SP1 and SP4 samples (**Figure 8.8**(a2)(d2)), which leads to high impedance of SP1 and SP4 soldered dummy SMT components compared to SP2 and SP3 soldered dummy SMT components with larger spreading area (**Figure 8.8**(b2)(c2)).

Moreover, the component with higher stand-off height obtained more space for the humidity interaction with flux residue. Therefore, the reduction of the impedance for the reflow flux residue in the component with 1 mm stand-off height is more pronounced than the component with 0.5 mm stand-off height under same climatic exposure, as shown in **Figure 8.7**(b)(c). Consequently, the EIS characteristic of SP2 and SP3 soldered SMT components shifted from capacitive to resistive behavior in the shaded region as shown in **Figure 8.7**(b), which indicates the water absorption of flux residue and dissociation of the WOA activator [14]. **Figure 8.7**(c) shows a decrease of impedance value of SP2 samples by extending the climatic exposure to 14 days, which could be either due to the release of acidic activators or the corrosion of solder alloys on SIR pattern induced by the WOA in flux residue. Under humidity exposure, the decreased

impedance result of SP2 agreed to the failure by exceeding critical leakage current level (**Figure 8.2**(a)). Similarly, the relatively higher impedance value obtained for SP3 sample indicates that good humidity robustness, which agreed with the lowest leakage current from DC testing as shown in **Figure 8.2**(a).

V. CONCLUSIONS

- Conductive ionic residues were released from the process-related flux residue after climatic exposure under at 60°C, 98% RH. The increased conductivity value for extracted solutions were due to the release of different activators due to the opening up of the residue film. The binary blended WOAs in SP1 flux residue and halide activators in SP4 flux residue accelerated hydrolytic degradation of the resin due to their lower DRH.

- Flux activator used in flux formulation resulted different spreading effect of flux residue after soldering process. With WOA flux activator, the larger spreading area of flux residue on SP2 reflow soldered SIR pattern induced higher charge transfer compared to SP1 reflow soldered SIR pattern, even though SP2 flux residue obtained the lower conductivity value.

- Type of flux activator used in flux formulation significantly influenced the leakage current value during accelerated climatic test. The lowest leakage current level obtained by SP3 flux residue could be due to Brönsted-Lowry acid base neutralization of WOA-amine activators, whereas the ECM failure of SP4 reflow soldered SIR pattern was attributed to the Low DRH and ionization of the corrosive halide under humid condition.

- Flux residue connected solder joints in the dummy SMT component with lower stand-off height due to capillary effect, which provided a hydrophilic media for charge transfer under humid conditions. However, increasing the stand-off height of component resulted in a flux free region between solder joints if the spreading area of the flux residue is small.

VI. REFERENCES

[1]   Mordor Intelligence, SURFACE MOUNT TECHNOLOGY MARKET - GROWTH, TRENDS, AND FORECASTS (2020 - 2025), 2019. https://www.mordorintelligence.com/industry-reports/surface-mount-technology-market.

[2]   E.H. Amalu, Y.T. Lui, N.N. Ekere, R.S. Bhatti, G. Takyi, Investigation Of The Effects Of Reflow Profile Parameters On Lead-free Solder Bump Volumes And Joint Integrity, in: AIP Conf. Proc., 2011. doi:https://doi.org/10.1063/1.3552519.

[3]   G.R. Blackwell, Experiences with the transition to surface mount technology in ECET labs, in: ASEE 2004 Annu. Conf. Expo. "Engineering Res. New Height., American Society for Engineering Education, 2004: pp. 5569–5573.

[4]   M.C. Li, A. Al-Refaie, C. Yang, DMAIC Approach to Improve the Capability of SMT Solder Printing Process, IEEE Trans. Electron. Packag. Manuf. 31 (2008) 126–133. doi:10.1109/TEPM.2008.919342.

[5]   R. Ambat, H. Conseil-Gudla, V. Verdingovas, Corrosion in Electronics, Encycl. Interfacial Chem. Surf. Sci. Electrochem. (2018) 134–144. doi:https://doi.org/10.1016/B978-0-12-409547-2.13437-7.

[6]   S. Lee, M. Jung, H. Lee, T. Kang, Y. Joo, Effect of Bias Voltage on the Electrochemical Migration Behaviors of Sn and Pb, IEEE Trans. Device Mater. Reliab. 9 (2009) 483–488. doi:10.1109/TDMR.2009.2026737.

[7]   P. Isaacs, T. Munson, Cleanliness Requirements: A Moving Target, in: 2019 Pan Pacific Microelectron. Symp. (Pan Pacific), 2019: pp. 1–10. doi:10.23919/PanPacific.2019.8696733.

[8]   E. Bastow, The Effect of Reflow Profiling on the Electrical Reliability of No-Clean Solder Paste Flux Residues, in: IPC APEX EXPO Proc., Las Vegas, 2014.

[9]   H. Conseil, M.S. Jellesen, R. Ambat, Contamination profile on typical printed circuit board assemblies vs soldering process, Solder. Surf. Mt. Technol. 26 (2014) 194–202. doi:10.1108/SSMT-03-2014-0007.

[10]   K. Piotrowska, M.S. Jellesen, R. Ambat, Thermal decomposition of solder flux activators under simulated wave soldering conditions, Solder. Surf. Mt. Technol. 29 (2017) 133–143. doi:10.1108/SSMT-01-2017-0003.

[11]   K.S. Hansen, M.S. Jellesen, P. Moller, P.J.S. Westermann, R. Ambat, Effect of solder flux residues on corrosion of electronics, in: 2009 Annu. Reliab. Maintainab. Symp., 2009: pp. 502–508. doi:10.1109/RAMS.2009.4914727.

[12]   P. Isaacs, T. Munson, What makes no-clean flux residue benign?, in: 2016 Pan Pacific Microelectron. Symp. (Pan Pacific), 2016: pp. 1–7. doi:10.1109/PanPacific.2016.7428404.

[13]   K. Piotrowska, R. Ambat, Residue-Assisted Water Layer Build-Up Under Transient Climatic Conditions and Failure Occurrences in Electronics, IEEE Trans. Components, Packag. Manuf. Technol. 10 (2020) 1617–1635. doi:10.1109/TCPMT.2020.3005933.

[14]   V. Verdingovas, M.S. Jellesen, R. Ambat, Solder Flux Residues and Humidity-Related Failures in Electronics: Relative Effects of Weak Organic Acids Used in No-Clean Flux Systems, J. Electron. Mater. 44 (2015) 1116–1127. doi:10.1007/s11664-014-3609-0.

[15]   K. Piotrowska, R. Ud Din, F.B. Grumsen, M.S. Jellesen, R. Ambat, Parametric Study of Solder Flux Hygroscopicity: Impact of Weak Organic Acids on Water Layer Formation and Corrosion of Electronics, J. Electron. Mater. 47 (2018) 4190–4207. doi:10.1007/s11664-018-6311-9.

[16]   K. Piotrowska, V. Verdingovas, R. Ambat, Humidity-related failures in electronics: effect of binary mixtures of weak organic acid activators, J. Mater. Sci. Mater. Electron. 29 (2018) 17834–17852. doi:10.1007/s10854-018-9896-0.

[17]   X. He, M.H. Azarian, M.G. Pecht, Evaluation of Electrochemical Migration on Printed Circuit Boards with Lead-Free and Tin-Lead Solder, J. Electron. Mater. 40 (2011) 1921–1936. doi:10.1007/s11664-011-1672-3.

[18]   M.S. Jellesen, D. Minzari, U. Rathinavelu, P. Møller, R. Ambat, Corrosion failure due to flux

residues in an electronic add-on device, Eng. Fail. Anal. 17 (2010) 1263–1272. doi:10.1016/j.engfailanal.2010.02.010.

[19] V. Verdingovas, M.S. Jellesen, R. Ambat, Relative effect of solder flux chemistry on the humidity related failures in electronics, Solder. Surf. Mt. Technol. 27 (2015) 146–156. doi:10.1108/SSMT-11-2014-0022.

[20] P. Veselý, D. Bušek, O. Krammer, K. Dušek, Analysis of no-clean flux spatter during the soldering process, J. Mater. Process. Technol. 275 (2020) 116289. doi:https://doi.org/10.1016/j.jmatprotec.2019.116289.

[21] M. Yamamoto, A. Takumi, K. Shiomi, M. Nakanishi, M. Watanabe, Soldering flux and solder paste composition, EP1897652A1, 2006. https://patents.google.com/patent/EP1897652A1/en.

[22] N.-C. Lee, 3 - Solder Paste Technology, in: N.-C.B.T.-R.S.P. Lee (Ed.), Reflow Solder. Process., Newnes, Burlington, 2001: pp. 37–55. doi:https://doi.org/10.1016/B978-075067218-4/50003-8.

[23] P. Gnanasekar, J. Chen, R. Goswami, H. Chen, Sustainable Shape-Memory Polyurethane from Abietic Acid : Superior Mechanical Properties and Shape Recovery with Tunable Transition Temperatures, ChemSusChem. 13 (2020) 5749–5761. doi:10.1002/cssc.202001983.

[24] A. Sharma, Y.-J. Jang, J.B. Kim, J.P. Jung, Thermal cycling, shear and insulating characteristics of epoxy embedded Sn-3.0Ag-0.5Cu (SAC305) solder paste for automotive applications, J. Alloys Compd. 704 (2017) 795–803. doi:https://doi.org/10.1016/j.jallcom.2017.02.036.

[25] R.P. Frankenthal, J.D. Sinclair, Electronic Materials and Devices, Corrosion of, in: Encycl. Mater. Sci. Technol., Elsevier, Oxford, 2001: pp. 2638–2644. doi:https://doi.org/10.1016/B0-08-043152-6/00473-3.

[26] S. Zhan, M.H. Azarian, M.G. Pecht, Surface insulation resistance of conformally coated printed circuit boards processed with no-clean flux, IEEE Trans. Electron. Packag. Manuf. 29 (2006) 217–223. doi:10.1109/TEPM.2006.882496.

[27] K. Piotrowska, S. Lagana, M. Jellesen, R. Ambat, Impact of Process-Related Flux Contamination on the Electronics Reliability Issues Under Detrimental Climatic Condtions, in: 2019 Pan Pacific Microelectron. Symp. (Pan Pacific), IEEE, Kauai, HI, USA, USA, 2019. doi:10.23919/PanPacific.2019.8696890.

[28] L. Lindau, B. Goldschmidt, Low temperature corrosion in bark fuelled, small boilers, Stockholm, 2008. https://www.osti.gov/etdeweb/servlets/purl/932355.

[29] D. Hu, J. Chen, X. Ye, L. Li, X. Yang, Hygroscopicity and evaporation of ammonium chloride and ammonium nitrate: Relative humidity and size effects on the growth factor, Atmos. Environ. 45 (2011) 2349–2355. doi:https://doi.org/10.1016/j.atmosenv.2011.02.024.

[30] K. Piotrowska, L. Feng, R. Ambat, Thermal decomposition of binary mixtures of organic activators used in no-clean fluxes and impact on PCBA corrosion reliability, Solder. Surf. Mt. Technol. 32 (2019) 93–103. doi:10.1108/SSMT-05-2019-0020.

[31] V. Verdingovas, M.S. Jellesen, R. Ambat, Influence of sodium chloride and weak organic acids (flux residues) on electrochemical migration of tin on surface mount chip components, Corros. Eng. Sci. Technol. 48 (2013) 426–435. doi:10.1179/1743278213Y.0000000078.

[32]   K. Piotrowska, M.S. Jellesen, R. Ambat, Water film formation on the PCBA surface and failure occurrence in electronics, in: 2018 IMAPS Nord. Conf. Microelectron. Packag., 2018: pp. 72–76. doi:10.23919/NORDPAC.2018.8423854.

[33]   D. Xu, X. Li, C. Wang, B. Xu, Study on wettability and corrosivity of a new no-clean flux for lead-free solder paste in electronic packaging technology, in: 2011 Second Int. Conf. Mech. Autom. Control Eng., 2011: pp. 1706–1708. doi:10.1109/MACE.2011.5987285.

[34]   Y. Shi, X. Wei, B. Tolla, The Role of Organic Amines in Soldering Materials, in: IPC APEX EXPO Conf. Proc., Circuit Insight, San Diego, USA, 2015.

[35]   M. Bixenman, D. Lober, A. Ailworth, K. Corporation, B. Tolla, D. Ph, J. Allen, D. Jean, K. Loomis, K. Corporation, Electrochemical Methods to Measure the Corrosion Potential of Flux Residues, in: IPC APEX EXPO, SMTNET, San Diego, USA, 2017.

[36]   B. Tolla, D. Jean, H. Bhavsar, Y. Shi, X. Wei, Reactivity of No-clean flux residues in electronic assemblies: a systematic study, in: SMTA Int., Rosemont, IL, USA, 2015.

9. Influence of no-clean solder flux residue on the corrosion protection of conformal coatings used in electronics

Feng Li, Vadimas Verdingovas, Ioannis Mantis, Morten Stendahl Jellesen, Rajan Ambat

Abstract: Conformal coatings are widely used on the electronic assemblies to protect the electronic device from the ionic contaminants, humidity, and dust in the environment. This study focused on the influence of the no-clean flux residue on the protection performance of the four frequently used conformal coatings under cyclic humidity conditions. A test Printed Circuit Board (PCB) with interdigitated surface insulation resistance (SIR) pattern was used as the test vehicle. Electrochemical impedance spectroscopy (EIS) was used to monitor the water uptake behavior of the coatings, followed by chronoamperometric DC method to evaluate the effect of penetrated moisture on failure due to leakage current or electrochemical migration (ECM) between the interdigitated electrodes. The surface morphology and adhesion was inspected using scanning electron microscopy and the corrosion product analysis was carried out using energy dispersive spectroscopy. Results suggested that the moisture barrier properties of the coating is relatively a minor factor contributing to the performance, while the adhesion of the coating, which compromised by the presence of no-clean flux residue has most significant influence. Among the coatings investigated, elastomeric acrylate showed better performance due to good adhesion even under contaminated conditions.

Keywords: Conformal coating, solder flux, electronic corrosion, humidity, reliability.

I.   INTRODUCTION

Driven by the concurrent reduction of the package size [1] and higher degrees of integration on integrated-circuit (IC) chips [2], the progress of electronics miniaturization was dramatically approached since 1990s. The closer spacing from miniaturized printed circuit board assemblies (PCBAs) and contamination on PCBAs reduced the corrosion reliability of electronics under humid conditions [3]. The contamination source of PCBAs mainly comes from the manufacturing process related flux residue [4] and external deposition of airborne contaminants [5]. The deposition of external contaminants is usually prohibited by the enclosure design, whereas the humidity and corrosive gases still can reach to the PCBA surface in the enclosure by diffusion through the walls and penetration through the openings [6][7][8]. On the other hand, the process related ionic contaminants were from etchants, plating, ionic contaminants leached out from the assembly [9][10], and flux residue can be related to the insufficient thermal degradation or over spray [4][11].

Flux residue on the surface of PCBAs acts as an important corrosion promoter for electronics [12]. The solid substances in the flux residue usually contains weak organic acids (WOAs) activators or resin/rosin component [13][14][15]. The hygroscopic nature of the flux activators triggers the humidity absorption from ambient at low humidity level [16]; hence the electrolyte layer formed between solder joints on the PCBAs leads to the ionization of WOAs [15][17] and induces intermittent or permanent corrosion problems [18].

Electrochemical migration (ECM) is a typical corrosion failure mode which takes place between two adjacent oppositely biased electrodes under humid conditions [19][20][21][22]. In the ECM process, dissolved metal ions from the anodic terminals migrate towards cathode where it will deposit to form the metallic dendrite and grow back to anode [5]. Dendrite bridging the gap leads to catastrophic failure due to reduction of surface insulation resistance [17] with substantial increase of leakage current [15][23], and short circuiting [19][22]. Conductive anodic filament (CAF) is another type of corrosion failure mode that leads to the loss of SIR [24][25]. The humidity accelerates the degradation of the fiber/epoxy interfacial bond, where the electrochemical cell forms to initiate corrosion [24]. The corrosion product in this case such as metal salts and oxides will precipitate due to the local occluded chemistry, which will be pushed from anode to cathode through the polymer [25]. Finally, the corrosion product bridge between anode and cathode, and the semi-conducting nature of the corrosion product will results in short circuit. To mitigate the humidity and condensation related electrical failures, conformal coatings have been broadly applied on the PCBAs as the last stage of the manufacturing process [26][27]. However, for the PCBA with conformal coating, due to the occluded nature of the electrolyte between PCBA-coating interface (if moisture reaches the interface and delaminate the coating), the corrosion product can be a mixture of metallic dendrite, metal hydroxides [21].

Conformal coating is a thin polymer film with thickness from 1 – 100 micrometers [28], which consists of the chemistries of acrylic, epoxy, urethane, silicone, parylene and floropolymer [26][29][30][31][32][33]. In the electronic manufacturing industry, the evaluation of physical or chemical properties such as shelf life, thermal shock, cure, viscosity, and flexibility etc. of conformal coatings are well defined in IPC-CC-830C standard [30]. However, the evaluation standard of the humidity robustness performance for the conformal coating is usually focused on the surface insulation resistance (SIR) test, and surface appearance such as cracking and adhesion loss under 25°C/50% RH within 24h. For harsh environment applications such as automotive industry [34], more rigorous tests are needed. Therefore, the SIR testing for the

conformal coating was conducted under 40°C/93% RH or 84°C/85% RH [35] with a variety of contaminants such as solder flux, SO_2, H_2S, Cl_2, NO_2 etc in the actual reliability assessment [27].

For acrylate coating and acrylic coating, Zou et al. [36] and Hunt et al. [37] reported both of the coatings did not pass the SIR testing over the NPL TB57 assembly with adipic acid, succinic acid, and glutaric acid contained flux residue under testing condition of 40°C/93% RH [35]; however, acrylate coating and acrylic coating passed the SIR testing over the IPC-B-24 test board with anonymous flux residue under the testing condition of 85°C/85% RH. Hunt et al. reported that the silicone coating passed the SIR testing over the NPL TB67 test board with adipic acid, succinic acid, and glutaric acid contained flux residue [37], while Rathinavelu et al. reported flux residue with anonymous carboxylic acid reduced the adhesion of silicone conformal coating and ECM failures were obtained on the IPC-B-24 SIR pattern under exposure of 25°C/98% RH [38]. As result, the SIR testing only provided the pass-fail criteria of the conformal coatings, which depend on the structure of the test vehicle, contamination types and exposed climate used for the study. Moreover, the SIR result for the conformal coating assessment also dependent on the thickness [35], cure method [36], chemistry of the precursor [37], and conformal flexibility on the contour of the terminals [27], which makes the general assessment more complicated. The mechanism of humidity diffusion induced failure for the conformal coatings is able to address the impact characters of the conformal coating on performance of the protection on PCBA with the no-clean flux residue from manufacturing process; however, limited investigation focused on this field. Electrochemical impedance spectroscopy (EIS) is a non-destructive, rapid technique, which is able to in-situ monitor the corrosion performance of the coated metals [39][40][41][42]. The impedance at low-frequency range was represent the barrier characteristic of the coating [41], while the capacitance at high-frequency range corresponds to water uptake of the coating [42].

Present investigation focus on understanding the moisture barrier properties and adhesion issues of conformal coating on a PCB surface based on the cleanliness of the PCB. A test PCB with surface insulation interdigitated pattern was used as the substrate. Three different types of commercial conformal coatings were selected for investigation namely: synthetic rubber, elastomeric acrylate, and urethane acrylate. In order to investigate the effect of no-clean flux residue protective performance, tests were carried out for all the coatings on a clean test PCB and PCBs contaminated with two types of no-clean flux residues mimicking a mild flux chemistry and aggressive flux chemistry. Test board SIR pattern and environmental exposure conditions used corresponds to IPC-B-24 standard compliant test board and international electronic commission (IEC 60068-2-30) standard, which provides a guideline for the assessment of all

fields of standardized electronics. Experimental techniques used for the investigation was a combination of two-electrode EIS technique for monitoring the moisture uptake in the coatings, while a subsequent DC chrono-amperometric measurement was conducted to understand the effect of moisture absorbed coating on the electrical performance of the test PCB. Surface morphology of the coating after the experiments including cross-sectional analysis is carried out using SEM, and chemical analysis using EDS.

II.   MATERIALS AND EXPERIMENTAL METHODS

Coated substrate for testing

Figure 9.1 shows the test vehicle used as the substrate for coating and electrochemical testing. Test printed circuit board (PCB) was made of glass-reinforced epoxy (FR-4) laminate. The SIR interdigitated pattern was designed based on the configuration of IPC-B-24 test board. The testing area was 13 mm × 25 mm with 0.3 mm of gap size and 0.4 mm of electrode width. The overlapping length of two electrodes was 10.8 mm × 41 sets. Surface finish for the interdigitated electrodes was hot air solder leveling using Sn-0.7Cu on the 35 µm thick Cu conductive lines. To prepare the substrate for the coating, 30 µL flux [35] was applied on isopropanol cleaned SIR pattern in order to imitate the presence of flux residue after manufacturing process. Applying 30 µL flux resulted in 162 µg/cm^2 Flux A residue and 372 µg/cm^2 Flux B residue on the SIR interdigitated pattern respectively due to different fraction of the solid content. **Table 9.1** shows the details of the fluxes used for contamination of SIR pattern. Flux A contains adipic acid as activator, which was known as mild flux with benign corrosivity, low hygroscopicity, and less active in terms of solderability. Flux B with blend glutaric-adipic acid activator has higher solid content and acid number than Flux A, which provides better solderability, but higher hygroscopicity and corrosivity. Another set of clean test vehicles with SIR pattern were used as reference samples.
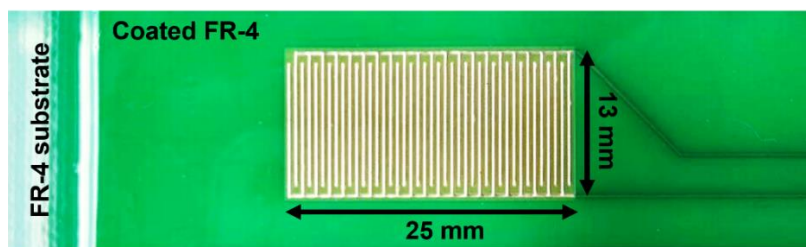
Figure 9.1 Coated PCB board with SIR pattern for the electrochemical testing.

Table 9.1 Fluxes used for imitating contamination on the SIR pattern.

	IPC J-STD-004 classification		Activator	Acid number		Contamination level

		Solid content (wt.%)		(mg KOH)	Applied volume (ml)	(µg/cm²)
Flux A	REL0	2.2	Adipic acid	15.80	30	162
Flux B	ORM0	4.0	Glutaric acid Adipic acid	36.85	30	372

Conformal coatings used for testing:

Three types of commercial conformal coatings were used in the present work as shown in **Table 9.2.** The application solutions of coatings were based on the manuals of the actual products, including thickness, applying method and curing method etc. In parallel, another set of non-coated PCB panels were used as reference.

Table 9.2 *Details of conformal coating application used in the present research.*

Conformal coating	Thickness over electrodes (µm)	Applying method	Curing method
Synthetic rubber	60	Spray	Ambient
Elastomeric acrylate	80	Spray	Ultraviolet
Urethane/acrylate	150	Spray	Ultraviolet

Climatic exposure and intermittent electrochemical testing
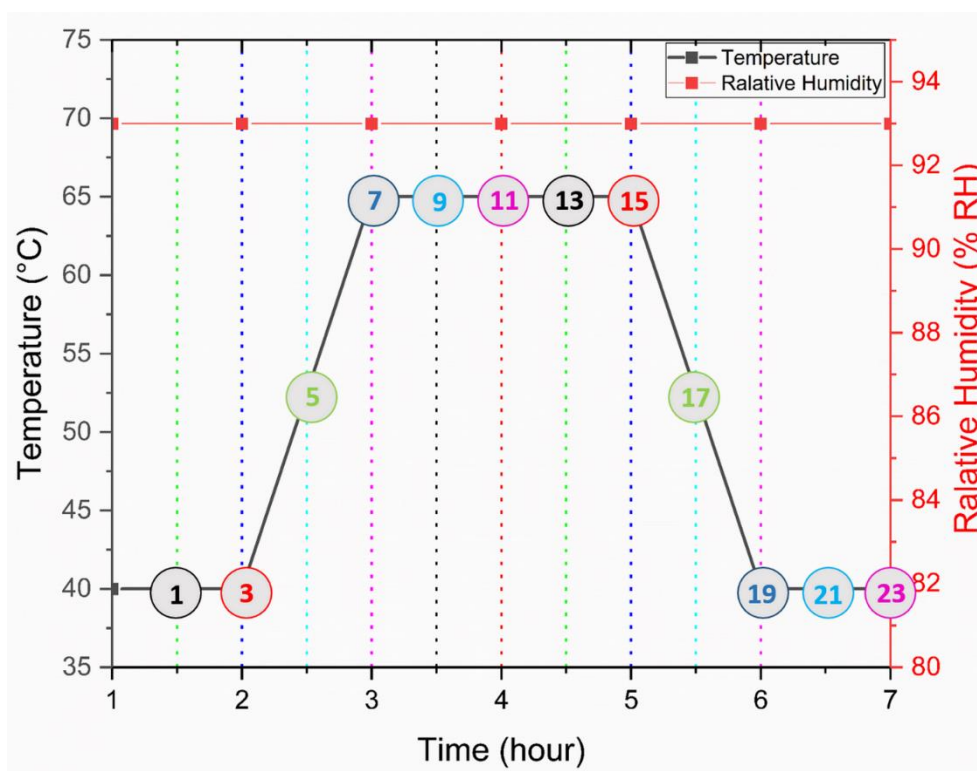
Figure 9.2 *Cyclic climatic profile used for the conformal coating testing.*

Climatic exposure was carried out in an "Espec PL-3KPH" climatic chamber with a sensitivity of ± 0.3°C and ± 2.5% for temperature and relative humidity (RH). The cyclic climatic profile used for testing in the present work was based on environmental testing of electronic equipment standard IEC 60068-2-30, as shown in **Figure 9.2**. For the accelerated climatic test, constant humidity exposure was set at 93% RH. When the temperature increases from 40°C to 65°C, transient condensation occurred on the PCB surface due to thermal delay as shown in stage 1-11, and moisture desorption occurred when the temperature shift back from 65°C to 40°C as shown in stage 13-23. Each cycle took 6 hours and lasted up to 52 cycles (total 13 days). This damp heat cyclic conditions accelerated the corrosion process of electronics under bias voltage.

The electrochemical measurements during humidity exposure was carried out using a "Biologic VSP" multichannel potentiostat. Electrochemical impedance spectroscopy (EIS) signal was applied on the two interdigitated electrodes, where one of the electrodes was used as both counter and reference electrode. For the first 5 days, EIS was used for monitoring moisture uptake and release in the coating. The scan range of frequency was from 100 kHz to 100 mHz with the amplitude of sinusoidal signal of 25 mV over the base voltage of 0 V. Each scan approximately took 5 mins, and a 10 min waiting period was inserted between each EIS scan. Therefore, in total 24 EIS scans were collected over one climatic cycle. The impedance value at 100 mHz was extracted to analyze the resistance evolution between two interdigitated electrodes over climate cycling, while the capacitance value was taken from frequency of 80 kHz in order to eliminate the electrochemical properties of the film and corrosion process of the electrodes [43].

Water uptake of the coating during cyclic climatic conditions was calculated based on Brasher and Kingsbury empirical formula (**Equation 9.1**) [42], where X_v is the percentage by volume fraction of water taken up in conformal coating, $Cp_{65°C}$ is the capacitance response after water absorption stage, $Cp_{40°C}$ is the capacitance response after water releasing stage, ε_w is the dielectric constant of water.

$$X_{\mathrm{v}} = \frac{\log(Cp_{65°C}/Cp_{40°C})}{\log\varepsilon_{\mathrm{w}}} \qquad \textit{Equation 9.1}$$

After 5 days EIS measurement, samples were subjected to a chrono-amperometry under 5 V DC bias for 7 day for the leakage current (LC) measurement in order understand the effect of moisture saturated coating on the failure. Following the 7 days DC testing, EIS was applied again in order to understand the influence of destructive DC method to the impedance value of the specimen. To obtain the robust statistics, 6 parallel tests were conducted for each type of coated samples.

Material characterization

In order to observe the corrosion of the SIR pattern and the blisters of the conformal coating, light optical microscopy inspection was conducted using a VHX digital microscope (Keyence, Japan). The morphology of the climatically exposed coating samples were inspected under secondary electron mode using a FEI Quanta 200 FEG scanning electron microscopy (SEM) at 3 kV. For the cross sectional analysis of the coated samples, the samples were cold-mounted in epoxy and polished up to using 50 nm neutral alumina. The morphology of corrosion product and the loss of adhesion at the interface was inspected using SEM. Chemical analysis of the corrosion product was carried out using energy dispersive spectroscopy (EDS) at 15 kV (Oxford Instrument, UK). To obtain the cross-sectional morphology of the coating, an initial cleaning of the cross-sectional area was carried out in the electron microscope using a 30 kV electron beam to remove the polymer debris from the polishing process. Moisture related degradation of the conformal coating structure was analyzed using Fourier-transform infrared spectroscopy (FT-IR) using a Nicolet iN10 MX infrared imaging microscope (Thermo Fisher Scientific, USA) with a Ge attenuated total reflectance (ATR) tip before and after climatic exposure.

III.   RESULTS

Surface appearance of the coated samples before climatic testing

Figure 9.3 shows the surface appearance of the coated SIR pattern. All the surface showed uniform coating layer without any air bubbles after the spray coating. For the test pattern coated with introduced surface contamination, flux residue can be seen beneath the coating for elastomeric acrylate coating and urethane acrylate coating pointed by arrows in the **Figure 9.3**(b3)(c3). Depending on the coating chemistry, urethane acrylate coating showed more visible changes to coating with Flux B residue followed by elastomeric acrylate coating. The LOM appearance of synthetic rubber coating did not show significant change with the flux residue, as shown in **Figure 9.3**(a1-a3). The surface morphology of elastomeric acrylate coating exhibited compact sphere appearance in **Figure 9.3**(b1), while the surface roughness of the synthetic rubber and urethane acrylate coatings were relative lower than elastomeric acrylate coating, as shown in **Figure 9.3**(a1)(c1). The cross-section micrograph in **Figure 9.3**(a1) shows the poor adhesion of synthetic rubber on the PCB substrate, whereas elastomeric acrylate and urethane acrylate coatings possessed robust adhesion as shown in **Figure 9.3**(b1)(c1).
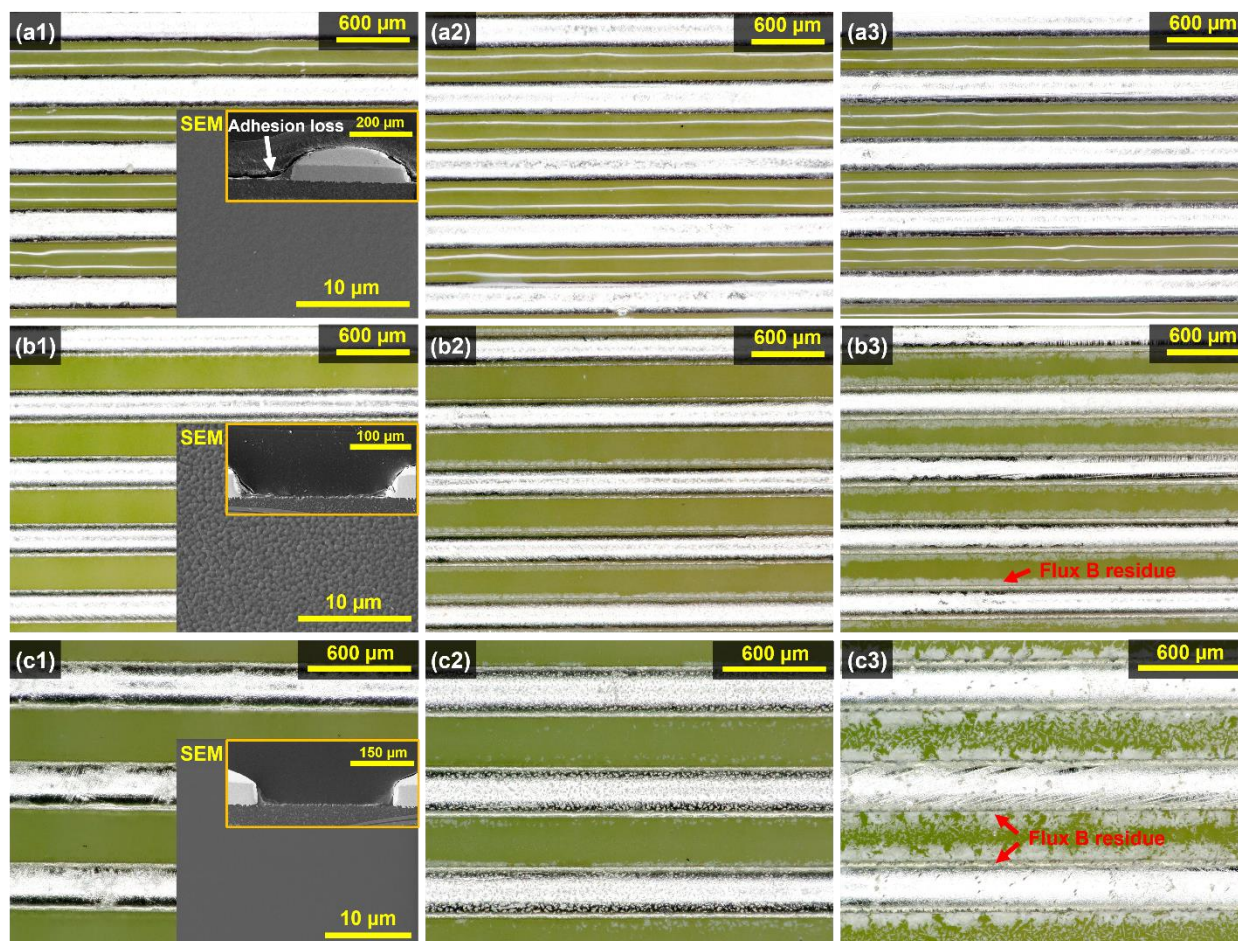
Figure 9.3 *LOM inspection of conformal coatings on SIR pattern before humidity testing with/without flux residue and the SEM micrograph of the surface morphology and cross-section: (a) synthetic rubber, (b) elastomeric acrylate, (c) urethane acrylate with the contamination condition of (1) flux free, (2) Flux A, and (3) Flux B.*

Electrochemical response of the coating during climatic cycling

a) Impedance analysis over first 5 days of exposure

Impedance spectra corresponding to the frequency range of 100 kHz to 100 mHz was collected over the 5 days of exposure with 24 scans during one cycle (**Figure 9.2**). **Figure 9.4** shows the typical full spectra showing the change in impedance and phase angle under testing temperature of 40°C and 65°C during the second climatic cycle in the first day, which is as stage 23 and stage 11 as shown in **Figure 9.2**. Generally, the impedance value at 100 mHz significantly dropped under testing temperature of 65°C compared to the impedance response at 40°C, as shown in **Figure 9.4**(a1)(b1)(c1). With the same type of coating, the impedance of flux free SIR pattern in **Figure 9.4**(a1) was the highest in comparison with the Flux A and Flux B contaminated SIR pattern shown in **Figure 9.4**(b1)(c1). With the Flux A contamination, the lowest impedance value

at 100 mHz was obtained for the synthetic rubber coated sample at 65°C, while the impedance response of elastomeric acrylate and urethane acrylate coated samples was higher than non-coated SIR pattern as shown in **Figure 9.4** (b1). The impedance response of Flux B contained samples at 100 mHz under 65°C was ranked as: elastomeric acrylate > urethane acrylate > synthetic rubber > non-coated sample.

Figure 9.4(a2) shows the phase angle change of flux free SIR pattern, which at high frequency remained at -90° when the testing temperature increased from 40°C to 65°C (as an example a vertical line shown at 10 kHz). However, a transition of the capacitance behavior (-90°) to resistance behavior (0°) was obtained for the Flux A and Flux B contained samples (**Figure 9.4**(b2)(c2)). The vertical line shown at 10 kHz for both cases shows shift of phase angle from -90 towards zero with synthetic rubber coated Flux A contained showing -70° under 65°C. In contrast, the increase of the phase angle is more pronounced for Flux B contained samples at 10 kHz as shown in **Figure 9.4**(c2). The phase angle of non-coated sample and synthetic rubber coated sample was at 0° under testing temperature of 65°C, while the phase angle of urethane acrylate coated samples increased from -75° to -25° as the temperature increased from 40°C to 65°C. The phase angle of the elastomeric acrylate coated sample was at -75° under 65°C.
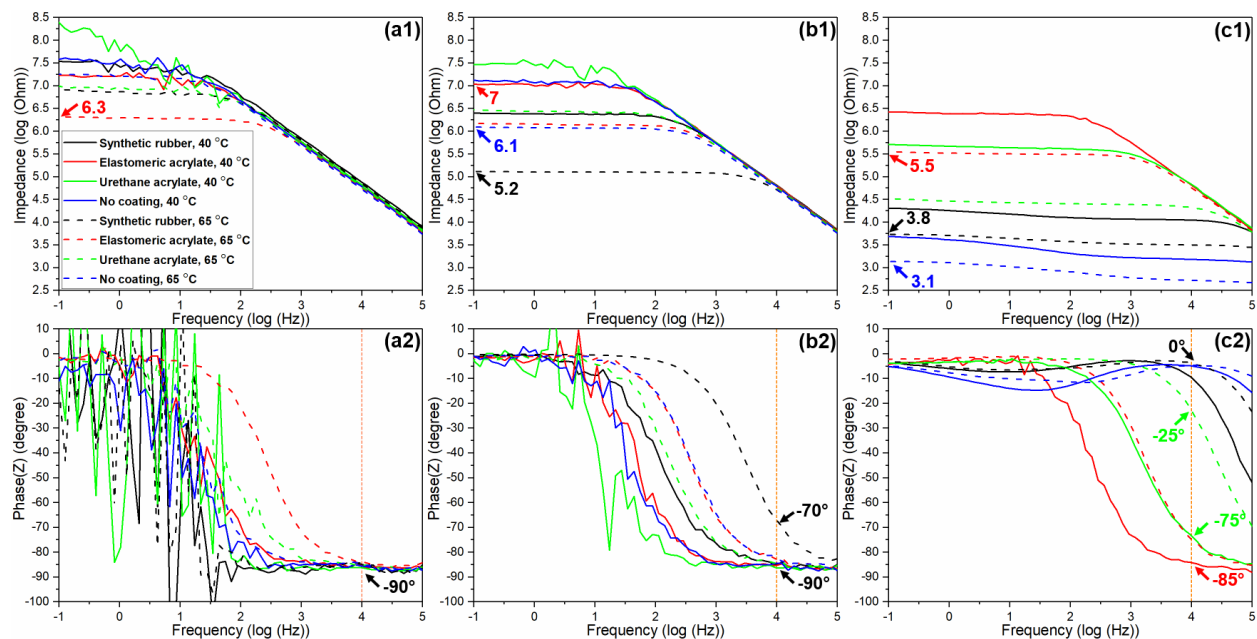
Figure 9.4 _(1) Impedance response and (2) phase angle of the (a) flux free, (b) Flux A, and (c) Flux B contained SIR pattern with/without conformal coating under testing temperature of 40°C and 65°C during the second climatic cycle._

Figure 9.5 shows the impedance evolution during five days EIS testing period at 100 mHz deduced from the full spectra recorded over the 5 days of exposure. Generally, the impedance value of flux free samples (**Figure 9.5**(a)) were higher than Flux A contaminated samples(**Figure 9.5**(b)), while Flux B residue contained samples obtained lowest impedance values (**Figure 9.5**(c)). Among flux free samples (**Figure 9.5**(a)), the synthetic rubber coated samples show a higher level of the impedance than non-coated samples. A slight increasing trend of the impedance over first 5 days was observed for elastomeric acrylate coated samples and non-coated samples. On the contrary, a decreasing trend was observed for urethane acrylate samples. For Flux A residue contained samples (**Figure 9.5**(b)), only synthetic rubber coated samples exhibited lower impedance than non-coated samples. The other two types of coated samples maintained a similar level of impedance as non-coated samples. For Flux B residue contained samples (**Figure 9.5**(c)), all the coated samples exhibited higher impedance level than non-coated samples. The ranking of the impedance over first 5 days as shown: elastomeric acrylate > urethane acrylate > synthetic rubber > non-coated samples. For the fluxes contaminated samples, an increasing trend of impedance over time was observed in first 5 days. EIS measurement was conducted after 7 days DC current aging, however no significant difference of impedance value was found in the case of flux free samples as shown in **Figure 9.5**(a). For flux contaminated sample, an increase in impedance was obtained as shown in **Figure 9.5**(b)(c).
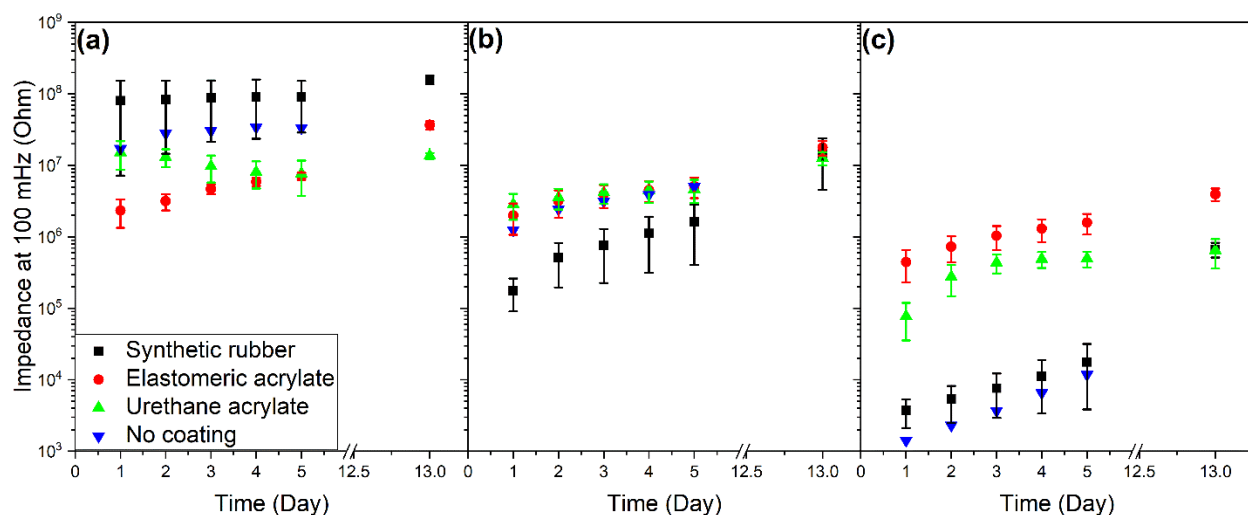
Figure 9.5 Evolution of impedance over 5 days at 100 mHz for various susbtrates: (a) flux free SIR PCB, (b) Flux A, and (c) Flux B contained test vehicles under testing temperature of 65°C.

Figure 9.6 shows the water uptake of the coatings with different contamination during climatic exposure calculated from the impedance data using **Equation 9.1**. Overall, no significant difference was observed for each set over the days of climatic exposure. In **Figure 9.6**(a) and (b),

no significant difference was found between the increased volume fraction of water for flux free samples and Flux A residue contained samples; however, **Figure 9.6**(c) shows the increased volume fraction of water for Flux B residue contained samples Compared to elastomeric acrylate coated samples, significant increase of the water volume fractions were obtained by the synthetic rubber and urethane acrylate coated Flux B contaminated SIR pattern as shown in **Figure 9.6**(c). For elastomeric acrylate coating, the flux residue on SIR pattern obtained minimum impact on moisture uptake compared to the flux free samples as shown in **Figure 9.6**(a)(b)(c).
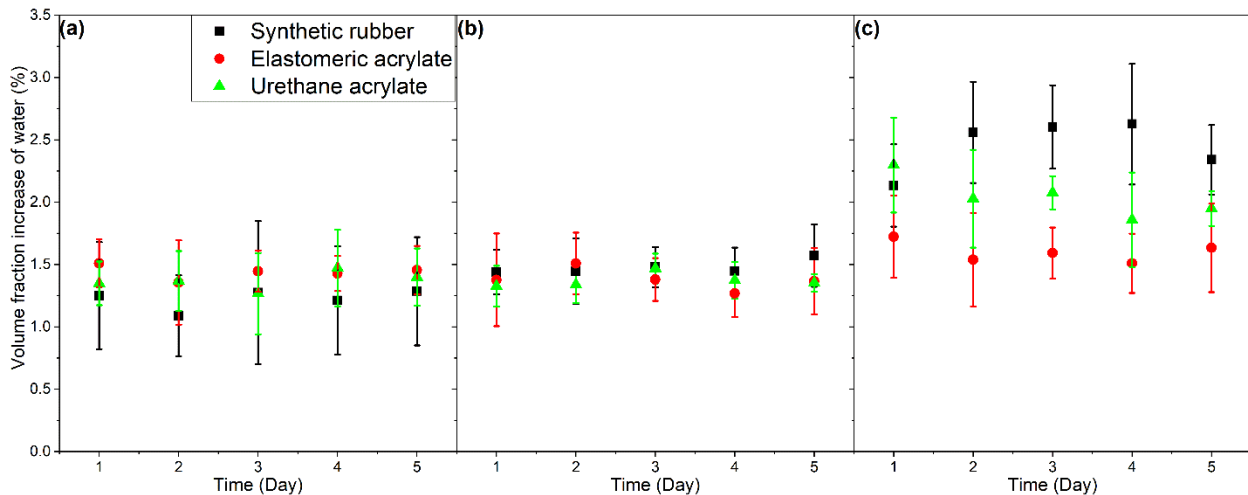
Figure 9.6 Volume fraction in coating calculated using impedance data: (a) flux free, (b) Flux A, and (c) Flux B contained test vehicles during climatic exposure.

b) DC voltage application for 7 days and leak current results

For each SIR PCBs exposed under humidity cycles, after 5 days of EIS measurements, 5V DC was applied to understand how the absorbed moisture can trigger failure. **Figure 9.7** shows the representative LC values of SIR patterns for various coatings and flux residue. Time scale in the graph is shown from 0 – 168 hours, however zero corresponds to the starting point of DC measurements ie. after 5 days of exposure to humidity cycles. With the same type of coating, the leakage current base value of flux B residue contained samples were higher than flux free and flux A residue contained samples. The leakage current of synthetic rubber coated samples with two types of flux residue exceed 10 µA as shown in **Figure 9.7**(b) and (c). The high leakage current was also confirmed in the case of Flux B residue contained non-coated samples (**Figure 9.7**(c)). **Table 9.3** summarized the failure rate of coatings, which was calculated based on 6 repetition of each type of test samples. No failure (NF) indicates the leakage current was below 10 µA during the testing period. Flux contaminated SIR pattern with synthetic rubber coating exhibited 100% failure rate. All the coated flux free samples maintained low leakage current, and

therefore no failure. No short circuit failure was observed for elastomeric acrylate and urethane acrylate coated samples with flux residue contamination.
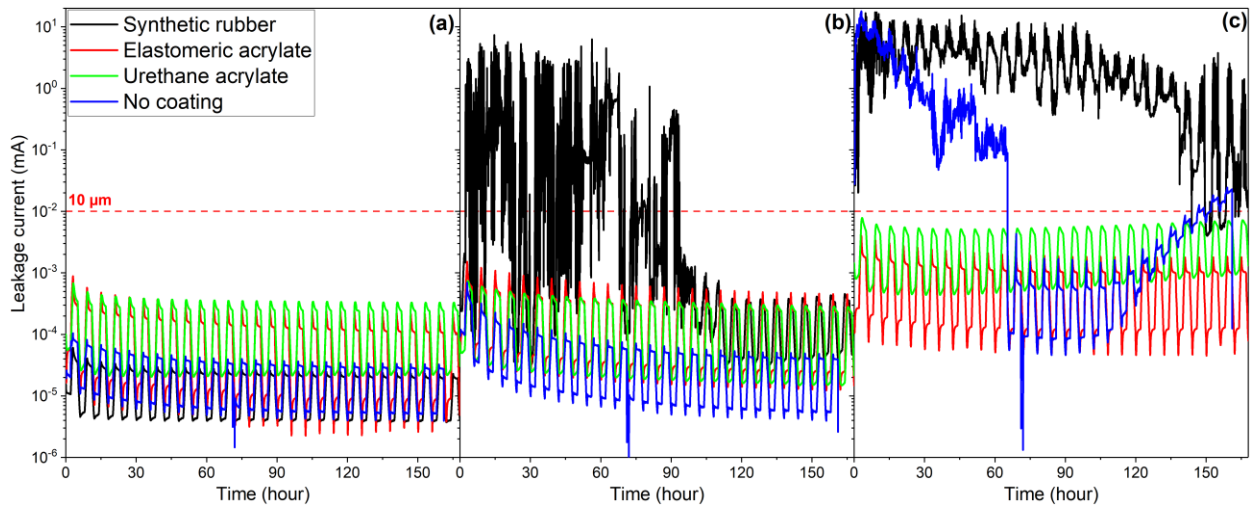
Figure 9.7 *Representative leakage current response of test vehicles for 7 days period under 5 V DC loading: (a) flux free, (b) Flux A, and (c) Flux B*

Table 9.3 *Summary of the short circuit failure rate of coated samples.*

Coatings	ContamiNFtion	Time to failure (hour)	Failure rate
	Flux A	2.3/4.2/28.8/5.3/10.5/15.8	100%
Synthetic rubber	Flux B	0.8/2.9/0.48/1.1/1.2/0.7	100%
	No flux	NF/NF/NF/NF/NF/NF	0%
	Flux A	NF/NF/NF/NF/NF/NF	0%
Elastomeric acrylate	Flux B	NF/NF/NF/NF/NF/NF	0%
	No flux	NF/NF/NF/NF/NF/NF	0%
	Flux A	NF/NF/NF/NF/NF/NF	0%
Urethane/acrylate	Flux B	NF/NF/NF/NF/NF/NF	0%
	No flux	NF/NF/NF/NF/NF/NF	0%

c) Surface and cross-section appearance of the coated samples after climatic testing

Figure 9.8 shows a general appearance of the conformal coating after climatic cycling test and the corrosion conditions of the interdigitated SIR pattern. Significant blisters can be seen on the the synthetic rubber coated PCBs with or without flux residue (**Figure 9.8**(a1-a3)), while no significant change was observed for elastomeric acrylate (**Figure 9.8**(b1-b3)). Urethane acrylate coating with Flux B residue shown in **Figure 9.8**(c2) exhibited a milky appearance after climatic cyclic test. In the case of Flux B contained samples, slight corrosion was observed in the elastomeric acrylate coated sample (**Figure 9.8**(b3)). On contrast, the synthetic rubber and urethane acrylate coated samples, severe corrosion was observed (**Figure 9.8**(a3)(c3)). For the

Flux A contained samples, pitting corrosion was observed on every second pitch lines of urethane acrylate coated samples (**Figure 9.8**(c2)), whereas short circuiting was observed in synthetic rubber coated sample (**Figure 9.8**(a2)).
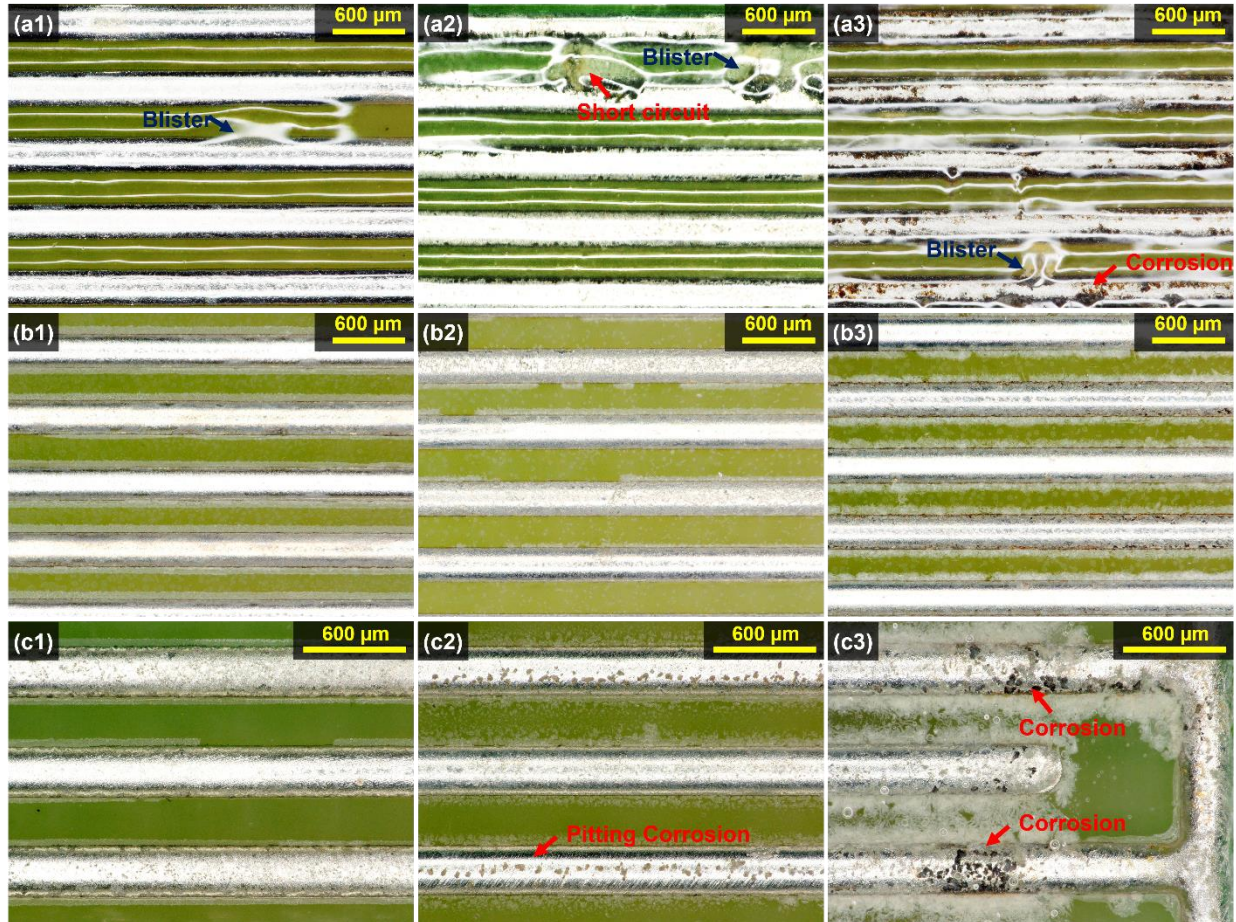
Figure 9.8 *LOM inspection of conformal coatings on SIR pattern after climatic testing: (a) synthetic rubber, (b) elastomeric acrylate, (c) urethane acrylate with the contamination condition of (1) flux free, (2) Flux A, and (3) Flux B.*

Figure 9.9 shows the SEM pictures of the morphology of conformal coatings after climatic exposure. In general for synthetic rubber and urethane acrylate coated samples, the defects induced by Flux B (**Figure 9.9**(a3)(c3)) were more pronounced than Flux A (**Figure 9.9**(a2)(c2)). Small cracking were obtained in the urethane acrylate coated sample shown in **Figure 9.9**(c2). However, no significant micro blisters was observed in the case of elastomeric acrylate coated samples. The size of the micro blister could be ranked as: synthetic rubber > urethane acrylate > elastomeric acrylate.
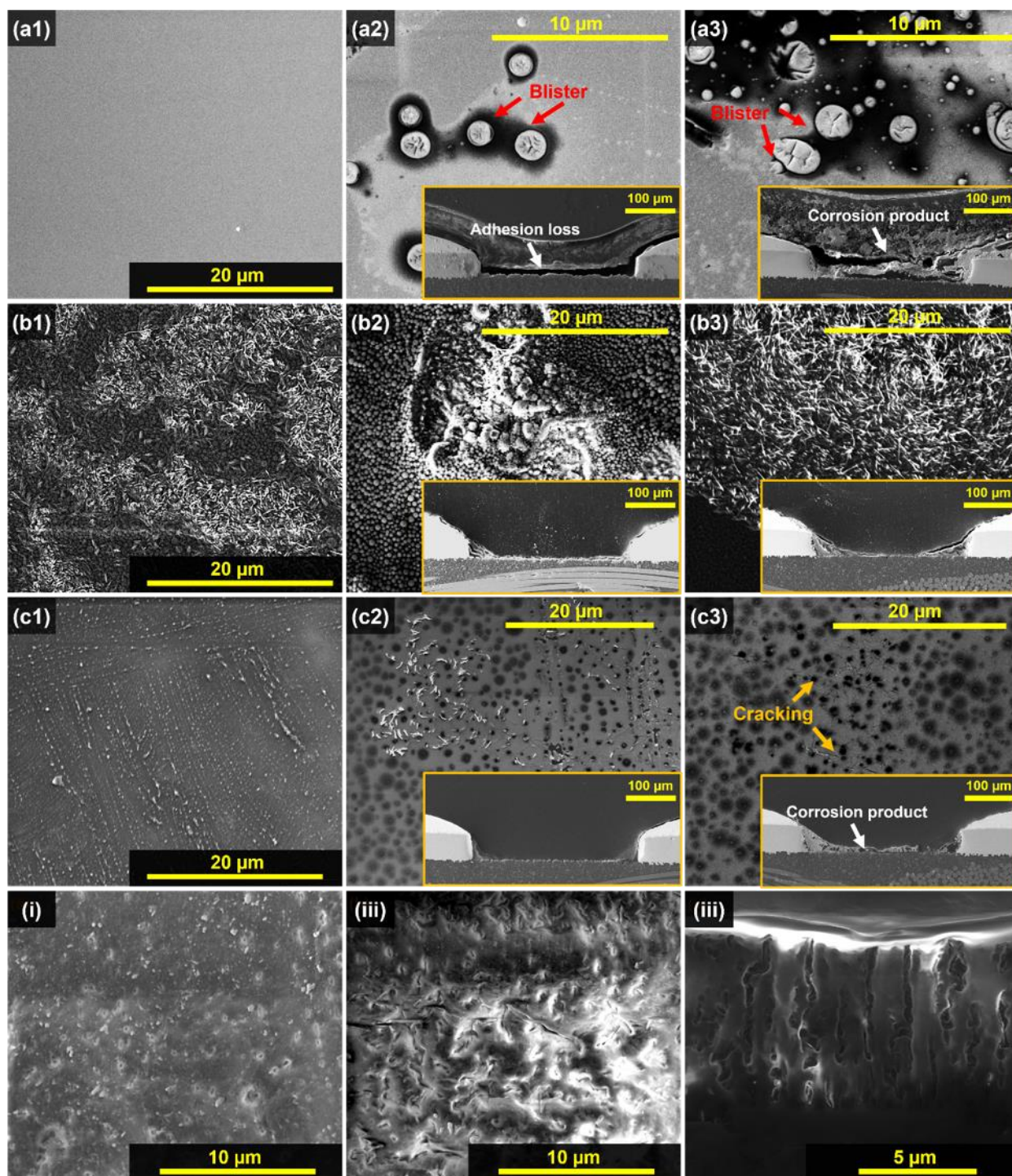
Figure 9.9 *Secondary electron micrographs of conformal coatings and cross-section of SIR pattern after climatic testing: (a) synthetic rubber, (b) elastomeric acrylate, (c) urethane acrylate with the contamination condition of (1) flux free, (2) Flux A, and (3) Flux B. and the cross-section of the Flux B contained test vehicles with (i) Urethane acrylate coating before climatic testing, (ii) Urethane acrylate after climatic testing, (iii) synthetic rubber after climatic testing.*

Figure 9.9 also shows the cross-sections of the coating after testing showing adhesion loss. Synthetic rubber showed poor adhesion (**Figure 9.9**(a2)(a3)) with severe corrosion attack underneath for Flux B residue sample bridging the gap (**Figure 9.9**(a3)). Good adhesion was confirmed in the case of elastomeric acrylate coated flux contaminated samples, as shown in **Figure 9.9**(b2)(b3). For urethane acrylate coated samples, corrosion product was only observed in the flux B case (**Figure 9.9**(c3)). The corrosion product was originated from anode and grow towards cathode along the interface between PCB substrate and urethane acrylate coating. The climatic exposure also changed the morphology of the coating, as shown in the cross-sectional **Figure 9.9(i-iii).** Before climatic exposure, the urethane acrylate coating was dense as shown in **Figure 9.9**(i). However, capillary channels were observed for the urethane acrylate coating on the Flux B contained test vehicle after climatic exposure (**Figure 9.9**(ii)). Similarly, capillary channels for the water transport were formed on synthetic rubber coated Flux B residue contained samples after climatic exposure (**Figure 9.9**(iii)).

For the case of urethane acrylate coated Flux B residue contained sample, EDS mapping result in **Figure 9.10** shows that the corrosion product bridged two electrodes and the corrosion product contains Sn and O with carbon resulting from the coating and Si is from the glass fiber of the PCB substrate.
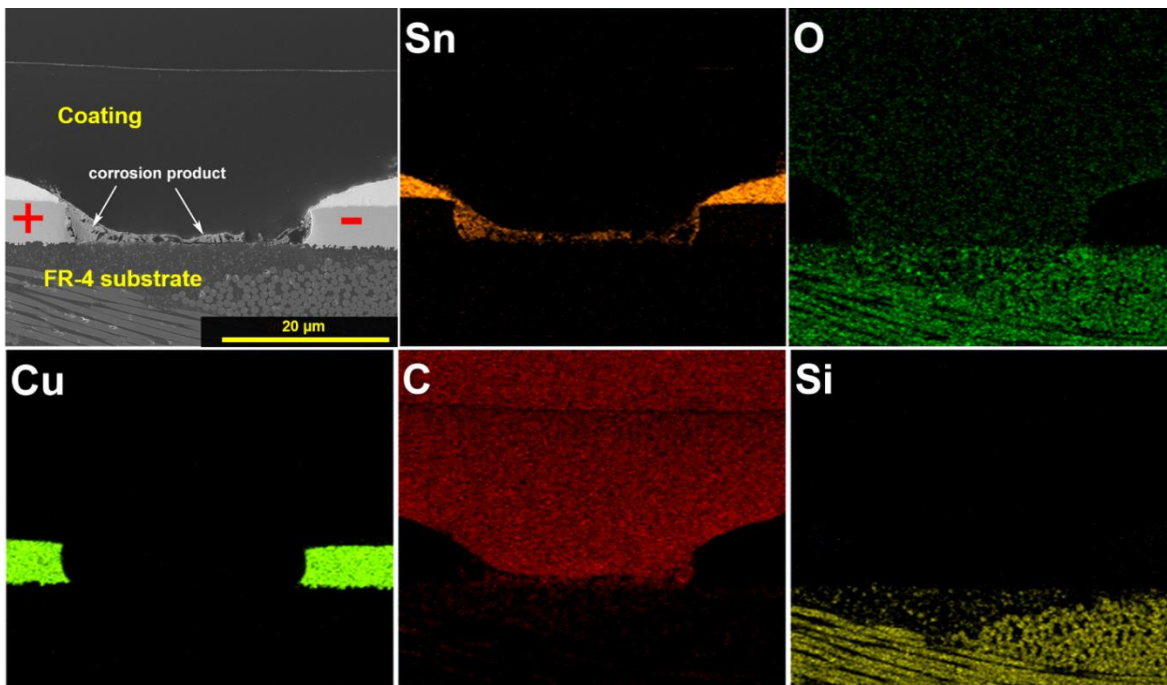
Figure 9.10 *EDS mappling of urethane acrylate coated test vehicle with Flux B residue (cross-sectional view)*

Figure 9.11 shows the FT-IR spectra of conformal coatings before and after climatic exposure. The shaded region in the range of 3000-3700 cm^{-1} indicates the O-H stretching peak of water absorbed in the coatings due to hydrolysis. No change was found from the spectra of three types of the coatings in the shaded region, which indicate that within the exposure time moisture absorption did not result in non-reversible effects involving reaction of water molecules with coating. The spectra of three types of coating maintained the same absorption nature climatic testing.
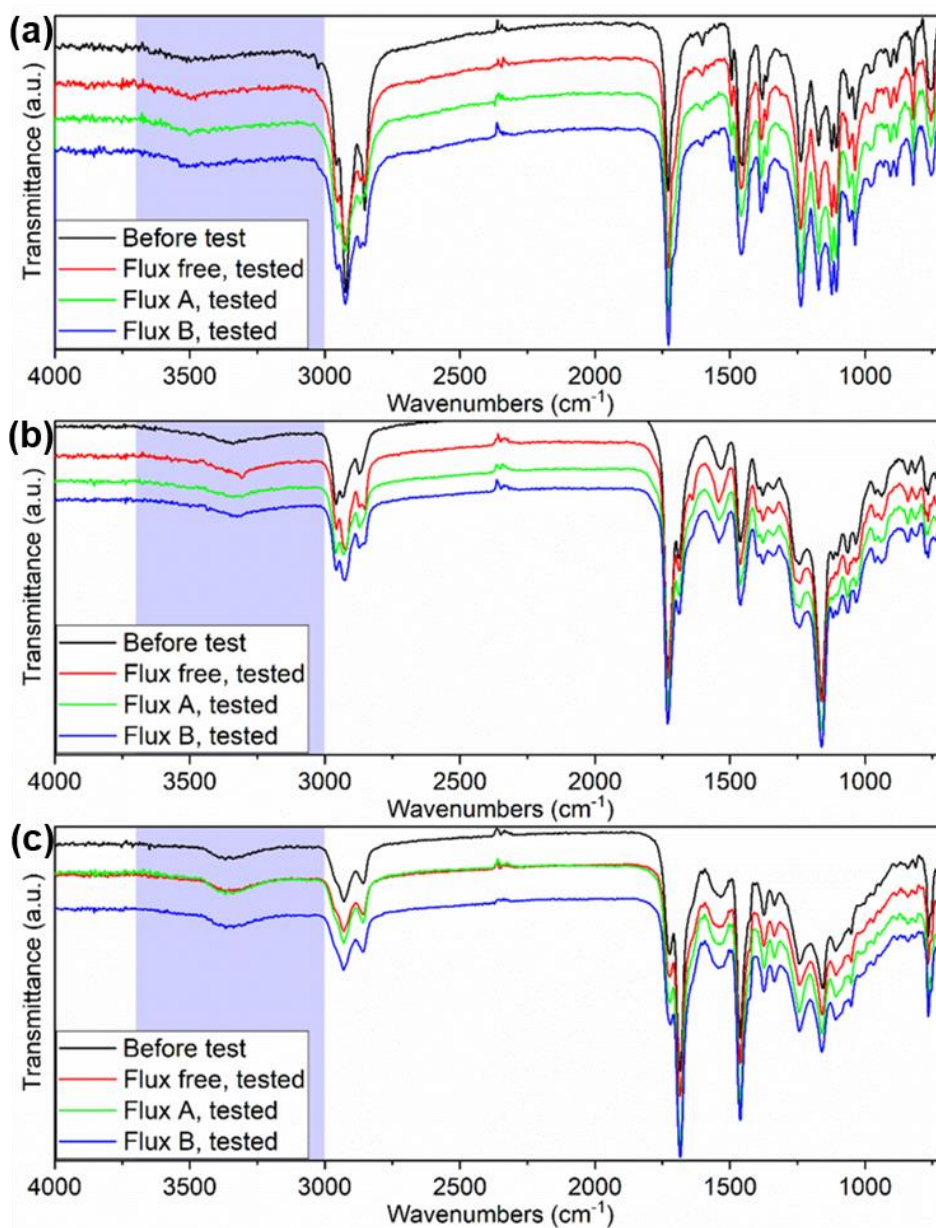
Figure 9.11 *FT-IR spectra of conformal coatings before and after climatic exposure: (a) synthetic rubber, (b) elastomeric acrylate, (c) urethane acrylate.*

IV.   DISCUSSION

Polymer conformal coatings used for PCBA applications are comparatively thin with not more than 150 μm thick. Therefore, moisture barrier properties for such coatings are limited as even the coating with lowest moisture diffusion coefficients can saturate the coatings within a short interval of time. Hence conformal nature of the coatings, and more importantly the adhesion to the PCBA surface is key factor determining its performance. Similar to any other substrate-coating interface, good adhesion ensure no delamination even if the coating saturate with moisture. Hygroscopic residues degrade the coating adhesion and allow water film build up at the interface due to deliquescence. Hence, the cleanliness of PCBAs is the most important factor for the performance of the conformation coating.

Present work clearly shows that flux free SIR pattern coated with conformal coating (irrespective of the type of conformal coating) possessed the highest impedance during moisture absorption as shown in **Figure 9.5**(a), and lowest leakage current as shown in **Figure 9.7**(a). With the flux residue contamination, elastomeric acrylate coating showed best performance because of the good adhesion at interface even with flux residues. However, the failure modes of the other three type of coated are different due to the adhesion issue due to flux residue, whereas the moisture barrier properties has minor impact for the performance of conformal coatings used in the present investigation.

The moisture barrier properties of the coating depend upon the humidity diffusion speed for the coatings. Tencer reported that the humidity equilibrium time in 1 cm thick polyurethane takes less than a week, which can be expressed by **Equation 9.2** [44]. τ indicates time constant for humidity ingress, L is thickness of the polymer, D is the diffusion coefficient (10^{-6} cm^2/s for polyurethane). From the equation, as an example, it is possible to estimate the time of humidity ingress for the urethane acrylate coating used in present work is less than 0.5 hour, which indicates that EIS signal reached to the humidity equilibrium stage over 2 hours of water absorption period and 2 hours releasing period in **Figure 9.2**. Therefore, impedance response was stabilized under water uptake stages (65°C) and water releasing stages (40°C) as shown in **Figure 9.4**.

$$\tau = \frac{L^2}{2D} \quad \textit{Equation 9.2}$$

<u>Role of the flux residue on the protection performance of the conformal coating</u>

Practically, the flux deposition level of 155-1550 μg/cm^2 were used in the electronic manufacturing process [45], which is comparable to the flux deposition level used in the present work, although after activation process, the level of residue on the PCBA surface can be lower. The flux used in

the present work contained glutaric acid and adipic acid, which possessed the boiling temperature of 273°C and 337.5°C respectively [15]. In actual electronic manufacturing process, the peak soldering temperature of the PCBA was between 235-245°C [46], which is not able to decompose or evaporate the glutaric acid and adipic acid in the flux residue. Therefore, the flux residue in the present work obtained similar chemical character as the flux residue from the manufacturing process. The gluraric acid in Flux B possessed higher hygroscopicity and solubility than adipic acid in Flux A, which triggers the water condensation at lower RH level and the formation of conductive path between electrodes [17]. In this work, the behavior of hygroscopicity and corrosivity of two types of flux residues was confirmed by the test on non-coated SIR pattern. The threshold leakage current value for the IPC-B-24 SIR pattern was define as 1-10 µA due to the ECM dendrite formation [47][48]. After 7 days DC testing, the leakage current induced by Flux A did not exceed the threshold value of 10 µA (**Figure 9.7**(b)), which indicates the flux A residue with adipic acid is benign from the corrosion point of view. However, the SIR pattern with glutaric acid contained Flux B residue exhibited high leakage current in mA level as shown in **Figure 9.7**(c), which indicates the higher hygroscopicity and corrosivity.

The WOAs can diffuse through the conformal coating under humid condition [37], which influence the impedance and leakage current of the flux residue contained test vehicles. The condensed water diffused through the conformal coating [49], which dissolved the WOAs at the PCB-coating interface to form the conductive media between interdigitated SIR electrodes. Under such condition, the electrical property of the coated test vehicle with Flux B residue transferred from capacitive nature to resistive in the EIS spectra within a frequency range over 10 KHz (**Figure 9.4**(c)), which is similar to water condensation on the PCBA [50]. For the coated test vehicles, the higher hygroscopicity and higher solubility of the glutaric acid contained flux B residue induced the lowest impedance value of the SIR pattern, which shows that in the second climatic cycle (**Figure 9.4**(c)). Over 5 days of cyclic climatic exposure, the impedance for the flux residue contained test vehicle increased due to the dilution of WOA by water condensation during of every climatic cycling as shown in **Figure 9.5**(b)(c); however, the dilution of WOA did not increase the impedance of flux residue contained test vehicles to the clean level (**Figure 9.5**(a)). In consequence, the high hygroscopic and ionic behavior of Flux B induced the higher leakage current values as shown in **Figure 9.7**(c) compared to coated flux free and mild Flux A contained test vehicles. Therefore, more corrosion pits were observed on the flux B contaminated SIR pattern as shown in **Figure 9.8**(a3)(b3)(c3). After DC leakage current measurement, significant increase of impedance response was obtained for all types of coating with flux contained SIR pattern as shown in **Figure 9.5**(b)(c), which could be attributed to the dilution of the flux residue

with repeated condensation and drying cycle making it to move around as well as leach out. On the other hand, the water absorption behavior of conformal coating was influenced by the flux residue. Under testing temperature of 40°C and 60°C, the deliquescence RH of adipic acid used in Flux A was 91.5% RH and 83.2% RH respectively, whereas the deliquescence RH of glutaric acid used in Flux B was 73.9% RH and 81.3% RH respectively [17]. Therefore, more water absorption was expected in the coated samples with flux residue than the coated flux free samples as shown in **Figure 9.6**, which induced higher stress in the conformal coating. This result in blister formation as shown in **Figure 9.9**(a2-3)(c2-3), while the capillary channel was formed in the cross-section of the coating for the water transportation (**Figure 9.9**(ii)(iii)). However, compared to coated clean SIR pattern shown in **Figure 9.6**(a), less hygroscopic Flux A residue contained test vehicle shows similar level of volume fraction of water in coatings (**Figure 9.6**(b)). In comparison, higher volume fraction of water in coating was obtained for the same type of coating with glutaric acid contained Flux B residue as shown in **Figure 9.6**(c). Due to higher solubility of glutaric acid, Flux B released more free ions in solution compared to the adipic acid in Flux A. According to **Equation 9.2**, the water volume fraction in coating is proportional to normalized capacitance, whereas the capacitance is proportional to the square root of ion concentration near the potential of zero charge [51]. Therefore, solubility and ionization of the WOA at PCB-coating interface influenced the water uptake in the coating. Over 5 days cyclic climatic exposure, the trend of the volume fraction of water for the flux residue contained test vehicle with same type of coating maintained at the same level as shown in **Figure 9.6**(b)(c), which could be attributed to the constant coating thickness for water uptake and the constant ion concentration due to WOA dissolution.

Corrosion protection performance assessment of the conformal coatings

Adhesion of the coating played a vital role on the protection performance of coating. The elastomeric acrylate and urethane acrylate coatings provide a barrier for the water film formation between electrode since the gap between electrodes was filled by conformal coatings, shown in **Figure 9.9**(b2-3)(c2-3). Comparatively, good adhesion of the elastomeric acrylate and urethane acrylate coating resulted in high impedance (**Figure 9.5**(b)(c)) and low leakage current (**Figure 9.6**(b)(c)) of flux residue contained test vehicles. However, adhesion of synthetic rubber with FR-4 laminate was not good as shown in **Figure 9.3**(a1). The gap formed between FR-4 substrate and synthetic rubber coating resulted the water accumulation and dissolution of the WOA, which induced corrosion failure. Due to the lag of moisture diffusion through the coating, the conductive electrolyte formed in the gap took longer time to be dried during climatic cycle compared to the non-coated test vehicles. Therefore, impedance value of synthetic rubber coated Flux A

contaminated SIR was lower than non-coated Flux A contained SIR pattern (**Figure 9.5**(b)). Under DC loading, the conductive electrolyte beneath the synthetic rubber coating bridged two oppositely bias electrode in the poor adhesion region as shown in **Figure 9.9**(a2), which induced a very high leakage current and short circuit (**Figure 9.7**(b) and **Figure 9.8**(b)). The formation of the corrosion product in **Figure 9.9**(a3) could be due to ECM, since the corrosion cell formed at the gap of the PCB-coating interface [52]. To sum up, the corrosion cell formation in the poor adhesion region and the lag of moisture diffusion resulted 100% failure rate of flux residue contained synthetic rubber coated SIR pattern (**Table 9.3**).

The compatibility of conformal coating and no-clean flux residue also influenced the performance of adhesion. **Figure 9.9**(b2) and (c2) show the good compatibility between elastomeric acrylate/urethane acrylate coatings and Flux A. However, the adhesion loss of urethane acrylate coating was observed in the Flux B contained test vehicle. Even though the leakage current for urethane acrylate coated SIR pattern in **Figure 9.7**(c) maintained a low value, the corrosion product presented at the PCB-urethane acrylate coating interface and initiated the tendency for short circuit failure as shown in the cross section image (**Figure 9.9**(c3)). Therefore, the leakage current measurement cannot be used as a sole assessment method without inspection of corrosion product for understanding the performance.

The impedance response at 100 mHz from EIS measurement (**Figure 9.5**) agreed the DC leakage current results shown in **Figure 9.7**. Compared to the DC testing, EIS results suggests that it is faster to make relative comparison of the conformal coating and it can provide better information on the kinetics of humidity transport through the coatings. However, the EIS method cannot evaluate the real failure mechanism. The impedance response of synthetic rubber coated Flux A contained SIR pattern (**Figure 9.5**(b)) was higher than urethane acrylate coated flux B contaminated SIR pattern (**Figure 9.5**(c)). However, urethane acrylate coated sample passed the DC testing (**Figure 9.6**(b)), whereas synthetic rubber coated Flux B contained sample failed (**Figure 9.7**(c)). Combined assessment using both techniques shows the importance of DC testing for the prediction of corrosion failures in the coated PCBA.

V.   CONCLUSIONS

- EIS measurement shows that moisture diffusion through the coating only has minor impact on the performance of conformation coating. Results also showed that the coatings with flux residue showed lower impedance due to the absorption moisture by the residue, which accelerated the failure of the coating.

- High impedance and low leakage current of coated clean SIR pattern suggest that the cleanliness is the key factor for the protection from conformal coatings . Together with cleanliness, compatibility of the coating with flux residue resulting in good adhesion results in better performance as found for elastomeric acrylate coating.

- Synthetic rubber coating is not suitable for the flux residue contaminated PCBA application due to poor adhesion. The corrosion cell formed in the blister due to the water diffusion and dissolution of ionic flux residue, which lead to the ECM failures with 100% failure rate.

- Low leakage current and high impedance was obtained for urethane acrylate coating with flux residue, however cross-sectional examination showed delamination and growth conductive corrosion products, which could have resulted in failure during extended exposure.

VI.   REFERENCES

[1]   K. Feldmann, J. Franke, F. Schüßler, Development of micro assembly processes for further miniaturization in electronics production, CIRP Ann. 59 (2010) 1–4. doi:https://doi.org/10.1016/j.cirp.2010.03.005.

[2]   H.M.B. Bird, S. Member, Approaches to Electronic Miniaturization, 18 (1995) 18–22.

[3]   R. Ambat, H. Conseil-Gudla, Improving intrinsic corrosion reliability of printed circuit board assembly, in: 2016 IEEE 18th Electron. Packag. Technol. Conf., 2016: pp. 540–544. doi:10.1109/EPTC.2016.7861538.

[4]   K.S. Hansen, M.S. Jellesen, P. Moller, P.J.S. Westermann, R. Ambat, Effect of solder flux residues on corrosion of electronics, in: 2009 Annu. Reliab. Maintainab. Symp., 2009: pp. 502–508. doi:10.1109/RAMS.2009.4914727.

[5]   M.S. Jellesen, D. Minzari, U. Rathinavelu, P. Moller, R. Ambat, Corrosion in Electronics at Device Level, ECS Trans. 25 (2010) 1–14. doi:10.1149/1.3321952.

[6]   D. Minzari, M.S. Jellesen, P. Møller, R. Ambat, Morphological study of silver corrosion in highly aggressive sulfur environments, Eng. Fail. Anal. 18 (2011) 2126–2136. doi:10.1016/j.engfailanal.2011.07.003.

[7]   H. Conseil, V.C. Gudla, M.S. Jellesen, R. Ambat, Humidity Build-Up in a Typical Electronic Enclosure Exposed to Cycling Conditions and Effect on Corrosion Reliability, IEEE Trans. Components, Packag. Manuf. Technol. 6 (2016) 1379–1388. doi:10.1109/TCPMT.2016.2590779.

[8]   S. Joshy, M. Jellesen, R. Ambat, Effect of interior geometry on local climate inside an electronic device enclosure, in: 2017 16th IEEE Intersoc. Conf. Therm. Thermomechanical Phenom. Electron. Syst., 2017: pp. 779–783. doi:10.1109/ITHERM.2017.7992565.

[9]   M. Pecht, E.M. Bumiller, D.A. Douthit, J. Pecht, Contamination of Electronic Assemblies, Tylor & Francis Group, 2002.

[10]   S.J. Krumbein, Electrolytic models for metallic electromigration failure mechanisms, IEEE Trans. Reliab. 44 (1995) 539–549. doi:10.1109/24.475971.

[11]   H. Conseil, M.S. Jellesen, R. Ambat, Contamination profile on typical printed circuit board assemblies vs soldering process, Solder. Surf. Mt. Technol. 26 (2014) 194–202. doi:10.1108/SSMT-03-2014-0007.

[12]   M.S. Jellesen, D. Minzari, U. Rathinavelu, P. Møller, R. Ambat, Corrosion failure due to flux residues in an electronic add-on device, Eng. Fail. Anal. 17 (2010) 1263–1272. doi:10.1016/j.engfailanal.2010.02.010.

[13]   D. Xu, X. Li, C. Wang, B. Xu, Study on wettability and corrosivity of a new no-clean flux for lead-free solder paste in electronic packaging technology, in: 2011 Second Int. Conf. Mech. Autom. Control Eng., 2011: pp. 1706–1708. doi:10.1109/MACE.2011.5987285.

[14]   K. Piotrowska, M.S. Jellesen, R. Ambat, Thermal decomposition of solder flux activators under simulated wave soldering conditions, Solder. Surf. Mt. Technol. 29 (2017) 133–143. doi:10.1108/SSMT-01-2017-0003.

[15]   V. Verdingovas, M.S. Jellesen, R. Ambat, Solder Flux Residues and Humidity-Related Failures in Electronics: Relative Effects of Weak Organic Acids Used in No-Clean Flux Systems, J. Electron. Mater. 44 (2015) 1116–1127. doi:10.1007/s11664-014-3609-0.

[16]   S. Zhan, M.H. Azarian, M.G. Pecht, Surface insulation resistance of conformally coated printed circuit boards processed with no-clean flux, IEEE Trans. Electron. Packag. Manuf. 29 (2006) 217–223. doi:10.1109/TEPM.2006.882496.

[17]   K. Piotrowska, R. Ud Din, F.B. Grumsen, M.S. Jellesen, R. Ambat, Parametric Study of Solder Flux Hygroscopicity: Impact of Weak Organic Acids on Water Layer Formation and Corrosion of Electronics, J. Electron. Mater. 47 (2018) 4190–4207. doi:10.1007/s11664-018-6311-9.

[18]   V. Vadimas, J. Salil, J.M. Stendahl, A. Rajan, Analysis of surface insulation resistance related failures in electronics by circuit simulation, Circuit World. 43 (2017) 45–55. doi:10.1108/CW-09-2016-0040.

[19]   X. Zhong, G. Zhang, Y. Qiu, Z. Chen, X. Guo, Electrochemical migration of tin in thin electrolyte layer containing chloride ions, Corros. Sci. 74 (2013) 71–82. doi:10.1016/J.CORSCI.2013.04.015.

[20]   B. Medgyes, B. Horváth, B. Illés, T. Shinohara, A. Tahara, G. Harsányi, O. Krammer, Microstructure and elemental composition of electrochemically formed dendrites on lead-free micro-alloyed low Ag solder alloys used in electronics, Corros. Sci. 92 (2015) 43–47. doi:10.1016/J.CORSCI.2014.11.004.

[21]   D. Minzari, M.S. Jellesen, P. Møller, R. Ambat, On the electrochemical migration mechanism of tin in electronics, Corros. Sci. 53 (2011) 3366–3379. doi:10.1016/j.corsci.2011.06.015.

[22]   D. Minzari, F.B. Grumsen, M.S. Jellesen, P. Møller, R. Ambat, Electrochemical migration of tin in electronics and microstructure of the dendrites, Corros. Sci. 53 (2011) 1659–1669. doi:10.1016/J.CORSCI.2011.01.009.

[23]   H. Conseil-Gudla, M.S. Jellesen, R. Ambat, Printed Circuit Board Surface Finish and Effects of Chloride Contamination, Electric Field, and Humidity on Corrosion Reliability, J. Electron. Mater. 46 (2017) 817–825. doi:10.1007/s11664-016-4974-7.

[24]   R. W.J., S. S.R., F. G.B., L.L., T. L.J., Microstructure of Conductive Anodic Filaments Formed during Accelerated Testing of Printed Wiring Boards, Circuit World. 21 (1995) 5–

9. doi:10.1108/eb044042.

[25] W.J. Ready, L.J. Turbini, R. Nickel, J. Fischer, A novel test circuit for automatically detecting electrochemical migration and conductive anodic filament formation, J. Electron. Mater. 28 (1999) 1158–1163. doi:10.1007/s11664-999-0151-6.

[26] D. Yun Chen, M. Osterman, Reliability of conformal coated surface mount packages, in: 2016 IEEE Accel. Stress Test. Reliab. Conf., 2016: pp. 1–5. doi:10.1109/ASTR.2016.7762293.

[27] M. Osterman, Effectiveness of Conformal Coat to Prevent Corrosion of Nickel-palladium-goldfinished Terminals, in: IPC APEX EXPO Conf. Proc., 2014.

[28] X. Shao, X. Chen, X. Yu, Y. Hu, L. Liu, F. Shi, W. Shao, J. Mo, Nondestructive Measurement of Conformal Coating Thickness on Printed Circuit Board With Ultra-High Resolution Optical Coherence Tomography, IEEE Access. 7 (2019) 18138–18145. doi:10.1109/ACCESS.2019.2896622.

[29] P. Dobriyal, S. Ramalingam, S.L. Lim, A. Kurella, Conformal coating challenges: Detection, rework and failure analysis, in: 2016 Pan Pacific Microelectron. Symp. (Pan Pacific), 2016: pp. 1–6. doi:10.1109/PanPacific.2016.7428411.

[30] IPC-CC-830C Qualification and Performance of Electrical Insulating Compound for Printed Wiring Assemblies, HIS Inc, Illinois, USA, 2018.

[31] U. Rathinavelu, M.S. Jellesen, P. Moller, R. Ambat, Effect of No-Clean Flux Residues on the Performance of Acrylic Conformal Coating in Aggressive Environments, IEEE Trans. Components, Packag. Manuf. Technol. 2 (2012) 719–728. doi:10.1109/TCPMT.2012.2186456.

[32] S. Michal, AFM-assisted investigation of conformal coatings in electronics, Anti-Corrosion Methods Mater. 63 (2016) 289–294. doi:10.1108/ACMM-09-2014-1426.

[33] H. Hal, Conformal coating removal techniques, Circuit World. 24 (1998) 13–19. doi:10.1108/030561201998000002.

[34] M. Cole, L. Hedlund, G. Hutt, T. Kiraly, L. Klein, S. Nickel, P. Singh, T. Tofil, Harsh environment impact on resistor reliability, in: SMTA Int. Conf., Orlando, USA, 2010.

[35] L. Zou, C. Hunt, Test Method for Conformal Coating Protection Performance of Electronic Assembly in Harsh Environments (NPL Report DEPC MPR 060), Teddington, Middlesex, 2007.

[36] K. Seelig, T. O'Neill, Conformal Coating over No-Clean Flux, SMT Surf. Mt. Technol. 29 (2014) 52–64.

[37] C. Hunt, A. Mensah, A. Buxton, R. Holman, Determining conformal coating protection, Solder. Surf. Mt. Technol. 18 (2006) 38–47. doi:10.1108/09540910610717893.

[38] U. Rathinavelu, M.S. Jellesen, R. Ambat, Effect of solder flux residue on the performance of silicone conformal coatings on printed circuit board assemblies, Corros. Eng. Sci. Technol. 48 (2013) 436–444. doi:10.1179/1743278213Y.0000000096.

[39] F.E. Bedoya-Lora, F. Echeverría, J.A. Calderón, Effectiveness of non-Fickian diffusion model on the water uptake determination of different organic coatings, Prog. Org. Coatings. 136 (2019) 105206. doi:https://doi.org/10.1016/j.porgcoat.2019.06.052.

[40] D.I. Njoku, M. Cui, H. Xiao, B. Shang, Y. Li, Understanding the anticorrosive protective mechanisms of modified epoxy coatings with improved barrier, active and self-healing functionalities: EIS and spectroscopic techniques, Sci. Rep. 7 (2017) 15597. doi:10.1038/s41598-017-15845-0.

[41] X. Liu, J. Xiong, Y. Lv, Y. Zuo, Study on corrosion electrochemical behavior of several different coating systems by EIS, Prog. Org. Coatings. 64 (2009) 497–503. doi:https://doi.org/10.1016/j.porgcoat.2008.08.012.

[42] D.M. Brasher, A.H. Kingsbury, Electrical measurements in the study of immersed paint coatings on metal. I. Comparison between capacitance and gravimetric methods of estimating water-uptake, J. Appl. Chem. 4 (1954) 67–72.

[43] G. Bierwagen, D. Tallman, J. Li, L. He, C. Jeffcoate, EIS studies of coated metals in accelerated exposure, Prog. Org. Coatings. 46 (2003) 149–158. doi:https://doi.org/10.1016/S0300-9440(02)00222-9.

[44] M. Tencer, Conductive aqueous layer formation at the gel-substrate interface in equilibrium with 100% RH environment, IEEE Trans. Components Packag. Technol. 23 (2000) 693–699. doi:10.1109/6144.888855.

[45] J.E. Sohn, U. Ray, Weak Organic Acids and Surface Insulation Resistance, Circuit World. 21 (1995) 22–26. doi:10.1108/eb044046.

[46] S.K. Kang, D.-Y. Shih, D. Leonard, D.W. Henderson, T. Gosselin, S. Cho, J. Yu, W.K. Choi, Controlling Ag3Sn plate formation in near-ternary-eutectic Sn-Ag-Cu solder by minor Zn alloying, JOM. 56 (2004) 34. doi:10.1007/s11837-004-0108-4.

[47] K. Piotrowska, M.S. Jellesen, R. Ambat, Water film formation on the PCBA surface and failure occurrence in electronics, in: 2018 IMAPS Nord. Conf. Microelectron. Packag., 2018: pp. 72–76. doi:10.23919/NORDPAC.2018.8423854.

[48] V. Verdingovas, M.S. Jellesen, R. Ambat, Relative effect of solder flux chemistry on the humidity related failures in electronics, Solder. Surf. Mt. Technol. 27 (2015) 146–156. doi:10.1108/SSMT-11-2014-0022.

[49] S. Manfred, Conformal coatings and their increasing importance for a safe operation of electronic assemblies, Circuit World. 33 (2007) 60–67. doi:10.1108/03056120710836954.

[50] S. Lauser, T. Richter, V. Vadimas, R. Ambat, Electrochemical Impedance Spectroscopy (EIS) for Monitoring the Water Load on PCBAs Under Cycling Condensing Conditions to Predict Electrochemical Migration Under DC Loads, in: 2019 IEEE 69th Electron. Components Technol. Conf., 2019: pp. 515–521. doi:10.1109/ECTC.2019.00084.

[51] B. Uralcan, I.A. Aksay, P.G. Debenedetti, D.T. Limmer, Concentration Fluctuations and Capacitive Response in Dense Ionic Solutions, J. Phys. Chem. Lett. 7 (2016) 2333–2338. doi:10.1021/acs.jpclett.6b00859.

[52] X. Zhong, G. Zhang, Y. Qiu, Z. Chen, W. Zou, X. Guo, In situ study the dependence of electrochemical migration of tin on chloride, Electrochem. Commun. 27 (2013) 63–68. doi:https://doi.org/10.1016/j.elecom.2012.11.010.

10. Overall discussion

This chapter provides an overall discussion of the results presented in the appended papers with a view of the overall goal of the project and application of the results in relation with humidity effects on electronics. Commercially used WOA flux activators played a vital role on the water condensation and corrosion problems due to the hygroscopic and ionic nature. The combined results from various activities in this project related to new activators compared the solderability and humidity robustness of organic amine, amino acids, and blend WOA-amine based flux activators in comparison with conventional WOA activators. Results from the investigations demonstrate the synergistic impact of the flux activators on humidity related reliability issues on electronics.

Contamination level in the condensed water was considered as the most effective impact on the time to ECM failure of SAC solder alloys. Chapter 4 shows the climatic reliability of SAC alloy was influenced by the elemental composition, and phase constitution and phase distribution in the bulk material under the same testing condition. ECM susceptibility illustrates the climatic reliability or corrosion reliability of solder alloys under actual service conditions with voltage bias loading. The ECM susceptibility of the SAC alloys bulk materials from water droplet testing and the reflow soldered SIR interdigitated pattern from accelerated climatic testing agreed with the corrosion current density obtained from the potentiodynamic polarization results. The passivation domain of SAC alloys from potential dynamic polarization testing is non-relevant to ECM susceptibility. Result indicates that the SAC alloys with more uniform microstructure obtained the best performance on the ECM susceptibility. To optimize the microstructure of the SAC, additivessuch as Ni, Sb and Bi additives were used during alloy manufacturing. As a consequence, new phases such as pure Bi phase and (Sn, Sb) solid solution were introduced to the microstructure of InnoLot alloy, which influenced the micro-galvanic corrosion mechanism of the SAC alloy. Pure Bi phase acted as the cathodic site during corrosion instead of Ag_3Sn IMCs as know before, whereas (Sn, Sb) solid solution acted as anode instead of β-Sn phase.

Combined results in the flux activator investigations from Chapter 5 exhibit the solderability of the tested organic amines are much less than WOA flux activators, which is either due to the lower boiling temperature or low activity of amino group under soldering condition. However, some tested amino acids in Chapter 6 and blend WOA-amine activators in Chapter 7 shows better solderability than commercial used WOA flux activators. The oxidation removal mechanism of organic amine, amino acids and WOAs are different. Under soldering condition, amino group in

organic amines and amino acids remove the CuO and Cu_2O due to redox reaction, which is different from the complexation and disproportionation reaction by the carboxylic group in WOA and amino acids. Chapter 5 demonstrates the reaction of metal oxides removal in aqueous amine solution is by protonation and complex formation, which is different from the reaction under soldering condition. One outcome from Chapter 5 is that the electrochemical analysis cannot be used for solderability assessment of amino group contained flux activators. Additionally, the relative lower wetting force of alkanolamine indicate that the hot plate spreading test cannot be solely used as the assessment method for solderability evaluation. Results in Chapter 6 demonstrate the solderability of the amino acid depends on the melting temperature, which is relevant to the prevention of the re-oxidation on the surface during the soldering condition. Compared to WOA activators, the higher wetting force obtained by tested amino acid could be attributed to the higher amount of zwitterions formation under soldering condition, which resulted in a more reactive positive charge group of $-NH3^+$ for oxide removal. The enhancement of the wetting speed of using amine additive in WOA activators was demonstrated in Chapter 7, which is due to the formation of more reactive $(R'CO)^+$ as well as $(R''NH)^-$ charge groups from the amide group in comparison with the carboxyl group in WOA activators under soldering process.

The humidity robustness of flux activator depends on water interaction with the function group under service condition, which affected by the critical RH for water condensation and the pH in electrolyte. The synergistic effect of hydroxyl group in alkanolamine and exposed humidity was demonstrated in Chapter 5, which resulted lower RH level for water condensation and ECM in comparison with commercial WOA activators. The hydroxyl group induced the water absorption due to intermolecular hydrogen bond formation. Similarly, Chapter 6 demonstrates the highest water absorption fraction was obtained by amino acid with hydroxyl group. Therefore, the flux activators with hydroxyl group are not suggested for the flux formulation from humidity robustness point of view. On the other hand, the active amino group in amino acids and organic amines significantly increased pH of electrolyte due to protonation, which triggered the formation of hydroxide ions for the neutralization of carboxyl groups. Consequently, the amino acids near pH neutral in Chapter 6 and the blend WOA-amine activators in Chapter 7 exhibit lower leakage current and high impedance response under high humidity exposure in comparison with commercial WOA flux activators. Moreover, chapter 8 shows the amine additive in the solder paste applications exhibited much lower leakage current during accelerated climatic test compared to the solder pastes using WOAs or halide activators.

For the SMT application in Chapter 8, flux activator used in reflow solder paste influenced the climatic reliability of SMD. Under harsh climatic exposure, the hygroscopic halide and binary blended WOAs activators promoted the water absorption in the encapsulation resin and accelerated the degradation of the resin polymer, which triggered the release of the ionic contaminations through the cracks and openings of the flux residue. Due to the hygroscopic and ionic nature of the flux activator, the flux residue presented between two opposite biased terminals start to absorb moisture, which generated a conductive path for the charge transfer between electrodes. By increasing the stand-off height of the SMT component, the decreased spreading area of the flux residue was due to the less presence of capillary effect beneath the component, and the flux free region was formed between electrodes as the barrier to enhance the SIR.

For the conformal coating protection of PCBA in Chapter 9, the moisture barrier property has minor impact in comparison with the adhesion due to the low thickness and the characteristic of water permeability. The cleanliness of the flux residue on the PCBA determines the performance of the conformal coatings. With the hygroscopic flux residue presented in the PCBA-coating interface, more water was absorbed in the coating, which lead to the stress crack on the coating after the cyclic climatic exposure. Under DC loads, the corrosion product was build up from the anodic terminals and grew toward adjacent cathodic terminal through the PCBA-coating interface. In the coating with poor adhesion, pocket was formed at the interphase for the water accumulation, which lead to the catastrophic ECM failure even if moderate flux residue presented at the interface. EIS is a non-destructive and rapid method for the analysis of water absorption and impedance change under climatic exposure, however DC testing and material characterization are mandatory for the corrosion failure analysis.

11. Overall conclusions

<u>SAC solder alloys in Chapter 4</u>

1) The additive element influenced the microstructure in the SAC alloy. More uniform phase distribution was obtained by the addition of Bi, Sb, and Ni in InnoLot alloy compared to conventional SAC 305 alloy. The difference of Ag content significantly influenced the microstructure homogeneity in the low Ag content alloys. More uniform microstructure was obtained for 0.05 wt.% Ni addition rather than for 0.1 wt.% Bi addition in the matrix of Sn - 0.8 wt.% Ag - 0.7 wt.% Cu alloy..

2) The corrosion reliability of SAC solder alloy is depend upon the homogeneity of microstructure and the phase constituents. Volta potential mapping result under ambient condition illustrated the galvanic coupling between cathodic Bi phase and anodic (Sn, Sb) solid solution in InnoLot alloy as well as cathodic Ag_3Sn IMCs and anodic β-Sn phase in the other four alloys. Pitting occurred preferentially on (Sn, Sb) solid solution adjacent of Bi phase in InnoLot alloy, while on β-Sn phase adjacent to Ag_3Sn IMCs in other four alloys.

3) ECM results from WD test and SIR comb pattern test confirmed the ECM failure agreed to the corrosion current density rather passivation domain of tested SAC solder alloy under 5 volt DC bias loading.

<u>Activators in wave solder flux in Chapter 5-7</u>

1) Solderability of the amino group contained flux activator depends on the boiling temperature, melting temperature, and activity of the functioning group for the oxides removal under soldering condition. The flux activator candidates with lower boiling temperature (EA and DEA, DIPA in Chapter 5) and higher melting temperature (Alanine in Chapter 6) are not able to protect the metal surface from re-oxidation. The activity of amino groups in alkanolamines resulted poor oxide removal under soldering condition compared to the commercial used adipic acid activator in Chapter 5, while the maximum wetting force of glutamine model flux was higher than adipic acid as shown in Chapter 6.

2) Hydroxyl group contained flux activators in Chapter 5-6 with relative higher boiling temperature induce water condensation at lower RH compared to commercial used WOA activators, which triggered higher leakage current and ECM dendrites formation. However, the increased testing temperature from 25 ℃ to 60 ℃ significantly decreased the leakage current induced by alkanolamines in Chapter 5. In addition, the leakage current and ECM occurrence were prohibited by the presence of amino group contained glutamine in Chapter 6.

3) The soldering properties depend on the reaction of amine additive and WOA flux activators. Both of tripropylamine and naphthylamine in Chapter 7 are able to form amides with succinic acids after flux formulation, while the adipic acid and amine additives did not form amide. Tripropylamine and naphthylamine additive in succinic acid based model improved of the wetting speed due to amide formation, whereas 0.2-0.4 wt.% tripropylamine additive in adipic acid based model fluxes significantly increased the maximum wetting force.

4) The amine additive used in Chapter 7 significantly increased the humidity robustness of WOA flux activator after soldering process. Tripropylamine and naphthylamine additives in adipic acid based model fluxes significantly increased the ERH and DRH in comparison with pure adipic acid flux under testing temperature of 60℃. The tripropylamine and naphthylamine additive in succinic acid model fluxes significantly decreased the leakage current level below threshold value of 10 µA under testing condition of 98% RH/25℃ and 98% RH/40℃ after simulated soldering process.

Activators in reflow solder flux in Chapter 8

1) Conductive ionic substances was released from the reflow flux residue after climatic exposure under at 60 °C, 98% RH. The increased conductivity value for extracted solutions were due to the release of different activators due to the opening up of the residue film. The binary blended WOAs activators and halide activators in residue accelerated hydrolytic degradation of the resin due to their lower DRH.

2) Flux activator used in flux formulation resulted different spreading effect of flux residue after soldering process. With WOA flux activator, the larger spreading area of flux residue on SIR pattern induced higher charge transfer, which is not related to the measured conductivity of the released substances from the residue after climatic exposure.

3) Type of flux activator used in flux formulation significantly influenced the leakage current value during accelerated climatic test. The lowest leakage current level was obtained by flux residue with amine additives due to Brönsted-Lowry acid base neutralization of WOA-amine activators. The ECM failure of reflow soldered SIR pattern was attributed to the low DRH and ionization of the corrosive halide under humid condition.

4) Due to capillary effect, reflow flux residue connected solder joints in the dummy SMT component with lower stand-off height, which provided a hydrophilic media for charge transfer under humid conditions. However, increasing the stand-off height of component resulted in a flux free region between solder joints if the spreading area of the flux residue is small.

Conformal coatings in Chapter 9

1) The moisture diffused through the coating only has minor impact on the performance of conformation coating. The coatings with flux residue showed lower impedance due to the absorption moisture by the residue, which accelerated the failure of the coating.

2) High impedance and low leakage current of coated clean SIR pattern suggest that the cleanliness is the key factor for the protection from conformal coatings. Together with cleanliness, compatibility of the coating with flux residue resulting in good adhesion results in better performance as found for elastomeric acrylate coating.

3) Synthetic rubber is not suitable for the flux residue contaminated PCBA application due to poor adhesion. The corrosion cell formed in the blister due to the water diffusion and dissolution of ionic flux residue, which lead to the ECM failures with 100% failure rate.

4) Low leakage current and high impedance was obtained for urethane acrylate coating with flux residue, however cross-sectional examination showed delamination and growth conductive corrosion products, which could have resulted in failure during extended exposure.

FURTHER PERSPECTIVES

Wave solder flux

The investigation of blended WOA-amine activator obtained the humidity robustness and excellent solderability. However, the influence of the degradation product of tripropylamine and succinic acid on the inhibition ECM is still unknown. Therefore, a continuation of the chemical analysis for the degradation product need to be conducted. The effect of blend WOA-amine activator on the corrosion process of Sn or SAC alloy can be monitored using Scanning Electrochemical Cell Microscopy with/without bias voltage loading. Moreover, the present work only confirmed the amide formation using succinic acid and selected amine additives, whereas the adipic acid did not reaction with amine additive. In order to obtain a proper flux formulation temperature for the robust flux manufacturing, the mechanism of the amide formation with different amine and WOA candidates required a further study, following with the reliability and solderability investigation of the new flux formulation.

Reflow solder flux

Investigation in this work demonstrates the risk of the flux residue spreading after the manufacturing process or under harsh climatic exposure. A further investigation is required to understand the reason of reflow flux spreading. Additionally, cracks and opening was observed after humidity exposure, which triggered the release of the conductive substances on the surface.

Therefore, to prevent the degradation and spreading of the reflow flux residue, new flux formulation for the reflow solder paste need to be investigated.

Conformal coating

To optimize the humidity robustness of the flux chemistry, organic amine will be or has been used as an important component in the flux for both wave soldering process and reflow soldering process. Limited information is available on the compatibility study of the conformal coating and flux residue with organic amine additives. A systematic investigation is required to understand the effect of the flux residue with organic amine additives on the adhesion and water absorption behavior of conformal coatings under harsh climatic exposure.

Since organic amine inhibited the corrosion performance at the surface on the PCBA. The organic amine or chemical with amino group can be used as the additive for the conformal coating. However, if the reaction between the WOA flux residue and organic amine in the coating induced more hygroscopic amide at PCBA-coating interface, more water will be absorbed by the conformal coating. Therefore, the solder flux and conformal coating can be designed as a couple products for the electronic manufacturing industry.